

UCLA

UCLA Electronic Theses and Dissertations

Title

Chemosensory mechanisms of host-seeking and host-infection behaviors in skin-penetrating parasitic nematodes

Permalink

<https://escholarship.org/uc/item/6zc6m726>

Author

Gang, Spencer S

Publication Date

2018

Peer reviewed|Thesis/dissertation

UNIVERSITY OF CALIFORNIA

Los Angeles

Chemosensory mechanisms of host-seeking and host-infection behaviors in
skin-penetrating parasitic nematodes

A dissertation submitted in partial satisfaction of the requirements for the degree
Doctor of Philosophy in Molecular Biology

by

Spencer Stephen Gang

2018

© Copyright by

Spencer Stephen Gang

2018

ABSTRACT OF THE DISSERTATION

Chemosensory mechanisms of host-seeking and host-infection behaviors in
skin-penetrating parasitic nematodes

by

Spencer Stephen Gang

Doctor of Philosophy in Molecular Biology

University of California, Los Angeles, 2018

Professor Elissa A. Hallem, Chair

Skin-penetrating parasitic nematodes infect approximately 1 billion people and are endemic in many developing regions worldwide. Nematode infections can lead to severe intestinal distress, anemia, stunted growth and cognitive impairment in children, and in some cases death. Skin-penetrating nematodes live in the environment as developmentally arrested third-stage infective larvae (iL3s) that actively search for mammals to infect, a process called host seeking. Despite the pervasive nature of these infections, very little is known about cellular and molecular mechanism that promote host-seeking behavior. In this dissertation I explore the behavioral strategies, and underlying chemosensory mechanisms, that allow skin-penetrating iL3s to detect hosts in the environment. I also characterize how iL3s use sensory mechanisms to resume their development upon entering the host. We focused on the human-parasitic threadworm *Strongyloides stercoralis* as a model for understanding chemosensory-driven behaviors in skin-penetrating nematodes. First, we investigated the host-seeking behaviors of *S. stercoralis* iL3s and compared its behavior to that of other parasitic nematodes. *S. stercoralis* iL3s are especially active in the environment, are stimulated by elevated temperatures approximating that of the human body, and also navigate

toward volatile odorants emitted from human skin and sweat. The odorant response profile of *S. stercoralis* iL3s was distinct from that of other parasitic nematodes that infect other mammals, indicating that olfaction may play a critical role in host specificity. We observed that the host-seeking behaviors of *S. stercoralis* iL3s are dramatically different from those of passively ingested parasitic nematode species. Thus, parasitic nematodes with different infection modes may identify and navigate to hosts in distinct ways, and in turn may require distinct environmental control measures. To address the molecular mechanisms of host seeking behavior, we leveraged the unique genetic tractability of *S. stercoralis* to develop CRISPR-Cas9-mediated targeted mutagenesis in parasitic nematodes. As a proof-of-concept for CRISPR-Cas9 feasibility in *S. stercoralis* we targeted the twitchin gene *Ss-unc-22* and generated iL3s with severe motility defects, the first mutant phenotype resulting from targeted mutagenesis observed in any parasitic nematode species. Our CRISPR-Cas9 technique was then applied to disrupt *S. stercoralis* genes with roles in chemosensation. We targeted the *Ss-tax-4* gene, a subunit of a cyclic nucleotide-gated ion channel, since its ortholog in the model free-living nematode *Caenorhabditis elegans* is known to be required for sensory-driven behaviors. *Ss-tax-4* iL3s were deficient in thermosensory-driven host seeking and could not positively thermotaxis in a temperature gradient, a robust behavior observed in wild-type iL3s. *Ss-tax-4* iL3s were also unable to navigate towards host-emitted 3-methyl-1-butanol (isoamyl alcohol), indicating that olfactory-driven host-seeking behaviors were also disrupted in the absence of functional chemosensory pathways. Next, we asked if chemosensory mechanisms were also necessary for iL3s to successfully establish an infection in the host. To address this question, we subjected *S. stercoralis* iL3s to host-like conditions *in vitro* and assessed iL3 activation, an initial developmental step inside the host where iL3s resume feeding behavior. iL3s consistently activated in the presence of 37°C and 5% CO₂ environments, but removal of either stimulus eliminated activation. *Ss-tax-4* iL3 were unable to activate in the presence of heat and CO₂, indicating that sensory function is also critical for in-host development. Our results suggest that two novel avenues for reducing the disease burden caused by skin-penetrating nematodes may be to interfere with chemosensory-driven host seeking in the

environment, or to inhibit sensory-driven development inside the host. Our results also lay the foundation for investigating the sensory neural circuits underlying the parasite-specific behaviors of an important group of helminths.

The dissertation of Spencer Stephen Gang is approved.

Alison Renee Frand

Kent L. Hill

Patricia J. Johnson

Elissa A. Hallem, Committee Chair

University of California, Los Angeles

2018

For Mo, Joe, Damien, and Tristram.

As the Joeism goes... "sometimes it's better to be lucky than good."

I've been incredibly lucky to have your guidance, example, and endless support.

Thank you for everything.

TABLE OF CONTENTS

Abstract.....	ii
Committee Page.....	v
Dedication.....	vi
List of Figures.....	viii
List of Tables.....	x
Acknowledgements.....	xi
Vita.....	xiv
Chapter 1:	
Introduction: Mechanisms of host seeking by parasitic nematodes.....	1
References.....	9
Chapter 2:	
Diverse host-seeking behaviors of skin-penetrating nematodes.....	12
Methods.....	19
References.....	22
Chapter 3:	
Experience-dependent olfactory behaviors of the parasitic nematode <i>H. polygyrus</i>	24
Methods.....	39
References.....	44
Chapter 4:	
Targeted mutagenesis in a human-parasitic nematode.....	48
Methods.....	64
References.....	76
Chapter 5:	
A critical role for thermosensation in host seeking by skin-penetrating nematodes.....	80
References.....	88
Methods.....	91
Chapter 6:	
Molecular mechanisms for olfactory-driven host seeking and in-host development in skin-penetrating nematodes.....	97
Methods.....	124
References.....	134
Chapter 7:	
Conclusions and future work.....	139
References.....	145

LIST OF FIGURES

Chapter 1

Figure 1: Ecology and life cycles of parasitic nematodes.....	3
Figure 2: Responses of different parasitic nematode species to CO ₂	4
Figure 3: Responses of mammalian-parasitic nematodes to volatile host cues.....	6
Figure 4: Skin-penetrating nematodes respond to thermosensory cues.....	7
Figure 5: Sensory neuron function is often conserved across free-living and parasitic nematodes.....	9

Chapter 2

Figure 1: Phylogenetic relationships and life cycles of parasitic nematodes.....	15
Figure 2: Foraging behaviors of skin-penetrating nematodes.....	16
Figure 3: Olfactory responses of mammalian-parasitic nematodes.....	18
Figure 4: Olfactory responses of <i>Strongyloides</i> species vary across life stages.....	19

Chapter 3

Figure 1: Navigational strategies of <i>H. polygyrus</i> in comparison to those of <i>S. ratti</i> and <i>S. stercoralis</i>	29
Figure 2: <i>H. polygyrus</i> iL3s are attracted to host feces.....	30
Figure 3: <i>H. polygyrus</i> iL3s are attracted to mammalian odorants.....	32
Figure 4: The navigational strategies of <i>H. polygyrus</i> are experience-dependent.....	34
Figure 5: <i>H. polygyrus</i> iL3s exhibit experience-dependent olfactory plasticity.....	35
Figure 6: Passively ingested nematodes but not skin-penetrating nematodes show experience-dependent modulation of CO ₂ -response valance.....	36
Figure 7: A model for host-seeking behavior in <i>H. polygyrus</i>	38

Chapter 4

Figure 1: A strategy for targeted mutagenesis in <i>S. stercoralis</i> using CRISPR-Cas9.....	51
Figure 2: CRISPR-Cas9 targeting of the <i>Ss-unc-22</i> gene results in iL3s with an uncoordinated phenotype.....	53
Figure 3: Nicotine induces twitching in <i>unc F₁</i> iL3s.....	54

Figure 4: CRISPR-mediated mutagenesis of <i>Ss-unc-22</i> results in putative deletion of the target locus.....	56
Figure 5: CRISPR-mediated homology-directed repair of <i>Ss-unc-22</i>	59
Figure 6: The <i>unc</i> phenotype is heritable following host passage.....	62
Chapter 5	
Figure 1: Human-parasitic iL3s show robust heat seeking.....	82
Figure 2: Experience-dependent plasticity regulates a switch between positive and negative thermotaxis.....	84
Figure 3: Thermal gradients can override olfactory attraction.....	86
Figure 4: The <i>S. stercoralis tax-4</i> homolog is required for heat seeking.....	87
Chapter 6	
Figure 1: Life cycles and ecology of nematode species.....	101
Figure 2: Olfactory responses are species and life-stage specific.....	103
Figure 3: <i>A. ceylanicum</i> and <i>S. stercoralis</i> have distinct fecal dispersal behaviors.....	106
Figure 4: The <i>S. stercoralis tax-4</i> gene is required for olfactory-driven host seeking.....	109
Figure 5: The <i>S. stercoralis tax-4</i> gene is required to detect sensory cues inside the host.....	110
Figure S1: Nematode chemotaxis assay.....	116
Figure S2: <i>S. stercoralis</i> wild-type iL3s navigate to host-emitted 3-methyl-1-butanol.....	117
Figure S3: Strategy of CRISPR-Cas9-mediated targeted mutagenesis of <i>Ss-tax-4</i> and genotyping for homology-directed repair (HDR).....	118
Figure S4: <i>In vitro</i> activation assay for <i>S. ratti</i> and <i>P. trichosuri</i> iL3s.....	119
Chapter 7	
Figure 1: The <i>S. stercoralis gcy-9</i> gene may be required for detection of CO ₂	142

LIST OF TABLES

Chapter 5

Key Resources Table.....	91
--------------------------	----

Chapter 6

Supplementary Table 1: Mammalian derived odorants tested.....	120
Supplementary Table 2: Plasmid vectors used in this study.....	121
Supplementary Table 3: Oligonucleotides used in this study.....	122
Supplementary Table 4: Summary of <i>Ss-tax-4</i> microinjections, F ₁ iL3 screening, and genotyping of <i>Ss-tax-4</i> knockout iL3s.....	123

ACKNOWLEDGEMENTS

To begin, I would like to thank my mentor Dr. Elissa Hallem for providing a truly exceptional graduate experience. Elissa is a remarkably gifted scientist who seems to have an endless supply of unique and exciting research questions to address, it was a privilege to help her explore a small fraction of them. What I appreciate most about Elissa is that she is an incredible motivator. Elissa's enthusiasm for science, unwavering support, and accessibility on a day-to-day basis shows that she is deeply invested in her mentees success, which in turn makes it very easy to want to work hard for her. I'm honored to have had the opportunity to learn from her example. I hope I can someday provide the same quality of mentorship that she has given me. Thank you, Elissa, for all of your time and effort on my behalf. I appreciated all of it immensely and look forward to following your research for many years to come.

I would also like to thank the members of the Hallem lab who helped support my research. In particular, I want to acknowledge our Project Scientist Dr. Michelle Castelletto. Michelle is a fantastic Parasitologist, amazing teacher, and critical resource for everything we do in the Hallem Lab. All of my accomplishments were only possible with Michelle's help and patient training. Michelle, thank you for everything. To everyone else in the Hallem Lab, thank you for providing an enjoyable and supportive work environment. It was a pleasure to work with such a talented and collaborative group every day.

I next would like to thank the members of my committee: Professors Alison Frand, Kent Hill, Patricia Johnson, and Alvaro Sagasti. Thank you for your encouragement and advice over the years. I am lucky to have had such a wonderful group of scientists guide me through my doctoral training. In addition, I would like to thank the members of the UCLA Parasitology group for feedback on my projects. It was a privilege to be part of great community of Parasitologist who provided different perspectives, and unique ideas, to help advance our research in the Hallem Lab.

I would also like to thank the Molecular Biology Institute and the department of Microbiology, Immunology, and Molecular Genetics, especially Pamela Hurley, Jen Miller,

Hillary Rubinich, and IMMP home area director Dr. Peter Bradley for their commitment to graduate student education.

Finally, it has been a privilege to have my graduate work supported by multiple different training grants and fellowship programs. I would like to thank the UCLA Whitcome Pre-Doctoral Fellowship in Molecular Biology, the Ruth L. Kirschstein T32 Microbial Pathogenesis Training Grant, and National Science Foundation East Asia and Pacific Summer Institutes Fellowship for their generous support. In addition to financial support, each of these programs helped broaden my exposure to science by providing valuable student-driven seminar series and journal clubs, engagement and outreach opportunities, and collaborations with scientists and fellow graduate students from around the world.

Chapter 1 is a version of: Gang S.S. and Hallem E.A. (2016) Mechanisms of host seeking by parasitic nematodes. *Mol Biochem Parasitol.* 208(1): 23-32. This review was part of a special issue on "Parasite communication and cell-cell interactions." It was written by Dr. Elissa Hallem and me.

Chapter 2 is a version of: Castelletto M.L., Gang S.S., Okubo R.P., Tselikova A.A., Nolan T.J., Platzer E.G., Lok J.B., Hallem E.A. (2014) Diverse host-seeking behaviors of skin-penetrating nematodes. *PLoS Pathog.* 10(8): e1004305. I contributed to this project by performing unstimulated, heat-stimulated, and mechanically-stimulated automated motility tracking of skin-penetrating infective larvae. I also performed nictation behavior assays on infective larvae. I followed up on this study by investigating the molecular basis of olfactory-driven host seeking and sensory-driven infection behaviors of skin-penetrating nematodes (Chapter 6). Dr. Astra Bryant followed up on my preliminary heat stimulation results by exploring the thermosensory-driven behaviors of skin-penetrating nematodes in greater detail, as described in Chapter 5.

Chapter 3 is a version of: Ruiz F., Castelletto M.L., Gang S.S., Hallem E.A. (2017) Experience-dependent olfactory behaviors of the parasitic nematode *Heligmosomoides polygyrus*. *PLoS Pathog.* 13(11): e1006709. I contributed to this project by performing *Strongyloides stercoralis* and *Strongyloides ratti* dispersal, crawling speed, and nictation

assays to compare the motility of skin-penetrating infective larvae to passively ingested *H. polygyrus*. I also performed *S. stercoralis* CO₂ assays with Dr. Michelle Castelletto demonstrating that skin-penetrating nematodes do not show experience-dependent modulation of CO₂-response valance.

Chapter 4 is a version of: Gang S.S., Castelletto M.L., Bryant A.S., Yang E., Mancuso N., Lopez J.B., Pellegrini M., Hallem E.A. (2017) Targeted mutagenesis in a human-parasitic nematode. *PLoS Pathog.* 13(10): e1006675. In coordination with my professor Dr. Elissa Hallem, and our Project Scientist Dr. Michelle Castelletto, I designed this study, executed the experiments, and interpreted the data. The manuscript was written by Dr. Elissa Hallem and me. Undergraduate researchers Emily Yang and Jackie Lopez assisted with molecular cloning and nicotine assay development, respectively. Dr. Astra Bryant assisted with motility tracking and provided valuable feedback and ideas on the manuscript. Dr. Matteo Pellegrini and Dr. Nick Mancuso assisted with bioinformatic analysis. Follow up experiments from this study focused on application of CRISPR-Cas9 to exploring molecular mechanisms of sensory-driven host seeking and host infection behaviors of skin-penetrating infective larvae.

Chapter 5 is a version of: Bryant A.S., Ruiz F., Gang S.S., Castelletto M.L., Lopez J.B. Hallem E.A. (2018) A critical role for thermosensation in host seeking by skin-penetrating nematodes. *Curr Biol* 28(14): 2338-2347. I contributed to this study by developing the CRISPR-Cas9 targeted mutagenesis strategy that was applied to the *Ss-tax-4* gene to demonstrate that sensory mechanisms are required for positive thermotaxis behaviors in skin-penetrating infective larvae.

Chapter 6 is a draft of a manuscript submission to be entitled, "Molecular mechanisms for olfactory-driven host seeking and in-host development in skin-penetrating nematodes." I wrote this draft with feedback from Dr. Elissa Hallem. With Dr. Elissa Hallem, I designed the study, executed experiments and interpreted data. Emily Yang, Feli Ruiz, and Dr. Michelle Castelletto assisted with life-stage-specific chemotaxis assays. Feli Ruiz performed fecal dispersal assays. Taylor Brown assisted with activation assays.

VITA

Education

B.S. in Biology

Santa Clara University, Santa Clara, CA (2006-2009)

Academic Awards

2015-2018 Ruth L. Kirschstein National Research Service Award AI007323

2015 Teaching Assistant Award, UCLA MIMG Department

2015 Philip Whitcome Fellowship, UCLA Molecular Biology Institute

2015 NSF East Asia and Pacific Summer Institutes Fellowship Award #1414655

2007-2009 John R. Box merit-based scholarship, Santa Clara University

Publications

Bryant A.S., Ruiz F., Gang S.S., Castelletto M.L., Lopez J.B., Hallem E.A. (2018) A critical role for thermosensation in host seeking by skin-penetrating nematodes. *Current Biology* 28(14): 2338-2347.

Gang S.S., Castelletto M.L., Bryant A.S., Yang E., Mancuso N., Lopez J.B., Pellegrini M., Hallem E.A. (2017) Targeted mutagenesis in a human-parasitic nematode. *PLoS Pathog.* 13(10): e1006675.

Ruiz F., Castelletto M.L., Gang S.S., Hallem E.A. (2017) Experience-dependent olfactory behaviors of the parasitic nematode *Heligmosomoides polygyrus*. *PLoS Pathog.* 13(11): e1006709.

Gang S.S., Hallem E.A. (2016) Mechanisms of host seeking by parasitic nematodes. *Mol Biochem Parasitol.* 208(1): 23-32.

Castelletto M.L., Gang S.S., Okubo R.P., Tselikova A.A., Nolan T.J., Platzer E.G., Lok J.B., Hallem E.A. (2014) Diverse host-seeking behaviors of skin-penetrating parasitic nematodes. *PLoS Pathog.* 10(8): e10004305.

Li X., Zhang R., Patena W., Gang S.S., Blum S.R., Ivanova N., Yue R., Robertson J.M., Lefebvre P.A., Fitz-Gibbon S.T., Grossman A.R., Jonikas M.C. (2016) An indexed, mapped

mutant library enables reverse genetics Studies of Biological Processes in *Chlamydomonas reinhardtii*. *Plant Cell* 28(2): 367-87.

Zhang R., Patena W., Armbruster U., Gang S.S., Blum S.R., Jonikas M.C. (2014) High-Throughput Genotyping of Green Algal Mutants Reveals Random Distribution of Mutagenic Insertion Sites and Endonucleolytic Cleavage of Transforming DNA. *Plant Cell* 26(4): 1398-1409.

Selected Presentations

Gang S.S., Castelletto M.L., Bryant A.S., Yang E., Hallem E.A. Targeted mutagenesis in a human-parasitic nematode. UCLA Parasitology Seminar Series. Los Angeles, CA. May 2018.

Gang S.S., Castelletto M.L., Brown T.M., Lee J., Hallem E.A. Host-seeking and infection strategies of parasitic nematodes. Molecular and Cellular Biology of Helminths X. Hydra, Greece. September 2016.

Gang S.S., Castelletto M.L., Barnia A., Okubo R., Tselikova A., Hallem E.A. Host-seeking strategies of skin-penetrating parasitic nematodes. The 5th Annual Southern California Eukaryotic Pathogen Symposium. Riverside, CA. October 2015.

Gang S.S., Castelletto M.L., Barnia A., Okubo R., Tselikova A., Hallem E.A. Host-seeking strategies of skin-penetrating parasitic nematodes. La Trobe University Department of Genetics Seminar Series. Melbourne, Australia. August 2014.

Chapter 1

Introduction: Mechanisms of host seeking by parasitic nematodes



Mechanisms of host seeking by parasitic nematodes



Spencer S. Gang, Elissa A. Hallem*

Department of Microbiology, Immunology, and Molecular Genetics and Molecular Biology Institute, University of California, Los Angeles, Los Angeles, CA 90095, United States

ARTICLE INFO

Article history:

Received 30 September 2015
Received in revised form 13 May 2016
Accepted 16 May 2016
Available online 17 May 2016

Keywords:

Parasitic nematodes
Parasitic helminths
Host-seeking behavior
Olfactory behavior
Skin-penetrating nematodes
Entomopathogenic nematodes

ABSTRACT

The phylum Nematoda comprises a diverse group of roundworms that includes parasites of vertebrates, invertebrates, and plants. Human-parasitic nematodes infect more than one billion people worldwide and cause some of the most common neglected tropical diseases, particularly in low-resource countries [1]. Parasitic nematodes of livestock and crops result in billions of dollars in losses each year [1]. Many nematode infections are treatable with low-cost anthelmintic drugs, but repeated infections are common in endemic areas and drug resistance is a growing concern with increasing therapeutic and agricultural administration [1]. Many parasitic nematodes have an environmental infective larval stage that engages in host seeking, a process whereby the infective larvae use sensory cues to search for hosts. Host seeking is a complex behavior that involves multiple sensory modalities, including olfaction, gustation, thermosensation, and humidity sensation. As the initial step of the parasite-host interaction, host seeking could be a powerful target for preventative intervention. However, host-seeking behavior remains poorly understood. Here we review what is currently known about the host-seeking behaviors of different parasitic nematodes, including insect-parasitic nematodes, mammalian-parasitic nematodes, and plant-parasitic nematodes. We also discuss the neural bases of these behaviors.

© 2016 Elsevier B.V. All rights reserved.

1. Host seeking by entomopathogenic nematodes

Entomopathogenic nematodes (EPNs) in the genera *Heterorhabditis* and *Steinernema* are parasites that infect and kill insects. EPNs are known as “beneficial nematodes” because they infect a wide variety of insect pests and disease vectors, and are used commercially throughout the world for biocontrol. EPNs are of interest not only as biocontrol agents, but also as models for understanding human-parasitic nematodes. EPNs are broadly distributed geographically, having been found on every continent except Antarctica [2]. Most EPNs, including many species commonly used for biocontrol such as *Steinernema carpocapsae* and *Heterorhabditis bacteriophora*, are generalists that are capable of infecting and killing many different insect species (Fig. 1A). However, some EPNs are specialists that primarily target a single type of insect [2]. For example, *Steinernema scapterisci* targets mole crickets [3] and *Steinernema diaprepesi* targets the larval stages of the root weevil *Diaprepes abbreviatus*, a citrus pest [4].

1.1. Life cycle of EPNs

EPNs are infective during a particular life stage called the infective juvenile (IJ), alternatively described as the infective third-stage larva (L3i). IJs invade insect hosts by entering through an orifice such as the mouth or spiracles, or by penetrating through the cuticle [5]. The IJs contain a bacterial endosymbiont in their gut, and upon host entry they deposit their symbiotic bacteria into the insect. The worms and bacteria rapidly kill the insect, typically within 48 h of host entry. The worms grow and reproduce inside the insect cadaver, feeding off bacteria and cadaver tissue until food sources are depleted. New IJs then form and disperse into the environment to search for new hosts (Fig. 1B) [5].

1.2. Host-seeking strategies of EPNs

The host-seeking strategies of EPN species are typically described as varying along a continuum ranging from ambushing, in which the IJs remain relatively stationary and latch on to passing hosts, to cruising, in which the IJs disperse in search of hosts [6]. Ambushers often nictate, where the IJ stands on its tail and waves to facilitate attachment to passing hosts. Some ambushing *Steinernema* species also jump, where the IJ stands on its tail, curls, and propels itself into the air [6]. In general, ambushers are most effective at targeting motile hosts, while cruisers are most effective

* Correspondence to: UCLA MIMG, 237 BSRB, 615 Charles E. Young Dr. E, Los Angeles, CA 90095, United States.

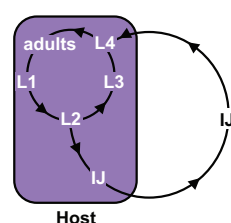
E-mail addresses: sgang@ucla.edu (S.S. Gang), ehallem@microbio.ucla.edu (E.A. Hallem).

<http://dx.doi.org/10.1016/j.molbiopara.2016.05.007>
0166-6851/© 2016 Elsevier B.V. All rights reserved.

A Ecology of select nematode species

Nematode	Common Name	Infection route	Common host(s)
<i>Caenorhabditis elegans</i>	n/a	free-living	none
<i>Steinernema carpocapsae</i>	n/a	active invasion	insect
<i>Heterorhabditis bacteriophora</i>	n/a	active invasion	insect
<i>Ancylostoma caninum</i>	hookworm	skin-penetration	dog, fox, cat
<i>Ancylostoma duodenale</i>	hookworm	skin-penetration	human
<i>Necator americanus</i>	hookworm	skin-penetration	human
<i>Nippostrongylus brasiliensis</i>	hookworm	skin-penetration	rat
<i>Strongyloides stercoralis</i>	threadworm	skin-penetration	human, primate, dog
<i>Strongyloides ratti</i>	threadworm	skin-penetration	rat
<i>Haemonchus contortus</i>	barber's pole worm	passive ingestion	ruminants
<i>Ascaris lumbricoides</i>	giant roundworm	passive ingestion	human

B Life cycle of EPNs



C Life cycles of select mammalian-parasitic nematode species

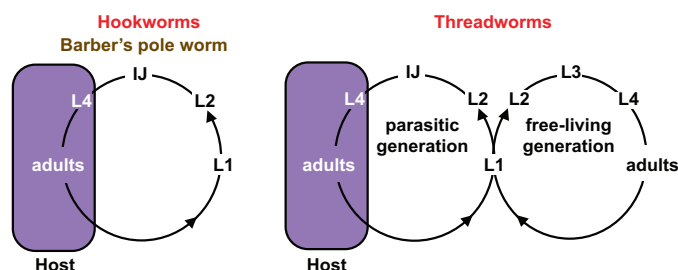


Fig. 1. Ecology and life cycles of parasitic nematodes. A. Ecology of select nematode species, with common hosts indicated [28,29,31,96–98]. Green = free-living, blue = entomopathogenic, red = skin-penetrating, brown = passively ingested. B. The life cycle of EPNs. EPN infective juveniles (IJs) infect by invasion through orifices or by penetration of the cuticle. The IJs and their associated bacteria rapidly kill the host. The nematodes develop and reproduce within the host cadaver for a number of generations, where they feed on bacteria in the insect body and the cadaver tissue. Once resources in the cadaver are exhausted, IJs emerge and search for a new host to infect [96]. C. Life cycles of mammalian-parasitic nematodes. Hookworms infect by skin penetration or orally. Inside the host, hookworms develop into adults that reproduce in the small intestine. Eggs are excreted with the host's feces and develop into IJs. IJs leave the feces in search of new hosts. Hookworms must infect a new host every generation [99]. Threadworms of the *Strongyloides* genus have a similar life cycle but can develop through a limited number of free-living generations outside the host. Some of the eggs excreted with the host's feces develop into IJs, while others develop into free-living adults that mate outside the host [28]. The life cycle outside the host of the barber's pole worm *Ha. contortus* is similar to that of hookworms, except that the IJs enter the host only by passive ingestion [97]. For B–C, L1–L4 are the first through fourth larval stages. For some parasitic nematode species IJs are alternatively described as infective third-stage larvae (L3i). Figures are adapted from Castelletto et al. (2014) [26].

at targeting non-motile hosts [7]. However, recent studies suggest that many species are capable of engaging in either ambushing or cruising depending on the environmental context. For example, although *Ste. carpocapsae* is generally considered a classical ambusher, it moves more in peat than sandy soil, suggesting that it can ambush or cruise depending on its environment [8]. The extent to which *Ste. carpocapsae* moves in the soil also depends on which insect hosts are present [7,9]. In addition, all EPN species examined so far exhibit robust chemotaxis in the presence of insect-derived odorants [10,11]. Thus, most EPNs appear to be capable of cruising toward host-emitted sensory cues under at least some conditions.

1.3. Responses of EPNs to olfactory cues

A number of studies have demonstrated that EPNs use olfactory cues to locate hosts to infect. IJs are attracted to the odor blends emitted by live insects and to a diverse array of insect-emitted odorants, including carbon dioxide (CO₂) (Fig. 2A–B) [10–15]. CO₂ is an essential host cue for EPNs: attraction to insect odor blends is greatly reduced or eliminated when CO₂ is removed (Fig. 2C) [11,12]. Jumping in *Steinernema* is stimulated by insect odor blends, CO₂, and host-specific odorants [10,11,16]. EPNs are also attracted to volatile components of insect feces [17]. A large-scale comparative analysis of olfactory behaviors across species revealed that different EPN species respond differently to odorants [10,11]; thus,

EPNs appear to have specialized olfactory systems that contribute to host selection.

EPNs also respond to odorants emitted by insect-damaged plants [18]. For example, the odorant (E)-β-caryophyllene is released by maize roots in response to insect feeding and attracts the EPN *Heterorhabditis megidis* [19]. Similarly, *Ste. diaprepesi* is attracted to volatiles released by plant roots that have been damaged by its host *D. abbreviatus* [4]. CO₂ acts synergistically with root volatiles to attract EPNs [18]. Thus, EPNs appear to use CO₂, insect odorants, and plant odorants to find insects to infect.

1.4. Responses of EPNs to other sensory cues

In addition to responding to olfactory cues, EPNs respond to a number of other sensory cues that may contribute to host seeking. For example, EPNs have been shown to aggregate at temperatures that approximate insect body temperature, which is slightly (<1 °C) above ambient temperature due to insect metabolic processes [20]. EPNs also respond to salt gradients. *Ste. carpocapsae* IJs can navigate in gradients of Na⁺, Mg²⁺, Ca²⁺, CO₃²⁻, and Cl⁻ and accumulate at different preferred concentrations for each ion [21]. EPNs also respond to electric fields, magnetic fields, vibration, and mechanical stimulation [22–26]. These other sensory responses are presumed to facilitate environmental navigation and/or host finding.

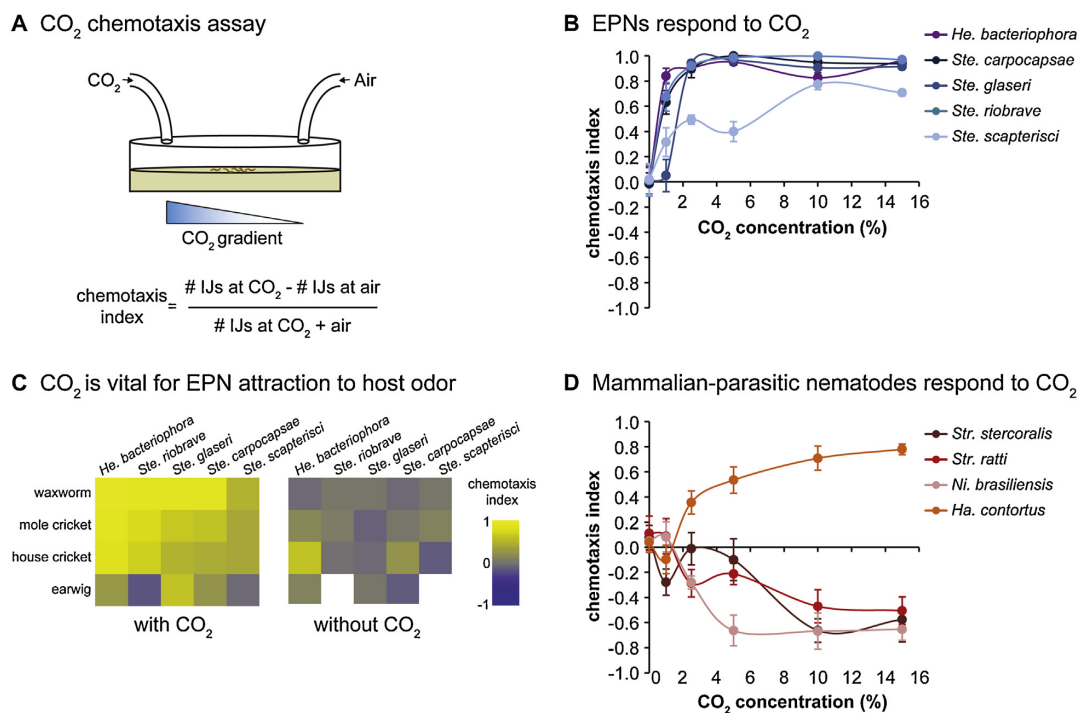


Fig. 2. Responses of different parasitic nematode species to CO₂. **A.** A CO₂ chemotaxis assay. CO₂ is pumped into one side of a plate, and an air control is pumped into the other side. IJs are placed in the center of the plate and allowed to migrate in the CO₂ gradient for 1 h. The number of IJs underneath the CO₂ inlet and the number underneath the air inlet are then counted, and a chemotaxis index (CI) is calculated according to the formula indicated. The chemotaxis index ranges from +1 to -1, with positive values indicating attraction to CO₂ and negative values indicating repulsion from CO₂. **B.** Responses of EPNs to CO₂ in a chemotaxis assay. All EPN species tested are attracted to CO₂ across concentrations. Data are from Dillman et al. (2012) [11]. **C.** CO₂ is required for normal attraction of EPNs to insect odor blends. Left, EPN responses to host odor blends in a chemotaxis assay. Right, EPN responses to host odor blends with CO₂ chemically removed. Attraction of EPNs to insect odor is reduced or eliminated in the absence of CO₂. Responses are shown as a heatmap; yellow indicates attraction and blue indicates repulsion. White boxes in the heatmap indicate EPN-host combinations that were not tested with CO₂ removed because they were not attractive with CO₂ present. Reproduced from Dillman et al. (2012) [11]. **D.** Responses of mammalian-parasitic nematodes to CO₂ in a chemotaxis assay. The skin-penetrating nematodes *Str. stercoralis*, *Str. ratti*, and *Ni. brasiliensis* are repelled by CO₂, while the passively ingested nematode *Ha. contortus* is attracted to CO₂. Data are from Castelletto et al. (2014) [26].

2. Host seeking by mammalian-parasitic nematodes

Nematode parasites of humans are widespread and pose dangerous health risks. Over one billion people worldwide harbor at least one nematode infection, mostly in low-income tropical and sub-tropical regions of the world [27]. Many parasitic nematode species are co-endemic and mixed infections are frequently observed. Parasitic nematode infections can cause chronic gastrointestinal distress, anorexia, anemia, and stunted physical and cognitive development in children. Select nematode species can cause severe symptoms such as permanent disfigurement and blindness, and some can even be fatal for infants and the immunocompromised [27]. In addition, nematode parasites of non-human animals are widespread, and preventing or controlling nematode infections in commercial livestock and household pets costs billions of dollars annually [1].

Many mammalian-parasitic nematodes infect only one or a limited number of host species. For example, *Strongyloides fulleroni kellyi* is a human parasite, while *Strongyloides stercoralis* has a limited host range that includes humans, primates, and dogs (Fig. 1A) [28]. Mammalian-parasitic nematodes can infect hosts by skin penetration, passive ingestion, or direct transmission via intermediate vectors [1]. Vector-borne parasitic nematodes such as *Wuchereria bancrofti* and *Onchocerca volvulus*, the causative agents of lymphatic filariasis and onchocerciasis, respectively, rely on

the host-seeking capabilities of their intermediate insect vectors to infect their definitive hosts [27]. By contrast, skin-penetrating nematodes and passively ingested nematodes use environmental and host-emitted stimuli to seek out nearby hosts or position themselves in advantageous locations for host ingestion. We focus here on skin-penetrating and passively ingested nematodes.

2.1. Life cycles of mammalian-parasitic nematodes

Skin-penetrating nematodes such as the human hookworms *Ancylostoma duodenale* and *Necator americanus*, and the human threadworm *Str. stercoralis*, have similar life cycles inside the host (Fig. 1A, C). Parasitic adults colonize the mucosa of the host intestine and shed eggs that are passed with feces. The nematodes develop on the host feces to the IJ stage, and the IJs then find and infect new hosts. The soil-dwelling IJs infect by skin penetration, commonly through the feet [28,29]. The IJs typically migrate through the circulatory system to the lungs, where they penetrate the alveoli and cause irritation and a dry cough. The IJs are coughed up and swallowed, and then pass through the stomach into the intestine, where they resume development into parasitic adults. Hookworms can also infect orally [30]. *Strongyloides* species can undergo one or a limited number of free-living generations outside of the host, and *Str. stercoralis* can cycle through multiple generations inside the same host (Fig. 1C) [28,29].

Passively ingested nematodes vary in their life cycles. For example, the human-parasitic giant roundworm *Ascaris lumbricoides* colonizes the host intestine and eggs are passed in the feces. *As. lumbricoides* larvae developmentally arrest while still inside the egg, and development resumes when the host ingests infective eggs [31]. In contrast, the ruminant parasite *Haemonchus contortus* is passively ingested as IJs and has a life cycle outside the host that is similar to that of skin-penetrating hookworms (Fig. 1A,C) [32]. However, unlike hookworms, the in-host life cycle of *Ha. contortus* is constrained to the gut. *Ha. contortus* IJs exsheath in the rumen and travel to the abomasum, where they develop into parasitic adults [33].

2.2. Host-seeking strategies of mammalian-parasitic nematodes

Like EPNs, mammalian-parasitic nematodes vary in their host-seeking strategies. In the absence of stimulation, the dog hookworm *Ancylostoma caninum* and the human hookworms *An. duodenale* and *Ne. americanus* have been described as ambushers that remain relatively motionless [34,35]. In the presence of host-emitted cues, the IJs crawl or nictate [34,35]. By contrast, the *Strongyloides* species appear to be cruisers that spend more time crawling than nictating in the absence of stimulation [26,36]. Human-parasitic *Str. stercoralis* IJs crawl faster than rat-parasitic skin-penetrating IJs and EPN IJs in the absence of sensory stimulation, suggesting that *Str. stercoralis* may have evolved longer-distance dispersal mechanisms to accommodate for more motile hosts [26]. In contrast, passively ingested *Ha. contortus* is less motile than the skin-penetrating species and appears to be an ambusher [26]. As with EPNs, some mammalian-parasitic nematodes have foraging behaviors that are intermediate between traditionally classified cruising and ambushing behaviors. For example, the rat hookworm *Nippostrongylus brasiliensis* is capable of crawling at a speed comparable to that of the skin-penetrating rat parasite *Strongyloides ratti*, yet unlike *Str. ratti*, *Ni. brasiliensis* prefers to nictate on certain surfaces [26]. Thus, like EPNs, mammalian-parasitic nematodes appear to modulate their foraging strategy depending on environmental conditions.

2.3. Responses of mammalian-parasitic nematodes to CO₂

There is now substantial evidence that mammalian-parasitic nematodes use host-emitted chemosensory cues to identify potential hosts. One important host cue for some mammalian-parasitic nematodes is CO₂, which is exhaled by mammals at concentrations of 4–5% during respiration (compared to 0.04% in air) [37]. CO₂ induces nictation behavior in *An. caninum* [34]. It also increases random crawling in *Str. stercoralis* and *An. caninum*, but decreases random crawling in *Ha. contortus* [36].

In the presence of a CO₂ gradient, the skin-penetrating nematodes *Str. stercoralis*, *Str. ratti*, and *Ni. brasiliensis* are repelled by high CO₂ but neutral to low CO₂ (Fig. 2D) [26]. Avoidance of high CO₂ by skin-penetrating nematodes is consistent with the fact that they typically infect around the feet and lower extremities, where CO₂ concentrations are less than 1% [38]. However, whether CO₂ is attractive in combination with other host cues has not yet been investigated. In contrast to the skin-penetrating nematodes, passively ingested *Ha. contortus* is attracted to CO₂ concentrations at or above 2.5% (Fig. 2D) [26]. *Ha. contortus* infects grazing animals and has been shown to migrate vertically between herbage and soil in response to changes in environmental factors such as temperature and humidity [39,40]. Attraction to host-emitted CO₂ may stimulate *Ha. contortus* to migrate up the herbage toward the mouths of grazing ruminants and thereby increase the chances of a successful infection.

2.4. Responses of mammalian-parasitic nematodes to soluble host cues

Mammalian-parasitic nematodes respond to a number of chemicals present in mammalian skin, sweat, and serum. For example, *An. caninum* is attracted to hydrophilic components extracted from dog skin [34]. In addition, *An. duodenale* and *Ne. americanus* show increased random crawling speeds and skin-penetration behaviors in the presence of human skin extract [35]. More quantitative studies are needed to determine if human hookworms are attracted to human skin extracts. In the case of threadworms, *Str. stercoralis* is attracted to dog skin extracts, human serum, and human sweat, while *Str. ratti* is attracted to mammalian serum components [41–43]. Furthermore, both *Str. stercoralis* and *Str. ratti* are capable of navigating in sodium chloride gradients and accumulate at concentrations comparable to the concentrations found in sweat [44,45].

2.5. Responses of mammalian-parasitic nematodes to volatile host cues

Humans and other mammals emit hundreds of odorants from skin, sweat, skin microbiota, and breath [46,47]. Since host-emitted odor blends are species-specific, olfaction is likely to contribute to the species-specificity of many parasites, including parasitic nematodes [48]. One of the first skin odorants identified as an attractant for mammalian-parasitic nematodes was urocanic acid. *Str. stercoralis* IJs are robustly attracted to urocanic acid even at low concentrations (Fig. 3A–B) [42]. Urocanic acid is found on the skin of many mammals, but in humans it is especially abundant on the feet, where *Str. stercoralis* infections commonly occur [42]. Thus, urocanic acid is likely to be an important host-seeking cue for *Str. stercoralis*.

More recently, *Str. stercoralis*, *Str. ratti*, *Ni. brasiliensis*, and *Ha. contortus* IJs were tested in chemotaxis assays to assess their responses to a large panel of human-emitted odorants (Fig. 3C–D) [26]. Each of the species tested showed a unique odor response profile, demonstrating that like EPNs, mammalian-parasitic nematodes have species-specific olfactory preferences (Fig. 3D) [26]. In the case of *Str. stercoralis*, nearly all of the strongest attractants identified are also known attractants for anthropophilic mosquitoes, suggesting that mosquitoes and nematodes may utilize similar olfactory cues to locate human hosts (Fig. 3D). Two of the attractive odorants identified, 7-octanoic acid and 6-methyl-5-hepten-2-one (sulcatone), are thought to be highly enriched in human body odor relative to the body odor of other mammals [49,50]. In addition, sulcatone response in certain *Aedes aegypti* mosquito populations was recently associated with preference for human hosts [50]. The finding that *Str. stercoralis* is attracted to sulcatone raises the possibility that it also uses sulcatone to preferentially target humans [26]. We note that sulcatone is also an insect pheromone [51,52], perhaps explaining why it is an attractant for EPNs as well as *Str. stercoralis*. In contrast to the skin-penetrating nematodes, passively ingested *Ha. contortus* was repelled by most skin and sweat odorants tested. However, *Ha. contortus* was attracted to fresh grass extracts, as well as methyl myristate and myristic acid, known components of cow and goat milk (Fig. 3D) [26]. These responses may allow *Ha. contortus* IJs to position themselves in grazing areas frequented by ruminants.

A quantitative comparison of olfactory behavior in skin-penetrating IJs, passively ingested IJs, EPN IJs, and dauer larvae of the free-living nematode *Caenorhabditis elegans* revealed that species with similar host ranges responded more similarly to odorants, even when phylogenetically distant (Fig. 3E–F) [26]. For example, *Str. ratti* and *Ni. brasiliensis* are distantly related but share a rodent host, and they respond more similarly to odorants

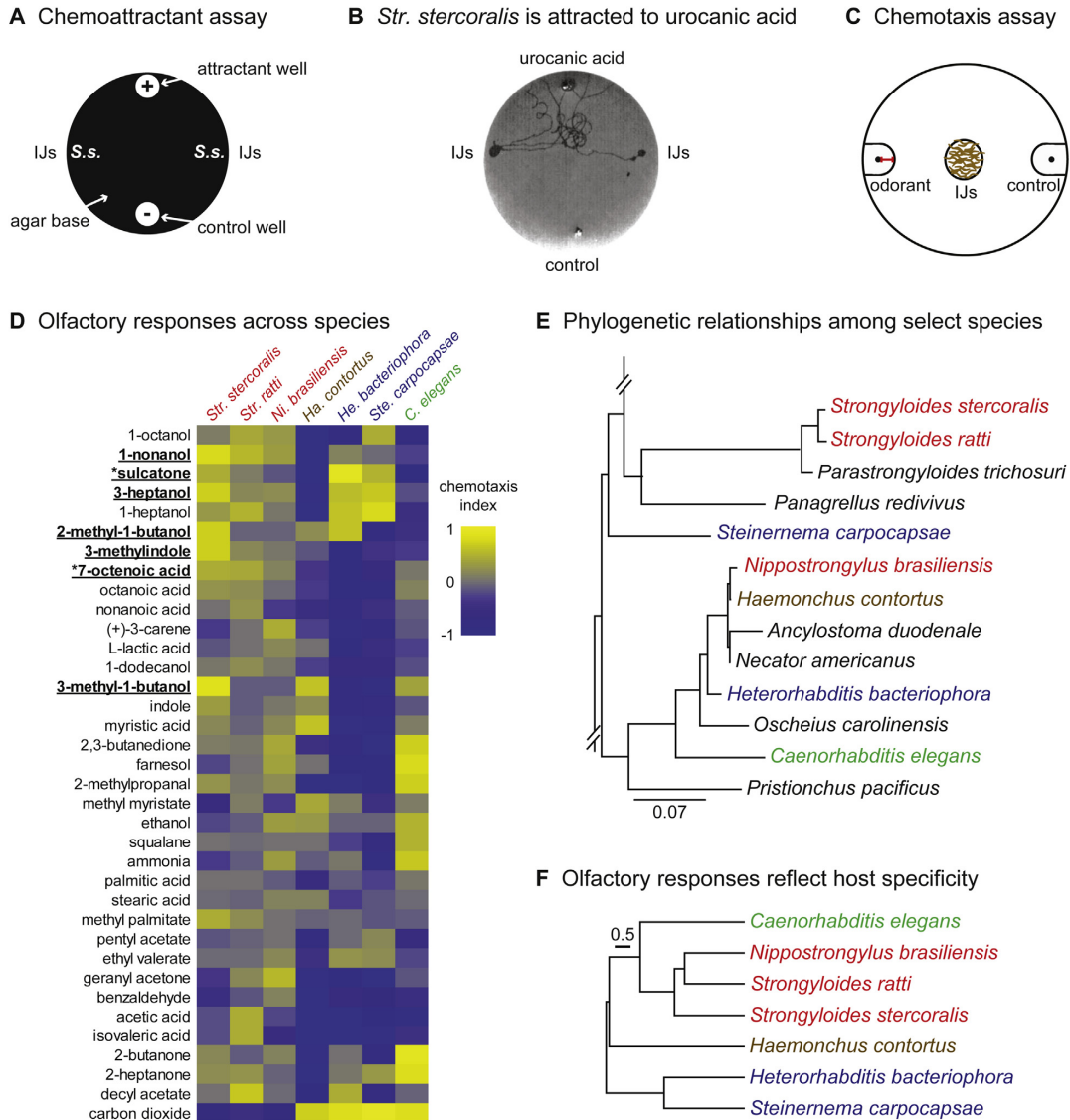


Fig. 3. Responses of mammalian-parasitic nematodes to volatile host cues. **A.** A chemoattractant assay for *Str. stercoralis* IJs. IJs are placed on each side of the plate and allowed to migrate in the chemical gradient for 28 min. **B.** *Str. stercoralis* IJs are attracted to urocanic acid. For A–B, data are reproduced from Safer et al. (2007) [42]. **C.** A chemotaxis assay for IJs. Odorant is placed on one side of the plate and control is placed on the other (black dots). IJs are placed in the center of the plate and allowed to migrate in the odorant gradient for 3 h. The number of IJs in each scoring region (extended circles around the black dots) is then counted and a chemotaxis index (CI) is calculated as: $CI = (\# \text{ IJs at odorant} - \# \text{ IJs at control}) / (\# \text{ IJs at odorant} + \# \text{ IJs at control})$. The chemotaxis index ranges from +1 to –1, with positive values indicating attraction to the odorant and negative values indicating repulsion from the odorant. Red scale bar = 1 cm. **D.** Olfactory responses across species. CI values are color-coded as shown to the right of the heatmap. For nematode species included, red = skin-penetrating; brown = passively ingested; blue = entomopathogenic; green = free-living. Odorants in bold and underlined are known attractants for anthropophilic mosquito species. Odorants denoted by an asterisk are abundant in humans relative to other mammals. **E.** Phylogenetic relationships among select nematode species, based on Castelletto et al. (2014) [26] and Dillman et al. (2012) [11]. Species tested for olfactory behavior are color-coded. **F.** Behavioral dendrogram constructed from odorant responses in D. Olfactory responses reflect preferred host rather than genetic relatedness. For C–F, data are from Castelletto et al. (2014) [26].

than *Str. ratti* and *Str. stercoralis*. Thus, the olfactory preferences of mammalian-parasitic nematodes reflect their host specificity rather than their phylogenetic relationships. These results suggest that mammalian-parasitic nematodes have specialized olfactory systems that support host finding and host selection.

2.6. Thermosensory behaviors of mammalian-parasitic nematodes

Skin-penetrating nematodes respond robustly to thermal stimulation. Both hookworms and *Strongyloides* species can navigate through thermal gradients and accumulate at temperatures approximating mammalian body temperature (Fig. 4A) [34,35,53,54]. In addition, *Str. ratti* and *Str. stercoralis* display rel-

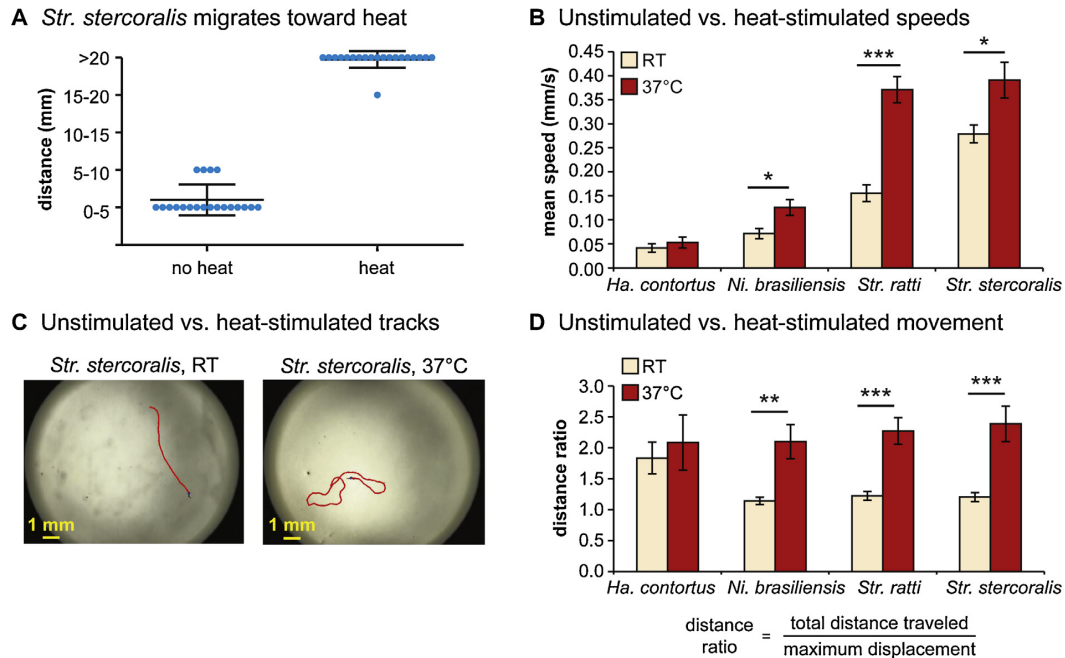


Fig. 4. Skin-penetrating nematodes respond to thermosensory cues. **A.** *Str. stercoralis* IJs migrate toward heat. In the absence of a thermal gradient, *Str. stercoralis* IJs do not migrate far from their placement point (“no heat” condition). When the IJs are placed at 26 °C in a thermal gradient ranging from 22 °C to 43 °C, they migrate toward the heated end (“heat” condition). Blue dots = migration distances of individual IJs from their initial placement point during a 1 min assay; center bars = mean migration distances; upper and lower bars = standard deviations. Dot-plot data are reproduced from Lopez et al. (2000) [54] with permission. **B.** Unstimulated vs. heat-stimulated speeds of mammalian-parasitic IJs. IJs of skin-penetrating nematode species exposed to an acute 37 °C stimulus increase their crawling speeds. **C.** Representative tracks of *Str. stercoralis* from 20 s recordings at room temperature versus 37 °C. **D.** Movement patterns at room temperature versus 37 °C. Distance ratios were calculated according to the formula shown; a greater distance ratio indicates a more curved trajectory. Skin-penetrating nematodes exposed to an acute 37 °C stimulus show curved crawling trajectories, indicative of local-search behavior. For B–D, data are from Castelletto et al. (2014) [26].

actively straight crawling trajectories at room temperature but increased crawling speeds and highly curved trajectories at 37 °C (Fig. 4B–D) [26]. This observation suggests that heat stimulates local search and thereby increases the likelihood of host attachment. In contrast, *Ha. contortus* does not migrate to a heat source and does not increase its crawling speed in response to heat (Fig. 4B) [26,55]. *Ha. contortus* instead migrates to its cultivation temperature, a behavioral strategy resembling that of *C. elegans* [55]. Thus, passively ingested IJs may not use heat as a host-seeking cue. However, more quantitative studies will be necessary to better understand how mammalian-parasitic nematodes move within temperature gradients.

2.7. Responses of mammalian-parasitic nematodes to other sensory cues

Mammalian-parasitic nematodes respond to a number of additional sensory cues that may contribute to host seeking or promote host contact in the environment. *An. caninum*, *An. duodenale*, and *Ne. americanus* IJs respond to vibration and humidity changes by actively crawling [30,34,35]. *An. duodenale* and *Ne. americanus* IJs are also activated by light, but only *Ne. americanus* migrates toward light [30,35]. Mechanical stimulation increases crawling speed in *Str. ratti* IJs [26]. How these responses to vibration, humidity, light, and mechanical stimulation contribute to host-seeking behaviors for skin-penetrating nematodes remains to be elucidated. Finally, *Ha. contortus* IJs exhibit migration toward light (phototaxis) and moisture (hygrotaxis) [39,40]. Phototaxis may allow *Ha. contortus* IJs to move vertically on herbage during the day when grazing

animals are more active. Hygrotaxis may serve as a protection mechanism, allowing IJs to migrate down herbage and into the relatively damp soil when surface conditions are unfavorable.

3. Host seeking by plant-parasitic nematodes

Some plant-parasitic nematodes (PPNs) also engage in host seeking, although their host-seeking behaviors remain poorly understood. For example, PPNs such as the potato cyst nematode *Globodera pallida* and root-knot nematodes in the genus *Meloidogyne* are attracted to plant roots [56–58]. Ethylene signaling in the plant modulates root attractiveness to PPNs, although whether ethylene signaling directly regulates the production of specific PPN attractants has not yet been determined [59]. *Meloidogyne* species are attracted to low pH, consistent with the fact that growing roots create a low pH environment [58]. CO₂ attracts a number of PPN species, including *Meloidogyne incognita* and *Rotylenchulus reniformis* [13,60]. However, at least in the case of *Meloidogyne* species, the observed attraction to CO₂ may be primarily a response to low pH rather than molecular CO₂ [58]. PPNs are also attracted to some of the same root volatiles emitted by insect-damaged plants that attract EPNs [61]. Thus, the emission of specific volatiles by plants in response to insect damage comes at a potential ecological cost.

4. The neural basis of host-seeking behavior

The neural basis of host-seeking behavior in parasitic nematodes is poorly understood, due to the technical difficulty of working with these organisms and a disconnect between the fields of par-

asitology and neurobiology. However, the neural basis of sensory behavior is well-studied in the model free-living nematode *C. elegans*, and neural anatomy and function are often conserved across free-living and parasitic nematode species [48,62,63]. In addition, *C. elegans* has a developmentally arrested, long-lived alternative life stage called the dauer larva, which is developmentally analogous to the IJ stage of parasitic nematodes [64]. *C. elegans* dauers form when environmental conditions are unfavorable and engage in phoresy, using insects and other invertebrates for transport to more favorable environmental niches [65,66]. A number of dauer behaviors, including nictation, are shared with parasitic IJs [66]. Thus, knowledge of the neural basis of behavior in *C. elegans*, particularly dauer behavior, can be leveraged to better understand the neural basis of host seeking in parasitic nematodes.

4.1. The neural basis of sensory behaviors in *C. elegans*

C. elegans responds robustly to sensory stimuli, including a wide variety of volatile compounds [67,68]; water-soluble compounds such as cations, anions, nucleotides, and amino acids [68]; pheromones [69]; the gases O₂ and CO₂ [70]; and temperature [71]. The responses to most chemicals and temperature are mediated primarily by head sensory neurons that extend processes toward the tip of the anterior of the worm [68]. Odorants and pheromones are detected by large families of seven-transmembrane domain G protein-coupled receptors (GPCRs) [68,72], while the gustatory response requires receptor guanylate cyclases (rGCs) [73]. CO₂ detection is mediated in part by the rGC GCY-9 [74–76]; however, GCY-9-independent mechanisms of CO₂ detection appear to operate in some sensory neurons but have not yet been characterized [77,78]. O₂ detection is mediated by soluble guanylate cyclases and globins [79–81]. Thermosensation involves rGCs and TRP channels [82].

Dauer-specific nictation behavior in *C. elegans* is mediated by a set of six cholinergic sensory neurons in the head called IL2 neurons [66]. The processes of the IL2 neurons undergo extensive remodeling during dauer development, and the furan homolog *kpc-1* is required for both dauer-specific IL2 remodeling and nictation behavior [83]. Whether IL2 neurons and/or a *kpc-1* homolog are required for host seeking by parasitic nematodes has not yet been investigated.

4.2. The neural basis of chemosensation in parasitic nematodes

A number of sensory neurons that contribute to host seeking have been identified in parasitic nematodes based on analogy with *C. elegans* neurons (Fig. 5A). For example, CO₂ chemotaxis in *C. elegans* was shown to require a pair of head sensory neurons called the BAG neurons, which directly sense molecular CO₂ [75,76,84,85]. Subsequently, BAG neurons were shown to mediate CO₂ chemotaxis in the EPNs *Ste. carpocapsae* and *He. bacteriophora*, and CO₂-evoked jumping in *Ste. carpocapsae* (Fig. 5B) [10]. Thus, the neural basis of CO₂ responsiveness is at least partly conserved across free-living and parasitic nematode species. Similarly, the ASE and ASH neurons mediate responses to gustatory cues in both *C. elegans* and the skin-penetrating human parasite *Str. stercoralis* [44]. The olfactory sensory neurons that mediate responses to host-specific odorants have not yet been identified in parasitic nematodes.

4.3. The neural basis of thermosensation in parasitic nematodes

In *C. elegans*, the primary thermosensory neurons are the AFD neurons, although the AWC and ASI chemosensory neurons are also thermosensory and contribute to thermotaxis [82]. The AFD neurons have a finger-like dendritic structure that results in an

increased surface area in the amphid chemosensory organs, which is thought to be important for temperature sensing [82]. The positional analogs of the AFD neurons in the dog hookworm *Ancylostoma caninum* and the passively ingested ruminant parasite *Ha. contortus* also have a finger-like dendritic structure and are also required for thermotaxis [53,55]. Moreover, the RIA interneurons, which function downstream of AFD to mediate thermosensation in *C. elegans* [82], were also found to be required for thermosensation in *Ha. contortus* [55]. Thus, as is the case for chemosensation, the neural basis of thermosensation is at least partly conserved across free-living and parasitic species.

Temperature sensing in *Str. stercoralis* may be somewhat different because *Str. stercoralis* does not have a pair of neurons with a finger-like dendritic structure [86]. Instead, *Str. stercoralis* has a pair of neurons, called the ALD neurons, with a lamellar dendritic structure that also results in a large surface area in the amphids [86]. Ablation of the ALD neurons in *Str. stercoralis* disrupted thermotaxis, demonstrating that the ALD neurons are required for thermosensory behavior (Fig. 5C) [54]. The anatomical position of the ALD neurons appears to most closely resemble that of the *C. elegans* AWC neurons [54]. However, whether ALD neurons are functionally more analogous to the *C. elegans* AWC or AFD neurons remains unclear.

4.4. Unanswered questions regarding neural circuit function in parasitic nematodes

The studies described above demonstrate that sensory neuron function is often conserved across free-living and parasitic species. However, the extent to which functional conservation across species exists at the interneuron level remains unknown. With the exception of the RIA interneurons mentioned above, interneuron function has not yet been explored in parasitic nematodes. The fact that sensory neuron function is often conserved across species, yet sensory microcircuits support species-specific behaviors, suggests that significant differences in interneuron function exist across species. While the connections between neurons have been almost completely mapped for *C. elegans* [87,88], connectome data is not yet available for parasitic nematodes. Thus, whether positionally analogous interneurons participate in the same microcircuits across species but have different functional properties, or whether positionally analogous interneurons participate in different microcircuits across species, is not yet clear.

The molecular basis of host seeking by parasitic nematodes also remains to be investigated. Some insights into possible molecular mechanisms of host seeking have come from studies of the necromenic nematode *Pristionchus pacificus*, which feeds off beetle cadavers [89]. Closely related *Pristionchus* species show species-specific responses to insect pheromones and plant volatiles [89]. Natural variation in the response to insect pheromone across *P. pacificus* strains is associated with the cGMP-dependent protein kinase gene *egl-4*, suggesting a role for cGMP signaling in the host-seeking behavior of *P. pacificus* [90]. Future studies will be necessary to determine whether cGMP signaling also regulates host seeking in parasitic nematodes.

5. Conclusions and future directions

In summary, parasitic nematodes use multiple sensory modalities to find and infect hosts, including olfaction, gustation, thermosensation, and hygrosensation. Moreover, all parasitic nematode infective larvae that have so far been examined respond robustly to sensory cues, suggesting that parasitic nematodes rely on these to maximize their chances of a successful infection regardless of their host range, host-seeking strategy, or infection route.

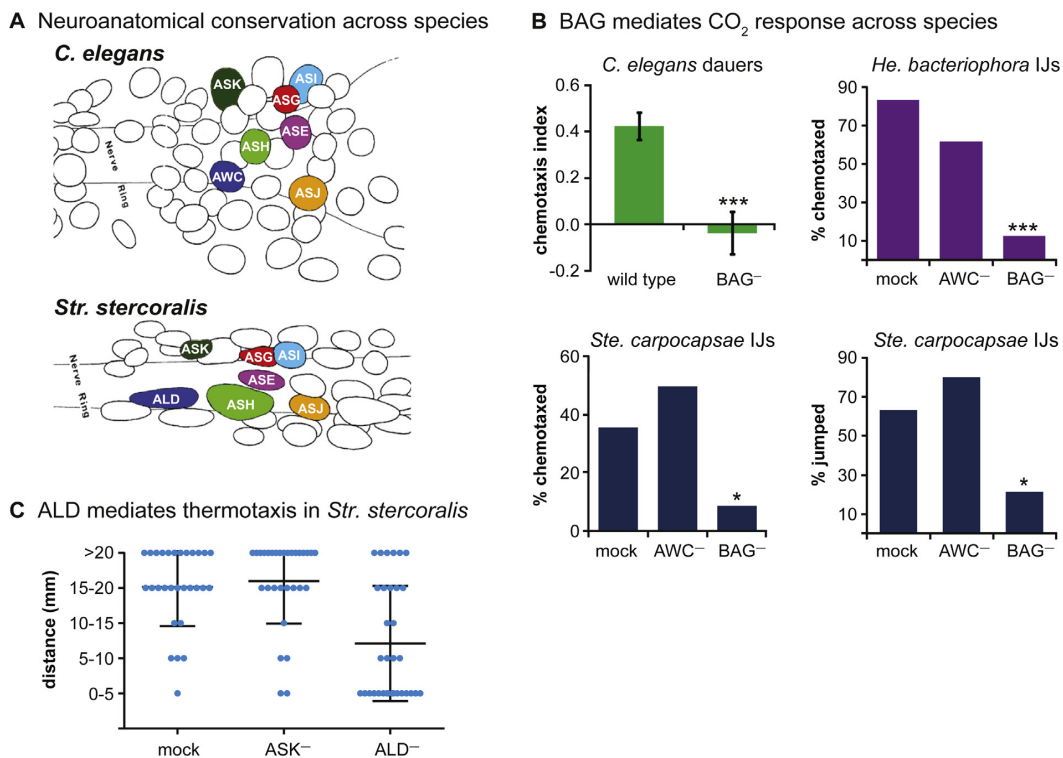


Fig. 5. Sensory neuron function is often conserved across free-living and parasitic nematodes. A. Schematics of neurons in the head regions of *C. elegans* and *Str. stercoralis*. Color-coding indicates a few of the analogous sensory neurons. Schematics are reproduced from Ashton et al. (1995) [86] with permission. B. BAG neurons mediate CO₂ response across species. Wild-type *C. elegans* dauer larvae are attracted to CO₂, but animals containing a genetic ablation of the BAG neurons (BAG⁻) do not chemotax to CO₂. Reproduced from Hallem et al. (2011) [10]. Wild-type *He. bacteriophora* and *Ste. carpocapsae* IJs, and IJs in which the AWC chemosensory neurons have been laser-ablated (AWC⁻), are attracted to CO₂. However, IJs in which the BAG neurons have been laser-ablated (BAG⁻) no longer chemotax to CO₂. BAG ablation also eliminates CO₂-evoked jumping by *Ste. carpocapsae* IJs (lower right graph). Reproduced from Hallem et al. (2011) [10]. C. ALD neurons mediate thermotaxis in *Str. stercoralis*. Wild-type *Str. stercoralis* IJs, and IJs in which the ASK chemosensory neurons have been laser-ablated (ASK⁻), migrate toward heat when placed at 26 °C in a thermal gradient ranging from 22 °C to 43 °C. However, IJs in which the ALD neurons have been laser-ablated (ALD⁻) do not migrate toward heat. Blue dots = migration distances of individual IJs from their initial placement point during a 1 min assay; center bars = mean migration distances; upper and lower bars = standard deviations. Dot-plot data are reproduced from Lopez et al. (2000) [54] with permission.

Although we are still at the early stages of understanding the neural basis of host seeking, a more detailed understanding of the molecular and cellular basis of this crucial behavior is likely to emerge over the next few years. Mechanistic studies of neural circuit function in parasitic nematodes are now feasible due to the large-scale sequencing of parasitic nematode genomes [91] and the development of new methods for genetic transformation of parasitic worms [92]. In addition, targeted gene disruption has recently been achieved in multiple free-living nematodes using the CRISPR-Cas9 system [93–95], and this system is likely to be applicable to parasitic nematodes. These exciting developments pave the way for in-depth molecular, cellular, and circuit-level analyses of the host-seeking behaviors of parasitic nematodes. A better understanding of neural circuit function in parasitic nematodes will provide important insights into how parasites target their hosts, and more generally, how the nervous systems of parasites have evolved to mediate parasitic behaviors such as host seeking and host invasion. In addition, a more mechanistic understanding of host seeking may enable the development of new strategies for preventing harmful nematode infections of animals and plants, and for enhancing the efficacy of beneficial nematodes as biocontrol agents.

Acknowledgments

We thank Taylor Brown, Michelle Castelletto, and Joon Ha Lee for insightful comments on the manuscript. This work was funded by the Whitcome Predoctoral Training Program, UCLA Molecular Biology Institute; Ruth L. Kirschstein National Research Service Award AI007323; and a National Science Foundation East Asia and Pacific Summer Institute Fellowship (Award #1414655) to S.S.G.; and a MacArthur Fellowship, McKnight Scholar Award, Searle Scholar Award, Rita Allen Foundation Fellowship, and NIH New Innovator Award (1DP2DC014596) to E.A.H.

References

- [1] D.P. Jasmer, A. Goverse, G. Smant, Parasitic nematode interactions with mammals and plants, *Annu. Rev. Phytopathol.* 41 (2003) 245–270.
- [2] W.M. Hominick, Biogeography, in: R. Gaugler (Ed.), *Entomopathogenic Nematology*, CABI Publishing, New York, 2002, pp. 115–143.
- [3] K.B. Nguyen, D.J. Hunt, Z. Mracek, Steinernematidae: species descriptions, in: K.B. Nguyen, D.J. Hunt (Eds.), *Entomopathogenic Nematodes: Systematics, Phylogeny, and Bacterial Symbionts*, Nematology Monographs and Perspectives, Brill, Leiden, 2007, pp. 121–609.
- [4] J.G. Ali, H.T. Alborn, L.L. Stelinski, Subterranean herbivore-induced volatiles released by citrus roots upon feeding by *Diaprepes abbreviatus* recruit entomopathogenic nematodes, *J. Chem. Ecol.* 36 (2010) 361–368.

- [5] B.C.A. Dowds, A. Peters, Virulence mechanisms, in: R. Gaugler (Ed.), Entomopathogenic Nematology, CAB International, New York, 2002, pp. 79–98.
- [6] E.E. Lewis, Behavioral ecology, in: R. Gaugler (Ed.), Entomopathogenic Nematology, CAB International, New York, 2002, pp. 205–223.
- [7] H.K. Bal, P.S. Grewal, Lateral dispersal and foraging behavior of entomopathogenic nematodes in the absence and presence of mobile and non-mobile hosts, *PLoS One* 10 (2015) e0129887.
- [8] M.J. Wilson, R.-U. Ehlers, I. Glazer, Entomopathogenic nematode foraging strategies – is *Steinernema carpocapsae* really an ambush forager? *Nematol* 14 (2012) 389–394.
- [9] V.S. Santhi, L. Salame, Y. Nakache, H. Koltai, V. Soroker, I. Glazer, Attraction of entomopathogenic nematodes *Steinernema carpocapsae* and *Heterorhabditis bacteriophora* to the red palm weevil (*Rhynchophorus ferrugineus*), *Biol. Control* 83 (2015) 75–81.
- [10] E.A. Hallem, A.R. Dillman, A.V. Hong, Y. Zhang, J.M. Yano, S.F. DeMarco, P.W. Sternberg, A sensory code for host seeking in parasitic nematodes, *Curr. Biol.* 21 (2011) 377–383.
- [11] A.R. Dillman, M.L. Guillermin, J.H. Lee, B. Kim, P.W. Sternberg, E.A. Hallem, Olfaction shapes host-parasite interactions in parasitic nematodes, *Proc. Natl. Acad. Sci. U. S. A.* 109 (2012) E2324–2333.
- [12] R. Gaugler, J.F. Campbell, P. Gupta, Characterization and basis of enhanced host-finding in a genetically improved strain of *Steinernema carpocapsae*, *J. Invertebr. Pathol.* 57 (1991) 234–241.
- [13] A.F. Robinson, Optimal release rates for attracting *Meloidogyne incognita*, *Rotylemchulus reniformis*, and other nematodes to carbon dioxide in sand, *J. Nematol.* 27 (1995) 42–50.
- [14] A.M. Koppenhofer, E.M. Fuzy, Attraction of four entomopathogenic nematodes to four white grub species, *J. Invertebr. Pathol.* 99 (2008) 227–234.
- [15] D.M. O'Halloran, A.M. Burnell, An investigation of chemotaxis in the insect parasitic nematode *Heterorhabditis bacteriophora*, *Parasitology* 127 (2003) 375–385.
- [16] J.F. Campbell, H.K. Kaya, Influence of insect-associated cues on the jumping behavior of entomopathogenic nematodes (*Steinernema* spp.), *Behavior* 137 (2000) 591–609.
- [17] J. Schmidt, J.N. All, Attraction of *Neoplectana carpocapsae* (Nematoda: Steinernematidae) to common excretory products of insects, *Environ. Entomol.* 8 (1979) 55–61.
- [18] T.C. Turlings, I. Hiltbold, S. Rasmann, The importance of root-produced volatiles as foraging cues for entomopathogenic nematodes, *Plant Soil* 358 (2012) 51–60.
- [19] S. Rasmann, T.G. Kollner, J. Degenhardt, I. Hiltbold, S. Toepfer, U. Kuhlmann, J. Gershenzon, T.C. Turlings, Recruitment of entomopathogenic nematodes by insect-damaged maize roots, *Nature* 434 (2005) 732–737.
- [20] J.A. Byers, J.O. Poinar, Location of insect hosts by the nematode, *Neoplectana carpocapsae*, in response to temperature, *Behavior* 79 (1982) 1–10.
- [21] A.E. Pye, M. Burman, *Neoplectana carpocapsae*: nematode accumulations on chemical and bacterial gradients, *Exp. Parasitol.* 51 (1981) 13–20.
- [22] T. Ilan, D.B. Kim-Shapiro, C.H. Bock, D.I. Shapiro-Ilan, Magnetic and electric fields induce directional responses in *Steinernema carpocapsae*, *Int. J. Parasitol.* 43 (2013) 781–784.
- [23] D.I. Shapiro-Ilan, J.F. Campbell, E.E. Lewis, J.M. Elkon, D.B. Kim-Shapiro, Directional movement of steinernematid nematodes in response to electrical current, *J. Invertebr. Pathol.* 100 (2009) 134–137.
- [24] D.I. Shapiro-Ilan, E.E. Lewis, J.F. Campbell, D.B. Kim-Shapiro, Directional movement of entomopathogenic nematodes in response to electrical field: effects of species, magnitude of voltage, and infective juvenile age, *J. Invertebr. Pathol.* 109 (2012) 34–40.
- [25] P. Torr, S. Heritage, M.J. Wilson, Vibrations as a novel signal for host location by parasitic nematodes, *Int. J. Parasitol.* 34 (2004) 997–999.
- [26] M.L. Castelletto, S.S. Gang, R.P. Okubo, A.A. Tselikova, T.J. Nolan, E.G. Platzer, J.B. Lok, E.A. Hallem, Diverse host-seeking behaviors of skin-penetrating nematodes, *PLoS Pathog.* 10 (2014) e1004305.
- [27] S. Lustigman, R.K. Prichard, A. Gazzinelli, W.N. Grant, B.A. Boatman, J.S. McCarthy, M.G. Basanez, A research agenda for helminth diseases of humans: the problem of helminthiasis, *PLoS Negl. Trop. Dis.* 6 (2012) e1582.
- [28] M.E. Viney, J.B. Lok, The biology of *Strongyloides* spp., In: *WormBook*, www.wormbook.org, 2015.
- [29] M.V. Periago, J.M. Bethony, Hookworm virulence factors: making the most of the host, *Microbes Infect.* 14 (2012) 1451–1464.
- [30] W. Haas, B. Haberl, S.I. Idris, S. Kersten, Infective larvae of the human hookworms *Necator americanus* and *Ancylostoma duodenale* differ in their orientation behaviour when crawling on surfaces, *Parasitol. Res.* 95 (2005) 25–29.
- [31] C. Dold, C.V. Holland, *Ascaris* and ascariasis, *Microbes Infect.* 13 (2011) 632–637.
- [32] L.J. O'Connor, S.W. Walkden-Brown, L.P. Kahn, Ecology of the free-living stages of major trichostrongylid parasites of sheep, *Vet. Parasitol.* 142 (2006) 1–15.
- [33] R. Laing, T. Kikuchi, A. Martinelli, I.J. Tsai, R.N. Beech, E. Redman, N. Holroyd, D.J. Bartley, H. Beasley, C. Britton, D. Curran, E. Devaney, A. Gilabert, M. Hunt, F. Jackson, S.L. Johnston, I. Kryukov, K. Li, A.A. Morrison, A.J. Reid, N. Sargison, G.I. Saunders, J.D. Wasmuth, A. Wolstenholme, M. Berriman, J.S. Gilleard, J.A. Cotton, The genome and transcriptome of *Haemonchus contortus*, a key model parasite for drug and vaccine discovery, *Genome Biol.* 14 (2013) R88.
- [34] M. Granzer, W. Hass, Host-finding and host recognition of infective *Ancylostoma caninum* larvae, *Int. J. Parasitol.* 21 (1991) 429–440.
- [35] W. Haas, B. Haberl, S.I. Idris, D. Kallert, S. Kersten, P. Stiegeler, Behavioural strategies used by the hookworms *Necator americanus* and *Ancylostoma duodenale* to find, recognize and invade the human host, *Parasitol. Res.* 95 (2005) 30–39.
- [36] J. Sciacca, W.M. Forbes, F.T. Ashton, E. Lombardini, H.R. Gamble, G.A. Schad, Response to carbon dioxide by the infective larvae of three species of parasitic nematodes, *Parasitol. Int.* 51 (2002) 53–62.
- [37] J.D. Pleil, A.B. Lindstrom, Measurement of volatile organic compounds in exhaled breath as collected in evacuated electropolished canisters, *J. Chromatogr. B: Biomed. Appl.* 665 (1995) 271–279.
- [38] I. Alkalay, S. Suetsugu, H. Constantine, M. Stein, Carbon dioxide elimination across human skin, *Am. J. Physiol.* 220 (1971) 1434–1436.
- [39] G. Rees, Observations on the vertical migrations of the third-stage larva of *Haemonchus contortus* (Rud.) on experimental plots of *Lolium perenne* S24, in relation to meteorological and micrometeorological factors, *Parasitology* 40 (1950) 127–143.
- [40] A.P. Callinan, J.M. Westcott, Vertical distribution of trichostrongylid larvae on herbage and in soil, *Int. J. Parasitol.* 16 (1986) 241–244.
- [41] M. Koga, S. Nuamtanong, P. Dekumyoy, T. Yoonuan, W. Maipanich, W. Rojkitikhun, J. Waikagul, Host-finding behavior of *Strongyloides stercoralis* infective larvae to sodium cation, human serum, and sweat, *Southeast Asian J. Trop. Med. Public Health* 36 (2005) 93–98.
- [42] D. Safer, M. Brenes, S. Dunipace, G. Schad, Urocanic acid is a major chemoattractant for the skin-penetrating parasitic nematode *Strongyloides stercoralis*, *Proc. Natl. Acad. Sci. U. S. A.* 104 (2007) 1627–1630.
- [43] M. Koga, I. Tada, *Strongyloides ratti*: chemotactic responses of third-stage larvae to selected serum proteins and albumins, *J. Helminthol.* 74 (2000) 247–252.
- [44] W.M. Forbes, F.T. Ashton, R. Boston, X. Zhu, G.A. Schad, Chemoattraction and chemorepulsion of *Strongyloides stercoralis* infective larvae on a sodium chloride gradient is mediated by amphidial neuron pairs ASE and ASH, respectively, *Vet. Parasitol.* 120 (2004) 189–198.
- [45] H. Tobata-Kudo, H. Higo, M. Koga, I. Tada, Chemokinetic behavior of the infective third-stage larvae of *Strongyloides ratti* on a sodium chloride gradient, *Parasitol. Int.* 49 (2000) 183–188.
- [46] M. Gallagher, C.J. Wysocki, J.J. Leyden, A.I. Spielman, X. Sun, G. Preti, Analyses of volatile organic compounds from human skin, *Br. J. Dermatol.* 159 (2008) 780–791.
- [47] A. Cork, K.C. Park, Identification of electrophysiologically-active compounds for the malaria mosquito, *Anopheles gambiae*, in human sweat extracts, *Med. Vet. Entomol.* 10 (1996) 269–276.
- [48] K.E. Chaisson, E.A. Hallem, Chemosensory behaviors of parasites, *Trends Parasitol.* 28 (2012) 427–436.
- [49] Y.T. Qiu, R.C. Smallegange, J.J. van Loon, W. Takken, Behavioural responses of *Anopheles gambiae sensu stricto* to components of human breath, sweat and urine depend on mixture composition and concentration, *Med. Vet. Entomol.* 25 (2011) 247–255.
- [50] C.S. McBride, F. Baier, A.B. Omond, S.A. Spitzer, J. Lutomiah, R. Sang, R. Ignell, L.B. Vosshall, Evolution of mosquito preference for humans linked to an odorant receptor, *Nature* 515 (2014) 222–227.
- [51] H. Funes, E. Zerba, P. Gonzalez-Audino, Effect of release rate and enantiomeric composition on response to pheromones of *Megaplatus mutatus* (Chapuis) in poplar plantations of Argentina and Italy, *Bull. Entomol. Res.* 103 (2013) 564–569.
- [52] E. Siljander, R. Gries, G. Khaskin, G. Gries, Identification of the airborne aggregation pheromone of the common bed bug, *Cimex lectularius*, *J. Chem. Ecol.* 34 (2008) 708–718.
- [53] V.M. Bhopale, E.K. Kupprion, F.T. Ashton, R. Boston, G.A. Schad, *Ancylostoma caninum*: the finger cell neurons mediate thermotactic behavior by infective larvae of the dog hookworm, *Exp. Parasitol.* 97 (2001) 70–76.
- [54] P.M. Lopez, R. Boston, F.T. Ashton, G.A. Schad, The neurons of class ALD mediate thermotaxis in the parasitic nematode, *Strongyloides stercoralis*, *Int. J. Parasitol.* 30 (2000) 1115–1121.
- [55] J. Li, X. Zhu, R. Boston, F.T. Ashton, H.R. Gamble, G.A. Schad, Thermotaxis and thermosensory neurons in infective larvae of *Haemonchus contortus*, a passively ingested nematode parasite, *J. Comp. Neurol.* 424 (2000) 58–73.
- [56] S. Rasmann, J.G. Ali, J. Helder, W.H. van der Putten, Ecology and evolution of soil nematode chemotaxis, *J. Chem. Ecol.* 38 (2012) 615–628.
- [57] K. Farnier, M. Bengtsson, P.G. Becher, J. Witzell, P. Witzgall, S. Manduric, Novel bioassay demonstrates attraction of the white potato cyst nematode *Globodera pallida* (Stone) to non-volatile and volatile host plant cues, *J. Chem. Ecol.* 38 (2012) 795–801.
- [58] C. Wang, G. Bruening, V.M. Williamson, Determination of preferred pH for root-knot nematode aggregation using pluronic F-127 gel, *J. Chem. Ecol.* 35 (2009) 1242–1251.
- [59] S.L. Fudali, C. Wang, V.M. Williamson, Ethylene signaling pathway modulates attractiveness of host roots to the root-knot nematode *Meloidogyne hapla*, *Mol. Plant Microbe Interact.* 26 (2013) 75–86.
- [60] M. Pline, D.B. Dusenbery, Responses of plant-parasitic nematode *Meloidogyne incognita* to carbon dioxide determined by video camera computer tracking, *J. Chem. Ecol.* 13 (1987) 873–888.
- [61] J.G. Ali, H.T. Alborn, L.L. Stelinski, Constitutive and induced subterranean plant volatiles attract both entomopathogenic and plant parasitic nematodes, *J. Ecol.* 99 (2011) 26–35.
- [62] F.T. Ashton, J. Li, G.A. Schad, Chemo- and thermosensory neurons: structure and function in animal parasitic nematodes, *Vet. Parasitol.* 84 (1999) 297–316.

- [63] F.T. Ashton, G.A. Schad, Amphids in *Strongyloides stercoralis* and other parasitic nematodes, *Parasitol. Today* 12 (1996) 187–194.
- [64] M. Crook, The dauer hypothesis and the evolution of parasitism: 20 years on and still going strong, *Int. J. Parasitol.* 44 (2014) 1–8.
- [65] L. Frezal, M.A. Felix, *C. elegans* outside the Petri dish, *Elife* 4 (2015) e05849.
- [66] H. Lee, M.K. Choi, D. Lee, H.S. Kim, H. Hwang, H. Kim, S. Park, Y.K. Paik, J. Lee, Nictation, a dispersal behavior of the nematode *Caenorhabditis elegans*, is regulated by IL2 neurons, *Nat. Neurosci.* 15 (2012) 107–112.
- [67] A.C. Hart, M.Y. Chao, From odors to behaviors in *Caenorhabditis elegans*, in: A. Menini (Ed.), *The Neurobiology of Olfaction*, CRC Press, Boca Raton, FL, 2010.
- [68] C.I. Bargmann, Chemosensation in *C. elegans*, In: *WormBook*, www.wormbook.org, 2006.
- [69] A.H. Ludewig, F.C. Schroeder, Ascaroside signaling in *C. elegans*, In: *WormBook*, www.wormbook.org 2013.
- [70] M.A. Carrillo, E.A. Hallem, Gas sensing in nematodes, *Mol. Neurobiol.* 51 (2015) 919–931.
- [71] M.B. Goodman, M. Klein, S. Lasse, L. Luo, I. Mori, A. Samuel, P. Sengupta, D. Wang, Thermotaxis navigation behavior, In: *WormBook*, www.wormbook.org, 2014.
- [72] C. Braendle, Pheromones: evolving language of chemical communication in nematodes, *Curr. Biol.* 22 (2012) R294–296.
- [73] C.O. Ortiz, S. Faumont, J. Takayama, H.K. Ahmed, A.D. Goldsmith, R. Pocock, K.E. McCormick, H. Kunimoto, Y. Iino, S. Lockery, O. Hobert, Lateralized gustatory behavior of *C. elegans* is controlled by specific receptor-type guanylyl cyclases, *Curr. Biol.* 19 (2009) 996–1004.
- [74] J.P. Brandt, S. Aziz-Zaman, V. Juozaityte, L.A. Martinez-Velazquez, J.G. Petersen, R. Pocock, N. Ringstad, A single gene target of an ETS-family transcription factor determines neuronal CO₂-chemosensitivity, *PLoS One* 7 (2012) e34014.
- [75] E.A. Hallem, W.C. Spencer, R.D. McWhirter, G. Zeller, S.R. Henz, G. Ratsch, D.M. Miller, H.R. Horvitz, P.W. Sternberg, N. Ringstad, Receptor-type guanylate cyclase is required for carbon dioxide sensation by *Caenorhabditis elegans*, *Proc. Natl. Acad. Sci. U. S. A.* 108 (2011) 254–259.
- [76] E.S. Smith, L. Martinez-Velazquez, N. Ringstad, A chemoreceptor that detects molecular carbon dioxide, *J. Biol. Chem.* 288 (2013) 37071–37081.
- [77] L.A. Fenk, M. de Bono, Environmental CO₂ inhibits *Caenorhabditis elegans* egg-laying by modulating olfactory neurons and evokes widespread changes in neural activity, *Proc. Natl. Acad. Sci. U. S. A.* 112 (2015) E3525–3534.
- [78] A.J. Bretscher, E. Kodama-Namba, K.E. Busch, R.J. Murphy, Z. Soltesz, P. Laurent, M. de Bono, Temperature, oxygen, and salt-sensing neurons in *C. elegans* are carbon dioxide sensors that control avoidance behavior, *Neuron* 69 (2011) 1099–1113.
- [79] J.M. Gray, D.S. Karow, H. Lu, A.J. Chang, J.S. Chang, R.E. Ellis, M.A. Marletta, C.I. Bargmann, Oxygen sensation and social feeding mediated by a *C. elegans* guanylate cyclase homologue, *Nature* 430 (2004) 317–322.
- [80] A. Persson, E. Gross, P. Laurent, K.E. Busch, H. Bretes, M. de Bono, Natural variation in a neural globin tunes oxygen sensing in wild *Caenorhabditis elegans*, *Nature* 458 (2009) 1030–1033.
- [81] P.T. McGrath, M.V. Rockman, M. Zimmer, H. Jang, E.Z. Macosko, L. Kruglyak, C.I. Bargmann, Quantitative mapping of a digenic behavioral trait implicates globin variation in *C. elegans* sensory behaviors, *Neuron* 61 (2009) 692–699.
- [82] I. Aoki, I. Mori, Molecular biology of thermosensory transduction in *C. elegans*, *Curr. Opin. Neurobiol.* 34 (2015) 117–124.
- [83] N.E. Schroeder, R.J. Androwski, A. Rashid, H. Lee, J. Lee, M.M. Barr, Dauer-specific dendrite arborization in *C. elegans* is regulated by KPC-1/Furin, *Curr. Biol.* 23 (2013) 1527–1535.
- [84] E.A. Hallem, P.W. Sternberg, Acute carbon dioxide avoidance in *Caenorhabditis elegans*, *Proc. Natl. Acad. Sci. U. S. A.* 105 (2008) 8038–8043.
- [85] M.A. Carrillo, M.L. Guillemin, S. Rengarajan, R. Okubo, E.A. Hallem, O₂-sensing neurons control CO₂ response in *C. elegans*, *J. Neurosci.* 33 (2013) 9675–9683.
- [86] F.T. Ashton, V.M. Bhopale, A.E. Fine, G.A. Schad, Sensory neuroanatomy of a skin-penetrating nematode parasite: *Strongyloides stercoralis*. I. Amphidial neurons, *J. Comp. Neurol.* 357 (1995) 281–295.
- [87] J.G. White, E. Southgate, J.N. Thomson, S. Brenner, The structure of the nervous system of the nematode *Caenorhabditis elegans*, *Philos. Trans. R. Soc. Lond. B* 314 (1986) 1–340.
- [88] L.R. Varshney, B.L. Chen, E. Paniagua, D.H. Hall, D.B. Chklovskii, Structural properties of the *Caenorhabditis elegans* neuronal network, *PLoS Comput. Biol.* 7 (2011) e1001066.
- [89] R.L. Hong, R.J. Sommer, Chemoattraction in *Pristionchus* nematodes and implications for insect recognition, *Curr. Biol.* 16 (2006) 2359–2365.
- [90] R.L. Hong, H. Witte, R.J. Sommer, Natural variation in *Pristionchus pacificus* insect pheromone attraction involves the protein kinase EGL-4, *Proc. Natl. Acad. Sci. U. S. A.* 105 (2008) 7779–7784.
- [91] A.R. Dillman, A. Mortazavi, P.W. Sternberg, Incorporating genomics into the toolkit of nematology, *J. Nematol.* 44 (2012) 191–205.
- [92] J. Lok, piggyBac: a vehicle for integrative DNA transformation of parasitic nematodes, *Mob. Genet. Elements* 3 (2013) e24417.
- [93] H. Witte, E. Moreno, C. Rödelsperger, J. Kim, J.S. Kim, A. Streit, R.J. Sommer, Gene inactivation using the CRISPR/Cas9 system in the nematode *Pristionchus pacificus*, *Dev. Genes Evol.* 225 (2015) 55–62.
- [94] T.W. Lo, C.S. Pickle, S. Lin, E.J. Ralston, M. Gurling, C.M. Schartner, Q. Bian, J.A. Doudna, B.J. Meyer, Precise and heritable genome editing in evolutionarily diverse nematodes using TALENs and CRISPR/Cas9 to engineer insertions and deletions, *Genetics* 195 (2013) 331–348.
- [95] A.E. Friedland, Y.B. Tzur, K.M. Esvelt, M.P. Colaiacovo, G.M. Church, J.A. Calarco, Heritable genome editing in *C. elegans* via a CRISPR-Cas9 system, *Nat. Methods* 10 (2013) 741–743.
- [96] A.R. Dillman, P.W. Sternberg, Entomopathogenic nematodes, *Curr. Biol.* 22 (2012) R430–R431.
- [97] J.S. Gilleard, *Haemonchus contortus* as a paradigm and model to study anthelmintic drug resistance, *Parasitology* 140 (2013) 1506–1522.
- [98] J.B. Lok, *Strongyloides stercoralis*: a model for translational research on parasitic nematode biology, In: *WormBook*, www.wormbook.org, 2007.
- [99] P.J. Hotez, S. Brooker, J.M. Bethony, M.E. Bottazzi, A. Loukas, S. Xiao, Hookworm infection, *N. Engl. J. Med.* 351 (2004) 799–807.

Chapter 2

Diverse host-seeking behaviors of skin-penetrating nematodes

Diverse Host-Seeking Behaviors of Skin-Penetrating Nematodes

Michelle L. Castelletto¹, Spencer S. Gang¹, Ryo P. Okubo¹, Anastassia A. Tselikova¹, Thomas J. Nolan², Edward G. Platzer³, James B. Lok², Elissa A. Hallem^{1*}

¹ Department of Microbiology, Immunology, and Molecular Genetics, University of California, Los Angeles, Los Angeles, California, United States of America, ² Department of Pathobiology, University of Pennsylvania, Philadelphia, Pennsylvania, United States of America, ³ Department of Nematology, University of California, Riverside, Riverside, California, United States of America

Abstract

Skin-penetrating parasitic nematodes infect approximately one billion people worldwide and are responsible for some of the most common neglected tropical diseases. The infective larvae of skin-penetrating nematodes are thought to search for hosts using sensory cues, yet their host-seeking behavior is poorly understood. We conducted an in-depth analysis of host seeking in the skin-penetrating human parasite *Strongyloides stercoralis*, and compared its behavior to that of other parasitic nematodes. We found that *Str. stercoralis* is highly mobile relative to other parasitic nematodes and uses a cruising strategy for finding hosts. *Str. stercoralis* shows robust attraction to a diverse array of human skin and sweat odorants, most of which are known mosquito attractants. Olfactory preferences of *Str. stercoralis* vary across life stages, suggesting a mechanism by which host seeking is limited to infective larvae. A comparison of odor-driven behavior in *Str. stercoralis* and six other nematode species revealed that parasite olfactory preferences reflect host specificity rather than phylogeny, suggesting an important role for olfaction in host selection. Our results may enable the development of new strategies for combating harmful nematode infections.

Citation: Castelletto ML, Gang SS, Okubo RP, Tselikova AA, Nolan TJ, et al. (2014) Diverse Host-Seeking Behaviors of Skin-Penetrating Nematodes. PLoS Pathog 10(8): e1004305. doi:10.1371/journal.ppat.1004305

Editor: Simon A. Babayan, University of Glasgow, United Kingdom

Received: February 6, 2014; **Accepted:** June 30, 2014; **Published:** August 14, 2014

Copyright: © 2014 Castelletto et al. This is an open-access article distributed under the terms of the Creative Commons Attribution License, which permits unrestricted use, distribution, and reproduction in any medium, provided the original author and source are credited.

Funding: This work was supported by a Sloan Research Fellowship, a Searle Scholar Award, and a Rita Allen Foundation Fellowship to EAH. The funders had no role in study design, data collection and analysis, decision to publish, or preparation of the manuscript.

Competing Interests: The authors have declared that no competing interests exist.

* Email: ehallem@microbio.ucla.edu

Introduction

Skin-penetrating nematodes such as the threadworm *Str. stercoralis* and the hookworms *Ancylostoma duodenale* and *Necator americanus* (Figure 1A) are intestinal parasites that infect approximately 1 billion people worldwide. Infection with skin-penetrating worms can cause chronic gastrointestinal distress as well as stunted growth and long-term cognitive impairment in children. Moreover, *Str. stercoralis* infection can be fatal for immunocompromised individuals and infants [1]. *Str. stercoralis* is endemic in tropical and sub-tropical regions throughout the world, including the United States, and is estimated to infect 30–100 million people worldwide [2]. Infection rates in rural and semi-rural areas are often high, particularly among children. For example, a recent study found that 25% of school children in semi-rural Cambodia were infected with *Str. stercoralis* [3]. A better understanding of how skin-penetrating worms target human hosts could lead to new strategies for preventing infections.

Skin-penetrating nematodes are infective only during a particular stage of their life cycle called the infective juvenile (IJ), a developmentally arrested third larval stage analogous to the *C. elegans* dauer [4]. IJs inhabit the soil and infect by skin penetration, often through the skin between the toes. Inside the host, IJs migrate through the circulatory system to the lungs, are coughed up and swallowed, and develop to adulthood in the

intestine [1]. IJs may also reach the intestine using other migratory routes [5]. Adult nematodes reproduce in the intestine, and eggs or young larvae are excreted in feces. In the case of hookworms, young larvae develop into IJs, which find and infect new hosts (Figure 1B). In the case of *Strongyloides* species, some larvae develop into IJs and others develop into free-living adults. In the human parasite *Str. stercoralis* and the rat parasite *Str. ratti*, which are subjects of this study, all progeny of free-living adults develop into IJs (Figure 1C). Some species of *Strongyloides*, such as the dog and cat parasite *Str. planiceps*, can undergo a limited number of sequential free-living generations [6]. Thus, *Strongyloides* can develop through at least one free-living generation outside the host. *Str. stercoralis* can also cycle through multiple parasitic generations in the same host, resulting in a potentially fatal disseminated infection [1].

Little is known about the process by which skin-penetrating nematodes find hosts [7]. IJs of some skin-penetrating species respond to heat and sodium chloride [8–12], suggesting a role for thermosensation and gustation in host seeking. In addition, *Str. stercoralis* is attracted to human blood serum and sweat [10,12], while *Str. ratti* is attracted to mammalian blood serum [13]. It has long been speculated that olfaction may be important for host seeking, since animals emit unique odor blends that could confer species-specificity [7]. However, the only specific odorant that has so far been found to elicit a response from a skin-penetrating

Author Summary

Parasitic worms are a significant public health problem. Skin-penetrating worms such as hookworms and the human threadworm *Strongyloides stercoralis* dwell in the soil before infecting their host. However, how they locate and identify appropriate hosts is not understood. Here we investigated the host-seeking behavior of *Str. stercoralis*. We found that *Str. stercoralis* moves quickly and actively searches for hosts to infect. We also found that *Str. stercoralis* is attracted to human skin and sweat odorants, including many that also attract mosquitoes. We then compared olfactory behavior across parasitic worm species and found that parasites with similar hosts respond similarly to odorants even when they are not closely related, suggesting parasitic worms use olfactory cues to select hosts. A better understanding of host seeking in skin-penetrating worms may lead to novel control strategies.

nematode is urocanic acid, a component of mammalian skin that attracts *Str. stercoralis* [14]. Thus, the extent to which skin-penetrating nematodes use olfactory cues to locate hosts is unclear.

Here we examined the host-seeking strategies and sensory behaviors of the human parasite *Str. stercoralis* as well as two other species of skin-penetrating nematodes, the rat parasites *Str. ratti* and *Nippostrongylus brasiliensis* (Figure 1A, D). We compared their behaviors to those of five other nematode species with diverse lifestyles and ecological niches: the passively ingested ruminant-parasitic nematode *Haemonchus contortus*; the entomopathogenic nematodes (EPNs) *Heterorhabditis bacteriophora*, *Steinernema glaseri*, and *Steinernema carpocapsae*; and the free-living nematode *Caenorhabditis elegans* (Figures 1A, D). This across-species analysis was used to fit the behaviors of skin-penetrating nematodes into an ecological framework, and to identify species-specific behavioral differences that reflect differences in phylogeny, host range, or infection route. We found that different species of mammalian-parasitic nematodes employ diverse host-seeking strategies, with the human parasite *Str. stercoralis* being a cruiser that actively seeks out hosts. We found that *Str. stercoralis* and the other skin-penetrating nematodes are attracted to skin and sweat odorants, while the passively ingested ruminant parasite *Ha. contortus* is attracted to the smell of grass. By comparing odor response profiles across species, we found that olfactory preferences reflect host specificity rather than phylogeny, suggesting a critical role for olfaction in the process of host finding and appropriate host selection. Our results provide insight into how skin-penetrating nematodes locate hosts to infect.

Results/Discussion

Mammalian-parasitic nematodes vary in their movement patterns

To gain insight into the host-seeking strategies used by mammalian-parasitic nematodes, we first examined their movement patterns in the absence of chemosensory stimuli. We compared their movement patterns to those of EPNs, which use well-characterized host-seeking strategies: some are “cruisers” that actively search for hosts, some are “ambushers” that wait for passing hosts, and some use an intermediate strategy [9,15]. We first examined motility using an assay in which IJs were allowed to distribute on an agar plate in the absence of chemosensory stimuli for one hour and the location of IJs on the plate was recorded. We

found that the motility of skin-penetrating IJs resembled that of EPN cruisers, with the human parasite *Str. stercoralis* being the most active (Figure 2A). By contrast, the motility of *Ha. contortus* resembled that of the ambushing EPN *Ste. carpocapsae* (Figure 2A). Thus, skin-penetrating IJs appear to be more active than passively ingested IJs.

To investigate the host-seeking strategies of skin-penetrating nematodes in more detail, we examined unstimulated movement of IJs using automated worm tracking [16]. We found that parasitic IJs vary dramatically in their crawling speeds, with the human parasite *Str. stercoralis* moving more rapidly than the other species tested (Figure S1A). The mean speeds of the skin-penetrating rat parasites were comparable to that of the most active EPN, *Ste. glaseri*, while the mean speed of *Ha. contortus* resembled that of the less active EPNs (Figure S1A). Turn probability also varied among species but did not correlate with speed (Figure S1B). Some but not all species crawled significantly faster following mechanical stimulation, and in fact the maximum speeds attained by *Str. stercoralis*, *Str. ratti*, and *Ste. glaseri* following mechanical stimulation were similar (Figure S1C–D, Movies S1 and S2). Thus, at least some of the differences in basal crawling speeds among species reflect differences in movement strategy rather than differences in the inherent speeds at which the IJs are capable of crawling.

The fact that *Str. stercoralis* has a higher basal speed than *Str. ratti* and *N. brasiliensis* is consistent with the possibility that host-seeking strategy evolved independently in these species to accommodate host behavior and ecology. *Str. ratti* and *N. brasiliensis* are parasites of nesting rodents, which are highly focal with circumscribed resting places. Since parasite transmission likely occurs within the confines of the nest, rapid mobility may not provide an adaptive advantage for these parasites. By contrast, *Str. stercoralis* is a parasite of humans, primates, and dogs, all of which are highly mobile. Rapid mobility may be necessary for *Str. stercoralis* to accommodate the mobility of its hosts.

Heat increases crawling speed and stimulates local searching in skin-penetrating nematodes

Heat is emitted by all mammals and is a known sensory cue for some mammalian-parasitic nematodes, including *Str. stercoralis* [11]. We therefore examined the responses of the mammalian-parasitic IJs to a 37°C heat stimulus. We found that the skin-penetrating nematodes increased their crawling speed in response to thermal stimulation, while the passively ingested nematode *Ha. contortus* did not (Figure 2B). Skin-penetrating nematodes may increase their speed in response to heat to maximize the likelihood of encountering host skin.

A comparison of IJ movement patterns at room temperature versus 37°C revealed that skin-penetrating IJs show dramatically different movement patterns at the different temperatures. The trajectories of individual IJs were relatively straight at room temperature but highly curved at 37°C (Figure 2C). To quantify these differences, we calculated a distance ratio consisting of the total distance travelled divided by the maximum displacement achieved. We found that all three species of skin-penetrating nematodes showed greater distance ratios at 37°C compared to room temperature (Figure 2D). These results suggest that heat may act as a cue that signifies host proximity and stimulates local searching. However, we note that the temperature at the surface of human skin is 32–35°C [17], and IJ movement within this temperature range remains to be examined.

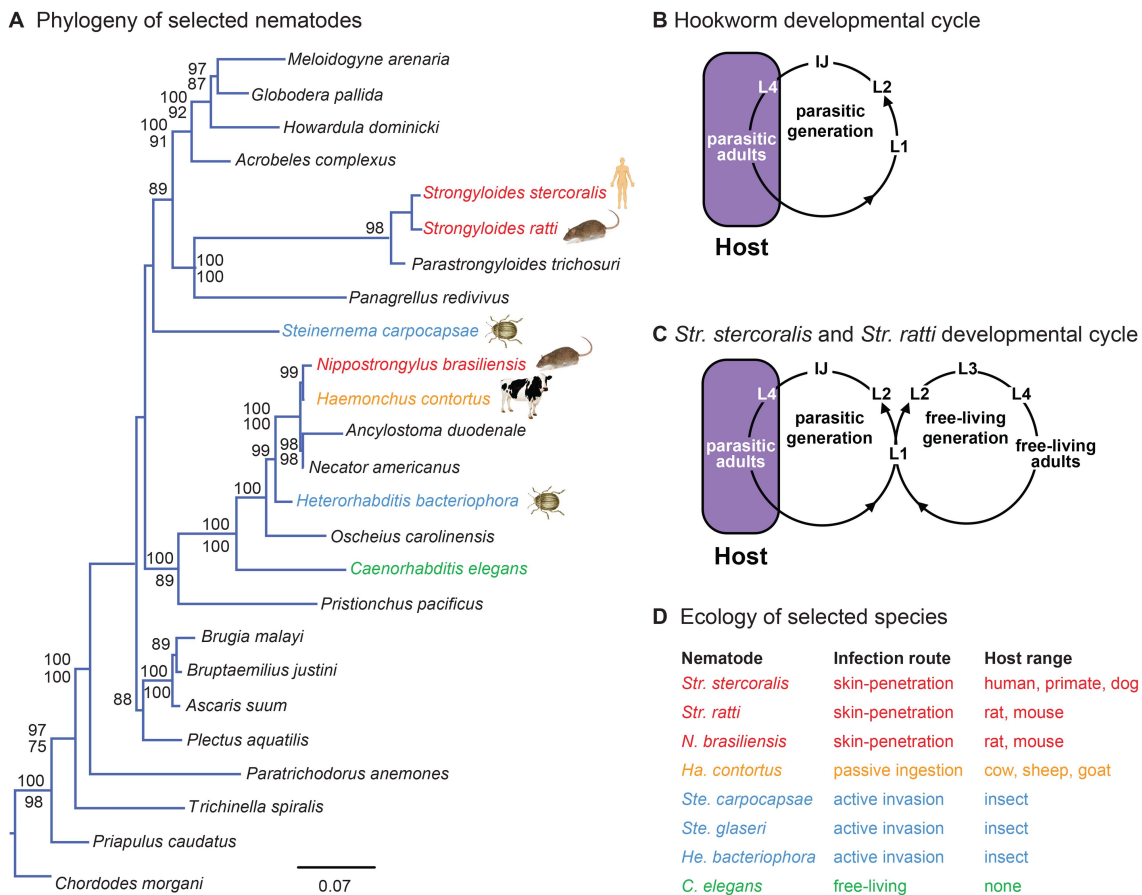


Figure 1. Phylogenetic relationships and life cycles of parasitic nematodes. **A.** Phylogeny of selected nematode species. Phylogenetic analysis is from Dillman *et al.*, 2012 [22]. Species used in the present study are highlighted. Red = skin-penetrating mammalian-parasitic nematode; gold = passively ingested mammalian-parasitic nematode; blue = entomopathogenic nematode; green = free-living nematode. For each of the selected species, icons depict one of their common hosts (human, rat, beetle, or cow). Phylogenetic relationships are based on ML and Bayesian analyses of nearly complete SSU sequences. Values above each branch represent Bayesian posterior probabilities; ML bootstrap indices appear below each branch. Values lower than 75 are not reported. *Priapulus caudatus* and *Chordodes morgani* were defined as outgroups. Detailed methods for phylogenetic tree construction are provided in Dillman *et al.*, 2012 [22]. **B–C.** Life cycles of skin-penetrating nematodes. **B.** Hookworms must infect a new host every generation. IJs infect hosts by skin-penetration. Nematodes develop to adulthood, reproduce, and lay eggs inside the host. Eggs are excreted in host feces and develop into IJs, which find and infect new hosts. **C.** *Str. stercoralis* and *Str. ratti* can develop through a single generation outside the host. Some larvae excreted in host feces develop into IJs; others develop into free-living adults that mate and reproduce outside the host. All progeny of free-living adults develop into IJs, which find and infect new hosts. L1–L4 are larval stages; IJ = infective juvenile. **D.** Ecology of selected nematode species.

doi:10.1371/journal.ppat.1004305.g001

Nictation behavior varies among mammalian-parasitic nematodes

An important component of host-seeking strategy for many parasitic nematodes is nictation, a behavior in which the worm stands on its tail and waves its head to facilitate attachment to passing hosts [9]. We examined the nictation behavior of mammalian-parasitic nematodes by performing nictation assays on an “artificial dirt” substrate consisting of dense agar with near-microscopic pillars [18], since IJs are not capable of standing on standard agar plates due to the high surface tension on the plates [18]. We found that nictation frequencies varied among species. *N. brasiliensis* showed a high nictation frequency comparable to that of the ambushing EPN *Ste. carpocapsae* (Figure 2E and Movie S3), suggesting that it spends most of its foraging time

nictating. By contrast, the *Strongyloides* species showed much lower rates of nictation (Figure 2E and Movie S4), suggesting they spend most of their foraging time crawling. *Ha. contortus* did not nictate on the artificial dirt substrate or any other substrate tested (see Materials and Methods), suggesting it may not be capable of nictating.

Mammalian-parasitic nematodes utilize diverse host-seeking strategies

Taken together, our results suggest that mammalian-parasitic nematodes employ diverse host-seeking strategies. The skin-penetrating *Strongyloides* species appear to be cruisers that are highly mobile and tend to crawl rather than nictate. By contrast, the passively ingested nematode *Ha. contortus* appears to be an

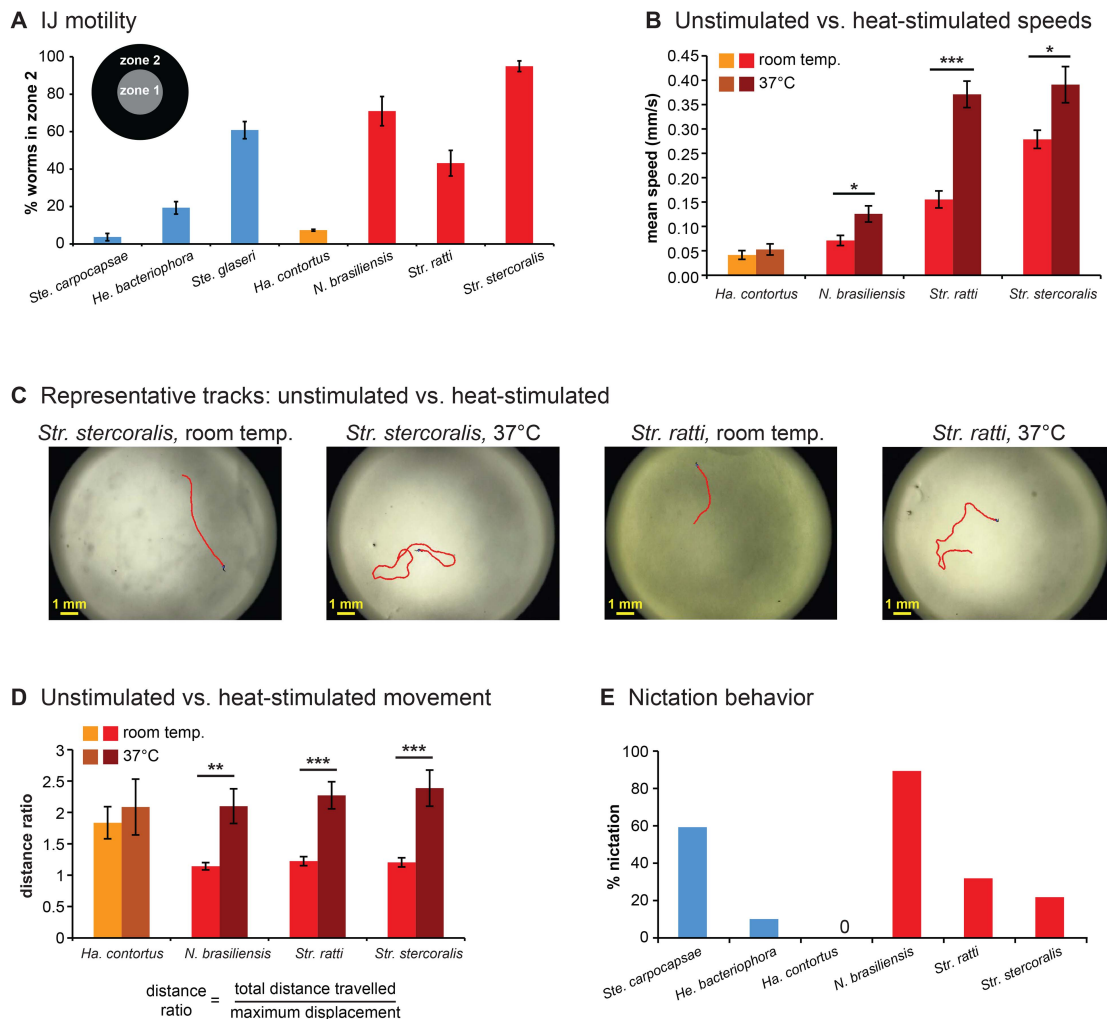


Figure 2. Foraging behaviors of skin-penetrating nematodes. **A** IJ motility in the absence of chemosensory stimulation. Motility varies across species ($P < 0.0001$, one-way ANOVA), with *Str. stercoralis* being the most active ($P < 0.01$, one-way ANOVA with Tukey-Kramer post-test). $n = 6-9$ trials for each species. For this graph and subsequent graphs with multiple species, red = skin-penetrating; gold = passively ingested; blue = entomopathogenic. Of the three entomopathogenic species, *Ste. carpocapsae* is considered an ambusher, *Ste. glaseri* is considered an active cruiser, and *He. bacteriophora* is considered a less active cruiser [15]. Statistical analysis is shown in Table S1. **B** Unstimulated vs. heat-stimulated mean speeds of mammalian-parasitic IJs. Heat-stimulated IJs were exposed to an acute 37°C stimulus and tracked at 37°C . ***, $P < 0.001$; *, $P < 0.01$, unpaired t test or Mann-Whitney test. $n = 5-10$ trials for each species. **C-D** Heat stimulates local search behavior. **C**. Representative tracks for *Str. stercoralis* and *Str. ratti* from 20 s recordings at room temperature versus 37°C . **D**. Movement patterns at room temperature versus 37°C . Distance ratios were calculated as the total track length divided by the maximum displacement attained during the 20 s recording period. A distance ratio of 1 indicates travel in a straight line; a distance ratio of >1 indicates a curved trajectory. ***, $P < 0.001$; **, $P < 0.01$, Mann-Whitney test. $n = 5-10$ trials. **E**. Nictation frequencies of IJs. Nictation was defined as standing or waving behavior of at least 5 s in duration over the course of a 2 min period. Nictation frequencies varied among species ($P < 0.0001$, chi-square test). *N. brasiliensis* showed a nictation frequency comparable to *Ste. carpocapsae* ($P > 0.05$, chi-square test with Bonferroni correction) and greater than *Str. stercoralis* or *Str. ratti* ($P < 0.01$, chi-square test with Bonferroni correction). Statistical analysis is shown in Table S4. $n = 20-28$ IJs for each species. For all graphs, error bars indicate SEM. doi:10.1371/journal.ppat.1004305.g002

ambusher that displays little unstimulated movement. *N. brasiliensis* can exhibit rapid, prolonged movement comparable to that of the cruisers but tends to nictate rather than crawl, suggesting it is also an ambusher. However, we note that foraging strategy is in some cases substrate-dependent, and different strains of a species can exhibit different host-seeking behaviors [19,20]. Thus, we

cannot exclude the possibility that the host-seeking strategies of these species may vary under conditions not tested here.

Str. stercoralis is attracted to human-emitted odorants

EPNs have been shown to use a diverse array of insect volatiles and herbivore-induced plant volatiles for host finding [21–30]. By

contrast, only one odorant has so far been identified as an attractant for *Str. stercoralis* [14]. We therefore tested the extent to which *Str. stercoralis* displays directed movement in response to human-emitted volatiles. We examined the responses of *Str. stercoralis* IJs to a large panel of odorants, most of which are known to be emitted by human skin, sweat, and skin microbiota (Table S5). Responses were examined using a chemotaxis assay (Figures S2 and S3) [21,22]. We found that *Str. stercoralis* was strongly attracted to a number of these odorants (Figure 3A). Nearly all of the attractants we identified for *Str. stercoralis* also attract anthropophilic mosquitoes (Figure 3A), suggesting that nematodes and mosquitoes target humans using many of the same olfactory cues. While many of the human-emitted odorants that attracted *Str. stercoralis* are also emitted by other mammals, 7-octenoic acid is thought to be human-specific [31] and may be used by *Str. stercoralis* to target humans. *Str. stercoralis* and disease-causing mosquitoes are co-endemic throughout the world [2], and our results raise the possibility of designing traps that are effective against both parasites.

We also examined responses to carbon dioxide (CO₂), which is emitted by aerobic organisms in exhaled breath and is an attractant for many parasites, including EPNs [9,21,22]. We found that *Str. stercoralis* was repelled by CO₂ at high concentrations and neutral to CO₂ at low concentrations, suggesting that CO₂ is not a host attractant (Figure 3A and Figure S4A). These results are consistent with the fact that *Str. stercoralis* infects by skin penetration, and only low levels of CO₂ are emitted from skin [32]. However, some EPNs respond synergistically to mixtures of CO₂ and other odorants [33], and we cannot exclude the possibility that *Str. stercoralis* is attracted to CO₂ in mixtures or under conditions not tested here.

Olfactory preferences of parasitic nematodes reflect host specificity

The fact that *Str. stercoralis* responds to human-emitted odorants suggests that olfaction plays an important role in host finding. However, the extent to which *Str. stercoralis* or any other mammalian-parasitic nematode uses olfactory cues for host selection is not known. To gain insight into whether olfaction contributes to host choice, we compared the olfactory responses of *Str. stercoralis* to those of six other species: *Str. ratti*, *N. brasiliensis*, *Ha. contortus*, *He. bacteriophora*, *Ste. carpocapsae*, and *C. elegans*. We found that all species responded to a wide array of odorants, indicating that as is the case for EPNs [21,22], even ambushers are capable of robust chemotaxis (Figure 3B and Figure S4). Moreover, each species exhibited a unique odor response profile, indicating that olfactory responses are species-specific even among closely related species such as *Str. stercoralis* and *Str. ratti* (Figure 3B). CO₂ response varied greatly among species. Like *Str. stercoralis*, *Str. ratti* and *N. brasiliensis* were repelled by CO₂ at high concentrations and neutral to CO₂ at low concentrations (Figure 3B and Figure S4B–C). By contrast, *Ha. contortus* IJs, like EPN IJs and *C. elegans* dauers [21,22], were attracted to CO₂ (Figure 3B and Figure S4D). To confirm that the observed responses to odorants were olfactory rather than gustatory, we examined the responses of *Str. stercoralis* and *Str. ratti* to a subset of odorants in a modified chemotaxis assay in which odorants were placed on the plate lid rather than the plate surface. We found that attractive responses were still observed when the odorants were placed on the plate lid, although the response of *Str. stercoralis* to one odorant was slightly reduced (Figure S5). Thus, the observed behavioral responses are primarily olfactory, but in some cases may include a gustatory component.

The olfactory preferences of the passively ingested mammalian parasite, *Ha. contortus*, are consistent with its known ecology. *Ha. contortus* IJs migrate from the feces of their ruminant hosts to grass blades, where they are ingested by grazing ruminants [34]. The fact that 5% CO₂, which approximates the concentration found in exhaled breath [35], was strongly attractive to *Ha. contortus* (Figure S4D) suggests that *Ha. contortus* may use exhaled CO₂ to migrate toward the mouths of potential hosts. By contrast, *Ha. contortus* was repelled by many of the skin and sweat odorants tested (Figure 3B), consistent with a lack of attraction to mammalian skin. Of the few attractive odorants we identified for *Ha. contortus*, two – methyl myristate and myristic acid – are known constituents of cow and goat milk [36–38] and may be used by *Ha. contortus* to migrate toward cows and goats. To test whether *Ha. contortus* also responds to plant-emitted odorants, we examined responses to freshly cut grass. We found that *Ha. contortus* is attracted to the smell of grass, while *Str. stercoralis* and *Ste. carpocapsae* are not (Figure 3C). These results suggest that *Ha. contortus* uses CO₂ in combination with other ruminant-emitted odorants and grass odorants to position itself for passive ingestion.

We then quantitatively compared odor response profiles across species, and found that species with similar hosts responded more similarly to odorants despite their phylogenetic distance (Figure 3D). For example, the distantly related rat parasites *Str. ratti* and *N. brasiliensis* responded similarly to odorants, as did the distantly related insect parasites *He. bacteriophora* and *Ste. carpocapsae*. The three skin-penetrating species responded more similarly to each other than to the other species tested, while the passively ingested mammalian parasite *Ha. contortus* responded very differently from all of the other species tested (Figure 3D). These results indicate that olfactory preferences reflect host specificity and infection mode rather than phylogeny, consistent with a key role for olfaction in host selection.

Olfactory preferences of *Strongyloides* species are life stage-specific

Skin-penetrating nematodes exit from hosts in feces as eggs or young larvae and subsequently develop into infective larvae outside the host. Thus, both infective and non-infective life stages are present in the environment (Figure 1B–C). This raises the question of whether host attraction is specific to the infective stage. We compared olfactory responses of free-living larvae, free-living adults, and IJs for both *Str. stercoralis* and *Str. ratti* in response to a subset of host odorants. We found that all three life stages were robustly attracted to host odorants, suggesting that host attraction is not downregulated in non-infective life stages (Figure 4). The free-living life stages of skin-penetrating worms are thought to reside primarily on host fecal matter, where they feed on bacteria present in the feces [39]. We therefore compared the responses of free-living larvae, free-living adults, and IJs to host feces. We found that responses differed dramatically across life stages: free-living larvae and adults were strongly attracted to feces, while IJs were neutral to host feces (Figure 4). Moreover, while *Str. ratti* IJs were neutral to both host and non-host feces, *Str. stercoralis* IJs were neutral to host feces but repelled by non-host feces (Figure 4).

Our results suggest a model in which all life stages are attracted to host skin odor, but strong attraction to host fecal odor by the free-living life stages causes them to remain on feces. Attraction to fecal odor is downregulated at the infective stage, enabling the IJs to migrate away from the feces in search of hosts. Repulsion of *Str. stercoralis* IJs from non-host feces may serve as an additional mechanism to prevent foraging in close proximity to non-hosts. To gain insight into the individual odorants that confer changes in

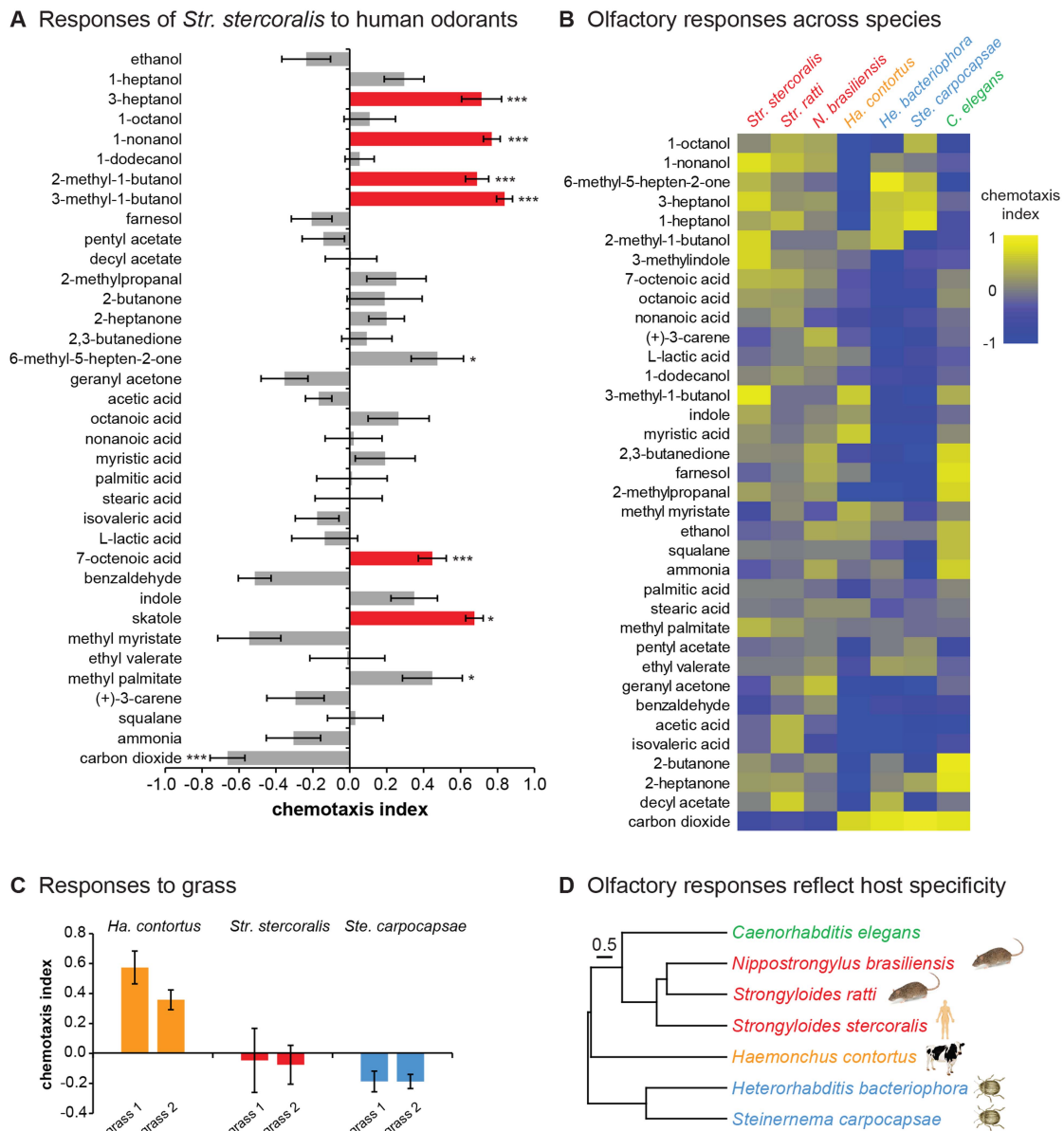


Figure 3. Olfactory responses of mammalian-parasitic nematodes. **A.** *Str. stercoralis* is attracted to a number of human-emitted odorants. Red = attractants for *Str. stercoralis* that also attract anthropophilic mosquitoes [31,52–58]. $n=6-23$ trials per odorant. *Str. stercoralis* did not respond to the chemotaxis controls (Figure S3). *, $P<0.05$; ***, $P<0.001$ relative to control, t-test (CO_2 vs. air and L-lactic acid vs. H_2O) or one-way ANOVA with Bonferroni post-test (all other odorants vs. paraffin oil). **B.** Olfactory responses across species. Response magnitudes are color-coded according to the scale shown to the right of the heat map, and odorants are ordered based on hierarchical cluster analysis. $n=6-14$ trials for each odorant-species combination. Each species exhibited a unique odor response profile ($P<0.0001$, two-way ANOVA with Tukey's post-test). Data for responses of EPNs and *C. elegans* to 10% CO_2 are from Dillman *et al.*, 2012 [22]. Red = skin-penetrating; gold = passively ingested; blue = insect-parasitic; green = free-living. **C.** Responses of *Ha. contortus* to grass odor. Responses to the odors of two different grass samples were examined. $n=8-17$ trials for each sample. **D.** Olfactory preferences reflect host specificity rather than phylogeny. The behavioral dendrogram was constructed based on the odor response profiles of each species. Hierarchical cluster analysis was performed using UPGMA (Unweighted Pair Group Method with Arithmetic Mean). Euclidean distance was used as a similarity measure. Hosts (humans, ruminants, rodents, or insects) for each species are indicated. Coph. Corr. = 0.96. For all graphs, error bars indicate SEM. doi:10.1371/journal.ppat.1004305.g003

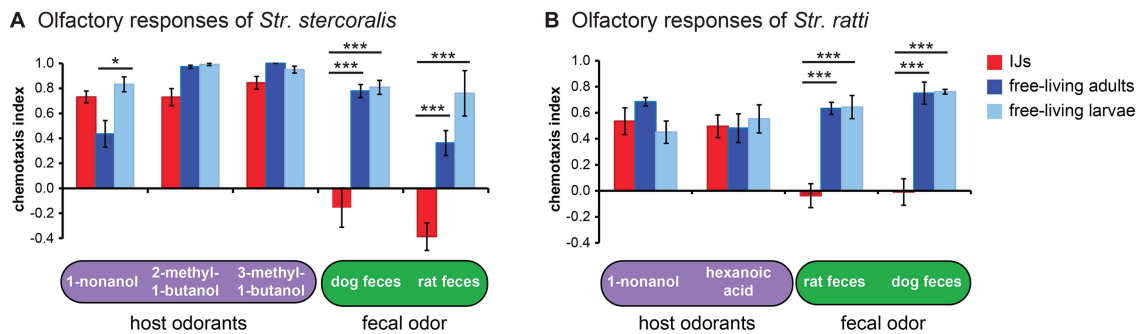


Figure 4. Olfactory responses of *Strongyloides* species vary across life stages. A–B. Responses of either *Str. stercoralis* (A) or *Str. ratti* (B) IJs, free-living adults, and free-living larvae to host odors and fecal odor. *, $P < 0.05$; ***, $P < 0.001$, two-way ANOVA with Tukey's post-test. $n = 4$ –12 trials for *Str. stercoralis* and $n = 6$ –26 trials for *Str. ratti* for each condition. Error bars indicate SEM. doi:10.1371/journal.ppat.1004305.g004

sensitivity to feces, we examined responses to two components of fecal odor, skatole and indole [40]. We found that the free-living stages of *Str. ratti* were highly attracted to both skatole and indole, while the IJs were neutral to both odorants (Figure S6A). Thus, altered sensitivity to these odorants may contribute to the developmental change in the response to fecal odor. By contrast, *Str. stercoralis* IJs were more attracted to skatole than the free-living life stages and all three life stages were relatively unresponsive to indole (Figure S6B), suggesting that other as yet unidentified odorants mediate the sensitivity of *Str. stercoralis* to fecal odor.

Implications for nematode control

Str. stercoralis infection is a worldwide cause of chronic morbidity and mortality. Current drugs used to treat nematode infections are inadequate for nematode control: some are toxic, drug resistance is a growing concern, and reinfection rates are high [41]. Our data suggest that *Str. stercoralis* IJs are fast-moving cruisers that actively search for hosts using a chemically diverse array of human-emitted odorants. The identification of odorants that attract or repel *Str. stercoralis* and other parasitic nematodes lays a foundation for the design of targeted traps or repellents, which could have broad implications for nematode control.

Materials and Methods

Ethics statement

Gerbils were used for host passage of *Str. stercoralis*, and rats were used for host passage of *Str. ratti* and *N. brasiliensis*. All protocols and procedures were approved by the UCLA Office of Animal Research Oversight (Protocol No. 2011-060-03B), which adheres to the AAALAC standards for laboratory animal use, and were in strict accordance with the *Guide for the Care and Use of Laboratory Animals*.

Nematodes, vertebrate animals, and insects

Strongyloides stercoralis UPD strain and *Strongyloides ratti* ED321 strain were provided by Dr. James Lok (University of Pennsylvania). *Nippostrongylus brasiliensis* was provided by Dr. Edward Platzer (University of California, Riverside). *Haemonchus contortus* was provided by Dr. Adrian Wolstenholme and Mr. Bob Storey (University of Georgia). *Heterorhabditis bacteriophora* Oswego strain and *Steinernema glaseri* VS strain were provided by David Shapiro-Ilan (USDA). *Steinernema carpocapsae* were

from the ALL strain [21,22,42]. *C. elegans* dauers were from the wild isolate CB4856 (“Hawaii”). Male Mongolian gerbils for culturing *Str. stercoralis* were obtained from Charles River Laboratories. Male or female Long-Evans or Sprague Dawley rats for culturing *Str. ratti* and *N. brasiliensis* were obtained either from Harlan Laboratories or second-hand from other investigators at UCLA through the UCLA Internal Animal Transfer supply system for surplus animals. *Galleria mellonella* larvae for culturing EPNs were obtained from American Cricket Ranch (Lakeside, CA).

Maintenance of *Str. stercoralis*

Str. stercoralis was serially passaged in gerbils and maintained on fecal-charcoal plates. Inoculation of gerbils with *Str. stercoralis* was performed essentially as previously described [43]. Briefly, *Str. stercoralis* IJs were isolated from fecal-charcoal plates using a Baermann apparatus [43]. Each gerbil was subcutaneously injected with 2000 IJs in 200 μ l sterile PBS. Gerbils became patent (as defined by the presence of nematodes in gerbil feces) on day 12 post-inoculation and remained patent for approximately 70 days. At 28 and 35 days post-inoculation, each gerbil received 2 mg methylprednisolone (Depo-Medrol, Pfizer) subcutaneously to induce an auto-infective cycle. To harvest infested feces, gerbils were housed overnight in cages containing a wire rack on the bottom of the cage. Fecal pellets fell below the rack onto damp cardboard and were collected the following morning. Feces were mixed with dH₂O and autoclaved charcoal (bone char from Ebonex Corp., Cat # EBO.58BC.04) in an approximately 1:1 ratio of charcoal to feces. The fecal-charcoal mixtures were poured into Petri dishes (10 cm diameter, 20 mm height) lined with wet filter paper, and were stored at 23°C until use. Nematodes used for behavioral analysis were isolated from fecal-charcoal plates using a Baermann apparatus [43] or from plate lids. To obtain free-living larvae (primarily post-parasitic L2s) for chemotaxis assays, nematodes were collected from fecal-charcoal plates after approximately 18 hrs. To obtain free-living adults for chemotaxis assays, nematodes were collected from fecal-charcoal plates after 48 hrs. To obtain IJs, nematodes were collected from fecal-charcoal plates starting at day 5 post-collection. IJs were used for behavioral assays within 2 weeks of fecal collection.

Maintenance of *Str. ratti*

Str. ratti was serially passaged in rats and maintained on fecal-charcoal plates. Inoculation of rats with *Str. ratti* was performed

essentially as previously described [44]. Briefly, *Str. ratti* IJs were isolated from fecal-charcoal plates using a Baermann apparatus. Each rat was subcutaneously injected with 700 IJs in 300 μ l sterile PBS. Rats became patent on day 6 post-inoculation and remained patent for up to 28 days post-inoculation. To harvest infested feces, rats were housed overnight in cages containing a wire rack on the bottom of the cage. Fecal pellets fell below the rack onto damp cardboard and were collected the following morning. Fecal-charcoal plates were prepared as described above for *Str. stercoralis* and stored at 23°C until use. Nematodes used for behavioral analysis were isolated from fecal-charcoal plates using a Baermann apparatus [43] or from plate lids. Free-living larvae, adults, and IJs were obtained from fecal-charcoal plates as described above for *Str. stercoralis*.

Maintenance of *N. brasiliensis*

N. brasiliensis was serially passaged in rats and maintained on fecal-charcoal plates. To inoculate rats, *N. brasiliensis* IJs were isolated from fecal-charcoal plates using a Baermann apparatus. Each rat was subcutaneously injected with 4000 IJs in 300 μ l sterile PBS. Rats became patent on day 6 post-inoculation and remained patent for up to 14 days. Infested feces were collected as described above for *Str. ratti*. Fecal-charcoal plates were prepared as described above for *Str. stercoralis*, except that vermiculite (Fisher catalog # S17729) was added to the feces and charcoal in an approximately 1:1:1 ratio of vermiculite to charcoal to feces. Plates were stored at 23°C until use. In some cases, either Nystatin (Sigma catalog # N6261) at a concentration of 200 U/ml or Fungizone (Gibco catalog #15290-018) at a concentration of 1 μ g/ml was added to the filter paper on the bottom of the plate to inhibit mold growth. Nematodes used for behavioral analysis were isolated from fecal-charcoal plates using a Baermann apparatus [43] or from plate lids. To obtain IJs, nematodes were collected from fecal-charcoal plates starting at day 7 post-collection. IJs were used for behavioral assays within 2 weeks of fecal collection.

Maintenance of *Ha. contortus*

Ha. contortus was stored in dH₂O at 8°C prior to use. IJs were tested within 6 months of collection. No differences in IJ movement or behavior were observed in freshly collected versus 6 month old IJs. IJ behavior declined after 6 months, so IJs older than 6 months were not tested.

Maintenance of entomopathogenic nematodes (EPNs)

EPNs were cultured as previously described [21]. Briefly, 5 last instar *Galleria mellonella* larvae were placed in a 5 cm Petri dish with a 55 mm Whatman 1 filter paper acting as a pseudo-soil substrate in the bottom of the dish. Approximately 250 μ l containing 500–1000 IJs suspended in water was evenly distributed on the filter paper. After 7–10 days the insect cadavers were placed on White traps [45]. Emerging IJs were collected from the White trap, rinsed 3 times with dH₂O, and stored in dH₂O until use. *Ste. carpocapsae* and *He. bacteriophora* were maintained at 25°C, while *Ste. glaseri* was maintained at room temperature. IJs were used for behavioral assays within 7 days of collection from the White trap.

Maintenance of *C. elegans*

C. elegans was cultured on NGM plates seeded with *E. coli* OP50 according to standard methods [46]. Dauer larvae were collected from the lids of plates from which the nematodes had consumed all of the OP50 and stored in dH₂O at room

temperature prior to use. Dauer larvae were used for behavioral assays within 2 weeks of collection from plate lids.

Motility assays

30–100 IJs were placed in the center of a chemotaxis plate [47]. IJs were allowed to distribute over the agar surface for 1 hr, after which the percentage of IJs in the outer zone (Zone 2) was determined. Zone 1 was a 4 cm diameter circle centered in the middle of the plate. Zone 2 consisted of the rest of the plate and included the edges of the plate, which acted as a trap since IJs that crawled onto the plate edge desiccated and could not return to the agar surface.

Recording worm movement for automated tracking

Recordings of worm movement were obtained with an Olympus E-PM1 digital camera attached to a Leica S6 D microscope. To quantify unstimulated movement, 4–5 IJs were placed in the center of a chemotaxis plate [47] and allowed to acclimate for 10 min. 20 s recordings were then obtained. Worms that either did not move, that stopped moving during the recording, or that crawled off the assay plate during the recording were excluded from the analysis. To quantify movement before and after mechanical stimulation, IJs were placed on chemotaxis plates and allowed to acclimate for 10 min. prior to tracking. Baseline movement was recorded for approximately 15 s. The plate lid was then removed, the IJ was gently agitated using a worm pick, and post-agitation movement was recorded for approximately 30 s. 5 s recording clips directly following agitation were used to calculate the maximum speeds shown in Figure S1D, and 5 s recording clips directly preceding and following agitation were used to generate the sample tracks shown in Figure S1C. Maximum speeds were calculated in WormAnalyzer (see below) based on changes in worm position over a seven frame (or 0.23 second) window. To quantify movement following thermal stimulation, assays were performed in a 37°C warm room. Chemotaxis assay plates were kept in the warm room prior to use. Individual IJs were transported into the warm room, transferred to assay plates, and immediately recorded for 20 s. For the room temperature control, IJs were similarly transferred to assay plates and immediately recorded for 20 s. Locomotion was quantified using WormTracker and WormAnalyzer multi-worm tracker software (Miriam Goodman lab, Stanford University) [16]. The following WormTracker settings were adjusted from the default settings (designed for *C. elegans* adults) for analysis of IJ movement: min. single worm area = 20 pixels; max. size change by worm between successive frames = 250 pixels; shortest valid track = 30 frames; auto-thresholding correction factor = 0.001. To calculate turn frequencies, the following WormAnalyzer settings were adjusted from the default settings for analysis of IJ speed: sliding window for smoothing track data = 30 frames; minimum run duration for pirouette identification = 2.9 s for *Str. stercoralis*, 5.3 s for *Ste. glaseri*, and 6 s for all other species (to compensate for differences in speed among species). All turns were confirmed by visual observation of worm tracks; turns not confirmed by visual observation were not counted. For calculations of maximum displacement in Figure 2D, the distance between the worm's start point and the farthest point the worm reached during the 20 s recording was calculated in ImageJ.

Nictation assays

Nictation was quantified on "micro-dirt" agar chips cast from polydimethylsiloxane (PDMS) molds as previously described [18], except that chips were made from 5% agar dissolved in dH₂O and were incubated at 37°C for 2 hr and then room temperature for

1 hr before use. The micro-dirt chip consisted of agar with near-microscopic pillars covering its surface (pillar height of 25 μm with a radius of 25 μm and an interval between pillars of 25 μm), which allowed IJs to nictate on top of the pillars. For each assay, 3–10 IJs were transferred to the micro-dirt chip and allowed to acclimate on the chip for 10 min. Each IJ was then monitored for 2 min. An IJ was scored as “nictating” if it raised its head off the surface of the chip for a period of at least 5 s during the 2 min assay period. Nictation behavior was also tested on sand. Sand nictation assays were performed essentially as previously described [21,48]. Sand (silicon dioxide, >230 mesh, CAS 60676-86-0) was distributed onto the surface of a chemotaxis plate using a sieve. IJs were transferred to the plate surface and allowed to acclimate for 10 min. Nictation behavior was then observed for two minutes. In all cases, nictation behavior on sand was consistent with nictation behavior on micro-dirt chips. In the case of *Ha. contortus*, we also tested for nictation on grass and vermiculite; no nictation was observed on any substrate tested. To test for nictation on grass, grass samples were collected from a lawn seeded with UC Verde Buffalo grass and perennial rye grass (the same lawn as for sample 1 below). The grass was cut into small chunks (~2.5 mm \times 2.5 mm) and distributed onto the surface of a chemotaxis plate. IJs were transferred onto the plate surface or directly onto blades of grass, and nictation was scored after a 10 min. acclimation period. Nictation was also scored after 20, 30, or 60 min., or the next day. No nictation was observed with *Ha. contortus* at any time point.

Odor chemotaxis assays

Odor chemotaxis assays were performed essentially as described [21,22] (Figure S2). Assays were performed on chemotaxis assay plates [47]. Scoring regions consisted of 2 cm diameter circles on each side of the plate along the diameter with the center of the circle 1 cm from the edge of the plate, as well as the rectangular region extending from the edges of the circle to the edge of the plate. Either 2 μl (for mammalian-parasitic IJs) or 1 μl (for insect-parasitic IJs and *C. elegans* dauers) of 5% sodium azide was placed in the scoring region as anesthetic. 5 μl of odorant was then placed on the surface of the assay plate in the center of one scoring region, and 5 μl of control (paraffin oil, dH₂O, or ethanol) was placed on the surface of the assay plate in the center of the other scoring region. Approximately 200 worms were placed in the center of the assay plate and left undisturbed on a vibration-reducing platform for 3 hours at room temperature. A chemotaxis index (CI) was then calculated as: $\text{CI} = (\# \text{ worms at odorant} - \# \text{ worms at control}) / (\# \text{ worms at odorant} + \# \text{ worms at control})$ (Figure S2). A positive CI indicates attraction; a negative CI indicates repulsion. A 3 hour assay duration was used because 3 hour assays were found to be most effective for EPNs [21,49]. However, 1 hour assays were also performed with *Str. ratti*, and no significant differences were observed in 1 hour vs. 3 hour assays (Table S6). Two identical assays were always performed simultaneously with the odor gradient in opposite directions on the two plates to control for directional bias due to room vibration; assays were discarded if the difference in the CIs for the two plates was ≥ 0.9 or if fewer than 7 worms moved into the scoring regions on one or both of the plates. Liquid odorants were tested undiluted unless otherwise indicated. Solid odorants were prepared as follows: 1-dodecanol, methyl palmitate, and methyl myristate were diluted 0.05 g in 2.5 ml paraffin oil; palmitic acid was diluted 10 g in 200 ml ethanol; myristic acid, skatole, and indole were diluted 0.05 g in 2.5 ml ethanol; and L-lactic acid was diluted 0.05 g in 2.5 ml dH₂O. Ammonia was purchased as a 2 M solution in ethanol. Solid odorants were tested at these concentrations unless otherwise

indicated. For assays in which odorants were placed on the plate lid rather than the plate surface (Figure S5), filter paper squares of approximately 0.5 cm in width were attached to the plate lid using double-stick tape. Odorant or control was then pipetted onto the filter paper, and chemotaxis was examined as described above.

CO₂ chemotaxis assays

CO₂ chemotaxis assays were performed essentially as described [21,22]. Assays were performed on chemotaxis assay plates [47], and scoring regions were as described above for odor chemotaxis assays (Figure S2). Gases were delivered at a rate of 0.5 ml/min through holes in the plate lids from gastight syringes filled with either a CO₂ mixture containing the test concentration of CO₂, 10% O₂, and the balance N₂, or a control air mixture containing 10% O₂ and 90% N₂. Certified gas mixtures were obtained from Air Liquide or Airgas. Assays were performed and scored as described above for odor chemotaxis assays, except that the assay duration was 1 hour.

Grass chemotaxis assays

Fresh grass samples were collected from the campus of the University of California, Los Angeles. Sample 1 was collected from a lawn seeded with UC Verde Buffalo grass and perennial rye grass, and sample 2 was collected from a lawn seeded with a custom blend of annual ryegrass, *Festuca*, Bonsai dwarf fescue, Bermuda grass, and bluegrass. 200 μl of dH₂O was added to 0.1 g grass. Grass was then ground in a small weigh boat, and 5 μl of the grass suspension was used in a chemotaxis assay with 5 μl dH₂O as a control. Grass was either used immediately for chemotaxis assays or stored at 4°C for no more than 3 days.

Fecal chemotaxis assays

Uninfected rat or dog feces was collected from animals in the UCLA vivarium. Responses to feces were tested using a modified chemotaxis assay in which feces was placed on the plate lid rather than the plate surface. Filter paper squares of approximately 0.5 cm in width were attached to the plate lid using double-stick tape. Fecal matter was moistened with dH₂O, smeared onto filter paper, and tested in a chemotaxis assay as described above for odor chemotaxis assays. We note that similar attraction to feces was observed when filter paper with feces was tested against filter paper with dH₂O, and no attraction was observed to wet filter paper when wet filter paper was tested against dry filter paper (data not shown).

Data analysis

Statistical analysis was performed using either GraphPad InStat, GraphPad Prism, or PAST [50]. The heatmap was generated using Heatmap Builder [51].

Supporting Information

Figure S1 IJ movement across species. **A.** Unstimulated mean speeds of IJs. IJ speed varies among species ($P < 0.0001$, Kruskal-Wallis test). *Str. stercoralis* crawled significantly faster than the other species tested ($P < 0.05$, Dunn’s post-test). Statistical analysis is shown in Table S2. $n = 20\text{--}31$ IJs for each species. **B.** Unstimulated turn frequencies of IJs in turns/s. Turn frequency varied among species ($P < 0.0001$, Kruskal-Wallis test with Dunn’s post-test) but did not correlate with speed ($R^2 = 0.22$ and $P = 0.28$, linear correlation analysis). Statistical analysis is shown in Table S3. $n = 20\text{--}31$ IJs for each species. **C.** Representative tracks of *St. carpocapsae*, *Str. ratti*, and *Str. stercoralis* before and after mechanical stimulation. Recordings show 5 s of pre-stimulation

movement and 5 s of post-stimulation movement. Red lines indicate the timing of the mechanical stimulation; red dot indicates the maximum speed attained during each recording; blue lines indicate the mean unstimulated speed for each species. **D.** Unstimulated vs. mechanically stimulated maximum speeds of IJs. ***, $P < 0.001$; **, $P < 0.01$, unpaired t test or Mann-Whitney test. $n = 20\text{--}31$ trials for unstimulated speed, 5–10 trials for stimulated speed. Maximum speed was used for this analysis since the species differed in how quickly they returned to basal speed following mechanical stimulation. For all graphs, error bars indicate SEM. (PDF)

Figure S2 Chemotaxis assay for IJs. Odorant is placed on one side of the plate and control is placed on the other side (black dots). IJs are placed in the center of the plate and allowed to distribute in the odor gradient for 3 hr. The number of IJs in each scoring region is then counted, and a chemotaxis index is calculated as shown (right). The chemotaxis index ranges from +1 to -1 , with a positive chemotaxis index indicating attraction and a negative chemotaxis index indicating repulsion. Red bar = 1 cm. (PDF)

Figure S3 Responses of *Str. stercoralis* to diluent controls. Responses of *Str. stercoralis* to paraffin oil vs. paraffin oil, water vs. water, and ethanol vs. ethanol in a chemotaxis assay. The diluents did not elicit responses from *Str. stercoralis*, resulting in an equal distribution of IJs on both sides of the assay plate. $n = 10\text{--}12$ trials for each condition. Error bars indicate SEM. (PDF)

Figure S4 Responses to odorants across concentrations. A–D. Responses of *Str. stercoralis* (A), *Str. ratti* (B), *N. brasiliensis* (C), and *Ha. contortus* (D) to increasing concentrations of odorants in a chemotaxis assay. $n = 6\text{--}21$ trials for each species-odorant combination. (PDF)

Figure S5 Responses to odorants are primarily olfactory rather than gustatory. A. Responses of *Str. stercoralis* in a standard chemotaxis assay where odorants are placed on the plate surface vs. a modified chemotaxis assay where odorants are placed on the plate lid. Responses to 3-heptanol and 1-nonanol were not significantly different, while the response to 3-methyl-1-butanol was slightly reduced. **, $P < 0.01$, two-way ANOVA with Bonferroni post-test. $n = 6\text{--}12$ trials for each condition. **B.** Responses of *Str. ratti* were not significantly different in the lid assay vs. the plate assay ($P > 0.05$, two-way ANOVA). $n = 6\text{--}16$ trials for each condition. For all graphs, error bars indicate SEM. (PDF)

Figure S6 Responses of *Strongyloides* species to selected fecal odorants. A. Responses of *Str. ratti* to skatole and indole across life stages. Both odorants were neutral for IJs but attractive for free-living larvae and adults. **, $P < 0.01$; ***, $P < 0.001$, two-way ANOVA with Tukey's post-test. $n = 8\text{--}13$ trials for each odorant. **B.** Responses of *Str. stercoralis* to skatole and

indole. *, $P < 0.05$, two-way ANOVA with Tukey's post-test. For all graphs, error bars indicate SEM. (PDF)

Table S1 Results of statistical analysis comparing motility across species. P values were determined by one-way ANOVA with Tukey-Kramer post-test. ***, $P < 0.001$; **, $P < 0.01$; *, $P < 0.05$; ns = not significant. Data are from Figure 2A. (DOCX)

Table S2 Results of statistical analysis comparing unstimulated mean speeds across species. P values were determined by Kruskal-Wallis test with Dunn's post-test. ***, $P < 0.001$; **, $P < 0.01$; *, $P < 0.05$; ns = not significant. Data are from Figure S1A. (DOCX)

Table S3 Results of statistical analysis comparing unstimulated turn frequencies across species. P values were determined by Kruskal-Wallis test with Dunn's post-test. ***, $P < 0.001$; **, $P < 0.01$; *, $P < 0.05$; ns = not significant. Data are from Figure S1B. (DOCX)

Table S4 Results of statistical analysis comparing nictation frequencies across species. P values were determined by chi-square analysis with Bonferroni corrections for multiple comparisons. **, $P < 0.01$; *, $P < 0.05$; ns = not significant. Data are from Figure 2E. (DOCX)

Table S5 Mammalian-derived odorants tested. Sources listed are not exhaustive. (DOCX)

Table S6 Comparison of 1 hour and 3 hour chemotaxis assays with *Str. ratti*. Results from 1 hour and 3 hour assays were not significantly different (two-way ANOVA). (DOCX)

Movie S1 Mechanical stimulation of a *Str. ratti* IJ. (MOV)

Movie S2 Mechanical stimulation of a *Str. stercoralis* IJ. (MOV)

Movie S3 Nictation of an *N. brasiliensis* IJ. (MOV)

Movie S4 Nictation of an *Str. ratti* IJ. (MOV)

Acknowledgments

We thank David Shapiro-Ilan, Adrian Wolstenholme, and Bob Storey for nematodes.

Author Contributions

Conceived and designed the experiments: MLC SSG EAH. Performed the experiments: MLC SSG RPO AAT. Analyzed the data: MLC SSG EAH. Contributed reagents/materials/analysis tools: TJN EGP JBL. Wrote the paper: EAH.

References

1. Schafer TW, Skopac A (2006) Parasites of the small intestine. *Curr Gastroenterol Rep* 8: 312–320.
2. Schar F, Trostorf U, Giardina F, Khieu V, Muth S, et al. (2013) *Strongyloides stercoralis*: global distribution and risk factors. *PLoS Negl Trop Dis* 7: e2288.
3. Khieu V, Schar F, Marti H, Sayasone S, Duong S, et al. (2013) Diagnosis, treatment and risk factors of *Strongyloides stercoralis* in schoolchildren in Cambodia. *PLoS Negl Trop Dis* 7: e2035.
4. Hotez P, Hawdon J, Schad GA (1993) Hookworm larval infectivity, arrest and amphiparatenesis: the *Caenorhabditis elegans* Daf-c paradigm. *Parasitol Today* 9: 23–26.
5. Schad GA, Aikens LM, Smith G (1989) *Strongyloides stercoralis*: is there a canonical migratory route through the host? *J Parasitol* 75: 740–749.
6. Yamada M, Matsuda S, Nakazawa M, Arizono N (1991) Species-specific differences in heterogenic development of serially transferred free-living

- generations of *Strongyloides planiceps* and *Strongyloides stercoralis*. *J Parasitol* 77: 592–594.
7. Ashton FT, Li J, Schad GA (1999) Chemo- and thermosensory neurons: structure and function in animal parasitic nematodes. *Vet Parasitol* 84: 297–316.
 8. Bhople VM, Kupprion EK, Ashton FT, Boston R, Schad GA (2001) *Ancylostoma caninum*: the finger cell neurons mediate thermotactic behavior by infective larvae of the dog hookworm. *Exp Parasitol* 97: 70–76.
 9. Chaisson KE, Hallem EA (2012) Chemosensory behaviors of parasites. *Trends Parasitol* 28: 427–436.
 10. Forbes WM, Ashton FT, Boston R, Zhu X, Schad GA (2004) Chemoattraction and chemorepulsion of *Strongyloides stercoralis* infective larvae on a sodium chloride gradient is mediated by amphidial neuron pairs ASE and ASH, respectively. *Vet Parasitol* 120: 189–198.
 11. Lopez PM, Boston R, Ashton FT, Schad GA (2000) The neurons of class ALD mediate thermotaxis in the parasitic nematode, *Strongyloides stercoralis*. *Int J Parasitol* 30: 1115–1121.
 12. Koga M, Nuamantong S, Dekumyop P, Yoonuan T, Maipanich W, et al. (2005) Host-finding behavior of *Strongyloides stercoralis* infective larvae to sodium cation, human serum, and sweat. *Southeast Asian J Trop Med Public Health* 36: 93–98.
 13. Koga M, Tada I (2000) *Strongyloides ratti*: chemotactic responses of third-stage larvae to selected serum proteins and albumins. *J Helminthol* 74: 247–252.
 14. Safer D, Brenes M, Dunipace S, Schad G (2007) Urocanic acid is a major chemoattractant for the skin-penetrating parasitic nematode *Strongyloides stercoralis*. *Proc Natl Acad Sci USA* 104: 1627–1630.
 15. Downes MJ, Griffin CT (1996) Dispersal behavior and transmission strategies of the entomopathogenic nematodes *Heterorhabditis* and *Steinernema*. *Biocontrol Sci Techn* 6: 347–356.
 16. Ramot D, Johnson BE, Berry TL, Carnell L, Goodman MB (2008) The parallel worm tracker: a platform for measuring average speed and drug-induced paralysis in nematodes. *PLoS ONE* 3: e2208.
 17. Liu Y, Wang L, Liu J, Di Y (2013) A study of human skin and surface temperatures in stable and unstable thermal environments. *J Therm Biol* 38: 440–448.
 18. Lee H, Choi MK, Lee D, Kim HS, Hwang H, et al. (2012) Nictation, a dispersal behavior of the nematode *Caenorhabditis elegans*, is regulated by IL2 neurons. *Nat Neurosci* 15: 107–112.
 19. Griffin CT (2012) Perspectives on the behavior of entomopathogenic nematodes from dispersal to reproduction: traits contributing to nematode fitness and biocontrol efficacy. *J Nematol* 44: 177–184.
 20. Wilson MJ, Ehlers R-U, Glazer I (2012) Entomopathogenic nematode foraging strategies – is *Steinernema carpocapsae* really an ambush forager? *Nematol* 14: 389–394.
 21. Hallem EA, Dillman AR, Hong AV, Zhang Y, Yano JM, et al. (2011) A sensory code for host seeking in parasitic nematodes. *Curr Biol* 21: 377–383.
 22. Dillman AR, Guillermin ML, Lee JH, Kim B, Sternberg PW, et al. (2012) Olfaction shapes host-parasite interactions in parasitic nematodes. *Proc Natl Acad Sci USA* 109: E2324–2333.
 23. Laznik Z, Trdan S (2013) An investigation on the chemotactic responses of different entomopathogenic nematode strains to mechanically damaged maize root volatile compounds. *Exp Parasitol* 134: 349–355.
 24. Ali JG, Albom HT, Stelinski LL (2010) Subterranean herbivore-induced volatiles released by citrus roots upon feeding by *Diaprepes abbreviatus* recruit entomopathogenic nematodes. *J Chem Ecol* 36: 361–368.
 25. Ali JG, Albom HT, Campos-Herrera R, Kaplan F, Duncan LW, et al. (2012) Subterranean, herbivore-induced plant volatile increases biological control activity of multiple beneficial nematode species in distinct habitats. *PLoS ONE* 7: e38146.
 26. Ali JG, Albom HT, Stelinski LL (2011) Constitutive and induced subterranean plant volatiles attract both entomopathogenic and plant-parasitic nematodes. *J Ecol* 99: 26–35.
 27. Hiltbold I, Baroni M, Toepfer S, Kuhlmann U, Turlings TC (2010) Selection of entomopathogenic nematodes for enhanced responsiveness to a volatile root signal helps to control a major root pest. *J Exp Biol* 213: 2417–2423.
 28. Kollner TG, Held M, Lenk C, Hiltbold I, Turlings TC, et al. (2008) A maize (E)- β -caryophyllene synthase implicated in indirect defense responses against herbivores is not expressed in most American maize varieties. *Plant Cell* 20: 482–494.
 29. Rasmann S, Kollner TG, Degenhardt J, Hiltbold I, Toepfer S, et al. (2005) Recruitment of entomopathogenic nematodes by insect-damaged maize roots. *Nature* 434: 732–737.
 30. Rasmann S, Ali JG, Helder J, van der Putten WH (2012) Ecology and evolution of soil nematode chemotaxis. *J Chem Ecol* 38:615–628.
 31. Qiu YT, Smallegange RC, van Loon JJ, Takken W (2011) Behavioural responses of *Anopheles gambiae sensu stricto* to components of human breath, sweat and urine depend on mixture composition and concentration. *Med Vet Entomol* 25: 247–255.
 32. Alkalay I, Suetsugu S, Constantine H, Stein M (1971) Carbon dioxide elimination across human skin. *Am J Physiol* 220: 1434–1436.
 33. Turlings TC, Hiltbold I, Rasmann S (2012) The importance of root-produced volatiles as foraging cues for entomopathogenic nematodes. *Plant Soil* 358: 51–60.
 34. Zajac AM (2006) Gastrointestinal nematodes of small ruminants: life cycle, anthelmintics, and diagnosis. *Vet Clin North Am Food Anim Pract* 22: 529–541.
 35. Pleil JD, Lindstrom AB (1995) Measurement of volatile organic compounds in exhaled breath as collected in evacuated electropolished canisters. *J Chromatogr B Biomed Appl* 665: 271–279.
 36. Mansson HL (2008) Fatty acids in bovine milk fat. *Food Nutr Res* 52: 10.
 37. Povolo M, Pelizzola V, Ravera D, Contarini G (2009) Significance of the nonvolatile minor compounds of the neutral lipid fraction as markers of the origin of dairy products. *J Agric Food Chem* 57: 7387–7394.
 38. Haenlein GFW (2004) Goat milk in human nutrition. *Small Ruminant Res* 51: 155–163.
 39. Viney ME, Lok JB (2007) *Strongyloides* spp. In *WormBook*, www.WormBook.org.
 40. Moore JG, Jessop LD, Osborne DN (1987) Gas-chromatographic and mass-spectrometric analysis of the odor of human feces. *Gastroenterology* 93: 1321–1329.
 41. Diawara A, Schwenkenbecher JM, Kaplan RM, Prichard RK (2013) Molecular and biological diagnostic tests for monitoring benzimidazole resistance in human soil-transmitted helminths. *Am J Trop Med Hyg* 88: 1052–1061.
 42. Bilgrami AL, Gauger R, Shapiro-Ilan DI, Adams BJ (2006) Source of trait deterioration in entomopathogenic nematodes *Heterorhabditis bacteriophora* and *Steinernema carpocapsae* during *in vivo* culture. *Nematology* 8: 397–409.
 43. Lok JB (2007) *Strongyloides stercoralis*: a model for translational research on parasitic nematode biology. In *WormBook*, www.WormBook.org.
 44. Shao H, Li X, Nolan TJ, Massey HC, Jr., Pearce EJ, et al. (2012) Transposon-mediated chromosomal integration of transgenes in the parasitic nematode *Strongyloides ratti* and establishment of stable transgenic lines. *PLoS Pathog* 8: e1002871.
 45. White GF (1927) A method for obtaining infective nematode larvae from cultures. *Science* 66: 302–303.
 46. Brenner S (1974) The genetics of *Caenorhabditis elegans*. *Genetics* 77: 71–94.
 47. Bargmann CI, Hartwig E, Horvitz HR (1993) Odorant-selective genes and neurons mediate olfaction in *C. elegans*. *Cell* 74: 515–527.
 48. Campbell JF, Kaya HK (2000) Influence of insect-associated cues on the jumping behavior of entomopathogenic nematodes (*Steinernema* spp.). *Behavior* 137: 591–609.
 49. O'Halloran DM, Burnell AM (2003) An investigation of chemotaxis in the insect parasitic nematode *Heterorhabditis bacteriophora*. *Parasitol* 127: 375–385.
 50. Hammer O, Harper DAT, Ryan PD (2001) *PAST: Paleontological statistics software package for education and data analysis*. *Palaentol Electronica* 4: 9pp.
 51. King JY, Ferrara R, Tabibiazar R, Spin JM, Chen MM, et al. (2005) Pathway analysis of coronary atherosclerosis. *Physiol Genomics* 23: 103–118.
 52. Mukabana WR, Mweresa CK, Otieno B, Omusula P, Smallegange RC, et al. (2012) A novel synthetic odorant blend for trapping of malaria and other African mosquito species. *J Chem Ecol* 38: 235–244.
 53. Verhulst NO, Mbadi PA, Kiss GB, Mukabana WR, van Loon JJ, et al. (2011) Improvement of a synthetic lure for *Anopheles gambiae* using compounds produced by human skin microbiota. *Malar J* 10: 28.
 54. Smallegange RC, Bukovinszkyne-Kiss G, Otieno B, Mbadi PA, Takken W, et al. (2012) Identification of candidate volatiles that affect the behavioural response of the malaria mosquito *Anopheles gambiae sensu stricto* to an active kairomone blend: laboratory and semi-field assays. *Physiol Entomol* 37: 60–71.
 55. Mathew N, Ayyanar E, Shanmugavelu S, Muthuswamy K (2013) Mosquito attractant blends to trap host seeking *Aedes aegypti*. *Parasitol Res* 112: 1305–1312.
 56. Mboera LE, Takken W, Mdira KY, Pickett JA (2000) Sampling gravid *Culex quinquefasciatus* (Diptera: Culicidae) in Tanzania with traps baited with synthetic oviposition pheromone and grass infusions. *J Med Entomol* 37: 172–176.
 57. Leal WS, Barbosa RM, Xu W, Ishida Y, Syed Z, et al. (2008) Reverse and conventional chemical ecology approaches for the development of oviposition attractants for *Culex* mosquitoes. *PLoS ONE* 3: e3045.
 58. Millar JG, Chaney JD, Mulla MS (1992) Identification of oviposition attractants for *Culex quinquefasciatus* from fermented Bermuda grass infusions. *J Am Mosq Control Assoc* 8: 11–17.

Chapter 3

Experience-dependent olfactory behaviors of the parasitic nematode

Heligmosomoides polygyrus

RESEARCH ARTICLE

Experience-dependent olfactory behaviors of the parasitic nematode *Heligmosomoides polygyrus*

Felicitas Ruiz¹, Michelle L. Castelletto¹, Spencer S. Gang², Elissa A. Hallem^{1,2*}

1 Department of Microbiology, Immunology, and Molecular Genetics, University of California, Los Angeles, Los Angeles, California, United States of America, **2** Molecular Biology Institute, University of California, Los Angeles, Los Angeles, California, United States of America

* ehallem@ucla.edu



Abstract

Parasitic nematodes of humans and livestock cause extensive disease and economic loss worldwide. Many parasitic nematodes infect hosts as third-stage larvae, called iL3s. iL3s vary in their infection route: some infect by skin penetration, others by passive ingestion. Skin-penetrating iL3s actively search for hosts using host-emitted olfactory cues, but the extent to which passively ingested iL3s respond to olfactory cues was largely unknown. Here, we examined the olfactory behaviors of the passively ingested murine gastrointestinal parasite *Heligmosomoides polygyrus*. *H. polygyrus* iL3s were thought to reside primarily on mouse feces, and infect when mice consume feces containing iL3s. However, iL3s can also adhere to mouse fur and infect orally during grooming. Here, we show that *H. polygyrus* iL3s are highly active and show robust attraction to host feces. Despite their attraction to feces, many iL3s migrate off feces to engage in environmental navigation. In addition, *H. polygyrus* iL3s are attracted to mammalian skin odorants, suggesting that they migrate toward hosts. The olfactory preferences of *H. polygyrus* are flexible: some odorants are repulsive for iL3s maintained on feces but attractive for iL3s maintained off feces. Experience-dependent modulation of olfactory behavior occurs over the course of days and is mediated by environmental carbon dioxide (CO₂) levels. Similar experience-dependent olfactory plasticity occurs in the passively ingested ruminant-parasitic nematode *Haemonchus contortus*, a major veterinary parasite. Our results suggest that passively ingested iL3s migrate off their original fecal source and actively navigate toward hosts or new host fecal sources using olfactory cues. Olfactory plasticity may be a mechanism that enables iL3s to switch from dispersal behavior to host-seeking behavior. Together, our results demonstrate that passively ingested nematodes do not remain inactive waiting to be swallowed, but rather display complex sensory-driven behaviors to position themselves for host ingestion. Disrupting these behaviors may be a new avenue for preventing infections.

OPEN ACCESS

Citation: Ruiz F, Castelletto ML, Gang SS, Hallem EA (2017) Experience-dependent olfactory behaviors of the parasitic nematode *Heligmosomoides polygyrus*. PLoS Pathog 13(11): e1006709. <https://doi.org/10.1371/journal.ppat.1006709>

Editor: Simon A Babayan, University of Glasgow, UNITED KINGDOM

Received: February 7, 2017

Accepted: October 24, 2017

Published: November 30, 2017

Copyright: © 2017 Ruiz et al. This is an open access article distributed under the terms of the [Creative Commons Attribution License](https://creativecommons.org/licenses/by/4.0/), which permits unrestricted use, distribution, and reproduction in any medium, provided the original author and source are credited.

Data Availability Statement: All relevant data are within the paper and its Supporting Information files.

Funding: This work was supported by a National Institutes of Health New Innovator Award (1DP2DC014596) to EAH. FR is a UCLA Center for Academic & Research Excellence (CARE) Scholar, and was supported by National Institute of General Medical Sciences grant R25GM055052 to T. Hasson. SSG was supported by a Microbial Pathogenesis Training Grant from the National

Institute of Allergy and Infectious Diseases (AI007323). EAH is a MacArthur Fellow and Howard Hughes Medical Institute Faculty Scholar. The funders had no role in study design, data collection and analysis, decision to publish, or preparation of the manuscript.

Competing interests: The authors have declared that no competing interests exist.

Author summary

Many parasitic nematodes infect by passive ingestion when the host consumes food, water, or feces containing infective third-stage larvae (iL3s). Passively ingested nematodes that infect humans cause severe gastrointestinal distress and death in endemic regions, and those that infect livestock are a major cause of production loss worldwide. Because these parasites do not actively invade hosts but instead rely on being swallowed by hosts, it has been assumed that they show only limited sensory responses and do not engage in host-seeking behaviors. Here, we investigate the olfactory behaviors of the passively ingested murine parasite *Heligmosomoides polygyrus* and show that this assumption is incorrect; *H. polygyrus* iL3s show robust attraction to a diverse array of odorants found in mammalian skin, sweat, and feces. Moreover, the olfactory responses of *H. polygyrus* iL3s are experience-dependent: some odorants are repulsive to iL3s cultured on feces but attractive to iL3s removed from feces. Olfactory plasticity is also observed in the ruminant parasite *Haemonchus contortus*, and may enable iL3s to disperse in search of new hosts or host fecal sources. Our results suggest that passively ingested nematodes use olfactory cues to navigate their environments and position themselves where they are likely to be swallowed. By providing new insights into the olfactory behaviors of these parasites, our results may enable the development of new strategies for preventing infections.

Introduction

Passively ingested gastrointestinal parasitic nematodes of humans and livestock are a significant health and economic problem. Human-infective nodular worms in the genus *Oesophagostomum* are a growing health concern in endemic regions of Africa, where they can cause abdominal pain, weight loss, diarrhea, and death [1–3]. Passively ingested parasites of livestock result in decreased production and economic loss worldwide. For example, *Haemonchus contortus* is an important parasite of ruminants that causes gastrointestinal distress, anemia, edema, and death in livestock [4]. In the United States alone, over 2.7 million goats and 2.6 million sheep are infected with *H. contortus* [5]. Infections with these parasites can be cleared using anthelmintic drugs, but frequent administration has led to increased drug resistance [6–9]. Although the host immune response to infection with passively ingested nematodes is well-studied [10–12], remarkably little is known about the behaviors of the parasites themselves. A better understanding of the behaviors exhibited by the environmental life stages of these parasites could facilitate the development of new strategies for preventing infections of humans and livestock, such as the use of targeted traps or repellents.

Parasitic nematodes that actively invade hosts by skin penetration are known to engage in sensory-driven host seeking [13]. For example, the human hookworms *Ancylostoma duodenale* and *Necator americanus*, and the dog hookworm *Ancylostoma caninum*, are relatively inactive in the absence of sensory stimuli but show increased activity in the presence of heat, CO₂, and/or skin extract [14–16]. Hookworms also migrate robustly toward a heat source [14, 17]. The human, non-human primate, and canine threadworm *Strongyloides stercoralis*, and the rat parasites *Strongyloides ratti* and *Nippostrongylus brasiliensis*, also respond robustly to host-emitted sensory cues. They are active in the absence of sensory stimuli [18], and show robust attraction to a wide variety of odorants emitted by human skin and sweat [18–20]. *S. ratti* is also known to be attracted to blood serum, and *S. stercoralis* to blood serum, sweat, and heat [19, 21, 22].

The sensory behaviors of passively ingested nematodes are much less understood. Some passively ingested worms are capable of responding to environmental sensory cues such as

temperature, humidity, and odorants [13]. For example, *H. contortus* uses temperature and humidity cues to migrate vertically through grass in response to changes in environmental conditions [23, 24]. Because passively ingested worms do not actively invade hosts, it has often been assumed that they do not host seek and do not respond to host-emitted sensory cues. However, we recently showed that *H. contortus* is attracted to some host-emitted odorants, raising the possibility that it can use olfactory cues to position itself in the vicinity of potential hosts [18]. Since many hosts develop immunity to passively ingested worms following repeated infection [25, 26], behaviors that expose these parasites to new hosts may be important for parasite propagation.

Here, we use the passively ingested gastrointestinal murine parasite *H. polygyrus* (also called *H. bakeri* [27, 28]) as a model system for studying the sensory behaviors of passively ingested gastrointestinal nematodes, and for testing the hypothesis that passively ingested nematodes engage in host seeking. As a mouse parasite, *H. polygyrus* is one of the only passively ingested nematodes that can be easily maintained in the lab [29, 30]. *H. polygyrus* is only infective as developmentally arrested iL3s, which are analogous to *Caenorhabditis elegans* dauers (S1 Fig) [31]. *H. polygyrus* iL3s were thought to primarily reside in host feces and infect when mice, which are coprophagic, eat infested feces [32, 33]. However, *H. polygyrus* iL3s can also attach to mouse fur and be ingested during grooming [34]. *H. polygyrus* iL3s were previously shown to nictate [33, 34], a behavior where the iL3 stands on its tail and waves its head [13], which may increase the probability of being swallowed during coprophagy or of becoming attached to mouse fur [34]. Once inside the host, the nematodes grow to adulthood and reproduce in the host intestine. *H. polygyrus* eggs then exit the host in feces and develop there into iL3s capable of infecting new hosts.

The fact that *H. polygyrus* develops on feces and infects mice from feces raises the question of whether *H. polygyrus* iL3s engage in environmental navigation using either host-emitted or environmental sensory cues, or whether they simply remain on feces and wait to be ingested. While this question had not been investigated thoroughly, *H. polygyrus* iL3s were previously found to be attracted to mouse urine and skin lipids, suggesting they are capable of responding to at least some host sensory cues [34]. However, the extent to which *H. polygyrus* iL3s engage in sensory behaviors that increase the likelihood that they will be swallowed by hosts remained unclear.

To address this question, we conducted a large-scale quantitative analysis of the unstimulated and odor-stimulated behaviors of *H. polygyrus*. We found that *H. polygyrus* iL3s were active in the absence of odor stimulation. In addition, they were attracted to host fecal odor. While they showed robust attraction to fresh feces, they showed reduced attraction to aged feces and ultimately migrated off their original fecal source to engage in environmental navigation. *H. polygyrus* iL3s were attracted to skin odorants as well as fecal odorants, suggesting that they are capable of migrating toward hosts as well as new host fecal sources. In addition, *H. polygyrus* iL3s showed experience-dependent olfactory plasticity, such that some host-emitted odorants were repulsive to iL3s cultured on feces but attractive to iL3s cultured off feces. Olfactory plasticity was also observed in the ruminant parasite *H. contortus*, and may be a general mechanism that enables passively ingested iL3s to shift from dispersal behavior to host-seeking behavior. Our results suggest that passively ingested nematodes disperse from feces and engage in host seeking to position themselves where they are likely to be ingested by new hosts.

Results

H. polygyrus iL3s are active in the absence of sensory stimulation

Parasitic nematodes are known to vary in their environmental navigation strategies: some are cruisers that actively navigate toward hosts; some are ambushers that are less active and

primarily attach to passing hosts; and some use an intermediate strategy [13]. To gain insight into the movement strategy used by *H. polygyrus*, we first examined the unstimulated movement of *H. polygyrus* iL3s, and compared their movement to that of *S. stercoralis* and *S. ratti* iL3s, which are known to be cruisers [18]. Using a dispersal assay in which iL3s were allowed to migrate on an agar surface in the absence of applied sensory stimulation for 1 hour, we found that *H. polygyrus* iL3s and *S. ratti* iL3s dispersed to a similar extent, whereas *S. stercoralis* iL3s dispersed more than either rodent parasite (Fig 1A). These results demonstrate that *H. polygyrus* iL3s are active in the absence of sensory stimulation and are capable of exhibiting a movement strategy resembling that of a cruiser. The increased movement of *S. stercoralis* iL3s relative to *H. polygyrus* and *S. ratti* iL3s may reflect the larger habitats of humans relative to nesting rodents [18]; since nesting rodents spend more time near their fecal deposits than do humans, non-human primates, and dogs, *S. stercoralis* iL3s may need to disperse farther into the environment to successfully locate a host.

Dispersal behavior reflects both crawling speed and other parameters such as crawling trajectory and tendency to pause during crawling. To gain more insight into the navigational strategy used by *H. polygyrus* iL3s, we tracked their crawling speed using automated worm tracking [35]. We found that *H. polygyrus* iL3s crawled more slowly than *S. ratti* iL3s, while *S. stercoralis* iL3s crawled much more rapidly than the rodent parasites (Fig 1B). The ability of *H. polygyrus* iL3s to disperse to the same extent as *S. ratti* iL3s despite their slower crawling speed suggests that *H. polygyrus* iL3s exhibit more linear and/or continuous movement than *S. ratti* iL3s.

We also evaluated the nictation behavior of *H. polygyrus*. Many skin-penetrating and passively ingested iL3s engage in nictation, a common ambushing behavior, as a means of increasing host contact. By standing up on a surface, nictating iL3s are more likely to touch and then transfer onto a passing host, or to be swallowed by a foraging host [13]. We assayed the nictation behavior of *H. polygyrus*, and compared it to that of *S. ratti* and *S. stercoralis*, using “micro-dirt” agar chips with near-microscopic pillars as an artificial dirt substrate (S2 Fig [36]). The pillars on the agar surface minimize surface tension, allowing the iL3s to stand. We found that all three of the species showed similarly low nictation frequencies: only ~20–30% of the tested iL3s nictated during the assay period (Fig 1C). The low nictation frequencies of *S. ratti* and *S. stercoralis* are consistent with a cruising navigational strategy [18]. The similarly low nictation frequency of *H. polygyrus*, combined with its active crawling behavior, suggests that it also behaves more like a cruiser than an ambusher. These results demonstrate that passively ingested iL3s do not remain inactive waiting to be swallowed by passing hosts. Rather, like skin-penetrating iL3s, they engage in environmental navigation.

H. polygyrus iL3s are attracted to host feces

If passively ingested iL3s utilize active strategies to position themselves in optimal locations for host ingestion, one strong prediction is that the species that infect coprophagic hosts (*e.g.*, mice) will be attracted to host feces. We examined the response of *H. polygyrus* iL3s to fresh fecal odor using a chemotaxis assay in which the iL3s could smell but not make contact with the feces. We found that *H. polygyrus* iL3s were strongly attracted to fresh mouse feces (Fig 2A and 2B). Moreover, they preferred mouse feces to gerbil or rabbit feces (Fig 2B and 2C), indicating that they can distinguish host from non-host feces. By contrast, *S. stercoralis* and *S. ratti* iL3s were neutral to host feces (Fig 2A) [18]. The different responses of *H. polygyrus* and *Strongyloides* iL3s to fecal odor are understandable in the context of their different lifestyles. Although the pre-infective larvae of both *H. polygyrus* and *Strongyloides* inhabit host feces, *H. polygyrus* iL3s can infect hosts from feces while skin-penetrating iL3s must migrate off feces

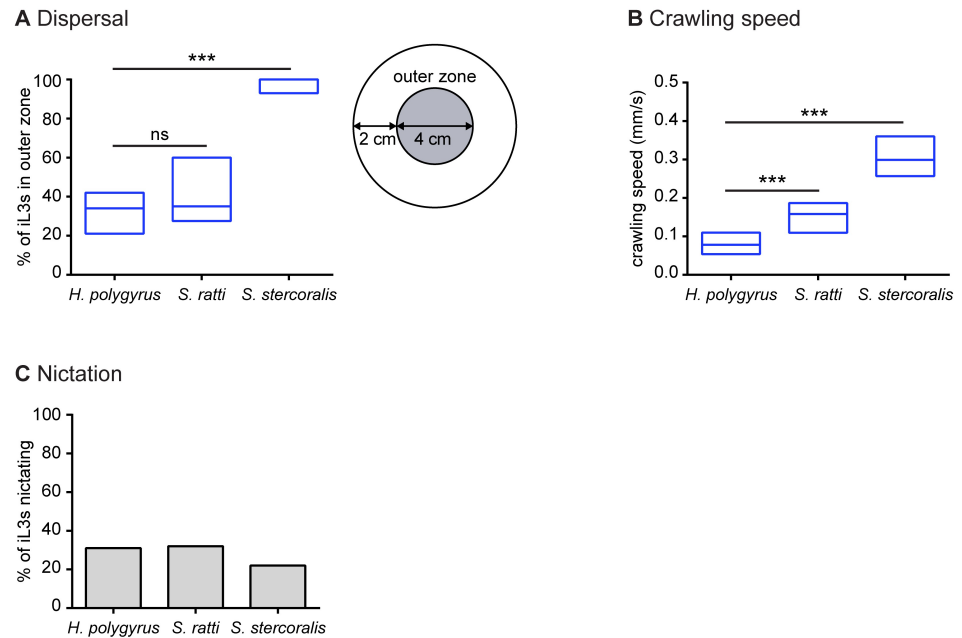


Fig 1. Navigational strategies of *H. polygyrus* in comparison to those of *S. ratti* and *S. stercoralis*. **A.** Dispersal behavior across species. iL3s were placed at the center of an agar plate and allowed to crawl freely for 1 hour in the absence of applied sensory stimuli. The percentage of iL3s in the outer zone, defined as the region of the plate outside a 4-cm-diameter circle (right), was determined. *H. polygyrus* and *S. ratti* iL3s dispersed to a similar extent, while *S. stercoralis* iL3s dispersed to a greater extent. *** $p < 0.001$, Kruskal-Wallis test with Dunn's post-test. $n = 9-11$ trials for each species and condition. **B.** Crawling speed across species. *H. polygyrus* iL3s crawled more slowly than *S. ratti* and *S. stercoralis* iL3s. *** $p < 0.001$, one-way ANOVA with Holm-Sidak's post-test. $n = 23-31$ iL3s per species. For **A-B**, graphs show medians and interquartile ranges. **C.** Nictation frequencies were similar across species ($p = 0.65$, chi-square test). $n = 22-70$ iL3s per species. Data for *S. ratti* and *S. stercoralis* are from Castelletto *et al.*, 2014 [18].

<https://doi.org/10.1371/journal.ppat.1006709.g001>

and onto host skin [13, 30]. Thus, attraction to host feces would likely be ecologically advantageous for *H. polygyrus* iL3s but not *Strongyloides* iL3s. In addition, we found that *H. polygyrus* iL3 were more attracted to fresh feces than aged feces (Fig 2D), suggesting that the iL3s use olfaction to identify favorable fecal sources. In contrast, they did not show a preference for feces from uninfected versus infected hosts (Fig 2D), suggesting that they are attracted to fresh host feces regardless of the infection status of the host. Attraction of *H. polygyrus* iL3s to fecal odor may cause some of the iL3s on a fresh fecal source to remain there, and may draw iL3s from fecal sources that have become suboptimal due to age, desiccation, or other conditions.

H. polygyrus iL3s disperse from feces to engage in environmental navigation

The robust attraction of *H. polygyrus* iL3s to fecal odor raised the question of whether the iL3s leave feces under normal conditions. To address this question, we performed two different fecal dispersal assays, the first to assess short-term dispersal over the course of hours and the second to assess long-term dispersal over the course of days. In the short-term dispersal assay, iL3s were placed on fresh feces in the center of an agar surface. The frequency with which the

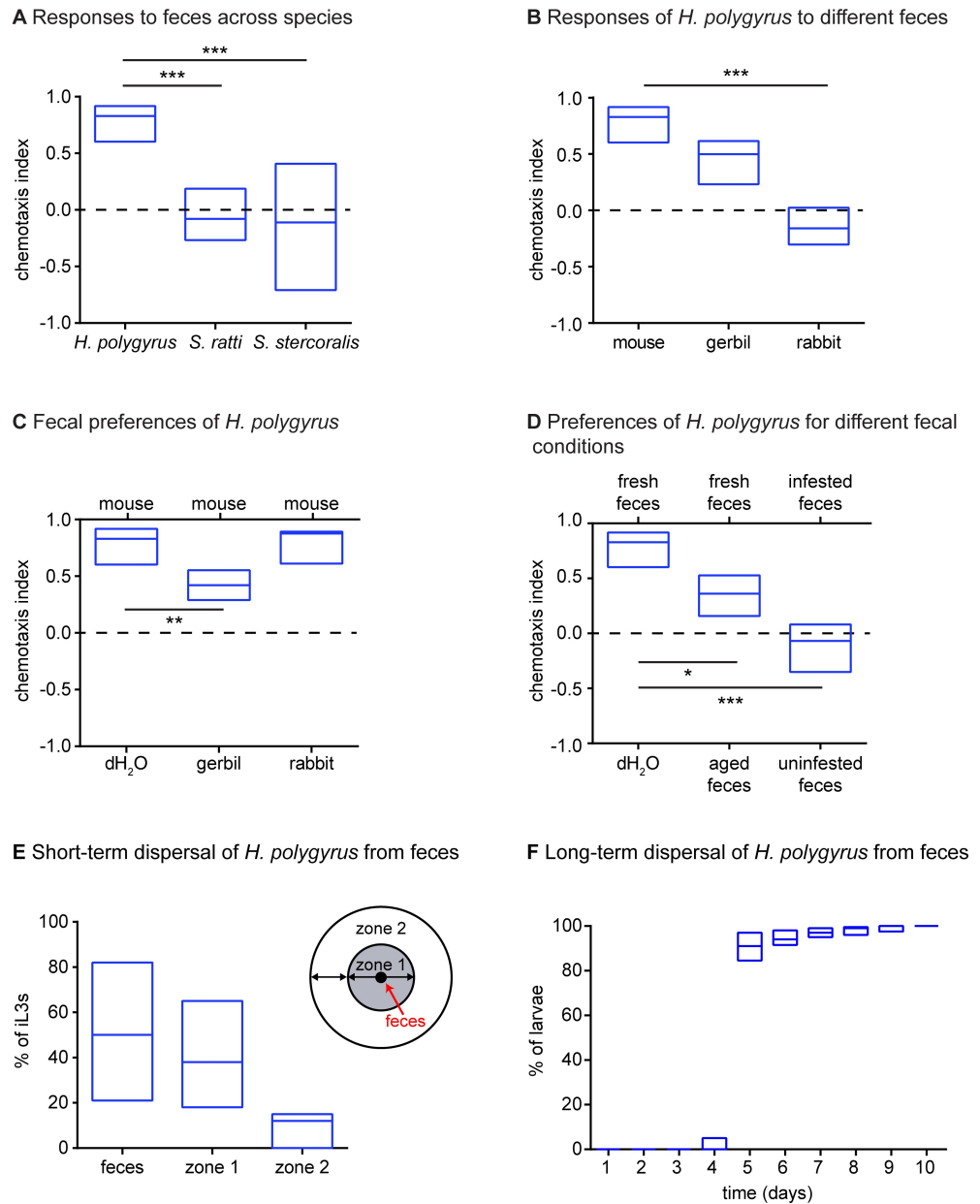


Fig 2. *H. polygyrus* iL3s are attracted to host feces. **A.** *H. polygyrus* iL3s were attracted to mouse feces. By contrast, *S. ratti* and *S. stercoralis* iL3s were not attracted to the feces of their hosts (rat and dog, respectively). *** $p < 0.001$, Kruskal-Wallis test with Dunn's post-test. $n = 12-14$ trials for each species. Data for *S. ratti* and *S. stercoralis* are from Castelletto *et al.*, 2014 [18]. **B-C.** *H. polygyrus* iL3s respond differently to feces from different animals (**B**), and prefer mouse feces to gerbil or rabbit feces (**C**). Labels above and below each box in **C** indicate the opposing cues in the fecal preference assay. ** $p < 0.01$, *** $p < 0.001$, Kruskal-Wallis test with Dunn's post-test. $n = 10-14$ trials per condition. **D.** *H. polygyrus* iL3s prefer fresh mouse feces to aged mouse feces, but

cannot distinguish mouse feces from infected animals versus uninfected animals. * $p < 0.05$, *** $p < 0.001$, Kruskal-Wallis test with Dunn's post-test. $n = 11$ – 14 trials per condition. **E.** In a short-term dispersal assay, *H. polygyrus* iL3s leave feces to engage in host seeking. iL3s were placed on fresh mouse feces and allowed to crawl freely for 1 hour. The number of iL3s either on the feces, in zone 1, or in zone 2 (right) was then quantified. Approximately half of the iL3 population migrated off of the feces. $n = 11$ trials, with 15–40 iL3s per trial. **F.** In a long-term dispersal assay, nearly all *H. polygyrus* iL3s eventually left their original fecal pellet to engage in host seeking. The cumulative percentage of nematodes that had migrated off of their original fecal pellet was quantified each day over the course of 10 days. $n = 13$ trials. For all graphs, lines indicate medians and interquartile ranges.

<https://doi.org/10.1371/journal.ppat.1006709.g002>

iL3s migrated off the feces and onto the agar was then quantified. We found that on average, 50% of the iL3 population left the fresh feces; in some trials, over 80% of the iL3s left the feces (Fig 2E). These results demonstrate that even for iL3s on fresh feces, which are presumably a favorable fecal source, a substantial portion of the iL3 population migrates off of the feces and engages in environmental navigation.

In the long-term dispersal assay, a fresh fecal pellet from an infected animal was collected, and one-half of the pellet was placed in the center of an agar surface. The frequency with which the nematodes migrated off of the feces and onto the agar was then quantified each day for a period of 10 days. Thus, this assay examined *H. polygyrus* dispersal in the more natural context of fecal aging. We found that nearly all of the nematodes remained on the feces until day 5. On day 5, by which time the nematodes had developed into iL3s [29], over 80% of the nematodes migrated off the feces (Fig 2F). By day 10, nearly 100% of the nematodes had migrated off of the feces (Fig 2F). In the same assay, we also examined nictation behavior and found that nictation occurs primarily on day 5 (S3 Fig), at the time when the majority of the population migrates off of the feces (Fig 2F). Together, these results argue against the possibility that some members of the iL3 population are ambushers while others are cruisers, and suggest instead that nearly all *H. polygyrus* iL3s ultimately engage in cruising behavior.

H. polygyrus iL3s are attracted to mammalian-derived odorants

Our results show that *H. polygyrus* iL3s will eventually leave their original fecal source and migrate toward new fecal sources to position themselves for ingestion during coprophagy. However, *H. polygyrus* iL3s can infect during grooming [34], raising the question of whether they also migrate toward hosts by detecting host-emitted olfactory cues. To investigate this possibility, we examined the responses of *H. polygyrus* iL3s to a large panel of odorants that included compounds found in mammalian skin and sweat using a chemotaxis assay (S4 Fig) [18]. We found that *H. polygyrus* iL3s showed robust attraction to 6 of the 35 odorants tested: 2-butanone; 2,3-butanedione; geranyl acetone; 3-methyl-1-butanol; 2-methyl-1-butanol; and 3-heptanol (Fig 3). In contrast, CO₂ was repulsive for *H. polygyrus* iL3s (Fig 3). All of the attractive odorants are emitted from mammalian skin, feces, and/or urine [18, 37–41]. Notably, 2-methyl-1-butanol, 3-methyl-1-butanol, and geranyl acetone are present in skin microbiota [42, 43] and are known attractants for skin-penetrating nematodes [18]. Attraction to these odorants could drive migration of *H. polygyrus* iL3s toward hosts.

To gain insight into how the olfactory preferences of *H. polygyrus* iL3s differ from those of other iL3s that engage in environmental navigation, we compared the odor-driven behaviors of *H. polygyrus* to those of 7 other nematode species: the skin-penetrating human-parasitic nematode *S. stercoralis*, the skin-penetrating rat-parasitic nematodes *S. ratti* and *N. brasiliensis*, the passively ingested ruminant-parasitic nematode *H. contortus*, the actively invading entomopathogenic nematodes *Heterorhabditis bacteriophora* and *Steinernema carpocapsae*, and the free-living bacterivorous nematode *C. elegans*. This comparison revealed that *H. polygyrus* responds differently to the odorant panel than the other species (S5A Fig), consistent with

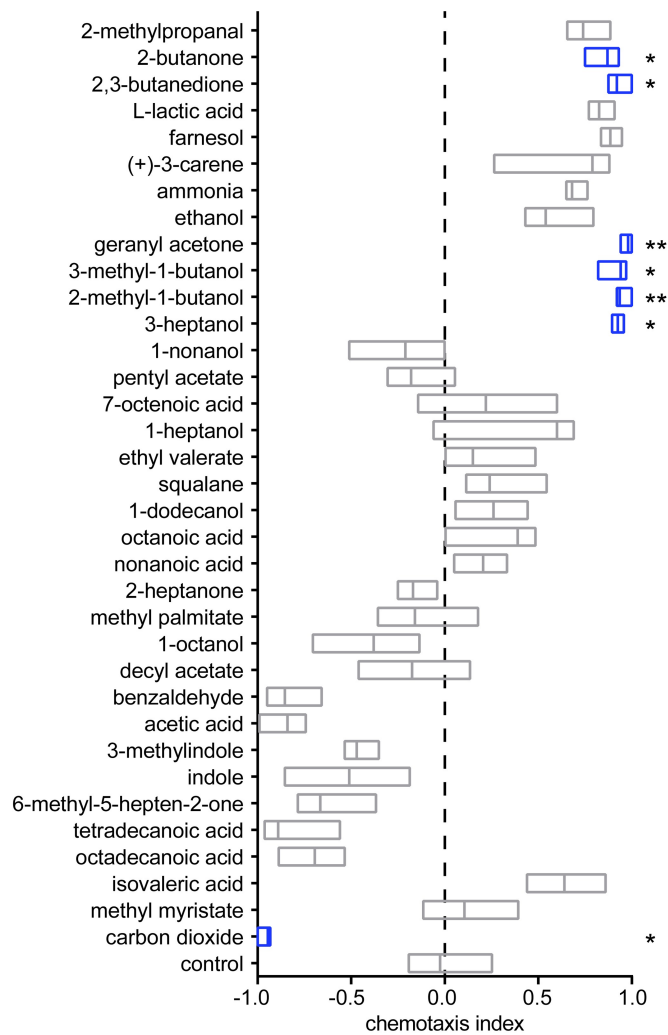


Fig 3. *H. polygyrus* iL3s are attracted to mammalian odorants. *H. polygyrus* iL3s were attracted to 6 of 35 tested odorants and were repelled by CO₂ in a chemotaxis assay. * $p < 0.05$ and ** $p < 0.01$ relative to the paraffin oil control, Kruskal-Wallis test with Dunn's post-test. Significant responses are highlighted in blue. $n = 8-28$ trials for each condition. Lines indicate medians and interquartile ranges.

<https://doi.org/10.1371/journal.ppat.1006709.g003>

previous studies demonstrating that parasitic nematodes show species-specific olfactory preferences [18, 44, 45]. Moreover, cluster analysis of the 8 species based on their olfactory preferences revealed that parasitic nematodes that infect the same hosts have more similar olfactory preferences than parasitic nematodes that infect different hosts (S5B Fig) [18, 44, 45]. In contrast, parasitic nematodes that infect different hosts but share the same mode of infection do not respond similarly to odorants. In particular, *H. polygyrus* and *H. contortus* are both

passively ingested but infect different hosts, and their olfactory preferences are dissimilar (S5B Fig). Thus, olfactory preferences appear to be determined primarily by host range rather than infection mode. The fact that distantly related species that target the same host respond similarly to odorants strongly suggests that parasitic nematode olfactory behavior has evolved to mediate specific parasite-host interactions.

The navigational strategies of *H. polygyrus* iL3s are shaped by their recently experienced environment

iL3s that have migrated off feces likely face a greater ethological drive to search for new hosts or fecal sources than iL3s that have remained on feces. We therefore wondered whether iL3s that have migrated off feces might exhibit different behaviors than iL3s on feces. To test this possibility, we compared the unstimulated migration of iL3s cultivated on feces to those of iL3s that had been removed from feces and maintained in dH₂O for 1 week. We found that the off-feces iL3s dispersed to a greater extent than the on-feces iL3s (Fig 4A), demonstrating that the unstimulated activity of *H. polygyrus* iL3s is subject to experience-dependent modulation. The greater dispersal of off-feces iL3s was not due to changes in crawling speed (Fig 4B); thus, the difference in dispersal reflects a difference in navigational strategy rather than motility. In addition, the nictation rate of on-feces vs. off-feces iL3s was unchanged (Fig 4C), demonstrating that removal from feces results in a specific change in crawling behavior. The increased dispersal of off-feces iL3s likely increases the probability of encountering a new host or fecal source.

H. polygyrus iL3s show experience-dependent olfactory plasticity

To further elucidate the effects of recently experienced environment on *H. polygyrus* behavior, we compared the olfactory preferences of on-feces vs. off-feces iL3s to a subset of mammalian odorants. The odorant panel was selected to include attractive, neutral, and repulsive odorants. We found that on-feces and off-feces iL3s responded differently to 2 of 8 tested odorants: CO₂ and benzaldehyde. Both odorants were repulsive for iL3s on feces but attractive for iL3s off feces (Fig 5A). For both on-feces and off-feces iL3s, CO₂-response valence, *i.e.* whether CO₂ was repulsive or attractive, was consistent across concentrations (S6 Fig). CO₂ is a critical host cue for many parasites, including many parasitic nematodes [13]; it is present at high concentrations in both exhaled breath and feces. Benzaldehyde is found in skin, breath, urine, and feces [18]. Thus, the olfactory responses of *H. polygyrus* iL3s to some host-associated odorants are subject to experience-dependent modulation as a result of recently experienced environmental conditions.

We then examined the relationship between cultivation environment and sensory behavior in more detail by investigating the time course of the change in CO₂- and benzaldehyde-response valence. We found that CO₂-response valence changed gradually over the course of days when iL3s were removed from feces (Fig 5B). Moreover, culturing iL3s under high CO₂ conditions prevented the shift in CO₂-response valence following removal from feces. While iL3s cultured off feces at ambient CO₂ (~0.04% CO₂ [46]) were attracted to CO₂, iL3s cultured off feces at high CO₂ (2.5% CO₂) were repelled by CO₂ (Fig 5C). Thus, CO₂-response valence is regulated by environmental CO₂ levels. Benzaldehyde-response valence also changed gradually over the course of days upon removal from feces and was also determined by environmental CO₂ levels (Fig 5D and 5E). These results suggest that the level of environmental CO₂ acts as a general regulator of olfactory behavior. Given that feces emit high levels of CO₂ [39], *H. polygyrus* iL3s may use environmental CO₂ levels to signal the presence or absence of feces, with the result that exposure to high CO₂ levels mimics the effects of exposure to feces.

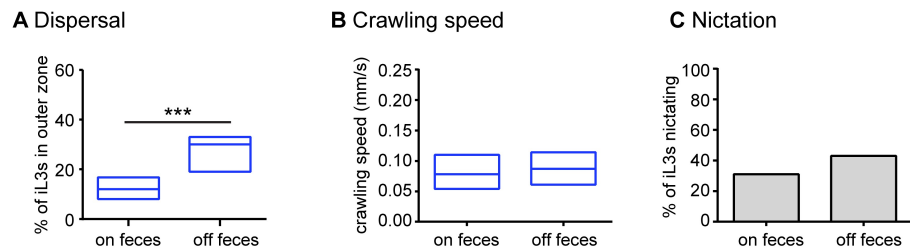


Fig 4. The navigational strategies of *H. polygyrus* are experience-dependent. **A.** Dispersal behavior of iL3s cultured on vs. off feces. *H. polygyrus* iL3s cultured off feces dispersed to a greater extent than *H. polygyrus* iL3s cultured on feces. *** $p < 0.001$, Mann-Whitney test. $n = 17$ – 36 trials per condition. Dispersal was assayed after 10 minutes. The outer zone is as defined in Fig 1A. **B.** Crawling speed did not differ for iL3s cultured on vs. off feces ($p = 0.82$, Mann-Whitney test). $n = 23$ – 31 iL3s per condition. For A–B, graphs show medians and interquartile ranges. **C.** Nictation frequency did not differ for iL3s cultured on vs. off feces ($p = 0.21$, Fisher's exact test). Graph shows the percentage of animals that nictated for each condition. Data were analyzed as a contingency table. $n = 61$ – 70 iL3s for each condition. For **A–C**, nematodes were allowed to develop on feces for 7 days until they reached the iL3 stage. The "on-feces" iL3s were then cultured on feces for 7 additional days, while the "off-feces" iL3s were cultured in dH_2O for 7 days. iL3s were tested on day 14.

<https://doi.org/10.1371/journal.ppat.1006709.g004>

Experience-dependent olfactory plasticity may be a mechanism that enables iL3s on feces to disperse from the feces, and iL3s that have been off feces for a prolonged period to instead migrate toward new hosts or fresh fecal sources.

H. contortus iL3s also show experience-dependent olfactory plasticity

Our finding that *H. polygyrus* iL3s exhibit experience-dependent olfactory plasticity raised the question of whether this behavior is unique to *H. polygyrus* or shared with other parasitic nematode species. To distinguish between these possibilities, we examined the CO_2 -evoked behaviors of *H. contortus*, *S. stercoralis*, and the skin-penetrating human-parasitic hookworm *Ancylostoma ceylanicum* cultured on versus off feces. We found that like *H. polygyrus* iL3s, *H. contortus* iL3s show experience-dependent plasticity in their response to CO_2 . In the case of *H. contortus*, CO_2 is neutral for iL3s cultured on feces but attractive for iL3s cultured off feces (Fig 6A). Since *H. contortus* iL3s are long-lived [47, 48], sometimes surviving in the environment for up to 8 months [48], we examined the CO_2 -evoked behavior of off-feces iL3s over the course of 5 weeks. We found that CO_2 changed from neutral to attractive after 1 week, and then remained attractive in subsequent weeks (Fig 6A). Thus, CO_2 remains a strong attractant for *H. contortus* iL3s that have been removed from feces for prolonged periods. Our results demonstrate that experience-dependent olfactory plasticity is not unique to *H. polygyrus*, but also occurs in other passively ingested nematodes. Experience-dependent modulation of CO_2 response may enable *H. contortus* iL3s to first migrate off feces and then navigate toward grazing hosts, which emit high concentrations of CO_2 in their exhaled breath.

In contrast to the passively ingested nematodes, the skin-penetrating nematodes tested did not show experience-dependent modulation of their CO_2 -evoked behavior. Both *S. stercoralis* iL3s and *A. ceylanicum* iL3s were repelled by CO_2 when cultured both on and off feces (Fig 6B and 6C). The lack of flexibility in their CO_2 -evoked behavior may reflect the fact that CO_2 attraction would likely not facilitate host finding by skin-penetrating worms, since very low levels of CO_2 are given off by the skin [49]. CO_2 avoidance may function as a dispersal mechanism to drive skin-penetrating iL3s off host feces; attraction to other sensory cues, such as skin and sweat odorants, may then drive the iL3s toward potential hosts [13]. Thus, the ability to

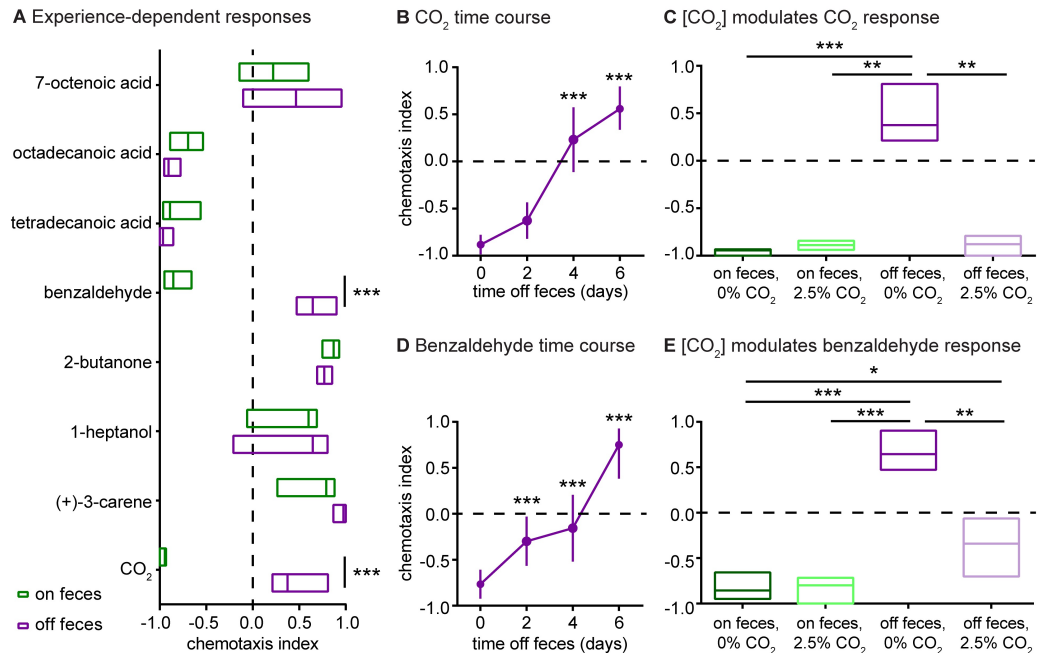


Fig 5. *H. polygyrus* iL3s exhibit experience-dependent olfactory plasticity. **A.** iL3s cultured on vs. off feces respond differently to a subset of odorants in a chemotaxis assay. Benzaldehyde and CO₂ were repulsive for on-feces iL3s but attractive for off-feces iL3s. ****p*<0.001, two-way ANOVA with Sidak's post-test. *n* = 8–28 trials for each condition. **B.** CO₂-response valence shifted from repulsive to attractive over the course of 6 days following removal from feces. Day 0 indicates the time of removal from feces. ****p*<0.001 relative to day 0, Kruskal-Wallis test with Dunn's post-test. *n* = 12–18 trials for each condition. **C.** Environmental CO₂ levels determine CO₂-response valence. iL3s cultured on feces at either ambient CO₂ ("0% CO₂") or high CO₂ ("2.5% CO₂") were repelled by 10% CO₂, iL3s cultured off feces at 0% CO₂ were attracted to 10% CO₂, and iL3s cultured off feces at 2.5% CO₂ were repelled by 10% CO₂. ***p*<0.01, ****p*<0.001, Kruskal-Wallis test with Dunn's post-test. *n* = 10–12 trials for each condition. **D.** Benzaldehyde-response valence shifted from repulsive to attractive over the course of 6 days following removal from feces. ****p*<0.001 relative to day 0, one-way ANOVA with Dunnett's post-test. *n* = 10–16 trials for each condition. **E.** Environmental CO₂ levels determine benzaldehyde-response valence. iL3s cultured on feces at either 0% CO₂ or 2.5% CO₂ were repelled by benzaldehyde, iL3s cultured off feces at 0% CO₂ were attracted to benzaldehyde, and iL3s cultured off feces at 2.5% CO₂ were slightly repelled by benzaldehyde. **p*<0.05, ***p*<0.01, ****p*<0.001, Kruskal-Wallis test with Dunn's post-test. *n* = 10–28 trials for each condition. Graphs show medians and interquartile ranges.

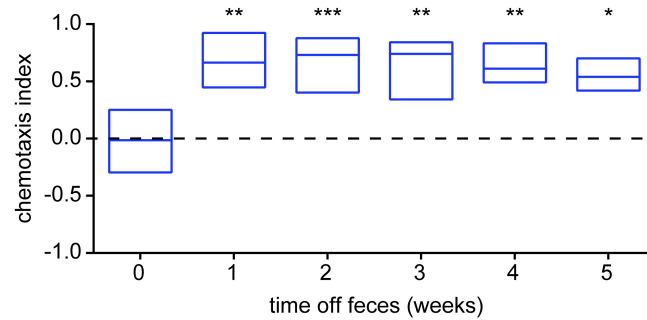
<https://doi.org/10.1371/journal.ppat.1006709.g005>

exhibit flexible responses to CO₂ may be a specific behavioral adaptation of passively ingested but not skin-penetrating nematodes.

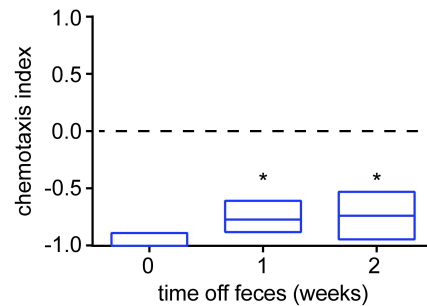
Discussion

Here we conducted the first large-scale quantitative behavioral analysis of *H. polygyrus* iL3s. We found that *H. polygyrus* iL3s were active even in the absence of sensory stimulation (Fig 1). These results argue against the classical notion that passively ingested iL3s remain stationary and wait to be swallowed, and suggest instead that these iL3s actively navigate their environments. We previously showed that *H. contortus* iL3s are less active than *S. ratti* and *S. stercoralis* iL3s [18]. However, the similar dispersal behaviors and nictation rates of *H. polygyrus* and *S. ratti* (Fig 1) suggest that some passively ingested nematodes are as active as skin-penetrating nematodes despite their passive mode of infection.

A *H. contortus* CO₂ response



B *S. stercoralis* CO₂ response



C *A. ceylanicum* CO₂ response

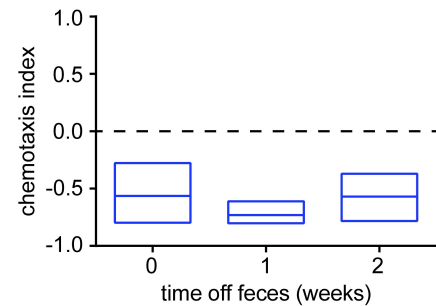


Fig 6. Passively ingested nematodes but not skin-penetrating nematodes show experience-dependent modulation of CO₂-response valence. **A.** Passively ingested *H. contortus* iL3s are neutral to CO₂ when cultured on feces, and is maintained for at least 5 weeks. Nematodes were allowed to develop on feces for at least 7 days. They were then either tested immediately, or stored in dH₂O for up to 5 weeks and then tested. The "on-feces" group included iL3s aged up to 9 weeks, confirming that CO₂ attraction occurred as a result of removal from feces rather than increased iL3 age. **p*<0.05, ***p*<0.01, ****p*<0.001, Kruskal-Wallis test with Dunn's post-test. *n* = 8–16 trials for each condition. **B-C.** Skin-penetrating *S. stercoralis* (**B**) and *A. ceylanicum* (**C**) iL3s do not show experience-dependent modulation of CO₂-response valence. Nematodes were allowed to develop on feces for 7 days (**B**) or 10 days (**C**) until they reached the iL3 stage. iL3s were then either tested immediately, stored in BU saline [64] for 7 days and then tested, or stored in BU saline for 14 days and then tested. CO₂ response was slightly attenuated in *S. stercoralis* iL3s cultured off feces, but did not shift from repulsion to attraction (**B**); CO₂ response was unchanged in *A. ceylanicum* iL3s cultured on vs. off feces (**C**). **p*<0.05, Kruskal-Wallis test with Dunn's post-test (**B**) or one-way ANOVA with Dunnett's post-test (**C**). *n* = 8–10 trials for each condition. Graphs show medians and interquartile ranges.

<https://doi.org/10.1371/journal.ppat.1006709.g006>

Our examination of the olfactory preferences of *H. polygyrus* iL3s revealed that they are attracted to fecal odor as well as mammalian skin and sweat odorants (Figs 2 and 3). These results suggest that passively ingested iL3s engage in odor-driven host seeking to position themselves near hosts or host feces, where they are likely to be ingested. Consistent with the attraction of *H. polygyrus* iL3s to both fecal odor and host odorants, *H. polygyrus* iL3s have been shown to infect hosts either from feces during coprophagy or from fur during grooming

[30, 32–34]. Thus, active migration toward new hosts or fecal sources may be a critical but often overlooked aspect of the environmental stage of the *H. polygyrus* life cycle.

The robust attraction of *H. polygyrus* iL3s to fecal odor could serve to keep some of the iL3s on favorable fecal sources, or to direct them away from suboptimal fecal sources toward more favorable sources. However, we found that even when iL3s are placed on fresh feces, which is presumably a favorable fecal source, approximately half of the population migrates off of the feces within an hour (Fig 2E). Moreover, we found that nearly all iL3s eventually leave their original fecal source to engage in environmental navigation (Fig 2F). These results suggest that all *H. polygyrus* iL3s are capable of engaging in environmental navigation, and that if they are not ingested with feces shortly after reaching the iL3 stage, they will leave their original fecal source and disperse into the environment. Once in the environment, they use olfactory cues to migrate toward hosts or new fecal sources (Fig 7).

At the population level, this behavioral flexibility may help to ensure maximal infection rates. Remaining on a known fecal source can in some cases be beneficial: if that fecal source is in or near a nest, the iL3s may encounter hosts by remaining in the nest. However, this behavioral strategy also carries risk: many mice forage and deposit feces far from their nests, in locations where the iL3s are less likely to encounter a mouse using a “sit-and-wait” strategy [34]. Under these circumstances, first dispersing from feces and then using host-emitted sensory cues to migrate toward new hosts or fecal sources is likely to be essential to continue the life cycle. Thus, maximal parasite survival may be achieved when iL3s that do not immediately encounter a host actively disperse in search of hosts. In future studies, it will be interesting to determine whether nematodes that exit the host early in an infection cycle show different dispersal behavior than nematodes that exit the host late in an infection cycle, or whether nematodes that emerge from hosts with a heavier worm burden show different dispersal behavior than nematodes that emerge from hosts with a lighter worm burden.

What is the mechanism that drives some iL3s to migrate off feces, and subsequently toward new hosts or fecal sources? We speculate that olfactory plasticity may function as this mechanism. We have shown that *H. polygyrus* iL3s display experience-dependent olfactory plasticity: some odorants are repulsive to iL3s that have been cultured on feces but attractive to iL3s that have been cultured off feces for a week (Fig 5). Repulsion of iL3s from odorants such as CO₂ and benzaldehyde, which are emitted by host feces [18, 39], may cause the iL3s to migrate off of their original fecal source and disperse into the environment. Once the iL3s have been in the environment for multiple days, these odorants become attractive, likely driving the iL3s toward new hosts or fecal sources.

The shift from repulsion to attraction for both CO₂ and benzaldehyde response is mediated by environmental CO₂ levels (Fig 5C and 5E). When iL3s are removed from feces but cultured in the presence of high CO₂, they remain repelled by both CO₂ and benzaldehyde. However, when iL3s are removed from feces and cultured at ambient CO₂, they become attracted to CO₂ and benzaldehyde. These results suggest that environmental CO₂ levels may be used as a proxy for the presence or absence of feces.

We found that like *H. polygyrus* iL3s, *H. contortus* iL3s show experience-dependent modulation of their CO₂-evoked behavior. *H. polygyrus* iL3s showed a shift in their CO₂ response from repulsive to attractive following removal from feces (Fig 5), while *H. contortus* iL3s showed a shift in their CO₂ response from neutral to attractive (Fig 6A). Thus, in both cases, CO₂ attraction is likely to be observed in nature in iL3s that have migrated off of feces and are engaging in environmental navigation. In contrast to the passively ingested nematodes tested, the skin-penetrating nematodes tested did not show experience-dependent modulation of their CO₂-evoked behavior (Fig 6B and 6C). Thus, experience-dependent plasticity based on the presence or absence of feces may be specific to passively ingested nematodes. The

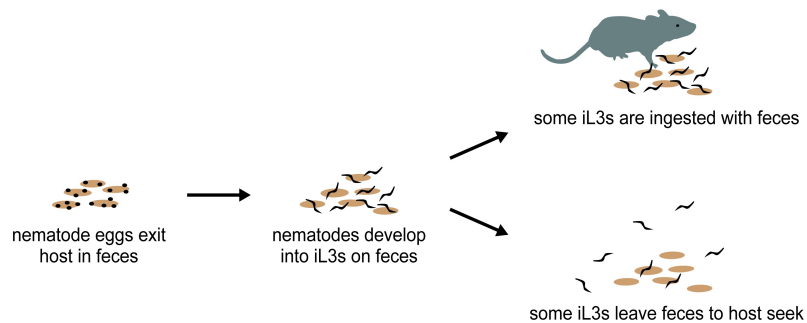


Fig 7. A model for host-seeking behavior in *H. polygyrus*. Nematode eggs exit the host in feces, and larvae develop on feces to the iL3 stage. iL3s either infect hosts from the feces on which they developed, or migrate off the feces and into the environment to search for hosts or new host fecal sources. Eventually, nearly all iL3s leave their original fecal source to engage in host seeking.

<https://doi.org/10.1371/journal.ppat.1006709.g007>

differences in CO₂-evoked behavior between passively ingested iL3s and skin-penetrating iL3s are consistent with their different ecologies. Skin-penetrating iL3s infect primarily via the skin, which emits low levels of CO₂ [49], so CO₂ attraction may not be beneficial for skin-penetrating iL3s regardless of their cultivation conditions. Passively ingested nematodes infect via the mouth, which emits high levels of CO₂ [50]. Thus, in the case of passively ingested nematodes, repulsive or neutral responses to CO₂ by iL3s on feces may initially drive them off feces, while subsequent attractive responses to CO₂ may drive them toward the mouths of respiring hosts. *H. contortus* is one of the most economically significant livestock parasites worldwide [5], and drug resistance resulting from repeated use of anthelmintic drugs is already a major challenge in combatting infections [9]. Our finding that the olfactory responses of *H. contortus* are experience-dependent could facilitate the development of odor-based traps or repellents that could be used in combination with grazing management interventions [51, 52] to prevent nematode infections.

The circuit mechanisms that drive experience-dependent valence changes in passively ingested nematodes remain to be determined. In *C. elegans*, CO₂-response valence is also subject to experience-dependent modulation: adults cultured at ambient CO₂ are repelled by CO₂, while adults cultured at high CO₂ are attracted to CO₂ [53]. Both CO₂ attraction and CO₂ repulsion by *C. elegans* are mediated by the BAG sensory neurons in the head and a group of downstream interneurons. The CO₂-evoked activity of these interneurons is subject to experience-dependent modulation, enabling them to generate opposite behavioral responses to CO₂ [53]. Since sensory neuroanatomy is generally conserved across nematode species [13], similar circuit mechanisms may operate in passively ingested parasitic nematodes to regulate CO₂-response valence.

The molecular mechanisms that drive experience-dependent valence changes in passively ingested nematodes are also not yet known. In *C. elegans*, CO₂-response valence is regulated by neuropeptide signaling [53]. However, CO₂-response valence in *C. elegans* changes over the course of hours [53], while CO₂-response valence in passively ingested parasitic nematodes changes over the course of days (Figs 5B and 6A). Thus, the valence change in parasitic nematodes could involve changes in gene expression and/or neuronal wiring, which occur on a slower timescale than neuropeptide signaling [54–59]. Elucidating the mechanisms that operate in passively ingested nematodes to control olfactory valence will require the development of genetic engineering techniques for these species, which have so far remained intractable to

molecular genetic manipulation [60]. Targeted mutagenesis using the CRISPR-Cas9 system has now been achieved in *Strongyloides* species [60–61], and may be applicable to other types of parasitic nematodes in the future.

Entomopathogenic nematodes and skin-penetrating nematodes also show olfactory plasticity, but in response to changes in their prior cultivation temperature [62]. In addition, the entomopathogenic nematode *Steinernema scapterisci* shows age-dependent olfactory plasticity in its response to CO₂: CO₂ changes from a repulsive cue in young iL3s to an attractive cue in older iL3s [62]. Thus, olfactory plasticity may be a general feature of parasitic nematode behavior that enables iL3s to modulate their sensory responses based on internal or external conditions so as to increase their chances of encountering a host.

Passively ingested nematodes comprise a group of human and livestock parasites whose behaviors have remained elusive. Increased drug resistance [6–9] necessitates the development of new strategies for their control. Our results suggest that passively ingested nematodes engage in robust and dynamic odor-driven host-seeking behaviors. A better understanding of these behaviors may lead to new strategies for preventing infections.

Materials and methods

Ethics statement

H. polygyrus was passaged in mice, *S. stercoralis* was passaged in gerbils, and *A. ceylanicum* was passaged in hamsters. All procedures and protocols were approved by the UCLA Office of Animal Research and Oversight (Protocol 2011-060-13B), which adheres to the standards of the AAALAC and the *Guide for the Care and Use of Laboratory Animals*.

Nematodes and mammalian hosts

Heligmosomoides polygyrus (also called *Heligmosomoides bakeri* [27]) was generously provided by Dr. Raffi Aroian (University of Massachusetts Medical School). *Strongyloides stercoralis* (UPD strain) was generously provided by Dr. James Lok (University of Pennsylvania), *Ancylostoma ceylanicum* (Indian strain, US National Parasite Collection Number 102954) was generously provided by Dr. John Hawdon (George Washington University), and *Haemonchus contortus* was generously provided by Dr. Anne Zajac (Virginia-Maryland College of Veterinary Medicine). Male or female C57BL/6 mice for propagation of *H. polygyrus* were obtained from the UCLA Division of Laboratory Animal Medicine Breeding Colony. Male Mongolian gerbils for propagation of *S. stercoralis* and male Syrian golden hamsters for propagation of *A. ceylanicum* were obtained from Envigo. *H. contortus* was not propagated in our laboratory.

Maintenance of *H. polygyrus* in mice

H. polygyrus was serially passaged in C57BL/6 male or female mice as described [30] and maintained on fecal-charcoal plates as described [18]. Briefly, mice were inoculated with ~150 iL3s administered in 100 μ L ddH₂O by oral gavage. Feces infested with *H. polygyrus* were collected between days 10 and 60 post-inoculation. Feces were obtained by placing mice overnight on wire cage bottoms above damp cardboard, and collecting the pellets from the cardboard the following morning. Fecal pellets were mixed with dH₂O and autoclaved charcoal granules to make fecal-charcoal plates. Plates were stored at room temperature until use. iL3s used for behavioral analysis were collected from fecal-charcoal plates using a Baermann apparatus [63]. iL3s cultured “on feces” were collected from fecal-charcoal plates on day 14 (with day 0 being the day of fecal collection) and tested immediately; iL3s cultured “off feces” were collected from fecal-charcoal plates on day 7, incubated in dH₂O for 7 days at room temperature, and

tested on day 14. For the odorant chemotaxis assays in Fig 3, iL3s were either collected from fecal-charcoal plates on days 7–14 and tested immediately or collected on days 7–14 and stored for up to 10 days in dH₂O at 4°C prior to testing (storage at 4°C in dH₂O is a standard cultivation condition for *H. polygyrus* [30]). In all cases where differences were observed following storage in dH₂O at 4°C, the data from iL3s stored at 4°C in dH₂O was excluded from the analysis. For the “off feces” time course in Fig 5, iL3s were collected from fecal-charcoal plates on day 7, incubated in dH₂O for the indicated number of days, and then tested. For assays involving iL3s cultured at 2.5% CO₂ either on or off feces, iL3s were collected from fecal-charcoal plates on day 7. iL3s for the on-feces condition were placed onto new fecal-charcoal plates containing autoclaved feces, stored in a CO₂ incubator with 2.5% CO₂ for 7 days, and collected from the fecal-charcoal plates using a Baermann apparatus immediately prior to testing. iL3s for the off-feces condition were incubated in dH₂O in a CO₂ incubator with 2.5% CO₂ for the indicated number of days and then tested.

Culturing of *H. contortus*

H. contortus was maintained on fecal-charcoal plates as described [18]. Plates were stored in an incubator at 23°C until use. iL3s used to test CO₂ response in Fig 6A were either cultured on fecal-charcoal plates for up to 9 weeks and then tested immediately; or removed from feces, stored in dH₂O for up to 5 weeks, and then tested. Notably, iL3s maintained on feces and tested immediately showed a neutral response to CO₂ regardless of their age, demonstrating that the CO₂ attraction of off-feces iL3s was due to their removal from feces and not their age.

Maintenance of *S. stercoralis* in gerbils

S. stercoralis was serially passaged in male Mongolian gerbils and maintained on fecal-charcoal plates as described [18]. Briefly, gerbils were inoculated with ~2,250 iL3s in 200 µL sterile PBS by subcutaneous injection. Feces infested with *S. stercoralis* were collected between days 14 and 45 post-inoculation. Feces were harvested and mixed with autoclaved charcoal granules to make fecal-charcoal plates as described above. Plates were stored in an incubator at 23°C until use. iL3s used to test CO₂ response in Fig 6B were cultured on fecal-charcoal plates until day 7; they were then either tested immediately, stored in BU saline [64] for 1 week and then tested, or stored in BU saline for 2 weeks and then tested.

Maintenance of *A. ceylanicum* in hamsters

A. ceylanicum was serially passaged in male Syrian golden hamsters and maintained on fecal-charcoal plates as described [18]. Briefly, hamsters were inoculated with ~100 iL3s in 100 µL sterile ddH₂O by oral gavage. Feces infested with *A. ceylanicum* were collected between days 14 and 45 post-inoculation. Feces were harvested and mixed with autoclaved charcoal granules to make fecal-charcoal plates as described above. Plates were stored in an incubator at 23°C until use. iL3s used to test CO₂ response in Fig 6C were cultured on fecal-charcoal plates until day 10; they were then either tested immediately, stored in BU saline [64] for 1 week and then tested, or stored in BU saline for 2 weeks and then tested.

Short-term dispersal assays for *H. polygyrus*

Short-term dispersal assays without feces (Figs 1A and 4A) were performed essentially as described [18]. For each trial, ~50–100 iL3s were placed on a 10-cm chemotaxis plate [65] on a vibration-reducing platform and allowed to disperse for either 1 hour (Fig 1A) or 10 minutes (Fig 4A) in the absence of applied sensory stimuli. The number of iL3s in the outer zone of the

plate (the region that excludes a 4-cm-diameter circle at the center of the plate) was then determined. For short-term fecal dispersal assays (Fig 2E), fresh fecal pellets were collected the morning of the assay from uninfected animals. One fecal pellet (~0.03 g) was placed in the center of a 10-cm chemotaxis plate. 15–40 iL3s were pipetted onto the pellet. The plates were then placed on a vibration-reducing platform for 1 hour. The number of iL3s either on the feces, off the feces but within a 4-cm-diameter circle around the feces (zone 1), or outside a 4-cm-diameter circle around the feces (zone 2) was then determined (Fig 2E). iL3s were not visible when they were on the fecal pellet, so the number of iL3s remaining on the feces at the end of the assay was determined by subtracting the number of iL3s in zones 1 and 2 from the total number of iL3s added to the feces. Note that for all dispersal assays, the outermost zone included the walls of the plate, which functioned as a trap such that most of the iL3s that crawled onto the walls of the plate remained there for the duration of the assay.

Long-term fecal dispersal and nictation assays for *H. polygyrus*

Long-term fecal dispersal assays (Fig 2F) were performed by first collecting fresh feces from infected animals; feces were collected as described above, but from a 4-hour collection period. Feces were collected from host animals that were each infected with ~75 iL3s. Individual fecal pellets of similar size were cut in half; one-half of a fecal pellet was then placed on each chemotaxis assay plate and incubated at room temperature. Every 24 hours (within a 3-hour window), the number of animals that had migrated out of the feces and onto the chemotaxis plate was quantified. After quantification, fecal pellets were transferred to fresh chemotaxis plates. On day 10, the fecal pellets were dissociated and the number of iL3s remaining in the fecal pellet was quantified. These numbers were then used to calculate the total number of worms that started out on each fecal pellet, and the cumulative percentage of worms that migrated off the fecal pellet each day. Nictation rates were also determined for each day by counting the number of worms observed to be nictating on the fecal pellet at each time of observation. These numbers were used, in combination with the number of worms remaining on the fecal pellet for each day (calculated as described above), to calculate the percentage of worms nictating on the fecal pellets at each time of observation (S3 Fig).

Automated tracking of worm movement

Automated tracking was performed as described [18]. For each recording session, 10–15 iL3s were placed on a chemotaxis plate and allowed to acclimate for 10 minutes. iL3 movement was then captured for 20 seconds using an Olympus E-PM1 digital camera attached to a Leica S6 D microscope. WormTracker and WormAnalyzer [35] were used to quantify crawling speed. WormTracker and WormAnalyzer settings were previously described [18].

Nictation assay

The nictation assays shown in Figs 1C and 4C were performed essentially as described (S2 Fig) [18, 62]. Briefly, agar chips for nictation assays were made from polydimethylsiloxane (PDMS) molds [36]. Chips were approximately 3 cm x 3.5 cm and contained near-microscopic posts that allowed the iL3s to stand. Chips were made using 4% agar dissolved in ddH₂O. Once the agar had solidified, chips were placed at 37°C for 2 hours followed by room temperature for 1 hour. 10–20 iL3s were transferred to the center of the chip in a 5 µL drop of dH₂O and allowed to acclimate for 10 minutes. Individual iL3s were then monitored for 2 minutes, and the number of iL3s that nictated during the observation period was recorded. Nictation was defined as an iL3 raising at least half of its body off the plate for at least 5 seconds (S2 Fig).

Fecal, odorant, and CO₂ chemotaxis assays

Chemotaxis assays were performed on chemotaxis plates as described [18, 44]. For fecal and odorant chemotaxis assays, 2 μ L 5% sodium azide was placed into the center of each scoring region. For fecal chemotaxis assays, feces were obtained from an overnight fecal collection. For assays involving feces from uninfected vs. infected animals (Fig 2D, right), feces were obtained from a 4-hour fecal collection. The feces were then incubated for 3 days at room temperature in a 10-cm Petri dish on filter paper moistened with 1 mL ddH₂O to prevent desiccation. For assays involving fresh vs. aged feces (Fig 2D, center), feces were obtained from a 4-hour fecal collection and stored in a 10-cm Petri dish without filter paper. “Fresh feces” refers to feces that were used on the day of collection, while “aged feces” refers to feces that were incubated in the Petri dish for 1 day. For all fecal assays, the feces were moistened to a paste with ddH₂O. 0.5-cm squares of filter paper were affixed to the lid of a chemotaxis plate using double-stick tape. 0.25 g fecal paste was placed onto one of the filter paper squares, and either 50 μ L ddH₂O (for normal fecal chemotaxis assays) or 0.25 g of feces (for fecal competition chemotaxis assays) was added to the other square.

For odorant chemotaxis assays (S4 Fig), 5 μ L odorant was pipetted into the center of one scoring region and 5 μ L control (paraffin oil, ddH₂O, or ethanol) was pipetted into the center of the other scoring region. Liquid odorants were tested undiluted. Solid odorants were dissolved to test concentrations as follows: tetradecanoic acid, indole, and 3-methylindole were diluted 0.05 g in 2.5 mL ethanol; octadecanoic acid was diluted 1 g in 80 mL ethanol; L-lactic acid was diluted 0.05 g in 2.5 mL ddH₂O; and ammonia was purchased as a 2 M solution in ethanol. ddH₂O was used as a control for L-lactic acid; ethanol was used as a control for tetradecanoic acid, octadecanoic acid, indole, 3-methylindole, and ammonia; and paraffin oil was used as a control for all other odorants. For CO₂ chemotaxis assays, gases were delivered at a rate of 0.5 mL/min through holes in the plate lids as previously described [18, 44]. Gas stimuli were obtained from Airgas, and consisted of the test concentration of CO₂, 21% O₂, and the balance N₂. Air controls consisted of 21% O₂ and 79% N₂. The test concentration of CO₂ consisted of 15% CO₂ for *H. contortus* and 10% CO₂ for all other species, unless otherwise indicated.

For all chemotaxis assays, ~200 iL3s were pipetted onto the center of the chemotaxis plate and allowed to distribute in the stimulus gradient on a vibration-reducing platform for 3 h (for fecal and odorant chemotaxis assays) or 1 h (for CO₂ assays). The number of iL3s in each scoring region was then quantified and a chemotaxis index was calculated as: (# iL3s at stimulus - # iL3s at control) / (# iL3s at stimulus + control). At least two identical assays were always performed simultaneously with the stimulus gradient oriented in opposite directions to control for directional bias due to room vibration or other causes; the pair of assays was discarded if the difference in the chemotaxis indices for the pair of plates was ≥ 0.9 or if either of the plates had <7 iL3s in the scoring regions. For the odorant chemotaxis assays in Fig 3, significance was calculated relative to a paraffin oil control.

Data analysis

Statistical analysis was performed using GraphPad Prism or PAST [66]. For each experiment, the D’Agostino-Pearson omnibus normality test was used to determine whether the data were normally distributed. If the data were normally distributed, parametric tests were used; otherwise, non-parametric tests were used. Graphs show medians and interquartile ranges to accurately depict the distribution and variance in our datasets. The heatmap in S5A Fig was generated using Heatmap Builder [67].

Supporting information

S1 Fig. The life cycle of *H. polygyrus*. iL3s infect when they are ingested by a mouse, either during fecal consumption or during grooming [30, 34]. The nematodes develop to adulthood in the mouse. Adults reproduce in the intestine, and nematode eggs exit the mouse in feces. The nematodes then develop on feces to the iL3 stage [30]. L1-L4 = 1st-4th larval stages. Figure design was adapted from Gang *et al.*, 2016 [13].
(PDF)

S2 Fig. A nictation assay for *H. polygyrus* iL3s. For the nictation assays described in Figs 1C and 4C, iL3s were placed on near-microscopic agar posts [36]. iL3s were allowed to acclimate to the posts for 10 minutes. The number of iL3s that nictated during a 2-minute period was then recorded. Nictation was defined as the iL3 raising at least half of its body off of the plate for at least 5 seconds. Photos show *H. polygyrus* iL3s either crawling but not nictating (left), or during different stages of nictation (center and right). Note that the iL3s can crawl between or over the posts, and can stand either on or between the posts. Scale bar = 500 μ m. Figure design was adapted from Lee *et al.*, 2012 [36].
(PDF)

S3 Fig. Nictation of *H. polygyrus* iL3s on their original fecal source. Individual fecal half-pellets from infected animals were examined each day over the course of 7 days, and the number of nematodes nictating at each time of observation was determined. Nictation was observed primarily on day 5 post-fecal collection. Nictation frequencies could not be determined beyond day 7 because nearly all of the nematodes had migrated off of the feces by this time (Fig 2F). n = 13 trials.
(PDF)

S4 Fig. A chemotaxis assay for iL3s. Stimulus is delivered to one side of the plate and control to the other side (black dots). For odorant chemotaxis assays, the odorant and control were placed directly on the surface of the plate. For CO₂ chemotaxis assays, CO₂ and an air control were delivered through holes in the plate lid. iL3s were placed at the center of the plate (double-sided arrow). After 1 hour (for CO₂-chemotaxis assays) or 3 hours (for odorant-chemotaxis assays), the number of iL3s in each scoring region (circles) was counted, and a chemotaxis index was calculated as indicated. The chemotaxis index ranges from +1 (maximal attraction) to -1 (maximal repulsion).
(PDF)

S5 Fig. A comparison of the olfactory preferences of different nematode species. A. Olfactory preferences vary across nematode species. Responses are shown as a heat map according to the scale shown at the lower right. Data for *H. polygyrus* are from Fig 3; data for all other species are from Castelletto *et al.*, 2014 [18]. Odorant order was determined by hierarchical cluster analysis (paired-group algorithm with Euclidean distance as a similarity measure, cophenetic correlation coefficient = 0.71). B. Olfactory preferences reflect host range rather than genetic relatedness. The behavioral dendrogram was constructed based on the olfactory behaviors of each species. Hierarchical cluster analysis was performed using a paired-group algorithm with Euclidean distance as a similarity measure, cophenetic correlation coefficient = 0.90. Nematode species are color-coded according to the key shown below the dendrogram. All species being compared have a developmentally arrested third-larval stage that engages in environmental navigation.
(PDF)

S6 Fig. CO₂ response of *H. polygyrus* iL3s across concentrations. On-feces iL3s were repelled by CO₂ (left) and off-feces iL3s were attracted to CO₂ (right) across concentrations in a CO₂-chemotaxis assay. * $p < 0.05$, ** $p < 0.01$, *** $p < 0.001$, Kruskal-Wallis test with Dunn's post-test. $n = 6$ –12 trials for each condition. Graphs show medians and interquartile ranges. (PDF)

Acknowledgments

We thank R. Aroian for generously providing *H. polygyrus*, J. Lok for generously providing *S. stercoralis*, J. Hawdon for generously providing *A. ceylanicum*, A. Zajac for generously providing *H. contortus*, and J. Lee and S. Park for generously providing PDMS molds for nictation assays. We also thank Tiffany Mao for technical assistance, and Astra Bryant and Mayra Carrillo for insightful comments on the manuscript.

Author Contributions

Conceptualization: Felicitas Ruiz, Elissa A. Hallem.

Formal analysis: Elissa A. Hallem.

Funding acquisition: Elissa A. Hallem.

Investigation: Felicitas Ruiz, Michelle L. Castelletto, Spencer S. Gang.

Methodology: Felicitas Ruiz, Michelle L. Castelletto, Spencer S. Gang, Elissa A. Hallem.

Project administration: Elissa A. Hallem.

Supervision: Elissa A. Hallem.

Writing – original draft: Felicitas Ruiz, Elissa A. Hallem.

Writing – review & editing: Felicitas Ruiz, Michelle L. Castelletto, Spencer S. Gang, Elissa A. Hallem.

References

1. Ghai RR, Chapman CA, Omeja PA, Davies TJ, Goldberg TL. Nodule worm infection in humans and wild primates in Uganda: cryptic species in a newly identified region of human transmission. *PLoS Negl Trop Dis*. 2014; 8(1):e2641. <https://doi.org/10.1371/journal.pntd.0002641> PMID: 24421915
2. Storey PA, Faile G, Hewitt E, Yelifari L, Polderman AM, Magnussen P. Clinical epidemiology and classification of human oesophagostomiasis. *Trans R Soc Trop Med Hyg*. 2000; 94(2):177–82. PMID: 10897362
3. Cibot M, Guillot J, Lafosse S, Bon C, Seguya A, Krief S. Nodular worm infections in wild non-human primates and humans living in the Sebitoli area (Kibale National Park, Uganda): do high spatial proximity favor zoonotic transmission? *PLoS Negl Trop Dis*. 2015; 9(10):e0004133. <https://doi.org/10.1371/journal.pntd.0004133> PMID: 26451592
4. Parkins JJ, Holmes PH. Effects of gastrointestinal helminth parasites on ruminant nutrition. *Nutr Res Rev*. 1989; 2(1):227–46. <https://doi.org/10.1079/NRR19890016> PMID: 19094355
5. Terrill TH, Miller JE, Burke JM, Mosjidis JA, Kaplan RM. Experiences with integrated concepts for the control of *Haemonchus contortus* in sheep and goats in the United States. *Vet Parasitol*. 2012; 186:28–37. <https://doi.org/10.1016/j.vetpar.2011.11.043> PMID: 22178411
6. Keiser J, Utzinger J. Efficacy of current drugs against soil-transmitted helminth infections: systematic review and meta-analysis. *JAMA*. 2008; 299(16):1937–48. <https://doi.org/10.1001/jama.299.16.1937> PMID: 18430913
7. Diawara A, Schwenkenbecher JM, Kaplan RM, Prichard RK. Molecular and biological diagnostic tests for monitoring benzimidazole resistance in human soil-transmitted helminths. *Am J Trop Med Hyg*. 2013; 88(6):1052–61. <https://doi.org/10.4269/ajtmh.12-0484> PMID: 23458960

8. Howell SB, Burke JM, Miller JE, Terrill TH, Valencia E, Williams MJ, et al. Prevalence of anthelmintic resistance on sheep and goat farms in the southeastern United States. *J Am Vet Med Assoc.* 2008; 233(12):1913–9. <https://doi.org/10.2460/javma.233.12.1913> PMID: 19072608
9. Gasser RB, Schwarz EM, Korhonen PK, Young ND. Understanding *Haemonchus contortus* better through genomics and transcriptomics. *Adv Parasitol.* 2016; 93:519–67. <https://doi.org/10.1016/bs.apar.2016.02.015> PMID: 27238012
10. Cooper D, Eleftherianos I. Parasitic nematode immunomodulatory strategies: recent advances and perspectives. *Pathogens.* 2016; 5(3):58.
11. McRae KM, Stear MJ, Good B, Keane OM. The host immune response to gastrointestinal nematode infection in sheep. *Parasite Immunol.* 2015; 37(12):605–13. <https://doi.org/10.1111/pim.12290> PMID: 26480845
12. Maizels RM. Parasitic helminth infections and the control of human allergic and autoimmune disorders. *Clin Microbiol Infect.* 2016; 22(6):481–6. <https://doi.org/10.1016/j.cmi.2016.04.024> PMID: 27172808
13. Gang SS, Hallem EA. Mechanisms of host seeking by parasitic nematodes. *Mol Biochem Parasitol.* 2016; 208:23–32. <https://doi.org/10.1016/j.molbiopara.2016.05.007> PMID: 27211240
14. Haas W, Haberl B, Idris SI, Kallert D, Kersten S, Stiegeler P. Behavioural strategies used by the hookworms *Necator americanus* and *Ancylostoma duodenale* to find, recognize and invade the human host. *Parasitol Res.* 2005; 95(1):30–9. <https://doi.org/10.1007/s00436-004-1257-7> PMID: 15614587
15. Haas W, Haberl B, Idris SI, Kersten S. Infective larvae of the human hookworms *Necator americanus* and *Ancylostoma duodenale* differ in their orientation behaviour when crawling on surfaces. *Parasitol Res.* 2005; 95(1):25–9. <https://doi.org/10.1007/s00436-004-1256-8> PMID: 15614586
16. Granzer M, Hass W. Host-finding and host recognition of infective *Ancylostoma caninum* larvae. *Int J Parasitol.* 1991; 21:429–40. PMID: 1917283
17. Bhopale VM, Kupprion EK, Ashton FT, Boston R, Schad GA. *Ancylostoma caninum*: the finger cell neurons mediate thermotactic behavior by infective larvae of the dog hookworm. *Exp Parasitol.* 2001; 97(2):70–6. <https://doi.org/10.1006/expr.2000.4575> PMID: 11281703
18. Castelletto ML, Gang SS, Okubo RP, Tselikova AA, Nolan TJ, Platzer EG, et al. Diverse host-seeking behaviors of skin-penetrating nematodes. *PLoS Pathog.* 2014; 10(8):e1004305. <https://doi.org/10.1371/journal.ppat.1004305> PMID: 25121736
19. Lopez PM, Boston R, Ashton FT, Schad GA. The neurons of class ALD mediate thermotaxis in the parasitic nematode, *Strongyloides stercoralis*. *Int J Parasitol.* 2000; 30(10):1115–21. PMID: 10996330
20. Safer D, Brenes M, Dunipace S, Schad G. Urocanic acid is a major chemoattractant for the skin-penetrating parasitic nematode *Strongyloides stercoralis*. *Proc Natl Acad Sci USA.* 2007; 104(5):1627–30. <https://doi.org/10.1073/pnas.0610193104> PMID: 17234810
21. Koga M, Nuamtanong S, Dekumyoy P, Yoonuan T, Maipanich W, Rojekkittikhun W, et al. Host-finding behavior of *Strongyloides stercoralis* infective larvae to sodium cation, human serum, and sweat. *Southeast Asian J Trop Med Public Health.* 2005; 36:93–8. PMID: 16438188
22. Koga M, Tada I. *Strongyloides ratti*: chemotactic responses of third-stage larvae to selected serum proteins and albumins. *J Helminthol.* 2000; 74(3):247–52. PMID: 10953225
23. Rees G. Observations on the vertical migrations of the third-stage larva of *Haemonchus contortus* (Rud.) on experimental plots of *Lolium perenne* S24, in relation to meteorological and micrometeorological factors. *Parasitol.* 1950; 40(1–2):127–43.
24. Callinan AP, Westcott JM. Vertical distribution of trichostrongylid larvae on herbage and in soil. *Int J Parasitol.* 1986; 16(3):241–4. PMID: 3744667
25. Reynolds LA, Filbey KJ, Maizels RM. Immunity to the model intestinal helminth parasite *Heligmosomoides polygyrus*. *Semin Immunopathol.* 2012; 34(6):829–46. <https://doi.org/10.1007/s00281-012-0347-3> PMID: 23053394
26. Nisbet AJ, Meeusen EN, Gonzalez JF, Piedrafita DM. Immunity to *Haemonchus contortus* and vaccine development. *Adv Parasitol.* 2016; 93:353–96. <https://doi.org/10.1016/bs.apar.2016.02.011> PMID: 27238008
27. Behnke J, Harris PD. *Heligmosomoides bakeri*: a new name for an old worm? *Trends Parasitol.* 2010; 26(11):524–9. <https://doi.org/10.1016/j.pt.2010.07.001> PMID: 20729145
28. Behnke JM, Menge DM, Noyes H. *Heligmosomoides bakeri*: a model for exploring the biology and genetics of resistance to chronic gastrointestinal nematode infections. *Parasitology.* 2009; 136(12):1565–80. <https://doi.org/10.1017/S0031182009006003> PMID: 19450375
29. Camberis M, Le Gros G, Urban J. Animal model of *Nippostrongylus brasiliensis* and *Heligmosomoides polygyrus*. *Curr Protoc Immunol.* 2003; 19:19.2.1–.2.27.

30. Johnston CJ, Robertson E, Harcus Y, Grainger JR, Coakley G, Smyth DJ, et al. Cultivation of *Heligmosomoides polygyrus*: an immunomodulatory nematode parasite and its secreted products. *J Vis Exp*. 2015;(98):e52412. <https://doi.org/10.3791/52412> PMID: 25867600
31. Viney ME, Thompson FJ, Crook M. TGF- β and the evolution of nematode parasitism. *Int J Parasitol*. 2005; 35(14):1473–5. <https://doi.org/10.1016/j.ijpara.2005.07.006> PMID: 16139836
32. Spurlock JM. Observations on host-parasite relations between laboratory mice and *Nematospiroides dubius* Baylis. *J Parasitol*. 1943; 29(5):303–11.
33. Ehrenford FA. The life cycle of *Nematospiroides dubius* Baylis (Nematoda, Heligmosomidae). *J Parasitol*. 1954; 40(4):480–1.
34. Hernandez AD, Sukhdeo MVK. Host grooming and the transmission strategy of *Heligmosomoides polygyrus*. *J Parasitol*. 1995; 81(6):865–9. PMID: 8544055
35. Ramot D, Johnson BE, Berry TL, Carnell L, Goodman MB. The parallel worm tracker: a platform for measuring average speed and drug-induced paralysis in nematodes. *PLoS ONE*. 2008; 3(5):e2208. <https://doi.org/10.1371/journal.pone.0002208> PMID: 18493300
36. Lee H, Choi MK, Lee D, Kim HS, Hwang H, Kim H, et al. Nictation, a dispersal behavior of the nematode *Caenorhabditis elegans*, is regulated by IL2 neurons. *Nat Neurosci*. 2012; 15(1):107–12.
37. Garner CE, Smith S, Costello BD, White P, Spencer R, Probert CSJ, et al. Volatile organic compounds from feces and their potential for diagnosis of gastrointestinal disease. *Faseb J*. 2007; 21(8):1675–88. <https://doi.org/10.1096/fj.06-6927com> PMID: 17314143
38. Goodrich BS, Gambale S, Pennycuik PR, Redhead TD. Volatiles from feces of wild male house mice—chemistry and effects on behavior and heart-rate. *J Chem Ecol*. 1990; 16(7):2091–106. <https://doi.org/10.1007/BF01026922> PMID: 24264078
39. de Lacy Costello B, Amann A, Al-Kateb H, Flynn C, Filipiak W, Khalid T, et al. A review of the volatiles from the healthy human body. *J Breath R*. 2014; 8(1): 014001.
40. Amann A, de Lacy Costello B, Miekisch W, Schubert J, Buszewski B, Pleil J, et al. The human volatile: volatile organic compounds (VOCs) in exhaled breath, skin emanations, urine, feces and saliva. *J Breath R*. 2014; 8(3).
41. De Angelis M, Montemurno E, Piccolo M, Vannini L, Lauriero G, Maranzano V, et al. Microbiota and metabolome associated with immunoglobulin A nephropathy (IgAN). *PLoS ONE*. 2014; 9(6).
42. Meijerink J, Braks MAH, Brack AA, Adam W, Dekker T, Posthumus MA, et al. Identification of olfactory stimulants for *Anopheles gambiae* from human sweat samples. *J Chem Ecol*. 2000; 26(6):1367–82.
43. Verhulst NO, Beijleveld H, Knols BGJ, Takken W, Schraa G, Bouwmeester HJ, et al. Cultured skin microbiota attracts malaria mosquitoes. *Malaria J*. 2009; 8:302.
44. Hallem EA, Dillman AR, Hong AV, Zhang Y, Yano JM, DeMarco SF, et al. A sensory code for host seeking in parasitic nematodes. *Curr Biol*. 2011; 21(5):377–83. <https://doi.org/10.1016/j.cub.2011.01.048> PMID: 21353558
45. Dillman AR, Guillermin ML, Lee JH, Kim B, Sternberg PW, Hallem EA. Olfaction shapes host-parasite interactions in parasitic nematodes. *Proc Natl Acad Sci USA*. 2012; 109(35):E2324–33. <https://doi.org/10.1073/pnas.1211436109> PMID: 22851767
46. Lahiri S, Forster RE 2nd. CO₂/H(+) sensing: peripheral and central chemoreception. *Int J Biochem Cell Biol*. 2003; 35(10):1413–35. PMID: 12818238
47. Okon ED, Enyenihi UK. Development and survival of *Haemonchus contortus* larvae on pastures in Ibadan. *Trop Anim Health Prod*. 1977; 9(1):7–10. PMID: 906089
48. Altaif KI, Yakoob AY. Development and survival of *Haemonchus contortus* larvae on pasture in Iraq. *Trop Anim Health Prod*. 1987; 19(2):88–92. PMID: 3629723
49. Alkalay I, Suetsugu S, Constantine H, Stein M. Carbon dioxide elimination across human skin. *Am J Physiol*. 1971; 220(5):1434–6. PMID: 5574662
50. Pleil JD, Lindstrom AB. Measurement of volatile organic compounds in exhaled breath as collected in evacuated electropolished canisters. *J Chromatogr B Biomed Appl*. 1995; 665(2):271–9. PMID: 7795807
51. van der Voort M, Van Meensel J, Lauwers L, de Haan MH, Evers AG, Van Huylenbroeck G, et al. Economic modelling of grazing management against gastrointestinal nematodes in dairy cattle. *Vet Parasitol*. 2017; 236:68–75. <https://doi.org/10.1016/j.vetpar.2017.02.004> PMID: 28288768
52. Stromberg BE, Averbek GA. The role of parasite epidemiology in the management of grazing cattle. *Int J Parasitol*. 1999; 29(1):33–9. PMID: 10048817
53. Guillermin ML, Carrillo MA, Hallem EA. A single set of interneurons drives opposite behaviors in *C. elegans*. *Curr Biol*. 2017; 27(17):2630–9. <https://doi.org/10.1016/j.cub.2017.07.023> PMID: 28823678

54. Grozinger CM, Sharabash NM, Whitfield CW, Robinson GE. Pheromone-mediated gene expression in the honey bee brain. *Proc Natl Acad Sci USA*. 2003; 100:14519–25. <https://doi.org/10.1073/pnas.2335884100> PMID: 14573707
55. Alaux C, Le Conte Y, Adams HA, Rodriguez-Zas S, Grozinger CM, Sinha S, et al. Regulation of brain gene expression in honey bees by brood pheromone. *Genes Brain Behav*. 2009; 8(3):309–19. <https://doi.org/10.1111/j.1601-183X.2009.00480.x> PMID: 19220482
56. Hiratani N, Fukai T. Hebbian wiring plasticity generates efficient network structures for robust inference with synaptic weight plasticity. *Front Neural Circuits*. 2016; 10:41. <https://doi.org/10.3389/fncir.2016.00041> PMID: 27303271
57. Tetzlaff C, Kolodziejcki C, Markelic I, Worgotter F. Time scales of memory, learning, and plasticity. *Biol Cybern*. 2012; 106(11–12):715–26. <https://doi.org/10.1007/s00422-012-0529-z> PMID: 23160712
58. Lee SH, Dan Y. Neuromodulation of brain states. *Neuron*. 2012; 76(1):209–22. <https://doi.org/10.1016/j.neuron.2012.09.012> PMID: 23040816
59. Dickinson PS. Neuromodulation of central pattern generators in invertebrates and vertebrates. *Curr Opin Neurobiol*. 2006; 16(6):604–14. <https://doi.org/10.1016/j.conb.2006.10.007> PMID: 17085040
60. Lok JB, Shao H, Massey HC, Li X. Transgenesis in *Strongyloides* and related parasitic nematodes: historical perspectives, current functional genomic applications and progress towards gene disruption and editing. *Parasitology*. 2016; 144(3):327–42. <https://doi.org/10.1017/S0031182016000391> PMID: 27000743
61. Gang SS, Castelletto ML, Bryant AS, Yang E, Mancuso N, Lopez JB, et al. Targeted mutagenesis in a human-parasitic nematode. *PLoS Pathog*. 2017; 13(10):e1006675. <https://doi.org/10.1371/journal.ppat.1006675> PMID: 29016680
62. Lee J, Dillman AR, Hallem EA. Temperature-dependent changes in the host-seeking behaviors of parasitic nematodes. *BMC Biol*. 2016; 14:36. <https://doi.org/10.1186/s12915-016-0259-0> PMID: 27154502
63. Lok JB. *Strongyloides stercoralis*: a model for translational research on parasitic nematode biology. In *WormBook*, www.wormbook.org. 2007.
64. Hawdon JM, Schad GA. Long-term storage of hookworm infective larvae in buffered saline solution maintains larval responsiveness to host signals. *J Helm Soc Wash*. 1991; 58:140–2.
65. Bargmann CI, Horvitz HR. Chemosensory neurons with overlapping functions direct chemotaxis to multiple chemicals in *C. elegans*. *Neuron*. 1991; 7(5):729–42. PMID: 1660283
66. Hammer Ø, Harper DAT, Ryan PD. PAST: Paleontological statistics software package for education and data analysis. *Palaeontol Electronica*. 2001; 4:9pp.
67. King JY, Ferrara R, Tabibiazar R, Spin JM, Chen MM, Kuchinsky A, et al. Pathway analysis of coronary atherosclerosis. *Physiol Genomics*. 2005; 23(1):103–18. <https://doi.org/10.1152/physiolgenomics.00101.2005> PMID: 15942018

Chapter 4

Targeted mutagenesis in a human-parasitic nematode

RESEARCH ARTICLE

Targeted mutagenesis in a human-parasitic nematode

Spencer S. Gang¹, Michelle L. Castelletto², Astra S. Bryant², Emily Yang², Nicholas Mancuso³, Jacqueline B. Lopez², Matteo Pellegrini⁴, Elissa A. Hallem^{1,2*}

1 Molecular Biology Institute, University of California, Los Angeles, California, United States of America, **2** Department of Microbiology, Immunology, and Molecular Genetics, University of California, Los Angeles, California, United States of America, **3** Department of Pathology and Laboratory Medicine, David Geffen School of Medicine, University of California, Los Angeles, California, United States of America, **4** Department of Molecular, Cell and Developmental Biology, University of California, Los Angeles, California, United States of America

* ehallem@ucla.edu



 OPEN ACCESS

Citation: Gang SS, Castelletto ML, Bryant AS, Yang E, Mancuso N, Lopez JB, et al. (2017) Targeted mutagenesis in a human-parasitic nematode. *PLoS Pathog* 13(10): e1006675. <https://doi.org/10.1371/journal.ppat.1006675>

Editor: Paul J. Brindley, George Washington University School of Medicine and Health Sciences, UNITED STATES

Received: May 23, 2017

Accepted: October 2, 2017

Published: October 10, 2017

Copyright: © 2017 Gang et al. This is an open access article distributed under the terms of the [Creative Commons Attribution License](https://creativecommons.org/licenses/by/4.0/), which permits unrestricted use, distribution, and reproduction in any medium, provided the original author and source are credited.

Data Availability Statement: All relevant data are within the paper and its Supporting Information files.

Funding: This work was funded by the Whitcome Predoctoral Training Program, UCLA Molecular Biology Institute, Ruth L. Kirschstein National Research Service Award AI007323, and National Science Foundation East Asia and Pacific Summer Institute Fellowship Award 1414655 (SSG); the UCLA Undergraduate Research Scholar Program (EY); the UCLA-Howard Hughes Medical Institute

Abstract

Parasitic nematodes infect over 1 billion people worldwide and cause some of the most common neglected tropical diseases. Despite their prevalence, our understanding of the biology of parasitic nematodes has been limited by the lack of tools for genetic intervention. In particular, it has not yet been possible to generate targeted gene disruptions and mutant phenotypes in any parasitic nematode. Here, we report the development of a method for introducing CRISPR-Cas9-mediated gene disruptions in the human-parasitic threadworm *Strongyloides stercoralis*. We disrupted the *S. stercoralis* twitchin gene *unc-22*, resulting in nematodes with severe motility defects. *Ss-unc-22* mutations were resolved by homology-directed repair when a repair template was provided. Omission of a repair template resulted in deletions at the target locus. *Ss-unc-22* mutations were heritable; we passed *Ss-unc-22* mutants through a host and successfully recovered mutant progeny. Using a similar approach, we also disrupted the *unc-22* gene of the rat-parasitic nematode *Strongyloides ratti*. Our results demonstrate the applicability of CRISPR-Cas9 to parasitic nematodes, and thereby enable future studies of gene function in these medically relevant but previously genetically intractable parasites.

Author summary

Parasitic worms are a widespread public health burden, yet very little is known about the cellular and molecular mechanisms that contribute to their parasitic lifestyle. One of the major barriers to better understanding these mechanisms is that there are currently no available methods for making targeted gene knockouts in any parasitic worm species. Here, we describe the first mutant phenotype in a parasitic worm resulting from a targeted gene disruption. We applied CRISPR-Cas9-mediated mutagenesis to parasitic worms in the genus *Strongyloides* and developed a method that overcomes many of the challenges that have previously inhibited generating mutant parasitic worms. We characterize heritable mutant phenotypes and outline a toolkit that will be applicable to many other genes

Pathways to Success Program (JBL); and a Burroughs-Wellcome Fund Investigators in the Pathogenesis of Disease Award, NIH New Innovator Award 1DP2DC014596, and Howard Hughes Medical Institute Faculty Scholar Award (EAH). The funders had no role in study design, data collection and analysis, decision to publish, or preparation of the manuscript.

Competing interests: The authors have declared that no competing interests exist.

with potential roles in parasitism. Importantly, we developed our method for gene knockouts in a human-parasitic worm. By directly investigating the genes and molecular pathways that enable worms to parasitize humans, we may be able to develop novel anthelmintic therapies or other measures for preventing nematode infections.

Introduction

Human-parasitic nematodes cause an annual disease burden of over 5 million disability adjusted life years (DALYs) [1,2]. Current drugs used to treat nematode infections are inadequate to eliminate this disease burden: reinfection rates are high in endemic areas and resistance to the few available anthelmintic drugs is a growing concern [2]. However, the development of new strategies for combating nematode infections has been severely limited by the lack of a method for gene disruption in parasitic nematodes [3]. While gene knockdowns by RNAi have been achieved in a few species, RNAi shows variable efficacy and has been used successfully for only a few genes [3]. Conversely, chemical mutagenesis screens have been used to generate mutant phenotypes but the causative mutations could not be identified [4]. As a result, the molecular mechanisms that drive development, behavior, and infectivity in parasitic nematodes remain poorly understood.

The clustered, regularly interspaced, short palindromic repeats (CRISPR) and CRISPR-associated nuclease Cas9 system [5], which evolved from an immune defense system in bacteria and archaea, has been used for targeted mutagenesis in both model and non-model organisms [6,7]. In this system, Cas9 creates double-strand breaks (DSBs) at the genomic location determined by two small RNAs: a CRISPR RNA (crRNA) complementary to the target site and a *trans*-activating crRNA (tracrRNA). The crRNA and tracrRNA are often synthetically combined into a single guide RNA (sgRNA) [5]. The DSBs are then most commonly repaired through either non-homologous end joining (NHEJ) or homology-directed repair (HDR) pathways, but alternative repair mechanisms have been reported in some cases [8]. Despite its application to a wide range of organisms, the CRISPR-Cas9 system has not been successfully utilized in parasitic nematodes. Reasons for this include the low tolerance of parasitic nematodes for exogenous DNA or protein, the labor-intensiveness and low efficiency of methods for delivering constructs for gene targeting, the need to propagate most parasitic nematodes inside an animal host, and the inaccessibility of host-dwelling life stages to genetic intervention [3].

The human-parasitic threadworm *Strongyloides stercoralis* is a powerful model system for mechanistic studies of parasitic nematode biology. *S. stercoralis* is a skin-penetrating intestinal nematode that infects approximately 100 million people worldwide; it can cause chronic gastrointestinal distress in healthy individuals but can be fatal for immunosuppressed individuals [9]. *S. stercoralis* and closely related species are unique among parasitic nematodes in that they can develop through a single free-living generation outside the host (Fig 1A) [10]. The free-living adults are amenable to transgenesis techniques adapted from the model nematode *Caenorhabditis elegans* [3,11], suggesting they may also be amenable to CRISPR-Cas9-mediated mutagenesis. Preliminary evidence that CRISPR-Cas9 can be used for gene disruptions in *S. stercoralis* was reported; however, DNA mutations were detected only at extremely low frequency in pooled populations of worms and individual worms with mutant phenotypes were not observed [11]. Thus, whether CRISPR-Cas9 can be used to study gene function in *S. stercoralis* was unclear.

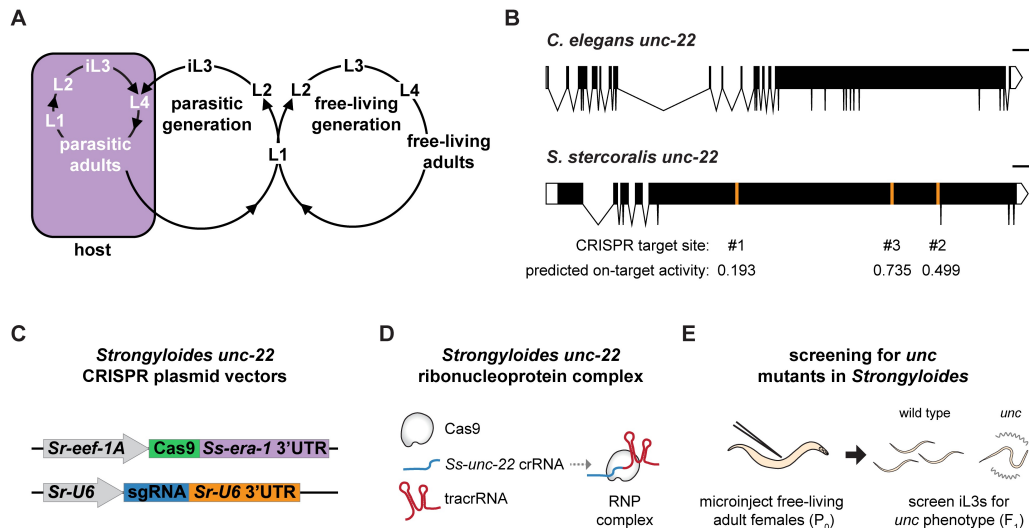


Fig 1. A strategy for targeted mutagenesis in *S. stercoralis* using CRISPR-Cas9. (A) The life cycle of *S. stercoralis*. iL3s enter hosts by skin penetration. The nematodes then develop into parasitic adults, which reside and reproduce in the small intestine. Their progeny exit the host in feces and develop into iL3s or free-living adults. The free-living adults mate and reproduce in the environment, and all of their progeny develop into iL3s. Thus, *S. stercoralis* can develop through a single generation outside the host [10]. *S. stercoralis* can also complete its life cycle within a single host [9]. L1-L4 = 1st-4th larval stages. Adapted from Gang and Hallem, 2016 [10]. (B) The *unc-22* genes of *C. elegans* and *S. stercoralis*. The *Ss-unc-22* gene structure depicted is based on the gene prediction from WormBase ParaSite [24,47]. The CRISPR target sites tested and their predicted on-target activity scores are indicated [50]. Scale bar = 1 kb. (C) Plasmid vectors for the expression of Cas9 and sgRNA in *S. stercoralis*. (D) RNP complex assembly. Cas9 protein, crRNA targeting *Ss-unc-22*, and tracrRNA are incubated *in vitro* to form RNP complexes [20]. (E) Strategy for targeted mutagenesis in *S. stercoralis*. Plasmid vectors or RNP complexes were introduced into developing eggs by gonadal microinjection of free-living adult females. F₁ iL3s progeny were screened for *unc* phenotypes, putatively resulting from mutation of *Ss-unc-22*.

<https://doi.org/10.1371/journal.ppat.1006675.g001>

Here we report the use of CRISPR-Cas9 to create loss-of-function DNA mutations and mutant phenotypes in *S. stercoralis*. We targeted the *S. stercoralis* twitchin gene *unc-22*, and subsequently isolated mutant nematodes with uncoordinated (*unc*) phenotypes characterized by decreased motility, sporadic spontaneous twitching, and persistent twitching when exposed to an acetylcholine receptor agonist. We found that CRISPR-Cas9-induced DSBs at *Ss-unc-22* are resolved by HDR when an appropriate repair template is provided. In the absence of an HDR template we found no evidence for small insertions or deletions (indels) at the target sites tested, but instead observed putative deletions of >500 base pairs at the target locus. We optimized CRISPR-Cas9 targeting conditions for *S. stercoralis*, and then demonstrated that *Ss-unc-22* mutations are heritable by passing mutant F₁ progeny through a host and collecting F₂ or F₃ nematodes with *unc* phenotypes. Our results pave the way for mechanistic studies of gene function in parasitic nematodes, which may enable the development of novel targeted therapies to improve human-parasitic nematode control.

Results

CRISPR-Cas9 targeting of *Ss-unc-22* causes an uncoordinated phenotype

To assess the functionality of CRISPR-Cas9-mediated mutagenesis in *S. stercoralis*, we focused on targeting the *S. stercoralis* ortholog of the *C. elegans unc-22* gene. *Ce-unc-22* encodes

twitchin, a large intracellular muscle protein homologous to mammalian connectin [12,13]. We selected *Ss-unc-22* because *Ce-unc-22* has been successfully mutagenized by multiple methods, including CRISPR-Cas9 [14–17]. In addition, disruption of *Ce-unc-22* results in an easily identifiable *unc* phenotype in both heterozygotes and homozygotes, with mutant nematodes showing dramatically impaired motility and intermittent body twitching [13]. We reasoned that the dominant phenotype resulting from loss of *Ss-unc-22* would enable us to easily identify mutagenized *S. stercoralis* in the F₁ generation even at low mutation frequencies. We introduced *Strongyloides*-specific CRISPR-Cas9 components targeting *Ss-unc-22* into the syncytial gonad of *S. stercoralis* free-living adult females (Fig 1A) [11,18]. We identified and tested three CRISPR target sites designed to target Cas9 to the largest exon of *Ss-unc-22* (Fig 1B). CRISPR-Cas9 constructs were delivered into *S. stercoralis* adults using two approaches. First, we utilized plasmid vectors to express *Strongyloides*-codon-optimized Cas9 and an sgRNA targeting *Ss-unc-22*. Cas9 was expressed under the control of the promoter for the putative *Strongyloides* elongation factor 1-alpha gene *eef-1A*. *C. elegans eef-1A* expresses in the germline, so it was predicted that germline expression would be conserved for *Strongyloides eef-1A* [19]. Expression of the sgRNA was driven by the putative *Strongyloides* U6 promoter (Fig 1C). Second, we targeted *Ss-unc-22* using a ribonucleoprotein (RNP) complex consisting of *in vitro*-assembled recombinant Cas9 protein, crRNA targeting *Ss-unc-22*, and tracrRNA (Fig 1D) [20]. We delivered CRISPR-Cas9 plasmid vectors or RNP complexes into free-living adult females, mated microinjected females with wild-type free-living males, and screened for *unc* phenotypes in F₁ progeny at the infective third-larval stage (iL3) (Fig 1A and 1E).

Following injection of *Ss-unc-22* CRISPR-Cas9 components into free-living adult females, we collected a distinct population of F₁ iL3s with a striking uncoordinated phenotype (hereafter referred to as *unc* F₁ iL3s) that was similar to the phenotype observed in *C. elegans unc-22* nematodes. *unc* F₁ iL3s showed impaired swimming behavior when compared to wild-type iL3s collected from non-injected controls (Fig 2A–2C, S1 and S2 Videos). Quantification of iL3 movement using automated tracking software [21] revealed that *unc* F₁ iL3s showed reduced crawling speeds relative to wild-type iL3s (Fig 2D, S3 and S4 Videos). We then tracked the trajectories of wild-type vs. *unc* F₁ iL3s over a 5-minute period and found that *unc* F₁ iL3s traversed significantly less distance than wild-type iL3s (Fig 2E). The swimming and crawling phenotypes of *unc* F₁ iL3s collected from injections were reminiscent of *C. elegans unc* phenotypes and suggested that we had successfully utilized CRISPR-Cas9 to disrupt *Ss-unc-22*.

The CRISPR-Cas9-induced *unc* phenotype is exacerbated by nicotine exposure

In *C. elegans*, the twitching phenotype of *Ce-unc-22* mutants is enhanced by exposure to acetylcholine receptor agonists such as nicotine [13]. We asked if F₁ iL3s collected following CRISPR-Cas9 injections showed a similar nicotine-induced twitching phenotype. To test this, we developed a nicotine assay for *S. stercoralis* iL3s (Fig 3A) and validated it by quantifying twitching behavior in wild-type and *unc-22 C. elegans* adults and dauers. We examined dauers as well as adults because the *C. elegans* dauer larval stage is a developmentally arrested life stage that is analogous to the parasitic iL3 [22]. Wild-type *C. elegans* adults and dauers were completely paralyzed after 8 minutes of nicotine exposure, while *Ce-unc-22* mutants showed severe twitching (S1 Fig). We observed a similar effect in *S. stercoralis* iL3s: nicotine induced paralysis in wild-type iL3s but caused nearly continuous twitching in some F₁ iL3s collected from CRISPR-Cas9 injections (S5 and S6 Videos).

We then used the distinct nicotine-twitching phenotype to assess the efficacy of different *Ss-unc-22* target sites and CRISPR-Cas9 delivery methods. We tested three different CRISPR

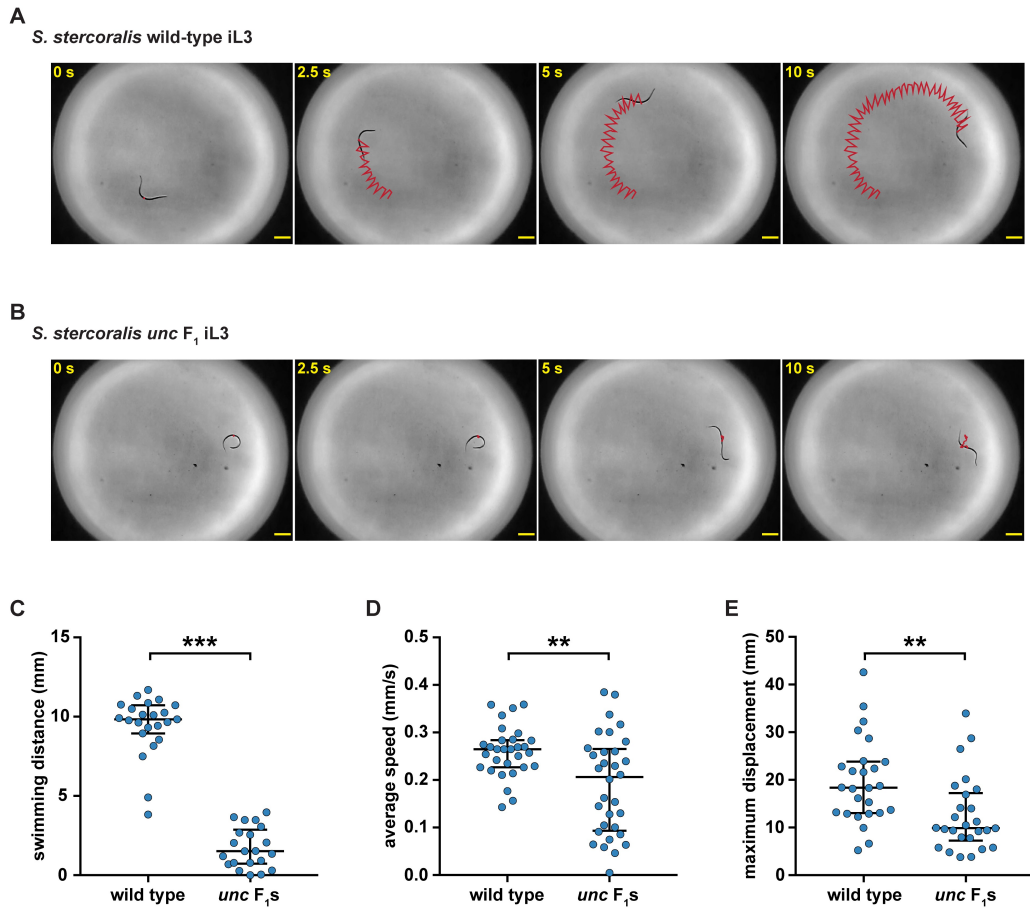


Fig 2. CRISPR-Cas9 targeting of the *Ss-unc-22* gene results in iL3s with an uncoordinated phenotype. (A–B) Time-lapse images of wild-type iL3s (A) vs. *unc F₁* iL3s (B) swimming in a water droplet. Wild-type iL3s showed continuous rapid movement in water; *unc F₁* iL3s experienced intermittent bouts of twitching, paralysis, and uncoordinated movement. For A and B, red lines indicate iL3 trajectories. Scale bars = 200 μ m. (C) Swimming distance for wild-type iL3s vs. *unc F₁* iL3s over a 10-s period. *unc F₁* iL3s swam shorter distances relative to wild-type iL3s. *** $P < 0.001$, Mann-Whitney test. $n = 21$ – 23 trials for each population. (D) Average crawling speed for wild-type iL3s vs. *unc F₁* iL3s over a 20-s period. *unc F₁* iL3s showed reduced crawling speeds relative to wild-type iL3s. ** $P < 0.01$, unpaired t test with Welch's correction. $n = 30$ – 32 trials for each population. (E) Maximum crawling displacement for wild-type iL3s vs. *unc F₁* iL3s over a 5-min period. *unc F₁* iL3s traversed less distance than wild-type iL3s. ** $P < 0.01$, Mann-Whitney test. $n = 26$ trials for each population. For C–E, graphs show medians and interquartile ranges. *unc F₁* iL3 data for B–E were obtained from plasmid vector delivery of CRISPR-Cas9 constructs at *Ss-unc-22* site #1.

<https://doi.org/10.1371/journal.ppat.1006675.g002>

target sites (Fig 1B) using either plasmid vector or RNP complex delivery of CRISPR-Cas9 components (Fig 1C and 1D). We found that all three target sites, and both CRISPR delivery methods, yielded a population of twitching *F₁* iL3s, and we observed increasing twitching frequency corresponding to increasing predicted on-target activity for each site (Fig 3B, S1 Table). Only site #2 showed a significant difference between plasmid vector and RNP complex delivery, with RNP complex delivery generating a higher frequency of twitching iL3s than plasmid vector delivery (Fig 3B, S1 Table). Overall, we observed a twitching phenotype in

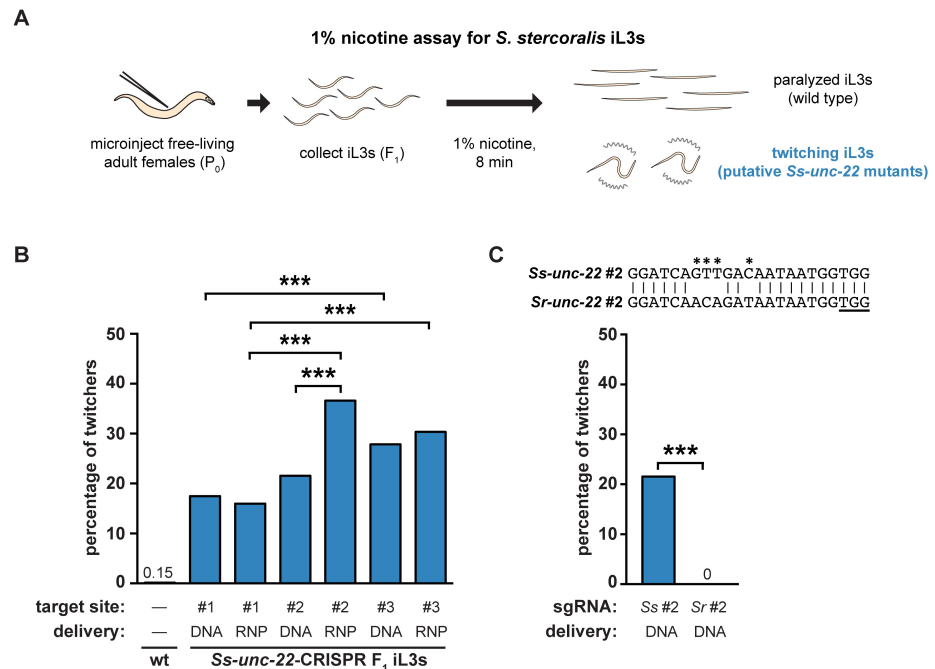


Fig 3. Nicotine induces twitching in *unc* F_1 iL3s. (A) A nicotine assay for *S. stercoralis* iL3s. Free-living adult females were injected with CRISPR constructs targeting *Ss-unc-22*. F_1 iL3s were collected and exposed to 1% nicotine. Wild-type iL3s gradually paralyzed over the course of 8 min, whereas *unc* F_1 iL3s twitched continuously. Some, but not all, of the F_1 iL3s contained putative *Ss-unc-22* mutations and twitched in nicotine. (B) Twitching frequency of *S. stercoralis* wild-type iL3s and the F_1 iL3s from microinjected females following nicotine exposure. For each condition, the *Ss-unc-22* target site and delivery method of the CRISPR-Cas9 constructs are indicated. DNA = plasmid vector delivery; RNP = ribonucleoprotein complex delivery. The twitching frequency of F_1 iL3s for all *Ss-unc-22* target sites and delivery methods tested differed from that of wild-type iL3s ($P < 0.001$, chi-square test with Bonferroni correction). Instances where twitching frequency differed between target sites or delivery methods are indicated. *** $P < 0.001$, chi-square test with Bonferroni correction. $n = 446-1,314$ iL3s per condition. (C) CRISPR-Cas9-mediated mutagenesis of *Ss-unc-22* requires a highly specific sgRNA. Plasmid vectors for the expression of Cas9 and a sgRNA targeting *S. ratti* site #2 were injected into *S. stercoralis*. The twitching phenotype in *S. stercoralis* F_1 iL3s was not observed when the *S. ratti* version of site #2 was used. *** $P < 0.001$, Fisher's exact test. $n = 484-677$ iL3s for each condition. The alignment of *S. stercoralis* and *S. ratti* site #2 is shown with the PAM underlined. Asterisks indicate nucleotide differences between the *S. stercoralis* and *S. ratti* targets.

<https://doi.org/10.1371/journal.ppat.1006675.g003>

~16–37% of the F_1 progeny depending on the target-site/delivery-method combination used (S1 Table). Thus, both plasmid vector and RNP delivery methods can be used for CRISPR-Cas9-mediated targeted mutagenesis in *S. stercoralis* to similar effect. Importantly, our results show that *unc* F_1 iL3s (resulting from putative *Ss-unc-22* mutations) can be generated at high efficiency in *S. stercoralis* by injecting a moderate number of P_0 females (S1 Table). Only one free-living generation is accessible for analysis before host infection is required to continue the life cycle. As a result, high efficiency of CRISPR-Cas9 editing in the F_1 is critical for either immediate investigation of first-generation mutants, or collection of sufficient numbers of mutant progeny to pass through a host and successfully generate a stable mutant line.

We also tested CRISPR-Cas9 activity in *Strongyloides ratti*, a parasite of rats, using the same method outlined for *S. stercoralis*. Like *S. stercoralis*, *S. ratti* can complete a free-living

generation outside the host and is amenable to transgenesis [3,11]. We tested two different CRISPR target sites for *Sr-unc-22* using plasmid vector delivery and screened F₁ iL3s in nicotine (S2A Fig). We found that both target sites yielded a population of twitching F₁ iL3s, and the nicotine-twitching frequency increased with predicted on-target activity (S2B Fig, S2 Table). The *S. ratti* nicotine-twitching phenotype was similar in severity to the phenotype observed in *S. stercoralis*. However, the twitching frequency was much lower in *S. ratti* than *S. stercoralis*, with only ~2–7% of F₁ progeny displaying the twitching phenotype when injecting a similar number of P₀ females (S2 Table). Our results demonstrate that CRISPR-Cas9 mutagenesis is applicable in both *S. stercoralis* and *S. ratti*, two important laboratory models for skin-penetrating parasitic nematode infections [23].

The genomes of *S. stercoralis* and *S. ratti* are very similar; their *unc-22* genes share >91% sequence identity [24]. The CRISPR target sequences for *Ss-unc-22* site #2 and *Sr-unc-22* site #2 differ by only four base pairs (Fig 3C). We asked whether CRISPR-Cas9 targeting was species-specific by injecting the plasmid vectors encoding Cas9 and the sgRNA for *S. ratti* site #2 into *S. stercoralis*. We found no evidence for twitching F₁ iL3s when the *S. ratti* version of the sgRNA was used (Fig 3C). Thus, CRISPR-Cas9-mediated mutagenesis of *Ss-unc-22* appears to require highly specific sgRNAs.

CRISPR-Cas9 mutagenesis causes putative deletion of the *Ss-unc-22* target locus

Most eukaryotes efficiently repair CRISPR-Cas9-induced DSBs through the NHEJ pathway [5–7,19,25]. NHEJ repair is error-prone and generally introduces small indels near the CRISPR cut site [5]. We asked if the *unc* F₁ iL3 motility and nicotine-twitching phenotypes observed for *S. stercoralis* resulted from CRISPR-Cas9-induced indels at *Ss-unc-22*. For each *Ss-unc-22* target site tested, we collected *unc* F₁ iL3s that twitched in nicotine (suggesting mutations to *Ss-unc-22*), PCR-amplified the region around the target, and genotyped for indels. Surprisingly, we were unable to detect indels at any of the three *Ss-unc-22* target sites tested. We attempted to identify indels through Sanger sequencing of the target region, heteroduplexed DNA detection by polyacrylamide gel electrophoresis (PAGE) [26], T7E1 endonuclease activity [27], and TIDE (Tracking of Indels by sequence DEcomposition) [28]. For all of the indel detection methods tested, we only observed *Ss-unc-22* wild-type sequence. However, when genotyping individual iL3s, we could reproducibly PCR-amplify the *Ss-unc-22* target region from wild-type iL3s but noted inconsistency in our ability to amplify the *Ss-unc-22* target region from *unc* F₁ iL3s (Fig 4A). Using control primers, we could however successfully amplify another location in the genome from the same *unc* F₁ iL3s where the *Ss-unc-22* target region amplified poorly (Fig 4A). Thus, PCR variability was specific to *unc* F₁ iL3s at the *Ss-unc-22* target region (Fig 4B). Based on the lack of detectable indels in *unc* F₁ iL3s, we hypothesized that the observed PCR variability at the *Ss-unc-22* target region likely resulted from CRISPR-Cas9-induced deletions that eliminated one, or both, of the primer binding sites. Given that the *C. elegans unc* phenotype is dominant [12,13], *unc* F₁ iL3s where the wild-type band was present are likely heterozygous, or mosaic, deletions of the *Ss-unc-22* target region. *unc* F₁ iL3s where the band was absent are putative homozygous deletions of *Ss-unc-22* (Fig 4B). We observed putative homozygous deletions for *Ss-unc-22* sites #2 and #3, the more efficient targets, but not *Ss-unc-22* site #1 (S3 Table).

To test the hypothesis that CRISPR-Cas9-mediated mutagenesis results in deletions at the target region, we performed a large-scale microinjection of free-living adults with the RNP complex targeting *Ss-unc-22* site #3. We focused on site #3 since it appeared to produce the most efficient mutagenesis of *Ss-unc-22* (Fig 3B). A single-stranded oligodeoxyribonucleotide

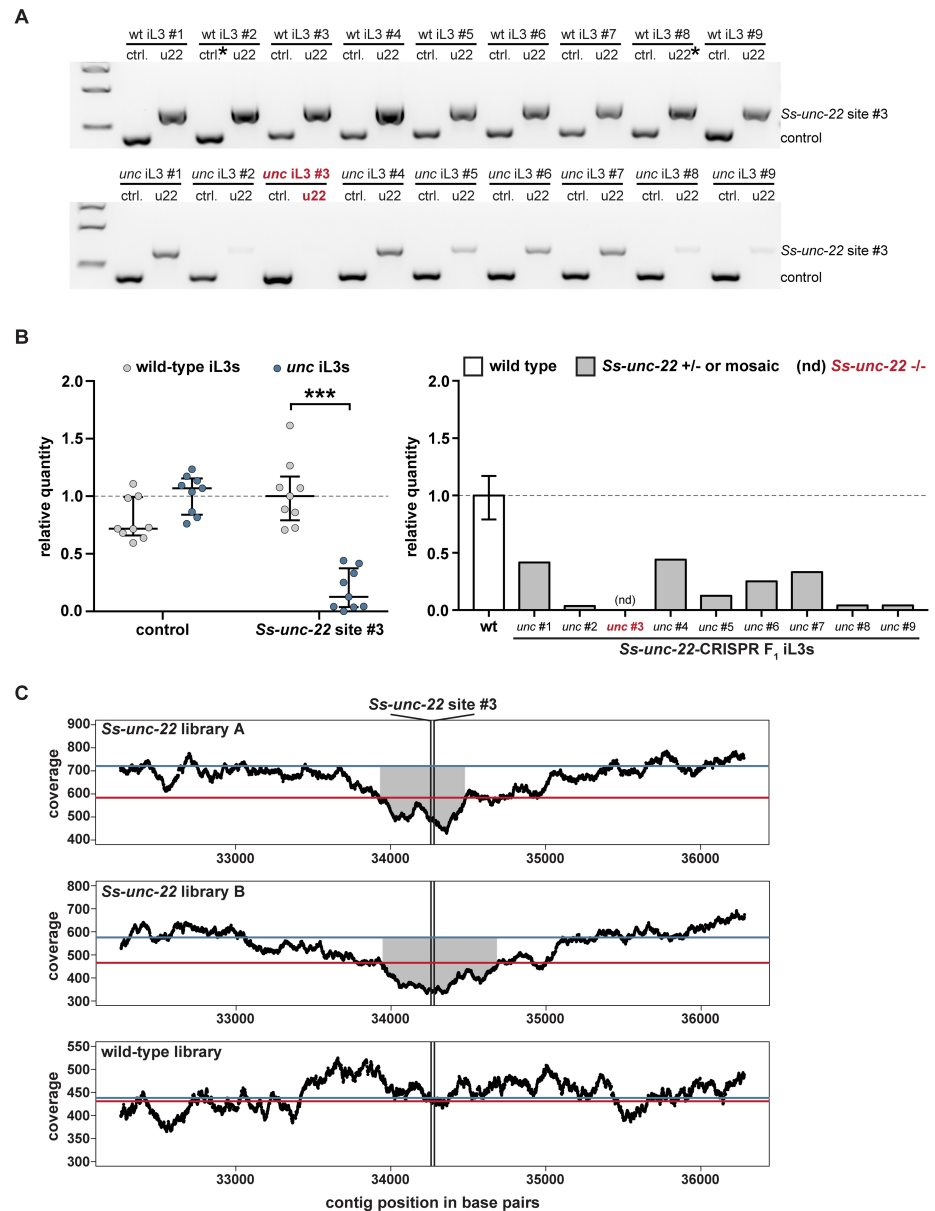


Fig 4. CRISPR-mediated mutagenesis of *Ss-unc-22* results in putative deletion of the target locus. (A) Representative gel of wild-type iL3s (top) or *unc* F₁ iL3s from RNP injections at site #3 (bottom). Genomic DNA from each iL3 was split into two reactions: ctrl. = control reaction amplifying 416 bp of the first exon of the *Ss-act-2* gene to confirm the presence of genomic DNA; u22 = reaction amplifying 660 bp around site #3. Size markers = 1.5 kb, 1 kb, and 500 bp from top to bottom. **(B)** The *Ss-unc-22* region is significantly depleted in *unc* F₁ iL3s. Left: relative quantity analysis of PCR products. All control bands and all u22 bands were quantified relative to their respective reference bands, denoted by asterisks in **A**. Values >1 indicate more PCR product than the reference while values <1 indicate less product. *** $P < 0.001$, two-way ANOVA with Sidak's post-test. Medians and interquartile ranges shown. Right: relative quantity of

the *Ss-unc-22* site #3 target region for each *unc* F₁ iL3 tested, and inferred genotypes. nd = PCR product not detected. (C) Whole-genome sequencing coverage plots for populations of *Ss-unc-22*-targeted F₁ iL3s or wild-type iL3s. A 4-kb window centered on the predicted cut site is shown [24,47]. Black lines = average coverage depth by position (reads per base); red lines = average genome-wide coverage; blue lines = average coverage for the *Ss-unc-22* gene. Coverage around *Ss-unc-22* site #3 is significantly depleted in both *Ss-unc-22* libraries relative to the *Ss-unc-22* gene average ($P < 0.05$; see Methods). No depletion is observed in the wild-type library ($P > 0.05$; see Methods). Gray shaded regions represent stretches of continuous significant coverage depletion around the cut site (*Ss-unc-22* library A = 510 bp, *Ss-unc-22* library B = 725 bp).

<https://doi.org/10.1371/journal.ppat.1006675.g004>

(ssODN) was also included in the injection mix to further improve targeting efficiency (described below). We collected a mixed population of wild-type and *unc* F₁ iL3s, where ~40% of the iL3s displayed the nicotine-twitching phenotype. From this mixed wild-type and *unc* F₁ population, we prepared two libraries for whole-genome sequencing, as well as a library prepared entirely from wild-type iL3s (S4 Table). We found that the *Ss-unc-22* libraries showed significant depletion in read coverage for an extended stretch of >500 base pairs around *Ss-unc-22* site #3, while no such depletion was observed in the wild-type library (Fig 4C). When targeting *Ss-unc-22* site #3, we found no evidence for read depletion at *Ss-unc-22* site #1 or site #2 in either *Ss-unc-22* library (S3 Fig). Similarly, we found no evidence for read depletion at an unrelated CRISPR target at a distant genomic location in the *Ss-tax-4* gene (see below) (S4 Fig). The observation that read coverage is depleted specifically around site #3 in the *Ss-unc-22* libraries, but not in the wild type, is consistent with the hypothesis that CRISPR-Cas9-mediated mutagenesis results in large deletions rather than small indels at the target locus. To further confirm the lack of small indels, we analyzed indel frequency in the deep-sequencing samples using the CRISPRessoWGS and CRISPRessoCompare computational suite [29]. The CRISPRessoWGS program is designed to analyze deep-sequencing reads aligned to a reference genome and quantify CRISPR-Cas9-editing outcomes, such as indels, at defined targets of interest [29]. We again found no evidence for indels at *Ss-unc-22* site #3 in either *Ss-unc-22* library, suggesting that all of the reads overlapping *Ss-unc-22* site #3 were obtained either from wild-type F₁ iL3s in the sample or from heterozygous/mosaic *unc* F₁ iL3s where deletion of the target locus was incomplete.

We note that while >500 base pairs around *Ss-unc-22* site #3 were found to be significantly depleted by whole-genome sequencing, the size of the deletion in many individual *unc* iL3s is likely to be substantially larger. There are a number of possible explanations for why a depleted region of only ~500 base pairs was observed in whole-genome sequencing analysis. First, whole-genome sequencing was performed on a mixed population of iL3s that included both wild-type and *unc* individuals. A mixed population was prepared because, given the labor-intensive nature of the microinjection procedure and screening process for *unc* iL3s, it was impractical to create an all-*unc* population of sufficient density for reliable whole-genome sequencing. As a result, many of the reads from the *Ss-unc-22* libraries were in fact from wild-type individuals. Second, the vast majority of individuals with the *unc* phenotype in the *Ss-unc-22* libraries were mosaics or heterozygotes, and therefore contained wild-type sequence in addition to edited sequence (Fig 4B). Third, each mutant F₁ iL3 in the *Ss-unc-22* libraries had a potentially different deletion, since the population was not clonal. For these reasons, it is likely that the only region that showed significant depletion is the deleted region that is shared among all of the *unc* iL3s. Many *unc* iL3s may contain larger deletions, as suggested by our PCR results, but these deletions may be positioned asymmetrically around the target site, with the exact breakpoints varying across individuals. The varied nature of these deletions, coupled with the mixture of wild-type and edited DNA sequence, made it impossible to detect larger deletions in the whole-genome sequencing experiments.

Our finding that CRISPR-Cas9-mediated DSBs resulted in deletion of the target locus raised the possibility of unintended disruption of nearby genes. We therefore asked if genomic loci upstream and downstream of *Ss-unc-22* site #3 were intact following CRISPR-Cas9-mediated deletions. To test this, we isolated rare *unc* F₁ iL3s with putative homozygous deletions of *Ss-unc-22*. For each iL3, we then PCR-amplified regions 10-kb upstream and downstream of the target site; the downstream target amplified in the second exon of the closest gene neighboring *Ss-unc-22* (S5A Fig). For all of the *unc* F₁ iL3s tested, we successfully amplified the upstream and downstream targets, suggesting that genomic loci near *Ss-unc-22* site #3 are intact following CRISPR-Cas9-mediated deletions (S5B Fig).

We attempted to map the precise endpoints of the *Ss-unc-22* deletion events in *unc* iL3s by PCR-amplifying regions of increasing size, up to 20 kilobases, around the CRISPR target site. However, we never observed PCR products smaller than the wild-type product. We always observed either the wild-type product or no product (Fig 4, S5 Fig). This is likely due to the fact that each deletion in an individual iL3 is potentially unique, making it difficult to optimally design primers to robustly PCR-amplify multiple different deletion events. Further complicating this approach, genomic DNA isolated from individual iL3s is low in concentration, and amplicons of >2–3 kb cannot be amplified reliably. Thus, mapping the endpoints of deletion events was not feasible from individual *unc* iL3s. Additionally, we cannot exclude the possibility that complex chromosomal rearrangements, inversion events, or deletions with inversion events occurred that could not be detected via the methods utilized in this study. Both large deletions and chromosomal rearrangements have been observed in *C. elegans* in some cases, and this phenomenon may be more common at certain genomic loci than others [30]. Similar chromosomal rearrangements may have precluded our ability to precisely map CRISPR-mediated mutation events at *Ss-unc-22* targets.

Taken together, our results suggest that CRISPR-Cas9-induced mutations to *Ss-unc-22* are not resolved by small indels near the target, but instead result in deletions around the target site. Importantly, we infer putative homozygous deletions of *Ss-unc-22* in ~2–5% of the *unc* F₁ iL3s genotyped by PCR (S3 Table). Given the challenges for targeted mutagenesis in parasitic nematodes, the ability to isolate homozygous deletions in the F₁ generation is critical because it allows for mutant analysis without the need for laborious host passage.

Homology-directed repair of CRISPR-Cas9-mediated mutations in *S. stercoralis*

CRISPR-Cas9-induced DSBs can also be resolved by HDR when a repair template is provided [5]. We asked if DSBs at *Ss-unc-22* could incorporate a repair template containing a fluorescent reporter by HDR, thereby providing an alternative to deletion of the target locus that would facilitate genotyping as well as identification of mutant nematodes. To address this question, we designed a plasmid containing a repair template for *Ss-unc-22* site #2. The repair template consisted of *mRFPmars* under the control of the promoter for the *Strongyloides* actin gene *Ss-act-2*, which expresses in contractile filaments of the nematode body wall [31]; the reporter was flanked by homology arms directly adjacent to the CRISPR-Cas9 cut site (Fig 5A). We injected plasmid vectors for the repair template, Cas9, and the sgRNA for site #2 into *S. stercoralis*. Interestingly, we found that injections including the repair template increased the percentage of *unc* F₁ iL3s twitching in nicotine when compared to injections without a repair template (S6A Fig, S5 Table). We then isolated *unc* F₁ iL3s that displayed a nicotine-twitching phenotype and screened for *mRFPmars* expression, predicting that a subset of these iL3s had successfully repaired CRISPR-Cas9-induced DSBs by HDR. We isolated *unc* F₁ iL3s with a range of *mRFPmars* expression patterns and fluorescence intensities (Fig 5B). *unc* F₁ iL3s that

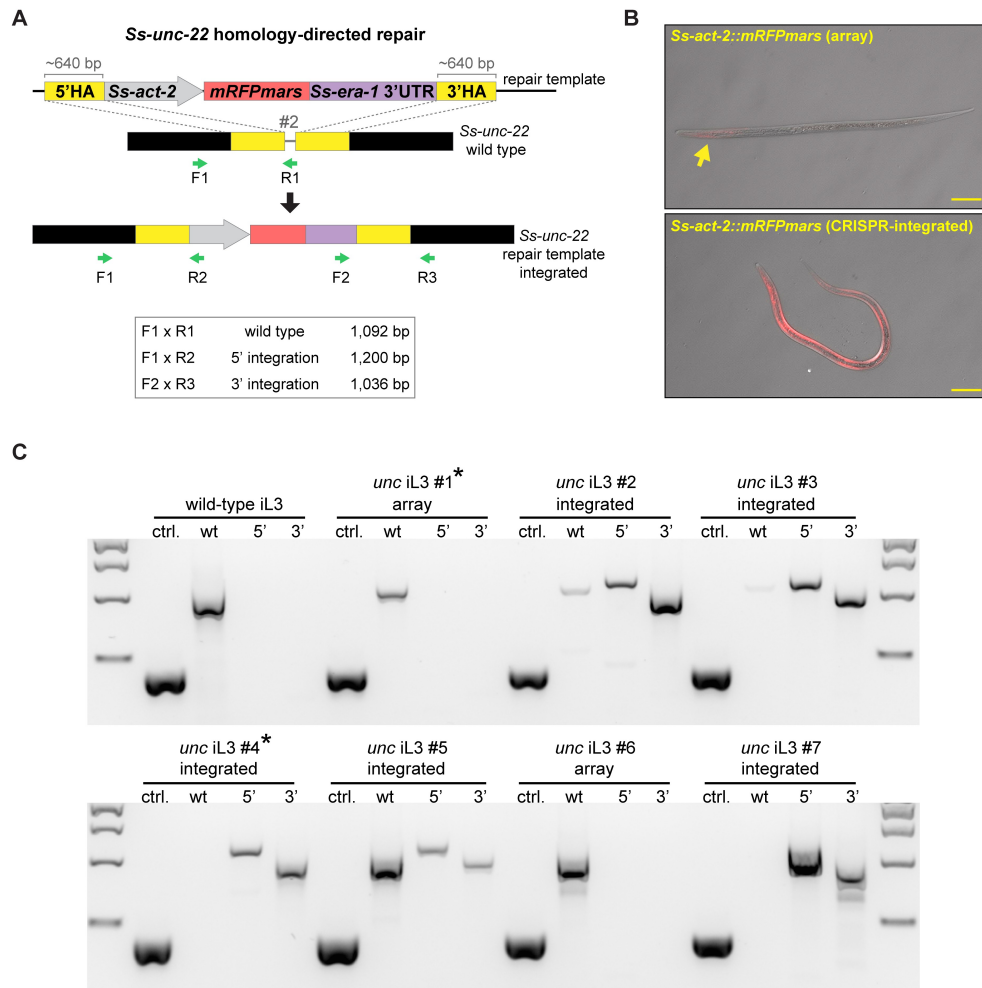


Fig 5. CRISPR-mediated homology-directed repair of *Ss-unc-22*. (A) Strategy for HDR at *Ss-unc-22* target site #2. *unc* F₁ iL3s that displayed both the nicotine-twitching phenotype and red fluorescence were selected as candidates for HDR and were genotyped using the primer sets indicated. 5' and 3' integration primer pairs amplify only following successful integration of *Ss-act-2::mRFPmars* into site #2. HA = homology arm. (B) Representative DIC + epifluorescence overlays of *unc* F₁ iL3s expressing *Ss-act-2::mRFPmars*. Top, iL3 expressing *mRFPmars* (sparse expression indicated by the arrow) from an extrachromosomal array. Bottom, iL3 expressing *mRFPmars* following HDR, showing near-uniform *mRFPmars* expression in the body wall. For both images, anterior is to the left. Scale bar = 50 μ m. (C) Representative genotypes of a wild-type iL3 and *unc* F₁ iL3s expressing *mRFPmars*. Genomic DNA from individual iL3s was split into four reactions: ctrl. = control reaction amplifying 416 bp of the first exon of the *Ss-act-2* gene to confirm the presence of genomic DNA; wt = reaction for the wild-type locus of site #2 where primer R1 overlaps the predicted CRISPR cut site; 5' = reaction for insertion of the 5' border of the integrated cassette; 3' = reaction for insertion of the 3' border of the integrated cassette. For genotypes: array = red *unc* F₁ iL3s that showed no evidence of integration; integrated = red *unc* F₁ iL3s with successful HDR. Some integrated iL3s had putative homozygous disruptions of *Ss-unc-22* site #2 (e.g. iL3s #4 and #7, which lacked the wt band). Asterisks indicate genotypes for iL3s shown in B. Size markers = 2 kb, 1.5 kb, 1 kb, and 500 bp from top to bottom.

<https://doi.org/10.1371/journal.ppat.1006675.g005>

expressed *mRFPmars* were genotyped for integration of the repair template using primer sets that spanned the 5' and 3' boundaries of the inserted cassette (Fig 5A). We found that >50% of the *unc* F₁ iL3s that expressed *mRFPmars* showed integration of the repair template at *Ss-unc-22* (Fig 5C, S6 Table). Importantly, we isolated several integrated iL3s that appeared to be putative homozygous knockouts of *Ss-unc-22*: these iL3s were found to lack a wild-type PCR product using a reverse primer that binds the target site (Fig 5C, S6 Table). These results demonstrate the feasibility of generating putative homozygous mutant iL3s in the F₁ generation using HDR. Sequencing from the 5' and 3' boundaries of the repair template confirmed its insertion at the target site (S7 Fig).

In *C. elegans*, CRISPR-Cas9-induced DSBs can also be resolved by HDR using an ssODN repair template [20,32]. The ssODN repair strategy has the advantage that ssODNs can be commercially synthesized to allow for rapid CRISPR target testing [20,32]. We asked if ssODNs are also suitable repair templates for HDR in *S. stercoralis*. We designed an ssODN for *Ss-unc-22* site #3 (S8A and S8B Fig) and injected it with RNP complexes targeting the same site. Our ssODN was designed in the sense orientation, because sense orientation ssODNs have been shown, in some cases, to be more effective HDR templates in *C. elegans* [33]. As with the presence of the *Ss-act-2::mRFPmars* repair template, the presence of the ssODN increased the percentage of *unc* F₁ iL3s twitching in nicotine (S6B Fig, S5 Table). However, we found no evidence for ssODN integration at *Ss-unc-22* site #3 (S8C and S8D Fig). To determine if the absence of ssODN integration was due to the target site selected, or delivery method, we also designed an ssODN for *Ss-unc-22* site #2 and injected it with plasmid vectors. Similarly, we saw no evidence for ssODN integration when using the same target site and delivery method that was used for *Ss-act-2::mRFPmars* integration. Our results raise the possibility that incorporation of ssODNs into CRISPR-Cas9-mediated DSBs may not be feasible in *S. stercoralis*.

To confirm that integration of the *Ss-act-2::mRFPmars* repair template by HDR was specific to CRISPR-Cas9-induced DSBs at *Ss-unc-22*, we repeated injections but removed the Cas9 plasmid vector. We did not observe *unc* F₁ iL3s twitching in nicotine when Cas9 was omitted, suggesting that *Ss-unc-22* site #2 was not disrupted in the absence of Cas9-induced DSBs (S9A Fig). Similarly, we found no evidence for *unc* F₁ iL3s twitching in nicotine when Cas9 was omitted from RNP complex injections (S9B Fig). Thus, DSBs at *Ss-unc-22* appear to be specifically triggered by CRISPR-Cas9 mutagenesis.

We next asked if CRISPR-Cas9-mutagenesis coupled with HDR of a fluorescent reporter was applicable to other *S. stercoralis* genes. To further validate our HDR approach, we targeted the *S. stercoralis* ortholog of the *C. elegans tax-4* gene. *Ce-tax-4* encodes a subunit of a cyclic nucleotide gated ion channel that is required for many chemosensory-driven responses in sensory neurons [34,35]. We identified a CRISPR target site for *Ss-tax-4* and modified the *mRFPmars* repair template to contain homology arms near the *Ss-tax-4* CRISPR-Cas9 cut site (S10A and S10B Fig). Following injection of the repair template, Cas9, and the sgRNA for *Ss-tax-4* site #1, we collected F₁ iL3s and screened for *mRFPmars* expression, again predicting that some of these iL3s would show integration events. As with HDR at *Ss-unc-22*, we isolated *mRFPmars*-expressing F₁ iL3s that showed *Ss-tax-4* integration events by PCR (S10C Fig, S6 Table). Sequencing from the 5' boundary of the repair template confirmed its insertion at the *Ss-tax-4* target site (S10D Fig).

Taken together, we conclude that DSBs in *S. stercoralis* are specifically triggered by CRISPR-Cas9-mediated mutagenesis, and can be precisely resolved by HDR when a plasmid repair construct is provided. Furthermore, as demonstrated with integration of *Ss-act-2::mRFPmars*, repair constructs containing a fluorescent reporter can be used to efficiently screen

for gene disruptions in the F₁ generation. This approach will likely be applicable to many genes of interest in the *S. stercoralis* genome.

Heritable transmission of *Ss-unc-22* mutations

One of the challenges for generating targeted gene disruptions in *S. stercoralis* is the need to passage F₁ progeny through a host to maintain the mutation of interest [3]. We developed two strategies to examine if CRISPR-Cas9-induced *Ss-unc-22* mutations are heritable following host passage. First, we injected CRISPR-Cas9 complexes into free-living adult females and collected F₁ iL3s where approximately 50% of the F₁ population twitched in nicotine. The mixed population of *unc* F₁ iL3s and wild-type iL3s was then used to infect gerbils, which are permissive laboratory hosts for *S. stercoralis* [36,37]. In a second approach, we injected free-living adult females, collected F₁ iL3s, enriched for nicotine-twitching *unc* iL3s, and infected gerbil hosts. As a control, we also infected gerbils with exclusively wild-type iL3s (Fig 6A, S7 Table).

Following host infection, we collected host feces from each germline transmission strategy, reared F₂ and F₃ progeny, and screened for the nicotine-twitching phenotype as an indicator of successful germline inheritance of *Ss-unc-22* mutations. From the mixed *unc* and wild-type infection strategy, we exclusively screened for the twitching phenotype in F₂ or F₃ iL3s. We successfully isolated nicotine-twitching *unc* F₂ or F₃ iL3s from the mixed infection over multiple fecal collection days but never observed twitching iL3s from the wild-type control (S7 Video). The average nicotine-twitching frequency of iL3s collected from the mixed infection was 1.2% (Fig 6B, S7 Table). From the *unc*-enriched infection, we screened for the twitching phenotype in both F₂ free-living adults and F₂ or F₃ iL3s. We isolated nicotine-twitching *unc* F₂ free-living adults from the *unc*-enriched infection but never observed twitching adults from the wild-type control (S8 and S9 Videos). The nicotine-twitching phenotype was observed in ~5% of F₂ adults (Fig 6B, S7 Table). When we screened F₂ or F₃ iL3s from the *unc*-enriched infection, we observed a nicotine-twitching frequency of 2.6% (Fig 6B, S7 Table). An ~5% twitching frequency in F₂ free-living adults and an ~2.5% twitching frequency in their F₃ iL3 progeny is consistent with the *unc* phenotype being dominant, and with *unc* F₃ iL3s resulting from mating events between an *unc* individual and a wild-type individual.

To further validate germline transmission of *Ss-unc-22* mutations, we also characterized the *unc* motility phenotypes of F₂ and F₃ iL3s. Twitching F₂ or F₃ iL3s were recovered from nicotine and their motility was compared to nicotine-recovered wild-type iL3s. *unc* F₂ or F₃ iL3s showed impaired swimming behavior when compared to wild-type iL3s (Fig 6C). Similarly, automated tracking revealed that *unc* F₂ or F₃ iL3s showed reduced crawling speeds relative to wild-type iL3s (Fig 6D). The *unc* phenotype observed for F₂ or F₃ iL3s was similar to that observed for F₁ iL3s (Fig 2). Thus, CRISPR-Cas9-mediated mutations are germline-transmissible, and mutant parasites can be propagated by host passage.

Discussion

Here we demonstrate the first targeted gene disruptions in a parasitic nematode resulting in a mutant phenotype. We exploited the complex life cycle of the human-parasitic threadworm *S. stercoralis* to deliver CRISPR-Cas9 constructs targeting *Ss-unc-22* into free-living adults, and characterized *Ss-unc-22* mutations in iL3 progeny (Fig 1). Using this strategy, we generated free-living adults and infective larvae with severe motility defects and altered nicotine sensitivity (Figs 2, 3 and 6). Furthermore, we optimized CRISPR-Cas9 targeting and obtained putative homozygous knockouts in the F₁ generation, a development that circumvents the necessity for labor-intensive host passage and allows for the immediate interrogation of mutant phenotypes in parasitic worms (Figs 4 and 5). A similar approach is likely to be immediately applicable to

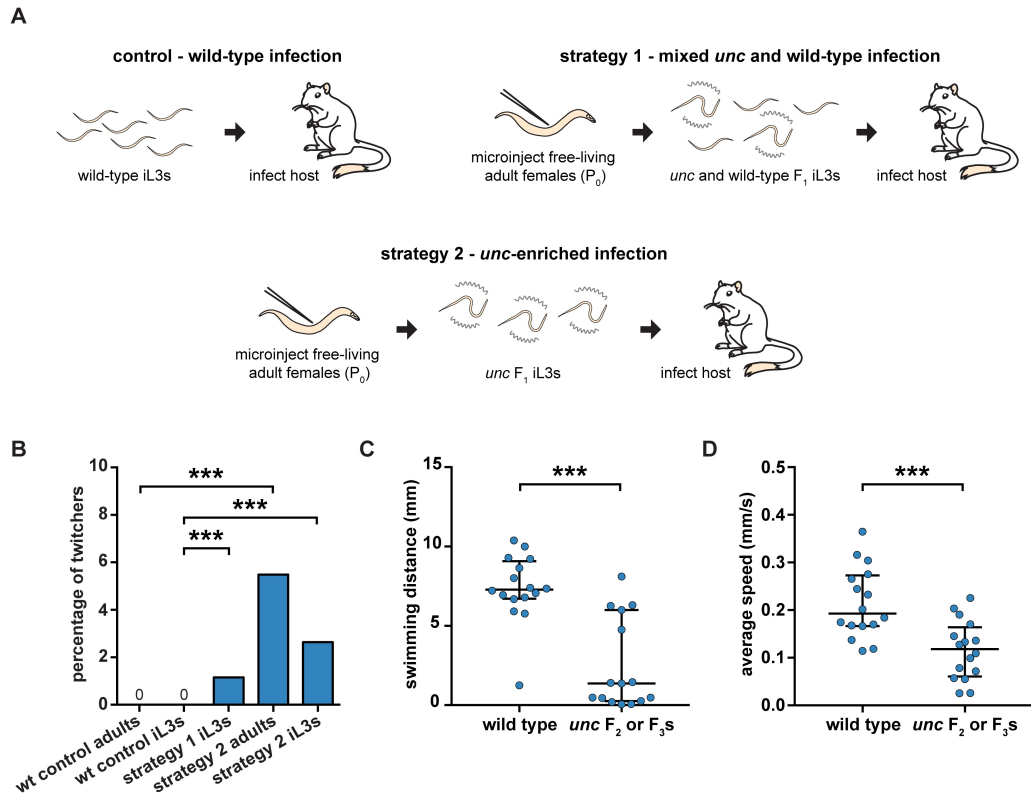


Fig 6. The *unc* phenotype is heritable following host passage. (A) Strategies for heritable transmission of *Ss-unc-22* mutations. Gerbil hosts were infected with either all wild-type iL3s, a 50/50 mix of *unc* and wild-type F_1 iL3s, or *unc*-enriched F_1 iL3s. F_2 and F_3 progeny were collected from host feces and screened for *unc* phenotypes. Note that iL3s collected from host feces can be the F_2 or F_3 generation depending on whether they developed into iL3s directly, or after a free-living generation (Fig 1A) [10]. (B) Twitching frequency of wild-type control progeny and F_2 or F_3 progeny collected from *unc* infections. The twitching frequency of the F_2 or F_3 iL3s collected from the mixed *unc* infection differed from that of wild-type iL3s. *** P <0.001, chi-square test with Bonferroni correction. $n = 1,908$ – $3,849$ iL3s per condition. The twitching frequency of F_2 adults collected from the *unc*-enriched infection differed from that of wild-type adults. *** P <0.001, chi-square test with Bonferroni correction. $n = 164$ – 332 adults per condition. The twitching frequency of F_2 or F_3 iL3s collected from the *unc*-enriched infection differed from that of wild-type iL3s. *** P <0.001, chi-square test with Bonferroni correction. $n = 2,694$ – $3,849$ iL3s per condition. (C) Swimming distance for wild-type iL3s vs. *unc* F_2 or F_3 iL3s over a 10-s period. *unc* iL3s swam shorter distances than wild-type iL3s. *** P <0.001, Mann-Whitney test. $n = 15$ – 16 worms for each population. (D) Mean crawling speed for wild-type iL3s vs. *unc* F_2 or F_3 iL3s over a 20-s period. *unc* iL3s showed reduced crawling speeds relative to wild-type iL3s. *** P <0.001, unpaired t test with Welch's correction. $n = 16$ worms for each population.

<https://doi.org/10.1371/journal.ppat.1006675.g006>

other parasitic nematode species, particularly those in the *Strongyloides* and *Parastrongyloides* genera, which are well-suited for gonadal microinjection of CRISPR-Cas9 plasmid vectors or RNP complexes [23,38,39]. Importantly, our results demonstrate that the CRISPR-Cas9 system is functional in parasitic nematodes and represents the first realistic opportunity for systematic gene knockout studies. With additional technical development, this approach may be adaptable to other parasitic nematodes with environmental life stages, such as numerous plant-parasitic and entomopathogenic nematode species.

Both *S. ratti* and *S. stercoralis* have been proposed as models for targeted mutagenesis in parasitic nematodes [3,11]. *S. ratti* has the advantage of requiring fewer iL3s to infect a host;

only ~10–20 *S. ratti* iL3s are needed to infect a rat, while >1,000 *S. stercoralis* iL3s are needed to reliably infect a gerbil. Thus, *S. ratti* has been considered the more efficient option for generating stable lines [3,37,40]. In contrast, *S. stercoralis* has been shown to be more tolerant of the gonadal microinjection procedure and F₁ nematodes express transgenes more efficiently [3,11,40]. We found that CRISPR-Cas9 mutagenesis in *Strongyloides* was strikingly similar to reported transgenesis outcomes; *unc-22* mutagenesis was more efficient in *S. stercoralis* than *S. ratti*, with 17–28% and 2–7% of F₁ iL3s twitching in nicotine, respectively, when using plasmid vector delivery of CRISPR-Cas9 and injecting a similar number of P₀ females (Fig 3, S2 Fig, S1 and S2 Tables). The higher mutagenesis efficiency we observed with *S. stercoralis* may reflect its increased tolerance of the microinjection procedure. However, future work targeting a number of different genes in *S. stercoralis* and *S. ratti* will be necessary to determine whether CRISPR-Cas9-mediated mutagenesis is more efficient in *S. stercoralis* at all target sites, or only in certain cases. Importantly, the rate of CRISPR-Cas9-mediated mutagenesis in *S. stercoralis* was sufficient for germline-transmission and host propagation, as we collected F₂ adults and F₂ or F₃ iL3s with *unc* phenotypes after host passage (Fig 6). However, we note that long-term propagation of the *Ss-unc-22* mutations was not practical given the low efficiency of F₂ and F₃ mutant recovery (Fig 6), presumably because the severe motility defects of *Ss-unc-22* iL3s reduced their ability to establish an infection in the host.

Based on the CRISPR-mediated disruption of *Ss-unc-22* and *Sr-unc-22* presented here, future studies pursuing targeted mutagenesis are likely to be feasible in both *S. stercoralis* and *S. ratti*, with each system having potential advantages. *S. stercoralis*, in addition to its direct health relevance as a human parasite, may prove to be a more valuable system for pursuing rapid investigation of homozygous knockouts in the F₁ generation. Our results show that F₁ mutagenesis was efficient enough to generate putative homozygous knockouts of *Ss-unc-22* (Figs 4 and 5). Further adding to the potential utility of *S. stercoralis*, a recent study demonstrated that heritable transgenesis is also possible by microinjection of plasmid constructs into the testicular syncytium of free-living males [41]. Future CRISPR-Cas9 strategies simultaneously targeting both *S. stercoralis* free-living males and females may further improve the incidence of F₁ homozygous knockouts. In contrast to *S. stercoralis*, gene disruptions in *S. ratti* are likely to be easier to maintain through successive rounds of host passage due to a more manageable infective dose. Additionally, given the wealth of information for host-parasite interactions between *S. ratti* and the rat host, gene knockout studies focused on host immune response, parasite immune manipulation or evasion, and anthelmintic drug administration may be well-suited to this system [42].

Targeted mutagenesis in parasitic nematodes presents a unique challenge in that mutant progeny must be propagated through a host to continue the life cycle. In some cases, knocking out a gene of interest may interfere with the ability of iL3s to infect a host. For example, we recovered only a small percentage of *unc* progeny in the F₂ and F₃ generations following host passage (Fig 6, S7 Table). As mentioned above, one hypothesis for the low frequency of *unc* F₂ and F₃ progeny is that *unc* iL3s are disadvantaged relative to wild-type iL3s during host infection. Host infection is a multi-step migratory process; iL3s infect by skin penetration, navigate to the circulatory system, penetrate the lungs, and are then thought to be coughed up and swallowed en route to parasitizing the intestinal tract [9]. We observed severe motility defects in *unc* F₁ iL3s that may handicap their ability to migrate inside the host (Fig 2). Supporting the hypothesis that *unc* motility defects might impede host infection, we consistently recovered fewer F₂ and F₃ nematodes from the host feces of *unc*-enriched infections than wild-type infections, despite infecting gerbil hosts with similar numbers of F₁ iL3s (S7 Table). Mutagenesis studies targeting genes that are essential for parasitic nematodes to infect or develop within the host could be difficult to maintain over multiple generations, although it may be possible to

maintain recessive mutations in these genes by passaging heterozygous iL3s through hosts. CRISPR-Cas9 mutagenesis that can efficiently generate homozygous knockouts in a single generation may prove to be the most realistic option for mutant analysis in these cases, and we have demonstrated that this approach is feasible in *S. stercoralis*. In contrast, target genes that are not required for infectivity or in-host development may be easier to maintain than the *Ss-unc-22* mutations generated here.

Our results suggest that *S. stercoralis* can correct CRISPR-Cas9-induced DSBs by HDR when a plasmid repair template is provided, but not an ssODN (Fig 5, S8 and S10 Figs). In the absence of HDR, we found no evidence for indels at the *Ss-unc-22* target sites tested but instead observed putative large deletions of the target locus (Fig 4). Many eukaryotes predominantly use NHEJ as a DSB repair mechanism [5–7,19,25]. However, whether *S. stercoralis* is capable of NHEJ remains unclear. In *C. elegans*, DSBs in somatic tissues are repaired by NHEJ, but recent work has demonstrated that germline CRISPR-induced DSBs are repaired by polymerase theta (POLQ)-mediated end joining [43]. Interestingly, CRISPR-Cas9 mutagenesis in *polq-1* deficient *C. elegans* routinely results in deletions averaging 10–15 kilobases, including at *Ce-unc-22* targets [43]. In addition, CRISPR-mediated deletions have also been observed in systems that are capable of NHEJ repair. For example, a recent report of CRISPR-Cas9 mutagenesis outcomes in mouse embryonic stem cells suggests that ~20% of edited cells resolve mutations by deletions of 250–9500 base pairs [44]. We hypothesize that *S. stercoralis* may favor deletion-based repair of DSBs over generating small indels near the cut site. While we were unable to map the precise endpoints of putative deletions at *Ss-unc-22*, our results suggest that the deletions were greater than 500 base pairs in *unc* F₁ iL3s, and that the regions 10 kilobases upstream and downstream of the target were unaltered (Fig 4, S5 Fig). We cannot, however, rule out the possibility of more complex DSB repair outcomes such as chromosomal rearrangements, inversion events, or rare indels not detected with the methods used here. Further work will be needed to characterize the DSB repair mechanism in the *S. stercoralis* germline in more detail.

In practical terms, HDR using a repair template may be the most straightforward application of CRISPR-Cas9-mediated mutagenesis in *Strongyloides* given that: 1) adding a repair template increases overall targeting efficiency (S6 Fig), 2) HDR is sufficient to generate putative homozygous knockouts in the F₁ generation (Fig 5, S6 Table), 3) HDR results in precise insertion of the construct of interest at the CRISPR target site instead of generating large deletions (Fig 5, S7 and S10 Figs), 4) incorporation of a fluorescent marker, like *mRFPmars*, simplifies mutant identification and isolation (Fig 5B), and 5) an HDR-based gene disruption strategy is likely to be applicable to many targets in the *S. stercoralis* genome (S10 Fig).

In-depth molecular studies in parasitic nematodes have not yet been feasible due to the lack of a toolkit for genetic intervention. We have developed the first practical method for targeted gene disruptions in parasitic nematodes using CRISPR-Cas9. Our results provide a foundation for making these previously intractable parasites more accessible to functional molecular analysis, which may accelerate the development of new strategies to prevent human-parasitic nematode infections.

Materials and methods

Ethics statement

Gerbils were used to passage *S. stercoralis*. Rats were used to passage *S. rattii*. All protocols and procedures used in this study were approved by the UCLA Office of Animal Research Oversight (Protocol No. 2011-060-21A), which adheres to AAALAC standards and the *Guide for the Care and Use of Laboratory Animals*.

Nematodes and hosts

C. elegans strains were either N2 Bristol (wild type) or CB66 *Ce-unc-22(e66)* and were obtained from the *Caenorhabditis* Genetics Center. *Strongyloides stercoralis* were the UPD strain and *Strongyloides ratti* were the ED321 strain [22]. Male Mongolian gerbils used to maintain *S. stercoralis* were obtained from Charles River Laboratories. Female Sprague-Dawley rats used to maintain *S. ratti* were obtained from Envigo Laboratories.

Maintenance of *S. stercoralis*

S. stercoralis was maintained by serial passage in male Mongolian gerbils as described [36]. *S. stercoralis* infective third-stage larvae (iL3s) were collected from fecal-charcoal cultures using a Baermann apparatus [36]. iL3s were cleaned of fecal debris by passage through ~0.5% low-gelling-temperature agarose (Sigma-Aldrich, Cat. # A0701) and washed 5 times in sterile 1x PBS. Isoflurane-anesthetized gerbils were inoculated by subcutaneous injection of ~2,250 iL3s suspended in 200 μ L sterile 1x PBS. Feces infested with *S. stercoralis* were collected during the patency period of infection, between days 14–45 post-inoculation. Fecal pellets were obtained by placing infected gerbils on wire cage racks overnight with wet cardboard lining the cage bottom; fecal pellets were collected the following morning. Fecal pellets were softened with dH₂O, crushed, and mixed in a 1:1 ratio with autoclaved charcoal granules (bone char from Ebonex Corp., Cat # EBO.58BC.04). Fecal-charcoal cultures were stored in Petri dishes (10-cm diameter x 20-mm height) lined with dH₂O-saturated filter paper. To collect free-living *S. stercoralis* adults, fecal-charcoal cultures were stored at 20°C for 48 h and adults were isolated using a Baermann apparatus. To collect iL3s, fecal-charcoal cultures were stored at 23°C for at least 5 days and iL3s were isolated using a Baermann apparatus.

Maintenance of *S. ratti*

S. ratti was maintained by serial passage in female Sprague-Dawley rats as described [45]. *S. ratti* iL3s were collected from fecal-charcoal cultures using a Baermann apparatus and washed 5 times in sterile 1x PBS. Rats were inoculated by subcutaneous injection of ~800 iL3s suspended in 300 μ L sterile 1x PBS. Feces infested with *S. ratti* were collected during the patency period of infection, between days 7–23 post-inoculation. Feces from infected rats were collected and made into fecal-charcoal cultures using the same procedure described above. To collect free-living *S. ratti* adults, fecal-charcoal cultures were stored at 20°C for 48 h and adults were isolated using a Baermann apparatus. To collect iL3s, fecal-charcoal cultures were stored at 23°C for at least 5 days and iL3s were isolated using a Baermann apparatus.

Maintenance of *C. elegans*

C. elegans N2 and CB66 were cultured at room temperature on 6-cm Nematode Growth Media (NGM) plates with *E. coli* OP50 bacteria using standard methods [46]. Young adult *C. elegans* used in nicotine assays were collected directly from NGM plates containing OP50. Dauer larvae used in nicotine assays were collected in dH₂O by washing them off of NGM plates where all the OP50 had been consumed. Dauers suspended in dH₂O were pelleted at 1,000 rpm for 2 min and the supernatant was removed. Pelleted nematodes were then treated with 5 mL of 1% SDS for 15 min at room temperature. After SDS treatment, the nematodes were washed 3x with dH₂O and transferred to a glass dish. Chemically resistant dauer larvae that survived the SDS treatment were selected and tested in nicotine assays.

Selection of CRISPR target sites for *Ss-unc-22*, *Sr-unc-22* and *Ss-tax-4*

The *Ss-unc-22* gene was identified based on sequence homology with *C. elegans unc-22*. Briefly, the *C. elegans* UNC-22 (isoform a) amino acid sequence was used as the query in the TBLASTN search tool to search against the *S. stercoralis* genome in WormBase ParaSite (PRJEB528, version WBPS9) [24,47]. The *S. stercoralis* gene SSTP_0000031900 was predicted as *Ss-unc-22* based on 55.3% pairwise amino acid identity with *Ce-unc-22*; SSTP_0000031900 was also predicted in WormBase ParaSite as a twitchin and an ortholog of *Ce-unc-22* [24,47]. Reciprocal BLAST of SSTP_0000031900 against the *C. elegans* genome predicted *Ce-unc-22* as the best hit. BLAST of SSTP_0000031900 against the *S. stercoralis* genome revealed no other obvious *unc-22* orthologs. We searched for CRISPR target sites in *Ss-unc-22* exon 7, the largest exon and the exon with the highest degree of conservation to *Ce-unc-22*. Potential CRISPR target sites were identified with Geneious 9 software using the Find CRISPR Sites plugin [48]. We restricted our CRISPR target sites to those with guanine residues in the 1st, 19th, and 20th positions in the target sequence (GN(17)GG) and the Cas9 PAM sequence (NGG); these guidelines were established in Farboud *et al.* 2015 for highly efficient guide RNA design in *C. elegans* [49]. We selected CRISPR target sites with a range of predicted on-target activity scores based on the algorithm developed in Doench *et al.* 2014, where scores range from 0 to 1, with higher scores representing higher predicted activity (Fig 1B) [50]. We discarded CRISPR target sites with off-target scores under 80% based on the algorithm developed in Hsu *et al.* 2013, where potential targets are rated from 0 to 100%, with higher scores indicating less off-target activity [51]. The same approach was taken to identify *Sr-unc-22* (SRAE_X000227400) in the *S. ratti* genome (PRJEB125, version WBPS9 on WormBase ParaSite) [24,47]. *S. ratti* CRISPR target sites were selected using the same restrictions outlined for *S. stercoralis*. The *Ss-tax-4* gene, SSTP_0000981000, was similarly identified based on sequence homology with *C. elegans tax-4*, and was also predicted in WormBase ParaSite as an ortholog of *Ce-tax-4* [24,47]. The *Ss-tax-4* CRISPR target was selected using the same restrictions outlined for *Ss-unc-22*. Gene structure diagrams for *S. stercoralis* (Fig 1B and S10A Fig) and *S. ratti* (S2A Fig) were generated with Exon-Intron Graphic Maker (Version 4, www.wormweb.org).

Plasmid vectors for targeted mutagenesis with CRISPR-Cas9

A summary of all plasmid vectors used in this study can be found in S8 Table. pPV540 expressing *Strongyloides*-codon-optimized Cas9 under the control of the *S. ratti eef-1A* promoter (previously called *eft-3* in *C. elegans* [19]) was a gift from Dr. James Lok. pPV540 includes the *S. stercoralis era-1* 3'UTR; *Strongyloides*-specific regulatory elements are required for successful expression of transgenes in *S. stercoralis* and *S. ratti* [52]. The sgRNA expression vectors for targeting *Ss-unc-22*, *Sr-unc-22*, and *Ss-tax-4* were synthesized by GENEWIZ in the pUC57-Kan backbone. The *S. ratti* U6 promoter and 3' UTR were identified by sequence homology with *C. elegans* U6 [19]; 500 bp and 277 bp regions of the *Sr-U6* promoter and 3' UTR, respectively, were included in each sgRNA expression vector. For all sgRNA constructs, a non-base-paired guanine was added to the 5' end (-1 position on the guide) of each sgRNA to improve RNA polymerase III transcription [49]. Target sequences are provided in S9 Table. The repair construct pEY09 was generated by subcloning approximately 640 bp 5' and 3' homology arms flanking *Ss-unc-22* site #2 into the *Strongyloides mRFPmars* expression vector pAJ50 (a gift from Dr. James Lok) [31]. *Ss-unc-22* site #2 was chosen for HDR based on the observation that it was targeted efficiently using plasmid-based delivery of CRISPR-Cas9 constructs (Fig 3B). The repair construct pMLC39 was generated by subcloning approximately 1-kb 5' and 3' homology arms flanking *Ss-tax-4* site #1 into pAJ50. Primer sets used to amplify the *Ss-unc-22* site #2 and *Ss-tax-4* site #1 5' and 3' homology arms from *S. stercoralis* genomic DNA can be

found in [S13 Table](#). Injection mixes containing plasmid vectors and concentrations used in this study can be found in [S10 Table](#). Plasmid vector injection mixes were diluted to the desired concentration in ddH₂O, centrifuged at 14,800 rpm on a bench-top centrifuge through a 0.22 μm tube filter (Costar Spin-X Cat. # 8106) for 15 min, and stored at room temperature prior to use in microinjection experiments. The total DNA concentration injected into free-living *Strongyloides* adult females was limited to a maximum of 100 ng/μL, as described in Junio *et al.* 2008 [31].

Ribonucleoprotein complexes for targeted mutagenesis with CRISPR-Cas9

RNP complexes were assembled *in vitro* essentially as described [20]. Lyophilized crRNAs targeting *Ss-unc-22* were synthesized commercially (Dharmacon Edit-R Synthetic Modified crRNA, 20 nM) and resuspended in nuclease-free dH₂O to 4 μg/μL. crRNA sequences are provided in [S11 Table](#). Lyophilized tracrRNA was synthesized commercially (Dharmacon U-002000–20, 20 nM) and resuspended in nuclease-free ddH₂O to 4 μg/μL. Lyophilized ssODN for *Ss-unc-22* site #3 was synthesized commercially (IDT Ultramer DNA Oligo, 4 nM) and resuspended in nuclease-free ddH₂O to 500 ng/μL. crRNA, tracrRNA, and ssODN stocks were stored at -20°C until use and kept on ice during RNP complex preparation. RNP injection mixes were made as shown in [S12 Table](#) and added to 10 μg of lyophilized recombinant Cas9 protein from *Streptococcus pyogenes* (PNA Bio Inc., Cat. #CP01). The solution was centrifuged for 2 min at 13,000 rpm in a bench-top centrifuge and incubated at 37°C for 15 min to assemble RNP complexes. RNP complex solution was stored on ice prior to use in microinjection experiments.

Microinjection of *Strongyloides* free-living adults

Gonadal microinjection of plasmid vectors or RNP complexes into the syncytial gonad of *S. stercoralis* or *S. ratti* free-living adult females was performed as described for *S. stercoralis*, *S. ratti*, and *C. elegans* [18,31,45]. Microinjected females were transferred to 6-cm NGM plates containing OP50 for recovery, and free-living wild-type adult males were added for mating. After a minimum injection recovery time of approximately 30 min, NGM plates were flooded with dH₂O and free-living males and females were transferred to 6-cm fecal-charcoal plates using non-stick sterile worm-transferring tips (BloomingBio, Cat. # 10020-200-B). Uninfected gerbil feces were collected as described above and used to make fecal-charcoal cultures for *S. stercoralis*. Uninfected rat feces were collected as described above and used to make fecal-charcoal cultures for *S. ratti*. Host feces were used for post-injection incubation based on the observation that the reproductive output of *Strongyloides* free-living adults is better on feces than with standard *C. elegans* culturing methods [53]. Fecal-charcoal cultures were maintained at 23°C. After 5–14 days, F₁ iL3s were recovered from the fecal-charcoal plates using a Baermann apparatus. The average number of F₁ iL3s collected from feces per injected female for *S. stercoralis* and *S. ratti* can be found in [S14 Table](#). iL3s were stored in dH₂O for 1–2 days at room temperature until behavioral analysis and subsequent genotyping. For each *Strongyloides* CRISPR-Cas9 target site and delivery method tested in this study, we microinjected P₀ adults and screened F₁ iL3s in a minimum of two separate experiments per condition.

Swimming assay

F₁ iL3s were recovered from fecal-charcoal cultures using a Baermann apparatus and stored in a glass dish in 2–5 mL of dH₂O. Individual iL3s were then transferred in 2–3 μL of dH₂O to a 10-cm chemotaxis plate [54]. 10-s recordings of the iL3 swimming in the dH₂O drop were

immediately obtained using an Olympus E-PM1 digital camera attached to a Leica M165 FC microscope. Swimming distances were calculated using the ImageJ Manual Tracking plugin by marking the frame-by-frame position change of the nematode centroid during the 10-s recording and summing the total distance traveled. F₂ or F₃ wild-type (paralyzed) or *unc* (twitching) iL3s were recovered from 1% nicotine treatment overnight on chemotaxis plates and tested for swimming behavior the next day.

Automated tracking of iL3 crawling

Automated tracking was performed as described [22]. Briefly, recordings of iL3 movement were obtained with an Olympus E-PM1 digital camera attached to a Leica S6 D microscope. To quantify movement, 3–5 iL3s were placed in the center of a chemotaxis plate in a 5 μ L drop of dH₂O. Once the drop dried, the iL3s were allowed to acclimate to the plate for 10 min. 20-s recordings were then obtained from each iL3, ensuring that each iL3 was only recorded once. Worm movement was quantified using WormTracker and WormAnalyzer software (Miriam Goodman lab, Stanford University) [21]. The following WormTracker settings were used: minimum single worm area = 20 pixels; maximum size change by worm between successive frames = 250 pixels; shortest valid track = 30 frames; auto-thresholding correction factor = 0.001. F₂ or F₃ wild-type (paralyzed) or *unc* (twitching) iL3s were recovered from 1% nicotine treatment overnight on chemotaxis plates and tested for crawling behavior the next day.

iL3 dispersal assay

Recordings of iL3 movement were obtained with a 5-megapixel CMOS camera (Mightex Systems) equipped with a manual zoom lens (Kowa American Corporation) suspended above a 22-cm x 22-cm chemotaxis plate. To quantify unstimulated movement, individual iL3s were placed in the center of the chemotaxis plate and allowed to acclimate for 10 min. 5-min recordings were then obtained. Images were captured at 1 Hz using Mightex Camera Demo software (V1.2.0) in trigger mode. Custom Matlab code (MathWorks) and a USB DAQ device (Lab-Jack) were used to generate trigger signals. To quantify maximum dispersal distance, the location of individual iL3s during the recording session was manually tracked using the ImageJ Manual Tracking plugin; maximum distance from initial iL3 location was calculated in Microsoft Excel. Researchers were blinded to twitching phenotype during manual tracking; recording sessions were scored in randomized order.

Nicotine assay

For adult *C. elegans* assays, 5–10 young adults were transferred from NGM plates containing OP50 onto a chemotaxis plate using a worm pick. 20 μ L of a 1% nicotine solution diluted in dH₂O was pipetted onto the nematodes. After 8 min in nicotine, individual nematode phenotypes were scored under a dissecting microscope. We characterized four distinct phenotypes: paralyzed = wild-type nicotine response [13]; partially paralyzed = instances where paralysis was nearly complete but we observed minor movements; unaffected = rare instances where the nematode appeared unaffected by nicotine treatment; and twitching = continuous twitching (the *unc-22* nicotine response [13]). The percentage of twitchers was calculated as: % twitchers = (# twitching nematodes) / (total # of nematodes screened) x 100. *C. elegans* dauer assays were performed essentially as described above. dH₂O drops containing 6–10 SDS-recovered dauers were pipetted onto chemotaxis plates. The drops were allowed to dry and 20 μ L of 1% nicotine solution was pipetted onto the dauers. After 8 min, phenotypes were scored and quantified as described above. *Strongyloides* free-living adults and iL3s were recovered from fecal-charcoal cultures using a Baermann apparatus and stored in a glass dish in 2–5 mL of dH₂O. A

chemotaxis plate was subdivided into four sections and ~10 μL of dH_2O containing nematodes was pipetted into each quadrant (~5–10 free-living adults or 20–50 iL3s per quadrant, 20–40 free-living adults or 80–200 iL3s per chemotaxis plate). The drops were allowed to dry and 40–50 μL of 1% nicotine solution was pipetted onto the worms. After 8 min, phenotypes were scored and quantified as described for *C. elegans*. For chi-square analysis, paralyzed, partially paralyzed, and unaffected phenotypes were combined into one “non-twitching nematodes” category and compared to “twitching nematodes.”

Strongyloides genomic DNA preparation

To obtain genomic DNA from *S. stercoralis* individual iL3s or small pools of iL3s, 1–15 iL3s were transferred to PCR tubes containing 5–6 μL of nematode lysis buffer (50 mM KCl, 10 mM Tris pH 8, 2.5 mM MgCl_2 , 0.45% Nonidet-P40, 0.45% Tween-20, 0.01% gelatin in ddH_2O) supplemented with ~0.12 $\mu\text{g}/\mu\text{L}$ Proteinase-K and ~1.7% 2-mercaptoethanol. Tubes were placed at -80°C for at least 20 min, then transferred to a thermocycler for digestion: 65°C (2 h), 95°C (15 min), 10°C (hold). Genomic DNA samples were stored at -20°C until use. For long-term genomic DNA integrity (>1 week), iL3 samples were stored undigested at -80°C ; thermocycler digestion was then performed immediately before testing. To obtain genomic DNA from large populations of ~5,000–10,000 *S. stercoralis* iL3s, we followed the “Mammalian Tissue Preparation” protocol for the GenElute Mammalian Genomic DNA Miniprep Kit (Sigma-Aldrich, Cat. # G1N10); genomic DNA was eluted in 100 μL of dH_2O and stored at -20°C until use. To obtain genomic DNA from wild-type iL3 populations or *unc* F₁ iL3 populations for deep sequencing (S4 Table), we followed the “Isolation of Genomic DNA from Tissues” protocol for the QIAamp UCP DNA Micro Kit (Qiagen, Cat. # 56204); genomic DNA was eluted in 15 μL of nuclease-free ultrapure ddH_2O and stored at -20°C until library preparation.

Genotyping for *Ss-unc-22* deletions

Primer sets used to amplify the regions around *Ss-unc-22* target sites, and regions 10-kb upstream and downstream of *Ss-unc-22* site #3, can be found in S13 Table. All deletion genotyping PCR reactions were performed with GoTaq G2 Flexi DNA Polymerase (Promega, Cat. # M7801) using the following thermocycler conditions: denature 95°C (2 min); PCR 95°C (30 s), 55°C (30 s), 72°C (1 min) x 35 cycles; final extension 72°C (5 min); 10°C (hold). All PCR products were resolved on ~1% agarose gels stained with GelRed (Biotium, Cat. # 41003) using a 1-kb marker (NEB, Cat. # N3232L). Quantification of PCR products shown in Fig 4B was performed with a ChemiDoc MP Imaging System using the Image Lab Version 5.1 Relative Quantity Tool. Individual control and *Ss-unc-22* site #3 bands from wild-type iL3s were randomly selected as reference bands. All other control and *Ss-unc-22* site #3 reactions were compared to the appropriate reference to determine relative quantity of PCR products. For all samples, 25 μL of PCR product were loaded on the gel and all samples were run on the same gel.

Genotyping for *Ss-unc-22* and *Ss-tax-4* HDR

Primer sets used to test for HDR at *Ss-unc-22* and *Ss-tax-4* target sites can be found in S13 Table. PCR reactions for HDR of the repair template pEY09 at *Ss-unc-22* site #2 and HDR of the repair template pMLC39 at *Ss-tax-4* site #1 were performed with GoTaq G2 Flexi DNA Polymerase using the same thermocycler conditions outlined above, except for *Ss-tax-4* genotyping, where the extension time was 2 min. PCR products were resolved on ~1% agarose gels stained with GelRed with a 1-kb marker. 5' and 3' integration bands for *Ss-unc-22*, and 5'

integration bands for *Ss-tax-4*, were gel-extracted using the QIAquick Gel Extraction Kit (Qiagen, Cat. # 28704) and subcloned into pGEM-T Easy (Promega, Cat. # A1360) for sequencing. PCR reactions to test for ssODN incorporation at *Ss-unc-22* site #3 were performed with Platinum Taq DNA Polymerase (ThermoFisher Cat. # 10966018) using the same thermocycler conditions described for GoTaq. PCR products were resolved on ~1% agarose gels stained with GelRed using a 100-bp marker.

Restriction enzyme digestion to test for ssODN incorporation

The primer set used to amplify the region around *Ss-unc-22* site #3 for ssODN EagI digest can be found in [S13 Table](#). PCR cleanup on wild-type and *unc* iL3 pools was performed using the QIAquick PCR purification kit (Qiagen, Cat. # 28104). For each sample, ~1 µg of template DNA was digested with EagI-HF (NEB, Cat. # R3505S) at 37°C for 1 h. Digested products were resolved on ~1% agarose gels stained with GelRed using 1-kb and 100-bp markers.

Illumina sequencing of *S. stercoralis*

Genomic DNA from populations of wild-type iL3s or *Ss-unc-22*-targeted F₁ iL3s were collected as described above. 2x 150 paired-end Illumina libraries were prepared from 1 µg genomic DNA using the KAPA Library Preparation Kit with beads for size selection and sample cleanup (Kapa Biosystems, Cat. # KK8232). Libraries were sequenced on the Illumina HiSeq3000 platform using the HiSeq 3000/4000 PE Cluster Kit according to the manufacturer's recommended protocol. Paired-end reads were mapped to the *S. stercoralis* reference genome using HISAT2 with the “—no-spliced-alignment” option [24,55]. To estimate read coverage, we performed a two-step approach. First, we computed per-site coverage using SAMtools for all sites that mapped to the reference. Second, to account for correlation between neighboring sites, we sampled 10,000 random sites to estimate coverage parameters under a negative-binomial distribution using custom Python and R scripts. The negative-binomial distribution is commonly used for modeling the random distribution of count data with an overdispersion parameter and has been used in many bioinformatics pipelines to model read coverage [56]. We performed this second step to estimate genome-wide coverage parameters as well as parameters restricted to *Ss-unc-22* sites. To compute the probability of observing coverage depletion at a given *Ss-unc-22* target site by chance, we performed a one-tailed test under the *Ss-unc-22*-fitted negative binomial. To calculate indel frequency at *Ss-unc-22* site #3, we took the mapped reads generated above and ran CRISPRessoWGS and CRISPRessoCompare with default parameters [29].

Fluorescence microscopy

unc F₁ iL3s with a nicotine-twitching phenotype were transferred to a chemotaxis plate and screened for *mRFPmars* expression under a Leica M165 FC microscope. *unc* F₁ iL3s expressing *mRFPmars* were mounted on a pad consisting of 5% Noble agar dissolved in ddH₂O. Epifluorescence images were captured using a Zeiss AxioImager A2 microscope with an attached Zeiss AxioCam camera. Images were processed using Zeiss AxioVision software. After imaging, individual *unc* F₁ iL3s were collected from agar pads and transferred to 5–6 µL of worm lysis buffer for HDR genotyping as described above.

Germline transmission of *Ss-unc-22* mutations

A summary of *Ss-unc-22* germline transmission strategies can be found in [S7 Table](#). To generate an ~50/50 mix of wild-type and *unc* F₁ iL3s, free-living adult females were injected with

RNP complex targeting *Ss-unc-22* site #3 with an ssODN. F₁ iL3s were collected and a subset of them were screened in 1% nicotine assays to estimate the nicotine-twitching frequency; ~52% of iL3s contained putative *Ss-unc-22* mutations based solely on phenotypic observation in nicotine. The remaining F₁ population was injected into gerbil hosts. To enrich for *unc* F₁ iL3s, RNP injections targeting site #3 were carried out as described for the 50/50 mixed infection. F₁ iL3s were collected and all nematodes were screened in 1% nicotine assays. Nicotine-twitching iL3s were selected, washed in ddH₂O, and recovered from nicotine treatment overnight. Paralyzed iL3s were discarded. *unc* F₁ iL3s recovered from nicotine were injected into gerbil hosts. In the control infection, wild-type iL3s were treated with nicotine to induce paralysis, washed in ddH₂O, and recovered from nicotine treatment overnight. Recovered wild-type iL3s were injected into gerbil hosts. Feces from all of the host infection strategies were collected as described above. F₂ and F₃ nematodes were screened for *unc* phenotypes using the nicotine, swimming, and crawling assays described above.

Statistical analysis

Statistical analysis was performed using standard statistical tests in GraphPad Prism Version 7.0. Deep-sequencing analysis was performed using custom Python and R scripts, and is described in detail above. The standard statistical tests used for all other experiments are described in the figure captions, and are also summarized below. For these experiments, the D'Agostino-Pearson omnibus normality test was first used to determine whether values came from a Gaussian distribution. If data were normally distributed, parametric tests were used; otherwise, non-parametric tests were used. A Mann-Whitney test or unpaired t-test with Welch's correction was used to compare swimming and crawling behaviors in wild-type iL3s vs. *unc* iL3s (Figs 2, 6C and 6D). A chi-square test with Bonferroni correction or Fisher's exact test was used to compare nicotine-induced twitching frequencies across genotypes or conditions (Figs 3 and 6B, S1, S2, S6 and S9 Figs). Depletion of *Ss-unc-22* site #3 in *unc* iL3s was quantified using a two-way ANOVA with Sidak's post-test (Fig 4B).

Supporting information

S1 Fig. Nicotine induces twitching in *C. elegans unc-22* adults and dauers. Twitching frequency of *C. elegans* wild-type and *unc-22* adults and dauers. Twitching frequency differs for *C. elegans* wild-type and *unc-22* adults and dauers. * $P < 0.05$, *** $P < 0.001$, chi-square test with Bonferroni correction. $n = 50-51$ nematodes for each genotype and life stage. (PDF)

S2 Fig. Targeted mutagenesis in *S. ratti* using CRISPR-Cas9. (A) The *unc-22* gene of *S. ratti*. The *Sr-unc-22* gene structure depicted is based on the gene prediction from WormBase Parasite [24,47]. The locations of the CRISPR target sites tested and predicted on-target activity scores are indicated [50]. Scale bar = 1 kb. (B) Twitching frequency of *S. ratti* wild-type iL3s and *Sr-unc-22*-targeted F₁ iL3s following 1% nicotine exposure. For each condition, the *Sr-unc-22* target site and delivery method of CRISPR constructs are indicated. Twitching frequency of F₁ iL3s for each target site differs from wild-type iL3s and from each other. * $P < 0.05$, ** $P < 0.01$, *** $P < 0.001$, chi-square test with Bonferroni correction. $n = 267-544$ iL3s for each condition. (PDF)

S3 Fig. Whole-genome sequencing reveals that *Ss-unc-22* sites #1 and #2 are not deleted when *Ss-unc-22* site #3 is targeted with CRISPR-Cas9. (A-B) Whole-genome sequencing coverage plots for *Ss-unc-22* site #1 (A) or site #2 (B) from populations of either *Ss-unc-22*-targeted F₁ iL3s from P₀ females injected with RNP complexes for site #3, or wild-type iL3s. A

4-kb window centered on the predicted cut sites is shown [24,47]. Black lines = average coverage depth by position (reads per base); red lines = average genome-wide coverage; blue lines = average coverage for the *Ss-unc-22* gene. Coverage around *Ss-unc-22* sites #1 and #2 is not depleted in *Ss-unc-22* libraries when *Ss-unc-22* site #3 is targeted ($P>0.05$; see [Methods](#)). Similarly, no coverage depletion is observed in the wild-type library ($P>0.05$; see [Methods](#)). For **B**, the gray shaded region represents significant depletion around *Ss-unc-22* site #3, which is only ~2.3 kb upstream of *Ss-unc-22* site #2. The arrow indicates that site #3 is upstream of the 4-kb window shown.

(PDF)

S4 Fig. Whole-genome sequencing reveals that a distinct CRISPR target site is not deleted when *Ss-unc-22* site #3 is targeted. Whole-genome sequencing coverage plots for a selected control gene, *Ss-tax-4* (SSTP_0000981000) containing an unrelated predicted CRISPR target site. A 4-kb window centered on the predicted cut site is shown [24,47]. Black lines = average coverage depth by position (reads per base); red lines = average genome-wide coverage; blue lines = average coverage for the *Ss-tax-4* gene. Coverage around *Ss-tax-4* site #1 is not depleted in *Ss-unc-22* libraries when *Ss-unc-22* site #3 is targeted ($P>0.05$; see [Methods](#)). Similarly, no coverage depletion is observed in the wild-type library ($P>0.05$; see [Methods](#)).

(PDF)

S5 Fig. CRISPR-Cas9-mediated deletions of *Ss-unc-22* site #3 do not disrupt nearby genomic loci. (A) The genomic region of *Ss-unc-22*. The gene structures of *Ss-unc-22*, and a downstream gene *Ss-rgr-1* (SSTP_0000032000), were based on the predictions from WormBase ParaSite [24,47]. Wild-type iL3s and *unc* F₁ iL3s were genotyped for the *Ss-unc-22* site #3 target, 10 kb upstream of the target, and 10 kb downstream of the target using the primer sets indicated. Scale bar = 1 kb. (B) Representative gel of a wild-type iL3 and *unc* F₁ iL3s from RNP injections at site #3. Genomic DNA from each iL3 was split into four reactions: ctrl. = control reaction amplifying 416 bp of the first exon of the *Ss-act-2* gene to confirm the presence of genomic DNA; u22 = reaction amplifying 660 bp around site #3; a = 10 kb upstream of site #3, b = 10 kb downstream of site #3. Genomic loci 10 kb upstream and downstream of site #3 are intact in *unc* F₁ iL3s with putative homozygous deletions of *Ss-unc-22*. Size markers = 1 kb and 500 bp from top to bottom.

(PDF)

S6 Fig. Addition of an HDR template improves *unc* F₁ iL3 nicotine-twitching frequency. (A) The twitching frequency in *unc* F₁ iL3s increases when a repair template containing *Ss-act-2::mRFPmars* is included in plasmid vector injections. $***P<0.001$, Fisher's exact test. $n = 677-788$ iL3s for each condition. (B) The twitching frequency in *unc* F₁ iL3s increases when an ssODN is included in RNP injections. $***P<0.001$, Fisher's exact test. $n = 619-830$ iL3s for each condition.

(PDF)

S7 Fig. Sequencing for HDR with the *Ss-act-2::mRFPmars* repair template at *Ss-unc-22* site #2. (A-B) Sequencing results showing insertion of the repair template spanning the 5' border of the integrated cassette (A) or the 3' border of the integrated cassette (B). The relevant regions of *Ss-unc-22*, the repair template, and the primer binding sites are highlighted and color-coded to match the schematic shown in [Fig 5A](#).

(PDF)

S8 Fig. ssODNs are not templates for HDR at *Ss-unc-22*. (A) Strategy for ssODN-mediated HDR of CRISPR mutations at *Ss-unc-22* site #3. RNP complexes targeting site #3 mixed with

ssODN were injected into free-living adult females. *unc* F₁ iL3s that displayed the twitching phenotype were selected as candidates for HDR and were genotyped for ssODN incorporation using the primer sets indicated. HA = homology arm. **(B)** The ssODN sequence for *Ss-unc-22* site #3. The ssODN contains stop codons in all reading frames, an *EagI* restriction site, and the sequence for the T7 primer flanked on either end by 5' and 3' homology arms that match the genomic DNA upstream and downstream of site #3. **(C)** The ssODN failed to incorporate at site #3 by PCR. Top gel: lane 1 = control to confirm primer R4 can amplify from *S. stercoralis* genomic DNA and is present in the reaction, lane 2 = control to confirm primer T7 can amplify from a plasmid vector and is present in the reaction, lanes 3–6 = reactions with primers T7 x R4 show no evidence for ssODN incorporation from pools of 10–15 wild-type iL3s or *unc* F₁ iL3s. Bottom gel: lanes 2–10 = reactions with primers T7 x R4 show no evidence for ssODN incorporation from an individual wild-type iL3 or individual *unc* F₁ iL3s. **(D)** The ssODN failed to incorporate at site #3 by *EagI* digest. Lanes 1–2 = *EagI* digest controls with plasmid vector, lanes 3–4 = *EagI* digest from >5,000 wild-type iL3s (population) or 10–15 wild-type iL3s (pool), lanes 5–8 = *EagI* digest from a mixed population of >5,000 twitching *unc* F₁ iL3s and not twitching wild-type iL3s (population), or 10–15 twitching *unc* F₁ iL3s (pools). Successful ssODN incorporation at *Ss-unc-22* site #3 would be expected to produce ~300 bp *EagI* digestion products. No digestion products were observed. Size markers = 100-bp ladder for **C**, or 100-bp and 1-kb ladder for **D**. (PDF)

S9 Fig. Removing Cas9 from injections abolishes *Ss-unc-22* targeted mutagenesis. **(A)** The nicotine-twitching phenotype was not observed in F₁ iL3s when the plasmid vector for the expression of Cas9 was excluded from the injection mix. ****P*<0.001, Fisher's exact test. n = 346–788 iL3s for each condition. **(B)** The nicotine-twitching phenotype was not observed in F₁ iL3s when Cas9 protein was excluded from RNP complex assembly. ****P*<0.001, Fisher's exact test. n = 353–1,284 iL3s for each condition. (PDF)

S10 Fig. CRISPR-mediated homology-directed repair of *Ss-tax-4*. **(A)** The *tax-4* genes of *C. elegans* and *S. stercoralis*. The *Ss-tax-4* gene structure is based on the gene prediction from WormBase Parasite [24,47]. The CRISPR target site tested and the on-target activity score are indicated [50]. Scale bars = 1 kb. **(B)** Strategy for HDR at *Ss-tax-4* target site #1. F₁ iL3s that displayed red fluorescence were selected as candidates for HDR and were genotyped using the primer sets indicated. The 5' integration primers only amplify following successful integration of *Ss-act-2::mRFPmars* into site #1. HA = homology arm. **(C)** Representative genotypes of F₁ iL3s expressing *mRFPmars* collected from *Ss-tax-4*-CRISPR microinjected females. Genomic DNA from individual iL3s was split into two reactions: wt = reaction for the wild-type locus of site #1; 5' = reaction for insertion of the 5' border of the integrated cassette. For genotypes: array = red iL3s that showed no evidence of integration; int. = red *Ss-tax-4* iL3s with successful HDR. Asterisks indicate iL3s that were sequenced for 5' integration at the *Ss-tax-4* locus. Size markers = 1-kb ladder. The gel was cropped for conciseness of presentation. **(D)** Sequencing results showing insertion of the repair template; the sequence spans the 5' border of the integrated cassette. The relevant regions of the *Ss-tax-4* repair template are highlighted and color-coded to match the schematic shown in **B**. (PDF)

S1 Table. Summary of CRISPR-Cas9 targeting efficiency for *Ss-unc-22*. Results for combined nicotine assay data presented in Fig 3B. The estimated number of F₁ iL3s collected from each injection experiment was based on the average number of iL3s per injected adult

calculated in [S14 Table](#).

(PDF)

S2 Table. Summary of CRISPR-Cas9 targeting efficiency for *Sr-unc-22*. Results for combined nicotine assay data presented in [S2 Fig](#). The estimated number of F₁ iL3s collected from each injection experiment was based on the average number of iL3s per injected adult calculated in [S14 Table](#).

(PDF)

S3 Table. Summary of *Ss-unc-22* deletions. Individual wild-type iL3s, and *unc* F₁ iL3s that displayed a nicotine-twitching phenotype, were collected and genomic DNA was prepared. For each iL3, the region around the *Ss-unc-22* target was PCR-amplified along with a control reaction from a different contig than *Ss-unc-22*, as shown in [Fig 4A](#). Instances where the *Ss-unc-22* target failed to amplify but the control reaction was present were considered putative homozygous deletions of *Ss-unc-22*.

(PDF)

S4 Table. Summary of sample preparation for *Ss-unc-22* whole-genome sequencing. *S. stercoralis* free-living adults were injected with RNP complexes targeting *Ss-unc-22* site #3, including an ssODN, and F₁ iL3s were collected. A subset of F₁ iL3s was screened for nicotine-twitching frequency to estimate the *Ss-unc-22* mutation rate and the remaining population was split in two for iL3 lysis, genomic DNA extraction, and Illumina library preparation. Wild-type iL3s were also screened for nicotine-twitching frequency and an Illumina library was prepared from a wild-type population in parallel with the *Ss-unc-22* libraries.

(PDF)

S5 Table. Summary of CRISPR-Cas9 targeting efficiency for *Ss-unc-22* with HDR constructs. Results for combined nicotine assay data presented in [S6 Fig](#). The estimated number of F₁ iL3s collected from each injection experiment was based on the average number of iL3s per injected adult calculated in [S14 Table](#). n.a. = not available; the number of free-living adults injected was not recorded for this experiment.

(PDF)

S6 Table. Summary of HDR in *S. stercoralis*. Free-living adult females were injected with CRISPR-Cas9 plasmid vectors and repair template targeting either *Ss-unc-22* site #2 or *Ss-tax-4* site #1. Individual F₁ iL3s expressing *mRFPmars* were genotyped for repair template integration as shown in [Fig 5](#) and [S10 Fig](#).

(PDF)

S7 Table. Host infection and germline transmission of *Ss-unc-22* mutations. Summary of host passage strategies for wild-type control, 50/50 mixed *unc* and wild-type, and *unc*-enriched infections. Results for total recovery of F₂ and F₃ progeny for each infection strategy, and the combined nicotine-assay data presented in [Fig 6B](#), are provided. n.a. = not available; the number of iL3s recovered was not recorded for these experiments.

(PDF)

S8 Table. Plasmid vectors for *Strongyloides* CRISPR-Cas9. pPV540, provided by Dr. James Lok, was modified from pPV402, which is described in Shao *et al.* 2012 [45]. pEY09 and pMLC39 were modified from pAJ50, which is described in Junio *et al.* 2008 [31].

(PDF)

S9 Table. *Strongyloides* CRISPR target sequences. The PAM for each target sequence is underlined. Note that each target sequence contains guanine residues in the 1st, 19th, and 20th

positions (GN(17)GG), as recommended in Farboud *et al.* 2015 [49].
(PDF)

S10 Table. Plasmid vector injection mixes for *Strongyloides* CRISPR-Cas9. Injection mixes introduced into *Strongyloides* free-living adult females were limited to a maximum final DNA concentration of 100 ng/μL, as previously described in Junio *et al.* 2008 [31].
(PDF)

S11 Table. *Ss-unc-22* crRNA sequences. The first 20 nucleotides of each crRNA match the genomic DNA of the CRISPR target site indicated. The remaining nucleotides are the *Streptococcus pyogenes* repeat sequence and are identical for all three crRNAs shown.
(PDF)

S12 Table. RNP injection mixes for *Ss-unc-22* CRISPR-Cas9. RNP injection mixes were based on the injection mixes described in Paix *et al.* 2015 [20].
(PDF)

S13 Table. Primer sets used in this study.
(PDF)

S14 Table. The average number of F₁ iL3s collected per microinjected free-living adult female for *S. stercoralis* and *S. ratti*. Injected free-living adult females were reared on host feces based on the observation that it results in higher reproductive output relative to other standard culturing methods [53]. iL3s were collected using a Baermann apparatus and all F₁ progeny were counted to calculate the average number of iL3s per injected adult.
(PDF)

S1 Video. An *S. stercoralis* wild-type iL3 swimming in dH₂O. Scale bar = 200 μm.
(MOV)

S2 Video. An *S. stercoralis unc* F₁ iL3 swimming in dH₂O. Scale bar = 200 μm.
(MOV)

S3 Video. An *S. stercoralis* wild-type iL3 crawling on agar. Scale bar = 1 mm.
(MOV)

S4 Video. An *S. stercoralis unc* F₁ iL3 crawling on agar. Scale bar = 1 mm.
(MOV)

S5 Video. An *S. stercoralis* wild-type iL3 paralyzed after 8 min in 1% nicotine. Scale bar = 100 μm.
(MOV)

S6 Video. An *S. stercoralis unc* F₁ iL3 twitching after 8 min in 1% nicotine. Scale bar = 100 μm.
(MOV)

S7 Video. An *S. stercoralis unc* F₂ or F₃ iL3 twitching after 8 min in 1% nicotine. Scale bar = 100 μm.
(MOV)

S8 Video. An *S. stercoralis* wild-type free-living adult female paralyzed after 8 min in 1% nicotine. Scale bar = 100 μm.
(MOV)

S9 Video. An *S. stercoralis unc* F₂ free-living adult female twitching after 8 min in 1% nicotine. Scale bar = 100 μm.
(MOV)

Acknowledgments

We thank Dr. James Lok (University of Pennsylvania) for providing plasmid vectors; Dr. Xinmin Li and Dr. Ling Dong (University of California Los Angeles, Technology Center for Genomics & Bioinformatics) for preparing libraries and running Illumina whole-genome sequencing samples; Dr. Michael Weinstein (University of California Los Angeles, Institute for Quantitative and Computational Biology) for helpful advice regarding whole-genome sequencing data analysis; and Tiffany Mao for technical assistance.

Author Contributions

Conceptualization: Spencer S. Gang, Michelle L. Castelletto, Elissa A. Hallem.

Formal analysis: Spencer S. Gang, Michelle L. Castelletto, Astra S. Bryant, Nicholas Mancuso, Elissa A. Hallem.

Funding acquisition: Elissa A. Hallem.

Investigation: Spencer S. Gang, Michelle L. Castelletto, Astra S. Bryant, Emily Yang, Jacqueline B. Lopez.

Methodology: Spencer S. Gang, Michelle L. Castelletto.

Project administration: Elissa A. Hallem.

Supervision: Matteo Pellegrini, Elissa A. Hallem.

Writing – original draft: Spencer S. Gang, Elissa A. Hallem.

Writing – review & editing: Spencer S. Gang, Michelle L. Castelletto, Astra S. Bryant, Elissa A. Hallem.

References

1. Pullan RL, Smith JL, Jasrasaria R, Brooker SJ. Global numbers of infection and disease burden of soil transmitted helminth infections in 2010. *Parasit Vectors*. 2014; 7:37. <https://doi.org/10.1186/1756-3305-7-37> PMID: 24447578
2. Boatman BA, Basanez MG, Prichard RK, Awadzi K, Barakat RM, Garcia HH, et al. A research agenda for helminth diseases of humans: towards control and elimination. *PLoS Negl Trop Dis*. 2012; 6(4):e1547. <https://doi.org/10.1371/journal.pntd.0001547> PMID: 22545161
3. Ward JD. Rendering the intractable more tractable: tools from *Caenorhabditis elegans* ripe for import into parasitic nematodes. *Genetics*. 2015; 201(4):1279–94. <https://doi.org/10.1534/genetics.115.182717> PMID: 26644478
4. Guo L, Chang Z, Dieterich C, Streit A. A protocol for chemical mutagenesis in *Strongyloides ratti*. *Exp Parasitol*. 2015; 158:2–7. <https://doi.org/10.1016/j.exppara.2015.03.001> PMID: 25765558
5. Doudna JA, Charpentier E. The new frontier of genome engineering with CRISPR-Cas9. *Science*. 2014; 346(6213):1258096. <https://doi.org/10.1126/science.1258096> PMID: 25430774
6. Chen L, Tang L, Xiang H, Jin L, Li Q, Dong Y, et al. Advances in genome editing technology and its promising application in evolutionary and ecological studies. *Gigascience*. 2014; 3:24. <https://doi.org/10.1186/2047-217X-3-24> PMID: 25414792
7. Tan W, Proudfoot C, Lillico SG, Whitelaw CB. Gene targeting, genome editing: from Dolly to editors. *Transgenic Res*. 2016; 25(3):273–87. <https://doi.org/10.1007/s11248-016-9932-x> PMID: 26847670

8. Peng D, Kurup SP, Yao PY, Minning TA, Tarleton RL. CRISPR-Cas9-mediated single-gene and gene family disruption in *Trypanosoma cruzi*. *MBio*. 2014; 6(1):e02097–14. <https://doi.org/10.1128/mBio.02097-14> PMID: 25550322
9. Schafer TW, Skopic A. Parasites of the small intestine. *Curr Gastroenterol Rep*. 2006; 8(4):312–20. PMID: 16836943
10. Gang SS, Hallem EA. Mechanisms of host seeking by parasitic nematodes. *Mol Biochem Parasitol*. 2016; 208(1):23–32. <https://doi.org/10.1016/j.molbiopara.2016.05.007> PMID: 27211240
11. Lok JB, Shao H, Massey HC, Li X. Transgenesis in *Strongyloides* and related parasitic nematodes: historical perspectives, current functional genomic applications and progress towards gene disruption and editing. *Parasitology*. 2017; 144(3):327–42. <https://doi.org/10.1017/S0031182016000391> PMID: 27000743
12. Moerman DG, Baillie DL. Genetic organization in *Caenorhabditis elegans*: fine-structure analysis of the *unc-22* gene. *Genetics*. 1979; 91(1):95–103. PMID: 17248882
13. Moerman DG, Benian GM, Barstead RJ, Schriefer LA, Waterston RH. Identification and intracellular localization of the *unc-22* gene product of *Caenorhabditis elegans*. *Genes Dev*. 1988; 2(1):93–105. PMID: 2833427
14. *C. elegans* Deletion Mutant Consortium. Large-scale screening for targeted knockouts in the *Caenorhabditis elegans* genome. *G3*. 2012; 2(11):1415–25. <https://doi.org/10.1534/g3.112.003830> PMID: 23173093
15. Thompson O, Edgley M, Strasbourger P, Flibotte S, Ewing B, Adair R, et al. The million mutation project: a new approach to genetics in *Caenorhabditis elegans*. *Genome Res*. 2013; 23(10):1749–62. <https://doi.org/10.1101/gr.157651.113> PMID: 23800452
16. Flibotte S, Edgley ML, Chaudhry I, Taylor J, Neil SE, Rogula A, et al. Whole-genome profiling of mutagenesis in *Caenorhabditis elegans*. *Genetics*. 2010; 185(2):431–41. <https://doi.org/10.1534/genetics.110.116616> PMID: 20439774
17. Kim H, Ishidate T, Ghanta KS, Seth M, Conte D Jr., Shirayama M, et al. A co-CRISPR strategy for efficient genome editing in *Caenorhabditis elegans*. *Genetics*. 2014; 197(4):1069–80. <https://doi.org/10.1534/genetics.114.166389> PMID: 24879462
18. Mello C, Fire A. DNA transformation. *Methods Cell Biol*. 1995; 48:451–82. PMID: 8531738
19. Friedland AE, Tzur YB, Esvelt KM, Colaiacovo MP, Church GM, Calarco JA. Heritable genome editing in *C. elegans* via a CRISPR-Cas9 system. *Nat Methods*. 2013; 10(8):741–3. <https://doi.org/10.1038/nmeth.2532> PMID: 23817069
20. Paix A, Folkmann A, Rasoloson D, Seydoux G. High efficiency, homology-directed genome editing in *Caenorhabditis elegans* using CRISPR-Cas9 ribonucleoprotein complexes. *Genetics*. 2015; 201(1):47–54. <https://doi.org/10.1534/genetics.115.179382> PMID: 26187122
21. Ramot D, Johnson BE, Berry TL Jr., Carnell L, Goodman MB. The parallel worm tracker: a platform for measuring average speed and drug-induced paralysis in nematodes. *PLoS One*. 2008; 3(5):e2208. <https://doi.org/10.1371/journal.pone.0002208> PMID: 18493300
22. Castelletto ML, Gang SS, Okubo RP, Tselikova AA, Nolan TJ, Platzer EG, et al. Diverse host-seeking behaviors of skin-penetrating nematodes. *PLoS Pathog*. 2014; 10(8):e1004305. <https://doi.org/10.1371/journal.ppat.1004305> PMID: 25121736
23. Viney ME, Lok JB. The biology of *Strongyloides* spp. 2015; In *WormBook*, www.wormbook.org.
24. Hunt VL, Tsai IJ, Coghlan A, Reid AJ, Holroyd N, Foth BJ, et al. The genomic basis of parasitism in the *Strongyloides* clade of nematodes. *Nat Genet*. 2016; 48(3):299–307. <https://doi.org/10.1038/ng.3495> PMID: 26829753
25. Lemmens BB, Tijsterman M. DNA double-strand break repair in *Caenorhabditis elegans*. *Chromosoma*. 2011; 120(1):1–21. <https://doi.org/10.1007/s00412-010-0296-3> PMID: 21052706
26. Zhu X, Xu Y, Yu S, Lu L, Ding M, Cheng J, et al. An efficient genotyping method for genome-modified animals and human cells generated with CRISPR/Cas9 system. *Sci Rep*. 2014; 4:6420. <https://doi.org/10.1038/srep06420> PMID: 25236476
27. Kim HJ, Lee HJ, Kim H, Cho SW, Kim JS. Targeted genome editing in human cells with zinc finger nucleases constructed via modular assembly. *Genome Res*. 2009; 19(7):1279–88. <https://doi.org/10.1101/gr.089417.108> PMID: 19470664
28. Brinkman EK, Chen T, Amendola M, van Steensel B. Easy quantitative assessment of genome editing by sequence trace decomposition. *Nucleic Acids Res*. 2014; 42(22):e168. <https://doi.org/10.1093/nar/gku936> PMID: 25300484
29. Pinello L, Canver MC, Hoban MD, Orkin SH, Kohn DB, Bauer DE, et al. Analyzing CRISPR genome-editing experiments with CRISPResso. *Nat Biotechnol*. 2016; 34(7):695–7. <https://doi.org/10.1038/nbt.3583> PMID: 27404874

30. Chiu H, Schwartz HT, Antoshechkin I, Sternberg PW. Transgene-free genome editing in *Caenorhabditis elegans* using CRISPR-Cas. *Genetics*. 2013; 195(3):1167–71. <https://doi.org/10.1534/genetics.113.155879> PMID: 23979577
31. Junio AB, Li X, Massey HC Jr., Nolan TJ, Todd Lamitina S, Sundaram MV, et al. *Strongyloides stercoralis*: cell- and tissue-specific transgene expression and co-transformation with vector constructs incorporating a common multifunctional 3' UTR. *Exp Parasitol*. 2008; 118(2):253–65. <https://doi.org/10.1016/j.exppara.2007.08.018> PMID: 17945217
32. Arribere JA, Bell RT, Fu BX, Artilles KL, Hartman PS, Fire AZ. Efficient marker-free recovery of custom genome modifications with CRISPR/Cas9 in *Caenorhabditis elegans*. *Genetics*. 2014; 198(3):837–46. <https://doi.org/10.1534/genetics.114.169730> PMID: 25161212
33. Katic I, Xu L, Ciosk R. CRISPR/Cas9 genome editing in *Caenorhabditis elegans*: evaluation of templates for homology-mediated repair and knock-ins by homology-independent DNA repair. *G3 (Bethesda)*. 2015; 5(8):1649–56.
34. Coburn CM, Bargmann CI. A putative cyclic nucleotide-gated channel is required for sensory development and function in *C. elegans*. *Neuron*. 1996; 17(4):695–706. PMID: 8893026
35. Komatsu H, Mori I, Rhee JS, Akaike N, Ohshima Y. Mutations in a cyclic nucleotide-gated channel lead to abnormal thermosensation and chemosensation in *C. elegans*. *Neuron*. 1996; 17(4):707–18. PMID: 8893027
36. Lok JB. *Strongyloides stercoralis*: a model for translational research on parasitic nematode biology. 2007; In WormBook, www.wormbook.org.
37. Nolan TJ, Megyeri Z, Bhopale VM, Schad GA. *Strongyloides stercoralis*: the first rodent model for uncomplicated and hyperinfective strongyloidiasis, the Mongolian gerbil (*Meriones unguiculatus*). *J Infect Dis*. 1993; 168(6):1479–84. PMID: 8245532
38. Grant WN, Skinner SJ, Newton-Howes J, Grant K, Shuttleworth G, Heath DD, et al. Heritable transgenesis of *Parastrongyloides trichosuri*: a nematode parasite of mammals. *Int J Parasitol*. 2006; 36(4):475–83. <https://doi.org/10.1016/j.ijpara.2005.12.002> PMID: 16500659
39. Grant WN, Stasiuk S, Newton-Howes J, Ralston M, Bisset SA, Heath DD, et al. *Parastrongyloides trichosuri*, a nematode parasite of mammals that is uniquely suited to genetic analysis. *Int J Parasitol*. 2006; 36(4):453–66. <https://doi.org/10.1016/j.ijpara.2005.11.009> PMID: 16500655
40. Li X, Shao H, Junio A, Nolan TJ, Massey HC Jr., Pearce EJ, et al. Transgenesis in the parasitic nematode *Strongyloides ratti*. *Mol Biochem Parasitol*. 2011; 179(2):114–9. <https://doi.org/10.1016/j.molbiopara.2011.06.002> PMID: 21723330
41. Shao H, Li X, Lok JB. Heritable genetic transformation of *Strongyloides stercoralis* by microinjection of plasmid DNA constructs into the male germline. *Int J Parasitol*. 2017; 47(9):511–515. <https://doi.org/10.1016/j.ijpara.2017.04.003> PMID: 28577882
42. Viney M, Kikuchi T. *Strongyloides ratti* and *S. venezuelensis*—rodent models of *Strongyloides* infection. *Parasitology*. 2017; 144(3):285–94. <https://doi.org/10.1017/S0031182016000020> PMID: 26935155
43. van Schendel R, Roerink SF, Portegijs V, van den Heuvel S, Tijsterman M. Polymerase Theta is a key driver of genome evolution and of CRISPR/Cas9-mediated mutagenesis. *Nat Commun*. 2015; 6:7394. <https://doi.org/10.1038/ncomms8394> PMID: 26077599
44. Egli D, Zuccaro MV, Kosicki M, Church GM, Bradley A, Jasin M. Inter-homologue repair in fertilized human eggs? *bioRxiv*. 2017; <https://doi.org/10.1101/181255>.
45. Shao H, Li X, Nolan TJ, Massey HC Jr., Pearce EJ, Lok JB. Transposon-mediated chromosomal integration of transgenes in the parasitic nematode *Strongyloides ratti* and establishment of stable transgenic lines. *PLoS Pathog*. 2012; 8(8):e1002871. <https://doi.org/10.1371/journal.ppat.1002871> PMID: 22912584
46. Brenner S. The genetics of *Caenorhabditis elegans*. *Genetics*. 1974; 77(1):71–94. PMID: 4366476
47. Howe KL, Bolt BJ, Cain S, Chan J, Chen WJ, Davis P, et al. WormBase 2016: expanding to enable helminth genomic research. *Nucleic Acids Res*. 2016; 44(D1):D774–80. <https://doi.org/10.1093/nar/gkv1217> PMID: 26578572
48. Kearse M, Moir R, Wilson A, Stones-Havas S, Cheung M, Sturrock S, et al. Geneious Basic: an integrated and extendable desktop software platform for the organization and analysis of sequence data. *Bioinformatics*. 2012; 28(12):1647–9. <https://doi.org/10.1093/bioinformatics/bts199> PMID: 22543367
49. Farboud B, Meyer BJ. Dramatic enhancement of genome editing by CRISPR/Cas9 through improved guide RNA design. *Genetics*. 2015; 199(4):959–71. <https://doi.org/10.1534/genetics.115.175166> PMID: 25695951
50. Doench JG, Hartenian E, Graham DB, Tothova Z, Hegde M, Smith I, et al. Rational design of highly active sgRNAs for CRISPR-Cas9-mediated gene inactivation. *Nat Biotechnol*. 2014; 32(12):1262–7. <https://doi.org/10.1038/nbt.3026> PMID: 25184501

51. Hsu PD, Scott DA, Weinstein JA, Ran FA, Konermann S, Agarwala V, et al. DNA targeting specificity of RNA-guided Cas9 nucleases. *Nat Biotechnol.* 2013; 31(9):827–32. <https://doi.org/10.1038/nbt.2647> PMID: 23873081
52. Li X, Massey HC Jr., Nolan TJ, Schad GA, Kraus K, Sundaram M, et al. Successful transgenesis of the parasitic nematode *Strongyloides stercoralis* requires endogenous non-coding control elements. *Int J Parasitol.* 2006; 36(6):671–9. <https://doi.org/10.1016/j.ijpara.2005.12.007> PMID: 16500658
53. Dulovic A, Puller V, Streit A. Optimizing culture conditions for free-living stages of the nematode parasite *Strongyloides ratti*. *Exp Parasitol.* 2016; 168:25–30. <https://doi.org/10.1016/j.exppara.2016.06.005> PMID: 27334397
54. Bargmann CI, Hartwig E, Horvitz HR. Odorant-selective genes and neurons mediate olfaction in *C. elegans*. *Cell.* 1993; 74(3):515–27. PMID: 8348618
55. Kim D, Langmead B, Salzberg SL. HISAT: a fast spliced aligner with low memory requirements. *Nat Methods.* 2015; 12(4):357–60. <https://doi.org/10.1038/nmeth.3317> PMID: 25751142
56. Love MI, Huber W, Anders S. Moderated estimation of fold change and dispersion for RNA-seq data with DESeq2. *Genome Biol.* 2014; 15(12):550. <https://doi.org/10.1186/s13059-014-0550-8> PMID: 25516281

Chapter 5

**A critical role for thermosensation in host seeking by
skin-penetrating nematodes**

A Critical Role for Thermosensation in Host Seeking by Skin-Penetrating Nematodes

Astra S. Bryant,¹ Felicitas Ruiz,¹ Spencer S. Gang,² Michelle L. Castelletto,¹ Jacqueline B. Lopez,¹ and Elissa A. Hallem^{1,2,3,*}

¹Department of Microbiology, Immunology, and Molecular Genetics, University of California, Los Angeles, Los Angeles, CA 90095, USA

²Molecular Biology Institute, University of California, Los Angeles, Los Angeles, CA 90095, USA

³Lead Contact

*Correspondence: ehallem@ucla.edu

<https://doi.org/10.1016/j.cub.2018.05.063>

SUMMARY

Skin-penetrating parasitic nematodes infect approximately one billion people worldwide and are a major source of neglected tropical disease [1–6]. Their life cycle includes an infective third-larval (iL3) stage that searches for hosts to infect in a poorly understood process that involves both thermal and olfactory cues. Here, we investigate the temperature-driven behaviors of skin-penetrating iL3s, including the human-parasitic threadworm *Strongyloides stercoralis* and the human-parasitic hookworm *Ancylostoma ceylanicum*. We show that human-parasitic iL3s respond robustly to thermal gradients. Like the free-living nematode *Caenorhabditis elegans*, human-parasitic iL3s show both positive and negative thermotaxis, and the switch between them is regulated by recent cultivation temperature [7]. When engaging in positive thermotaxis, iL3s migrate toward temperatures approximating mammalian body temperature. Exposing iL3s to a new cultivation temperature alters the thermal switch point between positive and negative thermotaxis within hours, similar to the timescale of thermal plasticity in *C. elegans* [7]. Thermal plasticity in iL3s may enable them to optimize host finding on a diurnal temperature cycle. We show that temperature-driven responses can be dominant in multisensory contexts such that, when thermal drive is strong, iL3s preferentially engage in temperature-driven behaviors despite the presence of an attractive host odorant. Finally, targeted mutagenesis of the *S. stercoralis* *tax-4* homolog abolishes heat seeking, providing the first evidence that parasitic host-seeking behaviors are generated through an adaptation of sensory cascades that drive environmental navigation in *C. elegans* [7–10]. Together, our results provide insight into the behavioral strategies and molecular mechanisms that allow skin-penetrating nematodes to target humans.

RESULTS AND DISCUSSION

Skin-penetrating parasitic nematodes are a group of soil-transmitted helminths that includes *Strongyloides stercoralis* as well as hookworms in the genera *Ancylostoma* and *Necator* [3, 11]. In humans, chronic nematode infections primarily affect the most impoverished communities around the world, with symptoms ranging from chronic gastrointestinal distress, to stunted growth and cognitive impairment in children, to death in the case of *S. stercoralis* [1–6]. Current treatments are often insufficient, as they target ongoing infections without preventing reinfection [12]. A better understanding of how parasitic worms locate and identify suitable hosts may lead to new therapeutic strategies for preventing infections.

Skin-penetrating worms have a complex life cycle that includes multiple environmental larval stages and culminates in parasitic adulthood inside a host (Figure S1A) [13]. These worms are infective during a developmentally arrested third-larval stage (iL3) analogous to the *C. elegans* dauer stage [14–16]. iL3s are soil dwelling and actively search for hosts using host-emitted sensory cues [13]. Skin-penetrating iL3s are only capable of using a narrow range of species as hosts [17–21]. Detection of a host animal likely involves both olfactory and thermosensory cues [13]. Early studies of thermosensation in skin-penetrating nematodes showed that the iL3s of many species respond to warmth [22–31]. However, the detailed thermosensory behaviors of parasitic nematodes require elucidation, and the molecular mechanisms that mediate thermosensation in these parasites have not yet been investigated.

Thermosensation has been extensively studied in *C. elegans*, which displays both thermotaxis navigation within their physiological temperature range (15°C–25°C) and active avoidance of noxious heat (>26°C) [7, 32–34]. Within their physiological range, *C. elegans* adults exhibit experience-dependent thermosensory behaviors, navigating in relation to a “remembered” cultivation temperature (T_C) [7, 34–40]. If the ambient temperature changes, the remembered T_C resets to the new ambient temperature within hours [7, 34, 37, 41–43]. At temperatures in the noxious heat range, *C. elegans* adults migrate down the thermal gradient [44]. In addition, noxious heat avoidance can overcome chemical attraction, as *C. elegans* adults fail to migrate toward attractive odorants placed at temperatures above their preferred range [33]. *C. elegans* dauers, which are more resistant to environmental stress, are insensitive to noxious thermal stimuli that repel adults [32].

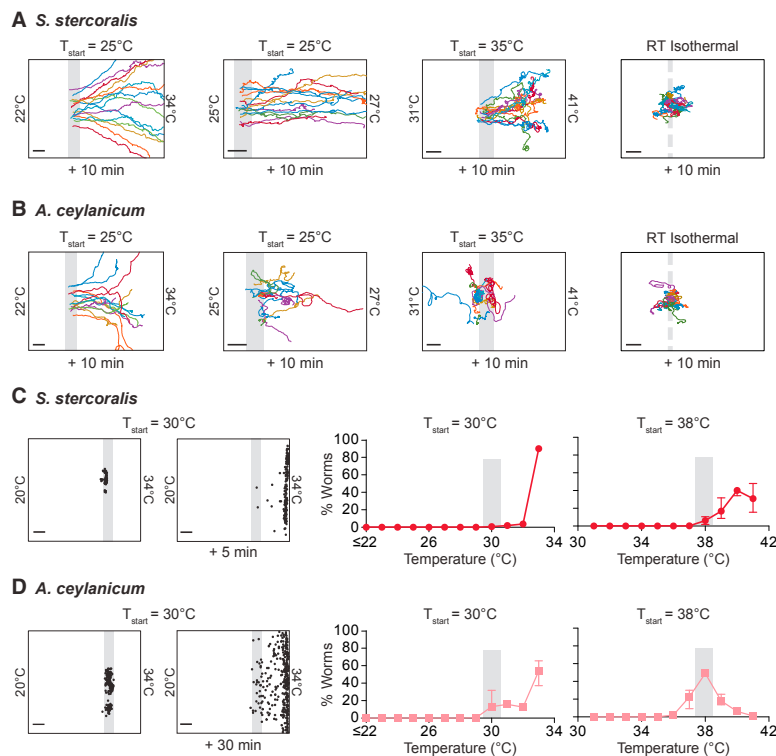


Figure 1. Human-Parasitic iL3s Show Robust Heat Seeking

(A) Left: Tracks of *S. stercoralis* iL3s heat seeking in a steep thermal gradient (22°C–34°C; 0.53°C/cm). Starting temperature (T_{start}): ~25°C; duration: 10 min; n = 15 worms. Center left: Tracks of *S. stercoralis* iL3s heat seeking in a shallow thermal gradient (24°C–27°C; 0.13°C/cm). T_{start} : ~25°C; duration: 10 min; n = 15 worms. Only a portion of the plate (25°C–27°C) is shown. Center right: Tracks of *S. stercoralis* iL3s moving in a 29°C–41°C gradient (0.53°C/cm). T_{start} : ~35°C; duration: 10 min; n = 15 worms. Only a portion of the gradient (31°C–41°C) is shown. Right: Tracks of *S. stercoralis* iL3s migrating on an isothermal room temperature (RT) plate. Duration: 10 min; n = 15 worms. Tracks reflect movement patterns in the absence of applied sensory stimulation. For each gradient, tracked worms were selected at random from ≤ 100 iL3s placed on the plates.

(B) Left: Tracks of *A. ceylanicum* iL3s heat seeking in a steep thermal gradient (22°C–34°C; 0.53°C/cm). Starting temperature (T_{start}): ~25°C; duration: 10 min; n = 15 worms. Center left: Tracks of *A. ceylanicum* iL3s heat seeking in a shallow thermal gradient (24°C–27°C; 0.13°C/cm). T_{start} : ~25°C; duration: 10 min; n = 15 worms. Only a portion of the plate (25°C–27°C) is shown. Center right: Tracks of *A. ceylanicum* iL3s moving in a 31°C–42°C gradient (0.49°C/cm). T_{start} : ~35°C; duration: 10 min; n = 15 worms. Only a portion of the gradient (31°C–41°C) is shown. Right: Tracks of *A. ceylanicum* iL3s migrating on an isothermal RT plate. Duration: 10 min; n = 20 worms. For each gradient, tracked worms were selected at random from ≤ 100 iL3s placed on the plates.

(C) Left: Representative distribution of *S. stercoralis* iL3s placed at 30°C in a 20°C–34°C gradient, either at the start of the experiment or 5 min later. Black dots indicate locations of individual iL3s (dots are not to scale). Center: Median final distribution of *S. stercoralis* iL3s in a ~20°C–34°C gradient (T_{start} : ~30°C; duration: 5 min; n = 16 trials with >50 iL3s per trial). Right: Median final distribution of *S. stercoralis* iL3s in a 30°C–42°C gradient (T_{start} : 38°C; duration: 15 min; n = 17 trials with >50 iL3s per trial). See also Video S1.

(D) Left: Representative distribution of *A. ceylanicum* iL3s placed at 30°C in a 20°C–34°C gradient, either at the start of the experiment or 30 min later. Black dots indicate locations of individual iL3s (dots are not to scale). Center: Median final distribution of *A. ceylanicum* iL3s in a ~20°C–34°C gradient (T_{start} : ~30°C; duration: 30 min; n = 16 trials with >50 iL3s per trial). Right: Median final distribution of *A. ceylanicum* iL3s in a 30°C–42°C gradient (T_{start} : 38°C; duration: 15 min; n = 15 trials with >50 iL3s per trial).

Graphs show medians and interquartile ranges; in some cases, error bars are too small to be visible. For all experiments, cultivation temperature (T_C): 23°C, scale bars: 2 cm, gray bars indicate T_{start} , and the width of the gray bars represents 1°C (except for shallow gradient tracks, where the width of the gray bars represents 0.25°C, and isothermal tracks, where the dashed gray bar indicates approximate starting location of the iL3s). See also Figures S1–S3 and Video S1.

Skin-Penetrating Human-Parasitic iL3s Heat Seek

To better understand the temperature-driven movement of parasitic nematodes, we first investigated the thermal preferences of two human-parasitic nematodes: *S. stercoralis* and *A. ceylanicum*. We imaged iL3 migration in precisely controlled, ethologically relevant thermal gradients using a large-format thermotaxis setup based on devices used for *C. elegans* [45] but modified for use with iL3s (Figure S1B). We found that human-parasitic iL3s display robust and sensitive heat seeking when exposed to temperatures above ambient (Video S1). When placed at 25°C, *S. stercoralis* and *A. ceylanicum* iL3s moved rapidly toward warmth in both steep (~0.53°C/cm) and shallow (0.13°C/cm) gradients (Figures 1A and 1B). This behavior contrasted sharply with the non-directional migration of iL3s in an isothermal environment (Figures 1A and 1B).

To identify the preferred temperature of human-parasitic iL3s engaged in heat seeking, we then measured the distribution of iL3s in warmer gradients that spanned human skin and core body temperatures (~31°C–34°C and ~37°C, respectively) [46, 47]. *A. ceylanicum* iL3s appeared to prefer temperatures near human core body temperature (~38°C), and *S. stercoralis* preferred slightly higher temperatures (~40°C), as indicated by a decrease in directional migration at these temperatures (Figures 1C and 1D). A preferred temperature set higher than host skin surface temperature may create strong migratory drive toward heat sources that does not attenuate as the iL3s approach a host.

The presence of a thermal gradient affected not only directional migration of iL3s but also their crawling speeds. iL3s in a steep thermal gradient crawled more rapidly than iL3s in a shallow thermal gradient or an isothermal environment (Figures

S2A and S2B). Both gradient steepness and absolute temperature contributed to changes in movement speed; for example, *S. stercoralis* iL3s thermotaxing in a steep gradient ranging over cooler temperatures traveled faster than iL3s thermotaxing in an equally steep gradient ranging over warmer temperatures (Figure S2A). These results suggest that the speed at which iL3s migrate within a thermal gradient is regulated by the strength of thermal drive, consistent with similar observations in *C. elegans* [36, 44]. The rapid crawling speed of human-parasitic iL3s in steep gradients, in combination with their sensitivity to shallow gradients, indicates that thermosensation is a potent sensory cue for skin-penetrating worms.

Navigation toward Host Temperatures Promotes Local-Search Behavior

When we tested iL3s at temperatures above ambient and below host body temperature (T_H), thermotaxis navigation occurred on a relatively straight trajectory. In contrast, as worms approached T_H , trajectories became more curved (Figures 1A and 1B). We quantified this change in tortuosity by calculating the distance ratio (total distance divided by maximum displacement) of individual worm tracks, where a greater distance ratio indicates a more curved trajectory. We found that iL3s in a steep thermal gradient near T_H had higher distance ratios than iL3s in a steep thermal gradient below T_H (Figures S2C and S2D). These results suggest that iL3s switch from long-range navigation to local search [48, 49] as they approach T_H .

In contrast to iL3s in thermal gradients below T_H , iL3s in isothermal environments below T_H showed highly curved trajectories (Figures 1A, 1B, S2C, and S2D), consistent with a previous study in a different parasitic nematode [23]. The fact that iL3s engage in local search both in isothermal conditions below T_H and in thermal gradients close to T_H suggests that local search is a basal behavior inhibited by thermal drive. Thus, iL3s transition from long-range navigation to local search when thermal drive has been sufficiently diminished by proximity to T_H . Local search near T_H may function to increase the likelihood that iL3s physically contact a nearby host [24]. It may also allow iL3s to sample the environment for gustatory or olfactory cues that may provide information about whether a nearby heat source indicates the presence of a host animal.

Human-Parasitic iL3s Engage in Positive and Negative Thermotaxis

In the experiments described above, iL3s were placed in thermal gradients at temperatures above ambient. Under these conditions, iL3s appeared to treat thermal cues as signaling the presence of a nearby host and displayed positive trajectories. When iL3s were instead placed near or below ambient temperature, a different mode of temperature-driven movement emerged: migration toward cooler temperatures (Figures 2A and 2B). For *S. stercoralis* iL3s, the switch point between positive and negative thermotaxis spanned a narrow temperature range. When iL3s were placed at 22°C, most showed negative thermotaxis (Figures 2A–2C). When iL3s were placed at 23°C, the population exhibited a bimodal response such that some iL3s engaged in positive thermotaxis and others engaged in negative thermotaxis (Figures 2A–2C). When placed at 25°C, nearly all of the iL3s engaged in positive thermotaxis (Figures 2A–2C). Negative ther-

motaxis could act as a dispersal mechanism to increase the chances of finding a host. It could also function to enhance subsequent discrimination between host-emitted heat and environmental temperature gradients.

The Switch between Positive and Negative Thermotaxis Is Regulated by Recent Experience

In *C. elegans*, both positive and negative thermotaxis are regulated by the T_C experienced by the worms within the past few hours [7, 34, 37, 41–43]. To test whether similar experience-dependent plasticity occurs in *S. stercoralis*, we first compared the behavior of *S. stercoralis* iL3s cultivated at 15°C for 7 days with control iL3s that were maintained at 23°C. Whereas 23°C-cultivated iL3s displayed both positive and negative thermotaxis when placed at 23°C in an ~20°C–34°C gradient (Figures 2A and 2B), iL3s cultivated at 15°C exclusively engaged in positive thermotaxis (Figure 2D). Thus, the decision to engage in positive or negative thermotaxis depends on T_C .

To investigate the time course of the switch, we took *S. stercoralis* iL3s grown at 23°C and cultivated them at either 23°C or 15°C for 2 hr, in parallel. We then recorded their behavior after placement at 22°C in an ~20°C–34°C gradient. In those conditions, only a small percentage of iL3s cultivated at 23°C engaged in positive thermotaxis (Figure 2E; Video S2). iL3s cultivated for 2 hr at 15°C were significantly more likely to display positive thermotaxis (Figure 2E; Video S3). Conversely, iL3s cultivated for 2 hr at 37°C were slightly less likely to engage in positive thermotaxis after placement at 30°C in an ~20°C–34°C gradient (Figure 2F); however, the majority of iL3s cultivated at 37°C continued to display positive thermotaxis, suggesting that thermal cues can drive host seeking even when environmental temperatures are high. Together, our results demonstrate that the time course of experience-dependent modulation in *S. stercoralis* is similar to that of T_C -dependent thermal plasticity in *C. elegans* [7, 34, 37, 41–43].

Soil-dwelling worms experience changes in environmental temperature on diurnal timescales [36, 50, 51]. Our results demonstrate that experience-dependent modulation of thermosensory responses in soil-dwelling iL3s occurs quickly enough to plausibly drive diurnal changes in host-seeking behavior. Moreover, the decrease in heat seeking we observed when T_C approximates T_H suggests that iL3s may be more likely to target humans when environmental temperatures are low. Interestingly, the rapid (hours-long) experience-dependent modulation of thermal preferences is in contrast to the slower (days-long) experience-dependent olfactory plasticity previously observed in some parasitic worms [52, 53]. Because olfactory environments are likely to be less influenced by diurnal changes than thermal environments, our results suggest that the temporal dynamics of sensory plasticity in iL3s may be tuned for the ethological relevance of environmental changes.

Similar Thermotaxis Behaviors Are Exhibited by Other Mammalian-Parasitic Nematodes

We next compared the thermal preferences of human-parasitic nematodes to those of an ethologically and evolutionarily diverse group of soil-dwelling nematodes (Figure S3A). For this analysis, we placed nematodes at 30°C in a steep thermal gradient; these conditions elicited robust positive thermotaxis from the

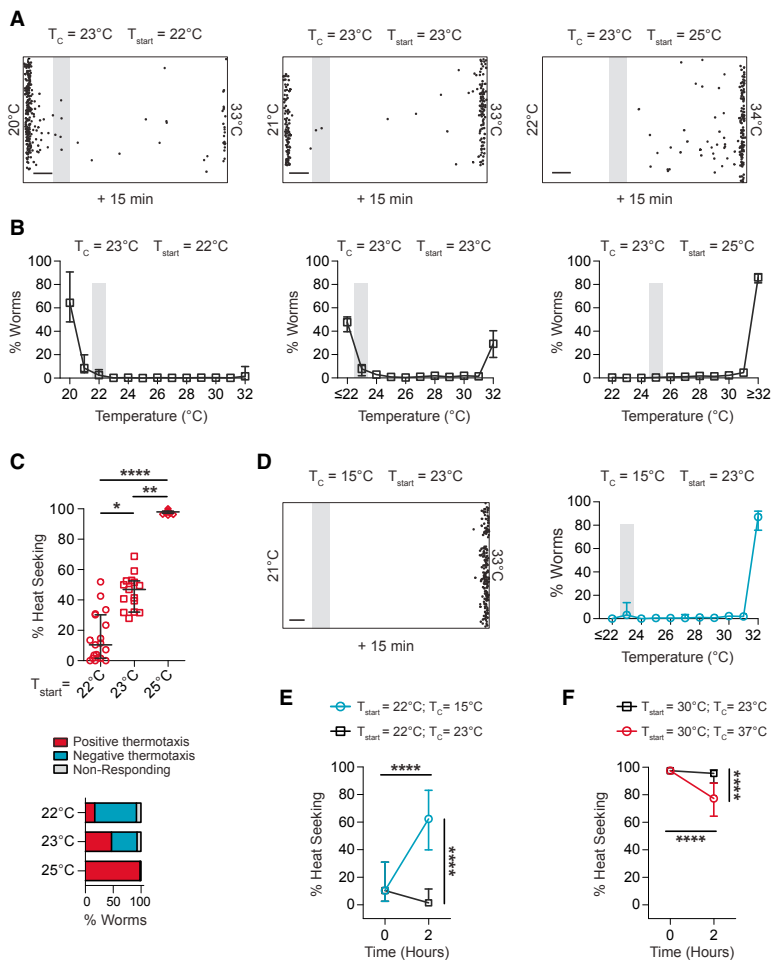


Figure 2. Experience-Dependent Plasticity Regulates a Switch between Positive and Negative Thermotaxis

(A) Left: Representative distribution of *S. stercoralis* iL3s placed at 22°C in a 20°C–33°C gradient after 15 min. iL3s display primarily negative thermotaxis. Center: Representative distribution of *S. stercoralis* iL3s placed at 23°C in a 21°C–33°C gradient after 15 min. iL3s display both positive and negative thermotaxis. Right: Representative distribution of *S. stercoralis* iL3s placed at 25°C in a 22°C–34°C gradient after 15 min. iL3s display primarily positive thermotaxis. T_C : 23°C; scale bars: 2 cm; gray bars indicate T_{start} ; width of the gray bars represents 1°C. Black dots indicate locations of individual iL3s (dots are not to scale).

(B) Left: Median final distribution of *S. stercoralis* iL3s placed at 22°C in a 20°C–33°C gradient. T_C : 23°C; duration: 15 min; $n = 19$ trials with >50 iL3s per trial. Center: Median final distribution of *S. stercoralis* iL3s placed at 23°C in an ~22°C–33°C gradient. $T_C = 23^\circ\text{C}$; duration: 15 min; $n = 15$ trials with >50 iL3s per trial. Right: Median final distribution of *S. stercoralis* iL3s placed at 25°C in an ~22°C–34°C gradient. $T_C = 23^\circ\text{C}$; duration: 15 min; gray bars indicate T_{start} ; width of the gray bars represents 1°C; $n = 15$ trials with >50 iL3s per trial. Graphs show medians and interquartile ranges. In some cases, error bars are too small to be visible.

(C) Top: Percent of heat-seeking (i.e., positively thermotaxing) *S. stercoralis* iL3s in an ~21°C–34°C gradient, by starting temperature. * $p < 0.05$; ** $p < 0.005$; **** $p < 0.0001$; Kruskal-Wallis test with Dunn's post-test. $n = 15$ –19 trials per condition, with >50 iL3s per trial. Graph shows medians and interquartile ranges. Bottom: Proportion of *S. stercoralis* iL3s placed at different starting temperatures that display positive or negative thermotaxis or that fail to migrate out of the initial 1°C temperature bin (non-responding). The percentage of iL3s that engage in thermotaxis (either positive or negative) is not significantly different

when iL3s are placed at 22°C versus 23°C ($p = 0.45$; chi-square test). However, each increase in starting temperature results in a significant increase in the likelihood of positive thermotaxis (22°C versus 23°C: $p < 0.001$; 23°C versus 25°C: $p < 0.001$; 22°C versus 25°C: $p < 0.001$; chi-square test with Bonferroni correction). Data are from the experiments shown in (B).

(D) Left: Representative distribution of *S. stercoralis* iL3s cultivated at 15°C for 7 days and then placed at 23°C in a 21°C–33°C gradient. iL3s display only heat seeking. Black dots indicate locations of individual iL3s (dots are not to scale). Right: Median final distribution of *S. stercoralis* iL3s cultivated at 15°C for 7 days and then placed at 23°C in an ~22°C–33°C gradient. Duration: 15 min; scale bar, 2 cm; $n = 15$ trials with >50 iL3s per trial. Graph shows medians and interquartile ranges. In some cases, error bars are too small to be visible.

(E) Time course of the T_C -dependent shift in thermal preference at temperatures below host body temperature (T_H). iL3s were initially cultured at 23°C and either shifted to 15°C (blue) or maintained at 23°C (black) for 2 hr. The iL3s were then placed at 22°C in a 20°C–33°C gradient. iL3s that had been cultured at 15°C for 2 hr showed an increased frequency of heat seeking. **** $p < 0.0001$; two-way ANOVA with Tukey's post-test. Duration: 15 min; $n = 14$ –15 trials per time point with >50 iL3s per trial. Graph shows medians and interquartile ranges. See also Videos S2 and S3.

(F) Time course of the T_C -dependent shift in thermal preference at temperatures near T_H . iL3s were initially cultured at 23°C and then either shifted to 37°C (red) or maintained at 23°C (black) for 2 hr. The iL3s were then placed at 30°C in a 21°C–33°C gradient. iL3s that had been cultured at 37°C for 2 hr showed a slightly decreased frequency of heat seeking. **** $p < 0.0001$; two-way ANOVA with Tukey's post-test. Duration: 15 min; $n = 14$ –15 trials per time point with >50 iL3s per trial. Graph shows medians and interquartile ranges. In some cases, error bars are too small to be visible.

See also Figure S4 and Videos S2 and S3.

human-parasitic iL3s (Video S1). We found that the other mammalian-parasitic species tested displayed robust positive thermotaxis under these conditions (Figure S3). Notably, we found that the passively ingested nematode *Heligmosomoides polygyrus* [54, 55] showed positive thermotaxis toward T_H (Fig-

ure S3D). Together with previous studies showing attraction of *H. polygyrus* iL3s to host-emitted chemosensory cues [52, 55], our results suggest that at least some passively ingested iL3s host seek to position themselves near potential hosts, where they are more likely to be swallowed. As a control for these

experiments, we examined the temperature-driven movement of an entomopathogenic nematode (EPN) and *C. elegans* when placed at 30°C in the same thermal gradient. As expected [32, 33, 51], neither the EPN nor *C. elegans* adults or dauers displayed positive thermotaxis under these conditions (Figures S3E–S3I). Thus, movement toward T_H is limited to nematodes that infect mammalian hosts. All of the mammalian-parasitic iL3s tested also showed similar experience-dependent positive and negative thermotaxis behaviors (Figure S4), consistent with a previous study of one of these species [29].

To compare the preferred temperature of each mammalian-parasitic species, we measured iL3 distribution in gradients spanning mammalian skin and core body temperatures. The thermal preferences of species that parasitize non-human mammals were similar to those of *A. ceylanicum* iL3s; they displayed minimal positive thermotaxis near T_H (Figures 1D, S3B–S3D, and S3J), suggesting that their preferred temperatures approximate T_H . The behaviors of *A. ceylanicum* and the parasitic worms of non-human mammals were significantly different from those of *S. stercoralis* (Figure S3J). Thus, our data suggest that, in comparison to other mammalian-parasitic nematode species, *S. stercoralis* is particularly specialized for temperature-driven tracking of potential hosts.

Thermal Drive Can Override Attraction to Host Odorants

Our results indicate that temperature is a potent host cue for iL3s. Previous studies demonstrated that iL3s are also attracted to host-emitted odorants [24, 48, 52, 56, 57], raising the question of whether thermal and olfactory cues interact to regulate host seeking. Other anthropophilic organisms, such as mosquitoes, exhibit context-dependent responses to host cues such that the presence of a potent host cue can alter the behavioral response to cues belonging to other modalities [58]. In parasitic worms, however, the interactions between different sensory modalities in the context of host attraction are not well understood.

To assess the interaction between thermosensation and chemosensation in parasitic worms, we tested the effects of a thermal gradient on the response of *S. stercoralis* iL3s to the highly attractive host odorant 3-methyl-1-butanol (also called isoamyl alcohol) [48]. When iL3s were exposed to 3m1b in an isothermal context at 27°C, they engaged in local search directed toward the odorant source (Figures 3A and 3B). In contrast, when 3m1b was placed at 27°C in a steep thermal gradient, iL3s did not engage in local search toward the 3m1b but rather displayed long-range navigation up the thermal gradient (Figures 3C and 3D). In the steep thermal gradient, the presence of the attractive odorant did not alter either the number of iL3s that reached the odorant source, the final temperature reached, or the tortuosity of the migratory path (Figures 3C–3F). When the odorant was instead placed near host body temperature in a higher thermal gradient, the presence of the odorant both reduced the final temperature reached and increased tortuosity (Figures 3G–3I), an effect that is likely due to both reduced thermal drive in the warmer gradient and increased odorant volatility. Thus, an odorant that is highly attractive in a monosensory context can be overwhelmed by the strong thermal drive experienced at temperatures below T_H .

Our results suggest that, at temperatures below T_H , iL3s may prioritize temperature-driven behaviors over chemosensory re-

sponses. We cannot exclude the possibility that sufficiently potent chemosensory cues could elicit attractive responses despite strong thermal drive. Nevertheless, if thermal cues are more effective drivers of directed navigation than chemosensory cues, skin-penetrating worms may utilize a host-seeking strategy wherein iL3s track down heat sources prior to determining whether they indicate a host animal. At temperatures near T_H , olfactory or gustatory cues that are selective for their host species may then cause iL3s to engage in short-range navigation toward the host and initiate host-infection behaviors [49].

S. stercoralis tax-4 Is Required for Positive Thermotaxis

To date, no studies have directly assessed the molecular basis of thermosensation or any other sensory modality in parasitic nematodes. In contrast, the molecular basis of *C. elegans* thermosensation has been extensively studied [34, 59, 60]. To begin to elucidate the molecular mechanisms that underlie parasitic nematode thermotaxis, we asked whether the distinct temperature-driven behaviors of parasitic and free-living nematodes arise from adaptations of shared thermosensory machinery. We focused on the *tax-4* gene, because the *C. elegans tax-4* gene encodes a cyclic nucleotide-gated channel subunit that is required for thermotaxis navigation [8–10, 61]. We used *S. stercoralis* for these experiments, because *Strongyloides* species are amenable to both transgenesis and CRISPR-Cas9-mediated mutagenesis [62–65]. We first examined the expression pattern of the *S. stercoralis tax-4* homolog (*Ss-tax-4*) and found that it is expressed in multiple head neuron pairs (Figure 4A), consistent with the expression pattern of *Ce-tax-4* [8, 10, 61]. We then tested the effects of *Ss-tax-4* gene disruption on parasite heat seeking. We used CRISPR-Cas9-mediated mutagenesis to generate *S. stercoralis* iL3s in which *Ss-tax-4* expression was fully disrupted, as previously described (Figures 4B–4D) [65]. Plasmids encoding Cas9, the single guide RNA, and a repair template for homology-directed repair were microinjected into *S. stercoralis* free-living adult females. The iL3 progeny from the microinjected females were individually tested in behavioral assays and then genotyped after testing.

To test the effect of *Ss-tax-4* disruption on iL3 thermotaxis, we compared the temperature-driven movements of *Ss-tax-4* iL3s to those of control iL3s generated by microinjections, in which Cas9 was excluded from the injection mix (“no-Cas9 controls”). As with wild-type worms, when no-Cas9 controls were placed at 30°C and allowed to migrate for 15 min, they moved rapidly up the thermal gradient (Figure 4E). In contrast, *Ss-tax-4* iL3s displayed multiple deficits in their temperature-driven behaviors (Figure 4F) such that their movements resembled those of wild-type iL3s in a room temperature isothermal context (Figure 4G). First, the movement of *Ss-tax-4* iL3s toward T_H was significantly reduced relative to that of the no-Cas9 controls (Figure 4H). Second, disruption of *Ss-tax-4* suppressed the thermal-drive-dependent inhibition of local search, resulting in distance ratios resembling those of wild-type iL3s on an isothermal plate (Figure 4I). Third, *Ss-tax-4* iL3s did not exhibit a temperature-dependent increase in crawling speed (Figure 4J). Thus, *Ss-tax-4* is required for normal iL3 thermotaxis. These results suggest that the robust heat-seeking behaviors of iL3s reflect a parasitic specialization of molecular pathways utilized for thermotaxis navigation in free-living worms.

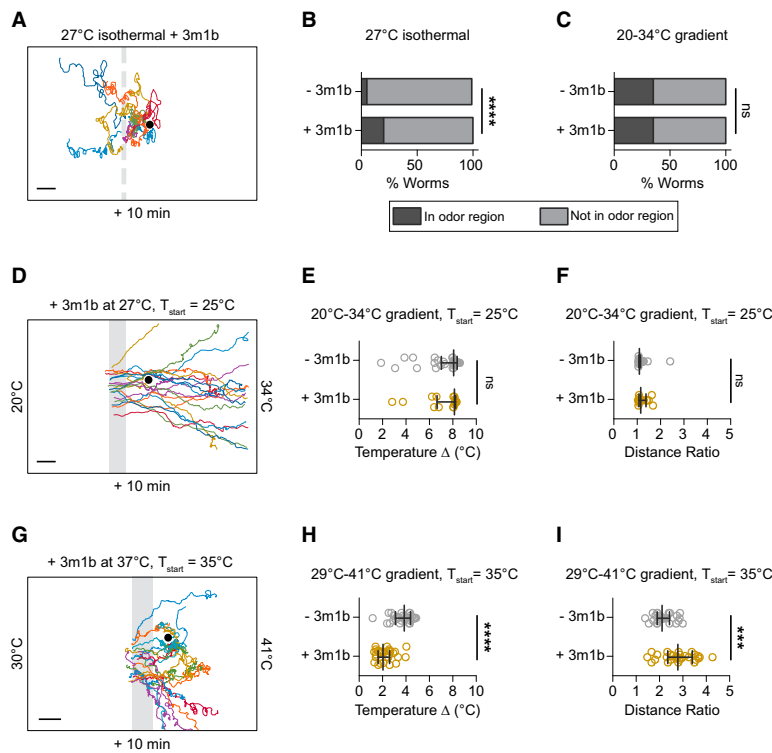


Figure 3. Thermal Gradients Can Override Olfactory Attraction

(A) *S. stercoralis* iL3 tracks on a 27°C isothermal plate; iL3s divert toward the attractive host odorant 3-methyl-1-butanol (3m1b; 5 μ L undiluted) placed ~2 cm away. T_C : 23°C; duration: 10 min; n = 10 worms. Dashed bar indicates approximate starting location of iL3s. The scale bar represents 2 cm. Tracked worms were selected at random from ≤ 100 iL3s placed on the plate.

(B) Percentage of *S. stercoralis* iL3s placed on a 27°C isothermal plate with or without 3m1b that either entered or failed to enter a 2-cm-diameter scoring region in 5 min. The scoring regions were positioned such that on plates with 3m1b, the 3m1b was centered in the scoring region. In an isothermal environment, the presence of 3m1b significantly increased the likelihood that worms entered the scoring region (****p < 0.0001; chi-square test). T_C : 23°C; n = 723–760 iL3s across 5 trials per condition.

(C) Percentage of *S. stercoralis* iL3s placed in a 20°C–34°C gradient with or without 3m1b that either entered or failed to enter a 2-cm-diameter scoring region in 5 min. The scoring regions were positioned such that, on plates with 3m1b, the 3m1b was centered in the scoring region. In the thermal gradient, the presence of 3m1b did not alter the percentage of worms entering the scoring region. T_{start} : ~25°C; $T_{odorant}$: 27°C; T_C : 23°C; n = 921–924 iL3s across 5 trials per condition. ns, not significant; chi-square test.

(D) *S. stercoralis* iL3 tracks in a 20°C–34°C gradient with 3m1b placed at 27°C. T_{start} : ~25°C; $T_{odorant}$: 27°C; T_C : 23°C; duration: 10 min; n = 20

worms. The scale bar represents 2 cm. Tracked worms were selected at random from ≤ 100 iL3s placed on the plate.

(E) The presence of 3m1b placed at 27°C in a 20°C–34°C gradient does not alter the final temperature reached by iL3s migrating in the gradient. Graph shows the change in temperature (final temperature – starting temperature) exhibited by individual iL3s migrating in a 20°C–34°C thermal gradient versus a combined 20°C–34°C thermal and chemosensory gradient. T_{start} : ~25°C; $T_{odorant}$: 27°C; T_C : 23°C; duration: 10 min; n = 20–40 iL3s per condition. ns, not significant; Mann-Whitney test. Lines show medians and interquartile ranges.

(F) The presence of 3m1b placed at 27°C in a 20°C–34°C gradient does not alter the tortuosity of *S. stercoralis* iL3 movement paths. Graph shows the distance ratios of individual iL3s migrating in a 20°C–34°C thermal gradient versus a combined 20°C–34°C thermal and chemosensory gradient. Distance ratios were calculated as the total track length divided by the maximum displacement; a higher value indicates a more highly curved trajectory. T_{start} : ~25°C; $T_{odorant}$: 27°C; T_C : 23°C; duration: 10 min; n = 20–40 worms per condition. ns, not significant; Mann-Whitney test. Lines show medians and interquartile ranges.

(G) *S. stercoralis* iL3 tracks in a 29°C–41°C gradient with 3m1b placed at 37°C. T_{start} : ~35°C; $T_{odorant}$: 37°C; T_C : 23°C; duration: 10 min; n = 20 worms. The scale bar represents ~2 cm. Only a portion of the plate (30°C–41°C) is shown. Tracked worms were selected at random from ≤ 100 iL3s placed on the plate.

(H) The presence of 3m1b placed at 37°C in a 29°C–41°C gradient decreases the final temperature reached by iL3s migrating in the gradient. Graph shows the change in temperature (final temperature – starting temperature) exhibited by individual iL3s migrating in a 29°C–41°C thermal gradient versus a combined 29°C–41°C thermal and chemosensory gradient. T_{start} : ~35°C; $T_{odorant}$: 37°C; T_C : 23°C; duration: 10 min; n = 30 worms per condition. ****p < 0.0001; Mann-Whitney test. Lines show medians and interquartile ranges.

(I) The presence of 3m1b placed at 37°C in a 29°C–41°C gradient increases the tortuosity of *S. stercoralis* iL3 movement paths. Graph shows the distance ratios of individual iL3s migrating in a 29°C–41°C thermal gradient versus a combined 29°C–41°C thermal and chemosensory gradient, calculated as described in (F). T_{start} : ~35°C; $T_{odorant}$: 37°C; T_C : 23°C; duration: 10 min; n = 30 worms per condition. ***p < 0.0005; Mann-Whitney test. Lines show medians and interquartile ranges.

Implications for Nematode Control

Soil-dwelling parasitic worms that infect humans and livestock are a major health and economic threat worldwide. Current treatments rely on periodic deworming, a strategy that has led to widespread drug resistance in livestock parasites and threatens to complicate the treatment of human patients in the near future [69–73]. Understanding the sensory modalities that guide host seeking by parasitic nematodes may enable new approaches for preventing infections. Here, we combined quantitative behavioral analyses with targeted mutagenesis to elucidate the

role of thermosensation in the host-seeking behaviors of mammalian-parasitic worms. We find evidence that heat acts as a critical host-emitted cue for multiple species of soil-transmitted helminths. Our results could inform the design of novel control strategies, such as worm traps that incorporate heating elements. Furthermore, our data suggest that parasitic nematodes modulate their response to thermal cues on a diurnal cycle such that they heat seek more robustly in cooler environments. Thus, populations at risk for infection may be more susceptible to being targeted by a host-seeking nematode in the early

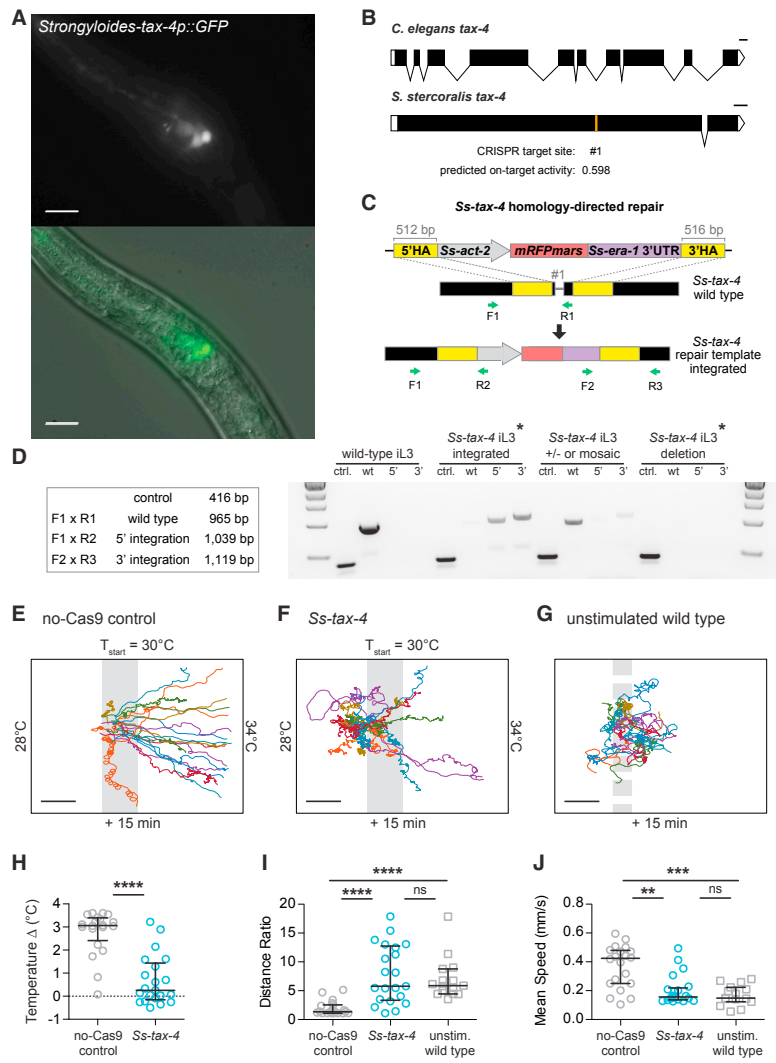


Figure 4. The *S. stercoralis tax-4* Homolog Is Required for Heat Seeking

(A) *Strongyloides-tax-4p::GFP* is expressed in the head neurons of an *S. stercoralis* larva. The scale bars represent 10 μm .

(B) The *tax-4* genes of *C. elegans* and *S. stercoralis*. The *Ss-tax-4* gene structure was based on the gene prediction by WormBase Parasite [65–67]. The location of the CRISPR target site is marked, and the on-target activity score is indicated. The scale bars represent 100 base pairs. Gene structure diagram is from Gang et al., 2017 [65].

(C) Strategy for homology-directed repair and single-worm genotyping at the *Ss-tax-4* target site [65]. The repair template contains an *mRFPmars* reporter gene under the control of the *Ss-act-2* promoter, which expresses in body wall muscle [68]. Free-living adult females (P_0) were microinjected with plasmids containing the CRISPR components (Cas9, single guide RNA, and repair template). F_1 iL3 progeny with near-uniform *Ss-act2p::mRFPmars* expression throughout the body wall were then genotyped using the primer sets indicated (green arrows). The wild-type primer set (F1/R1) exclusively amplifies the wild-type locus surrounding the *Ss-tax-4* target site. The 5' and 3' integration primers (F1/R2 and F2/R3, respectively) only amplify following successful integration of the repair template containing *Ss-act2p::mRFPmars* at the *Ss-tax-4* target site. Diagram is adapted from Gang et al., 2017 [65].

(D) Representative genotypes of a wild-type iL3 and F_1 iL3s expressing *mRFPmars* from P_0 females microinjected with the *Ss-tax-4* CRISPR components. ctrl., control reaction amplifying the first exon of the *Ss-act-2* gene to confirm the presence of genomic DNA; wt, reaction for the wild-type locus; 5', reaction for insertion of the 5' border of the repair template; 3', reaction for insertion of the 3' border of the repair template. Asterisks indicate genotypes categorized as *Ss-tax-4* homozygous knockouts. “+/- or mosaic” indicates iL3s that are either heterozygous or mosaic for an *Ss-tax-4* gene disruption [65]. Size markers, from top to bottom, are as follows: 3 kb; 2 kb; 1.5 kb; 1 kb; and 500 bp.

(E and F) CRISPR-Cas9 targeting of the *Ss-tax-4* gene results in iL3s with reduced preferences for warm temperatures. Tracks of individual no-Cas9

control F_1 iL3s (E) and *Ss-tax-4* F_1 iL3s (F) migrating for 15 min in an $\sim 22^{\circ}\text{C}$ – 34°C gradient are shown (T_{start} : $\sim 30^{\circ}\text{C}$; T_C : 23°C ; only a portion of the full gradient is shown). Worms were categorized as *Ss-tax-4* homozygous knockouts (“*Ss-tax-4*”) if the wild-type *Ss-tax-4* amplification band was absent during *post hoc* single-worm genotyping. Grey bars, T_{start} ; gray bar width: 1°C . The scale bars represent ~ 2 cm.

(G) Tracks of individual wild-type iL3s migrating for 15 min on an isothermal room temperature (RT) plate; tracks reflect unstimulated movement patterns. Dashed bar indicates approximate starting location of iL3s. T_C : 23°C . The scale bar represents 2 cm. Tracked worms were selected at random from ≤ 100 iL3s placed on the plate. The first 10 min of these tracks are also shown in Figure 1A and quantified in Figure S2.

(H) Change in temperature (final temperature – starting temperature) exhibited by individual iL3s migrating in an $\sim 22^{\circ}\text{C}$ – 34°C gradient (T_{start} : $\sim 30^{\circ}\text{C}$; T_C : 23°C). No-cas9 control iL3s migrated farther up the thermal gradient than *Ss-tax-4* iL3s. **** $p < 0.0001$; Mann-Whitney test.

(I) Distance ratio (maximum displacement divided by total distance traveled) for no-Cas9 control, *Ss-tax-4*, and unstimulated wild-type iL3s. The presence of the thermal gradient did not suppress local search in *Ss-tax-4* iL3s. **** $p < 0.0001$; Kruskal-Wallis test with Dunn’s post-test. For no-Cas9 control and *Ss-tax-4* iL3s, the thermal gradient is as follows: 22°C – 34°C gradient; T_{start} : $\sim 30^{\circ}\text{C}$; T_C : 23°C . Unstimulated worms were placed on an isothermal RT plate; T_C : 23°C .

(J) Mean speed of iL3s during thermotaxis navigation. *S. stercoralis* iL3s increased their crawling speed at warmer temperatures (no-Cas9 control versus unstimulated wild-type), as previously reported [48]. Disruption of *Ss-tax-4* prevented temperature-dependent speed changes. ** $p < 0.005$; *** $p < 0.001$; Kruskal-Wallis test with Dunn’s post-test. For no-Cas9 control and *Ss-tax-4* iL3s, the thermal gradient is as follows: 22°C – 34°C gradient; T_{start} : $\sim 30^{\circ}\text{C}$; T_C : 23°C . Unstimulated worms were placed on an isothermal RT plate; T_C : 23°C .

(H–J) Data are represented as median \pm interquartile range. $n = 15$ – 21 trials per condition.

morning and late evening, when people are active and environmental temperatures are low; this possibility has important implications for the development of preventative interventions [74]. Future studies of the cellular, molecular, and circuit bases of thermosensation in parasitic nematodes will provide further insights into the mechanisms that drive parasite-specific host-seeking behaviors.

STAR★METHODS

Detailed methods are provided in the online version of this paper and include the following:

- **KEY RESOURCES TABLE**
- **CONTACT FOR REAGENT AND RESOURCE SHARING**
- **EXPERIMENTAL MODEL AND SUBJECT DETAILS**
 - Maintenance of *Strongyloides stercoralis*
 - Maintenance of *Ancylostoma ceylanicum*
 - Maintenance of *Strongyloides ratti*
 - Maintenance of *Nippostrongylus brasiliensis*
 - Maintenance of *Heligmosomoides polygyrus*
 - Maintenance of *Steinernema carpocapsae*
 - Maintenance of *C. elegans*
- **METHOD DETAILS**
 - Thermotaxis assays
 - Behavioral effects of cultivation temperature
 - Thermotaxis assay data analysis
 - Multisensory assays
 - Generation of the *Strongyloides tax-4p::GFP* reporter construct
 - CRISPR-Cas9-mediated targeted mutagenesis of *Ss-tax-4*
 - Microinjection of *S. stercoralis* free-living adults
 - Selection of F₁ *Ss-tax-4* iL3s
 - *Ss-tax-4* thermotaxis assays
 - Genotyping for *Ss-tax-4* gene disruptions
 - Fluorescent microscopy
- **QUANTIFICATION AND STATISTICAL ANALYSIS**

SUPPLEMENTAL INFORMATION

Supplemental Information includes four figures, one table, and three videos and can be found with this article online at <https://doi.org/10.1016/j.cub.2018.05.063>.

ACKNOWLEDGMENTS

We thank Josh Hawk and Joon Ha Lee (Daniel Colon-Ramós lab) for helpful discussion regarding *C. elegans* thermotaxis as well as invaluable technical advice, Navonil Banerjee for insightful comments on the manuscript, and Tiffany Mao and Emily Yang for technical assistance. This work was supported by an A.P. Giannini Postdoctoral Fellowship and NIH Ruth L. Kirschstein National Research Service Award T32NS058280 (A.S.B.); the Whitcome Predoctoral Training Program, UCLA Molecular Biology Institute, and Ruth L. Kirschstein National Research Service Award T32AI007323 (S.S.G.); the UCLA-Howard Hughes Medical Institute Pathways to Success Program (J.B.L.); and a Burroughs-Wellcome Fund Investigators in the Pathogenesis of Disease Award, NIH New Innovator Award 1DP2DC014596, and Howard Hughes Medical Institute Faculty Scholar Award (E.A.H.).

AUTHOR CONTRIBUTIONS

Conceptualization, A.S.B. and E.A.H.; Methodology, A.S.B. and E.A.H.; Software, A.S.B.; Formal Analysis, A.S.B.; Investigation, A.S.B., F.R., and J.B.L.; Resources, A.S.B., F.R., S.S.G., and M.L.C.; Writing – Original Draft, A.S.B. and E.A.H.; Writing – Review & Editing, A.S.B., E.A.H., F.R., S.S.G., and M.L.C.; Project Administration, A.S.B. and E.A.H.; Funding Acquisition, E.A.H.

DECLARATION OF INTERESTS

The authors declare no competing interests.

Received: April 17, 2018

Revised: May 18, 2018

Accepted: May 22, 2018

Published: July 12, 2018

REFERENCES

1. Bethony, J., Brooker, S., Albonico, M., Geiger, S.M., Loukas, A., Diemert, D., and Hotez, P.J. (2006). Soil-transmitted helminth infections: ascariasis, trichuriasis, and hookworm. *Lancet* 367, 1521–1532.
2. Schafer, T.W., and Skopic, A. (2006). Parasites of the small intestine. *Curr. Gastroenterol. Rep.* 8, 312–320.
3. Bisoffi, Z., Buonfrate, D., Montresor, A., Requena-Méndez, A., Muñoz, J., Krolewiecki, A.J., Gotuzzo, E., Mena, M.A., Chiodini, P.L., Anselmi, M., et al. (2013). *Strongyloides stercoralis*: a plea for action. *PLoS Negl. Trop. Dis.* 7, e2214.
4. Buonfrate, D., Requena-Mendez, A., Angheben, A., Muñoz, J., Gobbi, F., Van Den Ende, J., and Bisoffi, Z. (2013). Severe strongyloidiasis: a systematic review of case reports. *BMC Infect. Dis.* 13, 78.
5. Nutman, T.B. (2017). Human infection with *Strongyloides stercoralis* and other related *Strongyloides* species. *Parasitology* 144, 263–273.
6. McKenna, M.L., McAtee, S., Bryan, P.E., Jeun, R., Ward, T., Kraus, J., Bottazzi, M.E., Hotez, P.J., Flowers, C.C., and Mejia, R. (2017). Human intestinal parasite burden and poor sanitation in rural Alabama. *Am. J. Trop. Med. Hyg.* 97, 1623–1628.
7. Hedgecock, E.M., and Russell, R.L. (1975). Normal and mutant thermotaxis in the nematode *Caenorhabditis elegans*. *Proc. Natl. Acad. Sci. USA* 72, 4061–4065.
8. Komatsu, H., Mori, I., Rhee, J.S., Akaike, N., and Ohshima, Y. (1996). Mutations in a cyclic nucleotide-gated channel lead to abnormal thermosensation and chemosensation in *C. elegans*. *Neuron* 17, 707–718.
9. Komatsu, H., Jin, Y.H., L'Etoile, N., Mori, I., Bargmann, C.I., Akaike, N., and Ohshima, Y. (1999). Functional reconstitution of a heteromeric cyclic nucleotide-gated channel of *Caenorhabditis elegans* in cultured cells. *Brain Res.* 821, 160–168.
10. Coburn, C.M., and Bargmann, C.I. (1996). A putative cyclic nucleotide-gated channel is required for sensory development and function in *C. elegans*. *Neuron* 17, 695–706.
11. Prichard, R.K., Basáñez, M.G., Boatman, B.A., McCarthy, J.S., García, H.H., Yang, G.J., Srija, B., and Lustigman, S. (2012). A research agenda for helminth diseases of humans: intervention for control and elimination. *PLoS Negl. Trop. Dis.* 6, e1549.
12. Jia, T.W., Melville, S., Utzinger, J., King, C.H., and Zhou, X.N. (2012). Soil-transmitted helminth reinfection after drug treatment: a systematic review and meta-analysis. *PLoS Negl. Trop. Dis.* 6, e1621.
13. Gang, S.S., and Hallem, E.A. (2016). Mechanisms of host seeking by parasitic nematodes. *Mol. Biochem. Parasitol.* 208, 23–32.
14. Viney, M.E., Thompson, F.J., and Crook, M. (2005). TGF- β and the evolution of nematode parasitism. *Int. J. Parasitol.* 35, 1473–1475.
15. Crook, M. (2014). The dauer hypothesis and the evolution of parasitism: 20 years on and still going strong. *Int. J. Parasitol.* 44, 1–8.

16. Hotez, P., Hawdon, J., and Schad, G.A. (1993). Hookworm larval infectivity, arrest and amphiparatensis: the *Caenorhabditis elegans* Daf-c paradigm. *Parasitol. Today (Regul. Ed.)* 9, 23–26.
17. Haley, A.J. (1961). Biology of the rat nematode *Nippostrongylus brasiliensis* (Travassos, 1914). I. Systematics, hosts and geographic distribution. *J. Parasitol.* 47, 727–732.
18. Viney, M., and Kikuchi, T. (2017). *Strongyloides ratti* and *S. venezuelensis* - rodent models of *Strongyloides* infection. *Parasitology* 144, 285–294.
19. Bezubik, B. (1965). Failure to establish infection in rats and guinea pigs exposed to the larvae of *Strongyloides papillosus*. *Acta Parasit. Polon.* 13, 349–354.
20. Nolan, T.J., Zhu, X., Ketschek, A., Cole, J., Grant, W., Lok, J.B., and Schad, G.A. (2007). The sugar glider (*Petaurus breviceps*): a laboratory host for the nematode *Parastrongyloides trichosuri*. *J. Parasitol.* 93, 1084–1089.
21. Viney, M.E., and Lok, J.B. (2015). The biology of *Strongyloides* spp (WormBook), pp. 1–17.
22. Barrett, J. (1968). The effect of temperature on the development and survival of the infective larvae of *Strongyloides ratti* Sandground, 1925. *Parasitology* 58, 641–651.
23. Croll, N.A., and Smith, J.M. (1972). Mechanism of thermopositive behavior in larval hookworms. *J. Parasitol.* 58, 891–896.
24. Granzer, M., and Haas, W. (1991). Host-finding and host recognition of infective *Ancylostoma caninum* larvae. *Int. J. Parasitol.* 21, 429–440.
25. Gupta, S.P. (1963). Mode of infection and biology of infective larvae of *Molineus barbatus* Chandler, 1942. *Exp. Parasitol.* 13, 252–255.
26. Haas, W., Haberl, B., Syafruddin, I., and Kersten, S.; Syafruddin (2005). Infective larvae of the human hookworms *Necator americanus* and *Ancylostoma duodenale* differ in their orientation behaviour when crawling on surfaces. *Parasitol. Res.* 95, 25–29.
27. Parker, J.C., and Haley, A.J. (1960). Phototactic and thermotactic responses of the filariform larvae of the rat nematode *Nippostrongylus muris*. *Exp. Parasitol.* 9, 92–97.
28. Reesal, M.R. (1951). Observations on the biology of the infective larvae of *Strongyloides agoutii*. *Can. J. Zool.* 29, 109–115.
29. Tobata-Kudo, H., Shimada, M., Koga, M., and Tada, I. (2000). *Strongyloides ratti*: thermokinetic behavior of third-stage larvae on a temperature gradient. *Exp. Parasitol.* 95, 196–201.
30. Bhopale, V.M., Kupprion, E.K., Ashton, F.T., Boston, R., and Schad, G.A. (2001). *Ancylostoma caninum*: the finger cell neurons mediate thermotactic behavior by infective larvae of the dog hookworm. *Exp. Parasitol.* 97, 70–76.
31. Lopez, P.M., Boston, R., Ashton, F.T., and Schad, G.A. (2000). The neurons of class ALD mediate thermotaxis in the parasitic nematode, *Strongyloides stercoralis*. *Int. J. Parasitol.* 30, 1115–1121.
32. Wittenburg, N., and Baumeister, R. (1999). Thermal avoidance in *Caenorhabditis elegans*: an approach to the study of nociception. *Proc. Natl. Acad. Sci. USA* 96, 10477–10482.
33. Glauser, D.A., Chen, W.C., Agin, R., Macinnis, B.L., Hellman, A.B., Garrity, P.A., Tan, M.W., and Goodman, M.B. (2011). Heat avoidance is regulated by transient receptor potential (TRP) channels and a neuropeptide signaling pathway in *Caenorhabditis elegans*. *Genetics* 188, 91–103.
34. Garrity, P.A., Goodman, M.B., Samuel, A.D., and Sengupta, P. (2010). Running hot and cold: behavioral strategies, neural circuits, and the molecular machinery for thermotaxis in *C. elegans* and *Drosophila*. *Genes Dev.* 24, 2365–2382.
35. Ito, H., Inada, H., and Mori, I. (2006). Quantitative analysis of thermotaxis in the nematode *Caenorhabditis elegans*. *J. Neurosci. Methods* 154, 45–52.
36. Ramot, D., Maclnris, B.L., Lee, H.C., and Goodman, M.B. (2008). Thermotaxis is a robust mechanism for thermoregulation in *Caenorhabditis elegans* nematodes. *J. Neurosci.* 28, 12546–12557.
37. Clark, D.A., Gabel, C.V., Lee, T.M., and Samuel, A.D. (2007). Short-term adaptation and temporal processing in the cryophilic response of *Caenorhabditis elegans*. *J. Neurophysiol.* 97, 1903–1910.
38. Jurado, P., Kodama, E., Tanizawa, Y., and Mori, I. (2010). Distinct thermal migration behaviors in response to different thermal gradients in *Caenorhabditis elegans*. *Genes Brain Behav.* 9, 120–127.
39. Mori, I., and Ohshima, Y. (1995). Neural regulation of thermotaxis in *Caenorhabditis elegans*. *Nature* 376, 344–348.
40. Ryu, W.S., and Samuel, A.D. (2002). Thermotaxis in *Caenorhabditis elegans* analyzed by measuring responses to defined thermal stimuli. *J. Neurosci.* 22, 5727–5733.
41. Kodama, E., Kuhara, A., Mohri-Shiomi, A., Kimura, K.D., Okumura, M., Tomioka, M., Iino, Y., and Mori, I. (2006). Insulin-like signaling and the neural circuit for integrative behavior in *C. elegans*. *Genes Dev.* 20, 2955–2960.
42. Mohri, A., Kodama, E., Kimura, K.D., Koike, M., Mizuno, T., and Mori, I. (2005). Genetic control of temperature preference in the nematode *Caenorhabditis elegans*. *Genetics* 169, 1437–1450.
43. Kuhara, A., and Mori, I. (2006). Molecular physiology of the neural circuit for calcineurin-dependent associative learning in *Caenorhabditis elegans*. *J. Neurosci.* 26, 9355–9364.
44. Schild, L.C., and Glauser, D.A. (2013). Dynamic switching between escape and avoidance regimes reduces *Caenorhabditis elegans* exposure to noxious heat. *Nat. Commun.* 4, 2198.
45. Goodman, M.B., Klein, M., Lasse, S., Luo, L., Mori, I., Samuel, A., Sengupta, P., and Wang, D. (2014). Thermotaxis navigation behavior (WormBook), pp. 1–10.
46. Benedict, F.G., Miles, W.R., and Johnson, A. (1919). The temperature of the human skin. *Proc. Natl. Acad. Sci. USA* 5, 218–222.
47. Burton, A.C. (1935). Human calorimetry: II. The average temperature of the tissues of the body: three figures. *J. Nutr.* 9, 261–280.
48. Castelletto, M.L., Gang, S.S., Okubo, R.P., Tselikova, A.A., Nolan, T.J., Platzer, E.G., Lok, J.B., and Hallem, E.A. (2014). Diverse host-seeking behaviors of skin-penetrating nematodes. *PLoS Pathog.* 10, e1004305.
49. Haas, W. (2003). Parasitic worms: strategies of host finding, recognition and invasion. *Zoology (Jena)* 106, 349–364.
50. Bennett, N.C., Jarvis, J.U.M., and Davies, K.C. (1988). Daily and seasonal temperatures in the burrows of African rodent moles. *S. Afr. J. Zool.* 23, 189–195.
51. Robinson, A.F. (1994). Movement of five nematode species through sand subjected to natural temperature gradient fluctuations. *J. Nematol.* 26, 46–58.
52. Ruiz, F., Castelletto, M.L., Gang, S.S., and Hallem, E.A. (2017). Experience-dependent olfactory behaviors of the parasitic nematode *Heligmosomoides polygyrus*. *PLoS Pathog.* 13, e1006709.
53. Lee, J.H., Dillman, A.R., and Hallem, E.A. (2016). Temperature-dependent changes in the host-seeking behaviors of parasitic nematodes. *BMC Biol.* 14, 36.
54. Monroy, F.G., and Enriquez, F.J. (1992). *Heligmosomoides polygyrus*: a model for chronic gastrointestinal helminthiasis. *Parasitol. Today (Regul.)* 8, 49–54.
55. Hernandez, A.D., and Sukhdeo, M.V.K. (1995). Host grooming and the transmission strategy of *Heligmosomoides polygyrus*. *J. Parasitol.* 81, 865–869.
56. Koga, M., Nuamtanong, S., Dekumyoy, P., Yoonuan, T., Maipanich, W., Rojekkittikhun, W., and Waikagul, J. (2005). Host-finding behavior of *Strongyloides stercoralis* infective larvae to sodium cation, human serum, and sweat. *Southeast Asian J. Trop. Med. Public Health* 36 (Suppl 4), 93–98.
57. Safer, D., Brenes, M., Dunipace, S., and Schad, G. (2007). Urocanic acid is a major chemoattractant for the skin-penetrating parasitic nematode *Strongyloides stercoralis*. *Proc. Natl. Acad. Sci. USA* 104, 1627–1630.

58. McMeniman, C.J., Corfas, R.A., Matthews, B.J., Ritchie, S.A., and Vosshall, L.B. (2014). Multimodal integration of carbon dioxide and other sensory cues drives mosquito attraction to humans. *Cell* 156, 1060–1071.
59. Aoki, I., and Mori, I. (2015). Molecular biology of thermosensory transduction in *C. elegans*. *Curr. Opin. Neurobiol.* 34, 117–124.
60. Glauser, D.A., and Goodman, M.B. (2016). Molecules empowering animals to sense and respond to temperature in changing environments. *Curr. Opin. Neurobiol.* 41, 92–98.
61. Bargmann, C.I. (2006). Chemosensation in *C. elegans* (WormBook), pp. 1–29.
62. Lok, J.B. (2007). *Strongyloides stercoralis*: a model for translational research on parasitic nematode biology (WormBook), pp. 1–18.
63. Lok, J.B., Shao, H., Massey, H.C., and Li, X. (2017). Transgenesis in *Strongyloides* and related parasitic nematodes: historical perspectives, current functional genomic applications and progress towards gene disruption and editing. *Parasitology* 144, 327–342.
64. Ward, J.D. (2015). Rendering the intractable more tractable: tools from *Caenorhabditis elegans* ripe for import into parasitic nematodes. *Genetics* 201, 1279–1294.
65. Gang, S.S., Castelletto, M.L., Bryant, A.S., Yang, E., Mancuso, N., Lopez, J.B., Pellegrini, M., and Hallem, E.A. (2017). Targeted mutagenesis in a human-parasitic nematode. *PLoS Pathog.* 13, e1006675.
66. Hunt, V.L., Tsai, I.J., Coghlan, A., Reid, A.J., Holroyd, N., Foth, B.J., Tracey, A., Cotton, J.A., Stanley, E.J., Beasley, H., et al. (2016). The genomic basis of parasitism in the *Strongyloides* clade of nematodes. *Nat. Genet.* 48, 299–307.
67. Howe, K.L., Bolt, B.J., Cain, S., Chan, J., Chen, W.J., Davis, P., Done, J., Down, T., Gao, S., Grove, C., et al. (2016). WormBase 2016: expanding to enable helminth genomic research. *Nucleic Acids Res.* 44 (D1), D774–D780.
68. Junio, A.B., Li, X., Massey, H.C., Jr., Nolan, T.J., Todd Lamitina, S., Sundaram, M.V., and Lok, J.B. (2008). *Strongyloides stercoralis*: cell- and tissue-specific transgene expression and co-transformation with vector constructs incorporating a common multifunctional 3' UTR. *Exp. Parasitol.* 118, 253–265.
69. Diawara, A., Schwenkenbecher, J.M., Kaplan, R.M., and Prichard, R.K. (2013). Molecular and biological diagnostic tests for monitoring benzimidazole resistance in human soil-transmitted helminths. *Am. J. Trop. Med. Hyg.* 88, 1052–1061.
70. Keiser, J., and Utzinger, J. (2008). Efficacy of current drugs against soil-transmitted helminth infections: systematic review and meta-analysis. *JAMA* 299, 1937–1948.
71. Kumar, N., Rao, T.K., Varghese, A., and Rathor, V.S. (2013). Internal parasite management in grazing livestock. *J. Parasit. Dis.* 37, 151–157.
72. Roeber, F., Jex, A.R., and Gasser, R.B. (2013). Impact of gastrointestinal parasitic nematodes of sheep, and the role of advanced molecular tools for exploring epidemiology and drug resistance - an Australian perspective. *Parasit. Vectors* 6, 153.
73. Felippelli, G., Lopes, W.D., Cruz, B.C., Teixeira, W.F., Maciel, W.G., Fávero, F.C., Buzzulini, C., Sakamoto, C., Soares, V.E., Gomes, L.V., et al. (2014). Nematode resistance to ivermectin (630 and 700µg/kg) in cattle from the Southeast and South of Brazil. *Parasitol. Int.* 63, 835–840.
74. Rund, S.S., O'Donnell, A.J., Gentile, J.E., and Reece, S.E. (2016). Daily rhythms in mosquitoes and their consequences for malaria transmission. *Insects* 7, E14.
75. Schindelin, J., Arganda-Carreras, I., Frise, E., Kaynig, V., Longair, M., Pietzsch, T., Preibisch, S., Rueden, C., Saalfeld, S., Schmid, B., et al. (2012). Fiji: an open-source platform for biological-image analysis. *Nat. Methods* 9, 676–682.
76. Kearse, M., Moir, R., Wilson, A., Stones-Havas, S., Cheung, M., Sturrock, S., Buxton, S., Cooper, A., Markowitz, S., Duran, C., et al. (2012). Geneious Basic: an integrated and extendable desktop software platform for the organization and analysis of sequence data. *Bioinformatics* 28, 1647–1649.
77. Hammer, Ø., Harper, D.A.T., and Ryan, P.D. (2001). PAST: Paleontological statistics software package for education and data analysis. *Palaeontol. Electronica* 4, 4.
78. Stiernagle, T. (2006). Maintenance of *C. elegans* (WormBook), pp. 1–11.
79. Hawdon, J.M., and Schad, G.A. (1991). Long-term storage of hookworm infective larvae in buffered saline solution maintains larval responsiveness to host signals. *J. Helm. Soc. Wash.* 58, 140–142.
80. White, G.F. (1927). A method for obtaining infective nematode larvae from cultures. *Science* 66, 302–303.
81. Karp, X. (2016). Working with dauer larvae (WormBook), pp. 1–19.

STAR★METHODS

KEY RESOURCES TABLE

REAGENT or RESOURCE	SOURCE	IDENTIFIER
Bacterial and Virus Strains		
<i>Escherichia coli</i> : Strain OP50	Caenorhabditis Genetics Center	OP50
Experimental Models: Organisms/Strains		
<i>Caenorhabditis elegans</i> : Strain CB48558	Caenorhabditis Genetics Center	<i>C. elegans</i> California wild isolate
<i>Strongyloides stercoralis</i> : UPD Strain	Dr. James Lok	<i>S. stercoralis</i>
<i>Ancylostoma ceylanicum</i> : Indian Strain	US National Parasite Collection Number 102954, courtesy of Dr. John Hawdon	<i>A. ceylanicum</i>
<i>Strongyloides ratti</i> : ED321 strain	Dr. James Lok	<i>S. ratti</i>
<i>Nippostrongylus brasiliensis</i>	Dr. Edward Platzler	<i>N. brasiliensis</i>
<i>Heligmosomoides polygyrus</i>	Dr. Raffi Aroian	<i>H. polygyrus</i>
<i>Steinernema carpocapsae</i> : ALL strain	[53]	<i>S. carpocapsae</i>
<i>Meriones unguiculatus</i> : Mongolian	Charles River Laboratories	Gerbils
<i>Mesocricetus auratus</i> : Syrian Golden	Envigo	Hamsters
<i>Rattus norvegicus</i> : Sprague Dawley	Envigo	Rats
<i>Rattus norvegicus</i> : Long Evans	Envigo	Rats
<i>Mus musculus</i> : C57BL/6	UCLA Division of Laboratory Animal Medicine Breeding Colony; Jackson Labs	Mice
<i>Galleria mellonella</i> larvae	Petco; American Cricket Ranch	Waxworms
Chemicals, Peptides, and Recombinant Proteins		
Charcoal granules (bone char)	Ebonex Corp.	Cat #EBO58BC.04
Oligonucleotides		
GTAACATTGACTTGATGGGTGG	[65]	<i>Ss-tax-4</i> CRISPR target sequence
See Table S1 for primer sequences.	N/A	N/A
Recombinant DNA		
<i>Sr-eef-1A_{pro}::Cas9::Ss-era-1</i> 3'UTR	Dr. James Lok [65]	pPV540; <i>Strongyloides</i> codon-optimized Cas9
<i>Sr-U6_{pro}::Ss-tax-4-sgRNA-1::Sr-U6</i> 3'UTR	[65]	pMLC47; sgRNA for <i>Ss-tax-4</i>
5'HA:: <i>Ss-act-2_{pro}::mRFPmars::Ss-era-1</i> 3'UTR::3'HA	This paper	pEY11; HDR construct for <i>Ss-tax-4</i>
<i>Sr-tax-4_{pro}::GFP::Ss-era-1</i> 3'UTR	This paper	pMC41
Software and Algorithms		
GraphPad Prism 6	GraphPad	http://www.graphpad.com
Zeiss AxioVision 4.8	Carl Zeiss	https://www.zeiss.com/microscopy/us/products/microscope-software/axiovision.html
Fiji	[75]	https://fiji.sc/
Geneious 9	[76]	https://www.geneious.com
PAST 3.19	[77]	https://folk.uio.no/ohammer/past/
MATLAB R2107B	MathWorks	https://www.mathworks.com/products/matlab.html
Mightex Cam Demo v1.2.1	Mightex Systems	http://www.mightexsystems.com/
FTC100D TEC controller	Accuthermo Technology	http://www.accuthermo.com/
Other		
3% thermotaxis agar (17 g agar, 3 g NaCl, 1 mL 1M CaCl ₂ , 1 mL 1M MgSO ₄ , 25 mL 1M KH ₂ PO ₄ pH 6.0, dH ₂ O to 1 L)	[45]	Thermotaxis agar
M9 solution (3 g KH ₂ PO ₄ , 6 g Na ₂ HPO ₄ , 5 g NaCl, 1 mL 1 M MgSO ₄ , dH ₂ O to 1 L)	[78]	M9 solution

(Continued on next page)

Continued

REAGENT or RESOURCE	SOURCE	IDENTIFIER
BU saline (7.10 g Na ₂ HPO ₄ , 2.99 g KH ₂ PO ₄ , 4.09 g NaCl, dH ₂ O to 1 L)	[79]	BU saline
2% NGM plates (3 g NaCl, 2.5 g Bacto Peptone, 20 g agar, 1 mL 5mg/mL cholesterol, 1 mL 1M CaCl ₂ , 1 mL 1M MgSO ₄ , 25 mL 1M KPO ₄ pH 6.0, dH ₂ O to 1 L)	[78]	2% NGM plates
USB-DAQ device	LabJack Corp	U3-LV
Isotemp Refrigerated/Heated Water Bath	Fisher Scientific	13-874-126
Commercial water block	Swiftech	MCW820
5-megapixel CMOS camera	Mightex Systems	BTE-B050-U
Zoom lenses	Kowa America Corp	LMZ69M
H-bridge amplifier	Accuthermo Technology	FTX300
TEC temperature controller	Accuthermo Technology	FTC100D
Peltier element	Multicomp	MCTE1-19913L-S
22x22 cm Bioassay dishes	Corning	431301
Wacom Intuos Art touch tablet and stylus	Wacom	CTH-690AK

CONTACT FOR REAGENT AND RESOURCE SHARING

Further information and requests for resources and reagents should be directed to and will be fulfilled by the Lead Contact, Dr. Elissa Hallem (ehallem@ucla.edu).

EXPERIMENTAL MODEL AND SUBJECT DETAILS

All protocols and procedures involving vertebrate animals were approved by the UCLA Office of Animal Research Oversight (Protocol 2011-060-22), which adheres to the standards of the AAALAC and the *Guide for the Care and Use of Laboratory Animals*.

Maintenance of *Strongyloides stercoralis*

S. stercoralis (UPD strain) was generously provided by Dr. James Lok (University of Pennsylvania). *S. stercoralis* was serially passaged through male and female Mongolian gerbils (Charles River Laboratories) and maintained on fecal-charcoal plates as previously described [48]. Gerbils were inoculated via subcutaneous injections with ~2,250 iL3s in 200 μ L of sterile PBS, under isoflurane anesthesia. To harvest fecal pellets, gerbils were housed overnight in cages with wire floors. The following morning, fecal pellets were recovered from damp cardboard below the wire floor. Feces containing *S. stercoralis* were collected for 14-45 days post-inoculation. Fecal-charcoal plates were made by mixing feces, dH₂O, and autoclaved charcoal granules (bone char from Ebonex Corp., Cat #EBO58BC.04). The mixture was poured into 10-cm-diameter Petri dishes lined with wet 10-cm-diameter Whatman filter paper. In some cases, fecal-charcoal plates were stored for ~2 days at 25°C; otherwise plates were stored for 2 days at 20°C. For micro-injection, free-living males and females were collected via a Baermann apparatus [62] from plates stored at 25°C for 1 day or plates stored at 20°C for 2 days. After 2 days, all remaining plates were moved to a 23°C incubator until use in thermotaxis assays. For thermotaxis assays, female iL3s were retrieved from 7-14 day old fecal-charcoal plates via a Baermann apparatus. *S. stercoralis* iL3s are exclusively female. Prior to testing, iL3s were stored in BU saline [79] or water for no more than 8 hours.

Maintenance of *Ancylostoma ceylanicum*

A. ceylanicum (Indian strain, US National Parasite Collection Number 102954) was generously provided by Dr. John Hawdon (George Washington University). *A. ceylanicum* was serially passaged through male Syrian golden hamsters (Envigo) and maintained on fecal-charcoal plates in a 23°C incubator as previously described [52]. Hamsters were inoculated with 70-100 iL3s in 100 μ L sterile water via oral gavage. Feces containing *A. ceylanicum* were collected as described above for 14-44 days post-inoculation. Fecal-charcoal plates were made as described above and stored at 23°C until use. For thermotaxis assays, male and female *A. ceylanicum* iL3s were retrieved from 7-18 day old fecal-charcoal plates via a Baermann apparatus [62]. Prior to testing, iL3s were stored in water for no more than 8 hours.

Maintenance of *Strongyloides ratti*

S. ratti (ED321 strain) was generously provided by Dr. James Lok (University of Pennsylvania). *S. ratti* was serially passaged through female Sprague Dawley rats (Envigo) and maintained on fecal-charcoal plates in a 23°C incubator as previously described [48]. Rats were inoculated with 800 iL3s in 300 μ L sterile PBS via subcutaneous injection. Feces containing *S. ratti* were collected as described

above for 7-23 days post-inoculation. Fecal-charcoal plates were made as described above and stored at 23°C until use. For thermotaxis assays, female *S. ratti* iL3s were retrieved from 7-14 day old fecal-charcoal plates via a Baermann apparatus [62]. *S. ratti* iL3s are exclusively female. Prior to testing, iL3s were stored in water for no more than 8 hours.

Maintenance of *Nippostrongylus brasiliensis*

N. brasiliensis was generously provided by Dr. Edward Platzer (University of California, Riverside). *N. brasiliensis* was serially passaged through female Long Evans rats (Envigo) and maintained on fecal-charcoal plates in a 23°C incubator, as previously described [48]. Rats were inoculated with ~4,000 iL3s in 300 µL sterile PBS via subcutaneous injection. Feces containing *N. brasiliensis* were collected as described above for 6-9 days post-inoculation. Fecal-charcoal plates were made as above and stored at 23°C until use. For thermotaxis assays, male and female *N. brasiliensis* iL3s were retrieved from 7-14 day old fecal-charcoal plates via a Baermann apparatus [62]. Prior to testing, iL3s were stored in water for no more than 8 hours.

Maintenance of *Heligmosomoides polygyrus*

H. polygyrus was generously provided by Dr. Raffi Aroian (University of Massachusetts Medical School). *H. polygyrus* was serially passaged in male and female C57BL/6 mice (UCLA Division of Laboratory Animal Medicine Breeding Colony or Jackson Labs) and maintained on fecal-charcoal plates at room temperature, as previously described [52]. Mice were inoculated with 100-150 iL3s in 100 µL sterile water via oral gavage. Feces containing *H. polygyrus* were collected as described above for 10-65 days post-inoculation. Fecal-charcoal plates were made as described above and stored at room temperature (21-23°C) until use. For thermotaxis assays, male and female *H. polygyrus* iL3s were retrieved from 7-14 day old fecal-charcoal plates via a Baermann apparatus [62]. Prior to testing, iL3s were stored in water for no more than 8 hours.

Maintenance of *Steinernema carpocapsae*

S. carpocapsae (ALL strain) was maintained via passage through waxworms, as previously described [53]. 3-6 last instar *Galleria mellonella* larvae were placed in a 5-cm Petri dish lined with 55-mm Whatman 1 filter paper. Approximately 250 µL of dH₂O containing 1000-2000 infective juveniles (IJs) was placed directly on the waxworms and on the filter paper. At 9 days post-exposure, infected waxworms were placed in White traps [80]; male and female IJs were collected from the White traps after 3-5 days. IJs were suspended in 10 mL ddH₂O in 50 mL tissue culture flasks and used for thermotaxis assays and to start new infections. Infection and storage of IJs was at room temperature. For thermotaxis assays, male and female IJs were used within 7 days of collection from White traps.

Maintenance of *C. elegans*

The California (CB4858) strain of *C. elegans* was used exclusively for this study. Experiments were carried out on young adult hermaphrodites and dauer larvae. To match cultivation conditions between *C. elegans* and the parasitic nematodes, *C. elegans* were maintained in the same 23°C incubator as the parasitic nematodes. Adults were raised on 2% Nematode Growth Media (NGM) plates containing a thin lawn of *Escherichia coli* OP50 bacteria, as per standard methods [78]. Adults were collected by washing them off of plates and into M9 solution [78] immediately prior to the assay. Suspended worms were collected in a watch glass; excess OP50 was rinsed off and worms were allowed to gravity settle. Dauers were generated from starved cultures [81]. In brief, ~5 L4 larvae or young adults were transferred to a fresh 2% NGM plate containing OP50. After approximately 10 days, dauers were collected from water droplets placed on the lid. Dauer formation plates were stored in the 23°C incubator, which significantly improved the rate of dauer formation. Dauer morphology was visually confirmed prior to thermotaxis experiments, and dauers were used for experiments within 7 days of their appearance on a plate.

METHOD DETAILS

Thermotaxis assays

Thermotaxis assays were performed using a large-format linear thermal stage adapted from those previously described [45]. A thermal gradient was established across an anodized aluminum slab (24 x 12 x 1/4 inch) that stands on two aluminum reservoir blocks (4 x 12 x 1.5 inch). Each reservoir block is attached to two 200-W thermoelectric heating/cooling devices (TECs, MCTE1-19913L-S, Multi-comp), which transfer heat/cold between the reservoir block and commercial water blocks (MCW820, Swiftech) attached to a temperature-controlled recirculating antifreeze coolant bath (5150 R28, Fisher Scientific). The outputs of the “hot” and “cold” side thermoelectric devices are controlled by independent closed-loop circuits that each include: a thermistor attached to the aluminum slab near the “hot” or “cold” edge of the gradient (#6568T46, McMaster Carr), a PID controller (FTC100D, AccuThermo Technology) and H-bridge amplifier (FTX300, AccuThermo Technology), and a 12V switching power supply (S-320-12, Oven Industries). The temperature range is set using FTC100D software (AccuThermo Technology). A square plastic dish (22 x 22 cm, Corning Bioassay Dishes, Fisher Scientific) filled with 3% thermotaxis agar solution (3% w/v agar, 51.37 mM NaCl; 1 mM CaCl₂; 1 mM MgSO₄; and 5 mM KPO₄) [45] was placed in the center of the aluminum slab, with glycerol between the dish and the aluminum surface to ensure strong thermal transfer. The size of the agar surface available for worm migration was empirically measured at ~22.5 x 22.5 cm; this value was used to calculate gradient steepness. Surrounding the agar plate, an array of red LED strips provided

dark-field illumination. Isothermal assays were performed using the same setup, except that a thermal gradient was not applied. For isothermal room temperature (RT) assays, “room temperature” was between 21°C and 23°C. For all isothermal assays, the surface temperature of individual isothermal plates varied by less than 1°C and any temperature variations were not directional.

Prior to the start of an experiment, the temperature range on the agar surface was manually confirmed using a laser thermometer. Worms were deposited on the agar surface in ~3 µL of BU saline (for *S. stercoralis*) [79], M9 solution (for *C. elegans*) [78], or dH₂O (for all other species). Worm movements were monitored using two 5 mega-pixel CMOS cameras (BTE-B050-U, Mightex Systems) equipped with zoom lenses (LMZ69M, Kowa). Each camera records approximately half of the 22-cm-long thermal plate. Image acquisition was triggered using a custom MATLAB script (MathWorks) that generated precisely timed TTL pulses via a USB DAQ device (U3-LV, LabJack Corp). The TTL pulses were passed to both cameras, which in turn sent acquired images to image acquisition software (see below).

Behavioral effects of cultivation temperature

For testing the effect of long-term cultivation temperature changes in iL3 behavior, 7-day-old fecal-charcoal plates were stored for an additional 7 days at either 15°C or 23°C. iL3s were collected using a Baermann apparatus [62] and stored in a watch glass containing BU saline [79] or dH₂O at their cultivation temperature. For testing the effect of short-term cultivation temperature changes, *S. stercoralis* iL3s were collected and placed in a watch glass containing BU saline [79]. Some worms were used immediately to generate the zero time point. The remaining worms were divided into two watch glasses; one watch glass was placed in an incubator set to 23°C, the other was placed in an incubator set to 15°C or 37°C. After 2 hours, iL3s were assayed using the thermotaxis setup described above.

Thermotaxis assay data analysis

The population-level movement of worms in a thermal gradient was calculated using Fiji [75]. Images corresponding to the desired experimental time point were divided into 1°C bins using the Grid command, and the number of worms in each bin was tallied using the Cell Counter plug-in. A Wacom tablet and stylus (CTH-690AK, Wacom Intuos Art) were used to aid the quantification of worm location. The percent of heat-seeking worms was calculated in Excel as the sum of worms found in temperature bins above T_{start} divided by the total number of worms. The percent of cold-seeking worms was calculated as the sum of worms found in temperatures below T_{start} divided by the total number of worms. The percent of “non-responding” worms was calculated as the number of worms that did not leave the 1°C T_{start} bin divided by the total number of worms.

For tracking individual iL3 trajectories, either single or a small group (< 100) of iL3s were placed on a thermotaxis plate and their migration imaged for 10-15 minutes at a rate of 0.5 frames/second. Worm locations were measured *post hoc* using the Manual Tracking plugin for Fiji. Custom MATLAB scripts (available upon request) were used to translate pixel-based x/y coordinates into cm- and temperature-based coordinates, which were then plotted. These scripts also calculated: overall mean speed, mean speed within specified temperature bins, distance ratio (maximum distance traveled divided by the maximum displacement), and final temperature difference (final temperature minus starting temperature).

Multisensory assays

For measuring the effect of a host odorant on the migration of individual iL3s, in both thermal gradients and isothermal conditions, 5 µL undiluted 3-methyl-1-butanol was placed on the thermotaxis plate immediately prior to placement of iL3s. The effect of 3m1b was quantified by counting the number of iL3s that entered a 2-cm-diameter scoring region surrounding the odorant droplet. Only iL3s that entered the scoring region within the first 5 minutes of the assay were counted. Control (–3m1b) values were generated by counting the number of iL3s that entered a similarly positioned scoring region on a plate without odorant.

Generation of the *Strongyloides tax-4p::GFP* reporter construct

The *S. ratti tax-4* gene (SRAE_2000234000) was identified based on sequence homology with *C. elegans tax-4* and was predicted in WormBase Parasite as an ortholog of *Ce-tax-4* [66, 67]. To generate the *Sr-tax-4p::GFP* construct, ~2,100 base pairs of the *Sr-tax-4* promoter upstream of the predicted *Sr-tax-4* ATG was PCR-amplified and cloned into the *Strongyloides* expression vector pPV254 (containing *Ss-act-2p::GFP*; a gift from Dr. James Lok) in place of the *Ss-act-2* promoter. Primer sequences are listed in Table S1. To generate *Sr-tax-4p::GFP*-expressing transgenics, the plasmid encoding *Sr-tax-4p::GFP* (pMC41) was microinjected at 50 ng/µL.

CRISPR-Cas9-mediated targeted mutagenesis of *Ss-tax-4*

The *S. stercoralis tax-4* gene (SSTP_0000981000) was previously targeted for CRISPR-Cas9-mediated mutagenesis [65]; we utilized the same CRISPR target site in this study. In brief, the *Ss-tax-4* gene was identified based on sequence homology with *C. elegans tax-4* and was also predicted in WormBase Parasite as an ortholog of *Ce-tax-4* [65–67]. The CRISPR target site was identified using the Find CRISPR Site plugin for the Geneious 9 software [76]. Gene-structure diagrams for *S. stercoralis* and *C. elegans* were generated with Exon-Intron Graphic Maker (Version 4, <http://www.wormweb.org>). The single guide RNA (sgRNA) expression vector for targeting *Ss-tax-4* (pMC47) was synthesized by GENEWIZ and included 500- and 277-bp regions of the *S. ratti* U6 promoter and 3' UTR, respectively. The target sequence for *Ss-tax-4* is listed in the Key Resources Table. To generate the repair template

(pEY11), 539-bp 5' and 671-bp 3' homology arms flanking *Ss-tax-4* site #1 were cloned into the *Ss-act-2p::mRFPmars* expression vector pAJ50 (a gift from Dr. James Lok). The *Ss-act-2* gene encodes actin; the *Ss-act-2* promoter drives expression of mRFPmars in body-wall muscle [68]. pEY11 was modified from pEY09 [65] to maximize targeting efficiency and improve homology-directed repair at *Ss-tax-4*.

Primer sequences are listed in the [Key Resources Table](#) and [Table S1](#). Injection mixes contained 60 ng/μL pMC47, 20 ng/μL pEY11, and 20 ng/μL pPV540 (*Strongyloides*-codon-optimized Cas9 driven by the *S. ratti eef-1A* promoter; a gift from Dr. James Lok). For generating no-Cas9 controls, injection mixes contained only 60 ng/μL pMC47 and 20 ng/μL pEY11. Plasmid vectors were diluted to the desired concentration in ddH₂O and filtered using a bench-top centrifuge and a 0.22-μm tube filter (Costar Spin-X, Cat #8106).

Microinjection of *S. stercoralis* free-living adults

Plasmid vectors were injected into the syncytial gonad of *S. stercoralis* free-living adult females as previously described [65, 68]. For CRISPR-Cas9-mediated mutagenesis, a repair template containing *Ss-act-2p::mRFPmars* was included to enable selection of transgenic F₁ progeny, as described above. In addition, the *Ss-tax-4* iL3s tested were generated from multiple injection runs. For all microinjection experiments, microinjected females were placed with wild-type adult males on fecal-charcoal plates containing uninfected gerbil feces for a minimum of 6 days prior to testing.

Selection of F₁ *Ss-tax-4* iL3s

F₁ iL3 progeny of microinjected females were recovered using a Baermann apparatus [62], washed three times in dH₂O, and then collected in BU saline [79]. ~15 μL of F₁ iL3-containing BU saline was placed on an OP50-seeded 2% NGM plate and screened for *mRFPmars* expression using a Leica M165 FC microscope. A previous study found that near-uniform *mRFPmars* expression in the body wall is predictive of successful homology-directed repair [65]. In contrast, sparse *mRFPmars* expression correlates with extrachromosomal-array-mediated expression. Thus, only iL3s displaying near-uniform *mRFPmars* expression were picked into a small watch glass containing BU saline; a percentage of these worms were expected to show either deletions or integration of the repair template at the target region [65]. *mRFPmars*-expressing iL3s were tested in thermotaxis assays within 8 hours of screening.

Ss-tax-4 thermotaxis assays

Single *mRFPmars*-expressing *S. stercoralis* iL3s were placed at 30°C in a 20–34°C thermal gradient and allowed to navigate for up to 15 minutes. Worm movements were imaged at 0.5 frames/second using the image acquisition setup described above. Image acquisition lasted for 15 minutes, until the iL3 reached the edge of the gradient, or until it left the cameras' fields of view, whichever came first. Following the cessation of recording, single iL3s were recollected for individual genomic DNA preparations. Individual iL3 trajectories were tracked as described above. Thus, all behavioral assays were performed by a researcher blind to the iL3 genotype.

Genotyping for *Ss-tax-4* gene disruptions

mRFPmars-positive iL3s in which *Ss-tax-4* expression was fully disrupted either by deletion or integration events (hereafter called *Ss-tax-4* iL3s) were identified by *post hoc* single-worm genotyping, as previously described [65]. After completion of thermotaxis assays, iL3s were transferred from thermotaxis plates into PCR tubes containing 5 μL of nematode lysis buffer (50 mM KCl, 10 mM Tris pH 8, 2.5 mM MgCl₂, 0.45% Nonidet-P40, 0.45% Tween-20, 0.01% gelatin in ddH₂O, ~0.12 μg/μL Proteinase-K, and ~1.7% 2-mercaptoethanol). Tubes were placed at –80°C for a minimum of 20 minutes, then digested in a thermocycler (65°C (2 h), 95°C (15 min), 10°C (hold)). Digested single-iL3 DNA samples were stored at –20°C until use, for no more than 12 hours. Single DNA preparations were divided between four PCR reactions: a control reaction that amplified part of the endogenous *Ss-act-2* gene, a reaction that amplified only wild-type *Ss-tax-4*, and reactions for 5' and 3' integration of repair template pEY11 into the *Ss-tax-4* targeting site. Primer sequences are listed in the [Key Resources Table](#). All PCR reactions were performed with GoTaq G2 Flexi DNA Polymerase (Promega, Cat #M7801) using the following thermocycler conditions: denature 95°C (2 min); PCR 95°C (30 s), 55°C (30 s), 72°C (2 min) x 35 cycles; final extension 72°C (5 min); 10°C (hold). PCR products were resolved on ~1% agarose gels treated with GelRed (Biotium, Cat #41003) using a 1-kb ladder (NEB, Cat #N3232L). For all samples, 30 μL of PCR product were loaded on the gel, and all samples from a single iL3 were run on the same gel. The strength of the *Ss-tax-4* wild-type band in *Ss-tax-4* worms was calculated relative to that of a wild-type iL3. Quantification was performed using a ChemiDoc MP Imaging System. Worms were categorized as *Ss-tax-4* if the Image Lab Version 5.1 Relative Quantity Tool failed to detect a wild-type *Ss-tax-4* amplification band. Some *Ss-tax-4* iL3s had either 5' or 3' integration bands, reflecting integration of pEY11; other iL3s lacked wild-type and integration bands, likely indicating a large deletion at the *Ss-tax-4* target site, as previously observed [65].

Fluorescent microscopy

Images of animals expressing *Ss-tax-4::GFP* were acquired as previously described [65]. F₁ L2 or L3 larvae on a 2% NGM plate with OP50 were screened for GFP expression using a Leica M165 FC microscope. L2 or L3 larvae expressing GFP were exposed to 10 mM levamisole in BU saline [79], and then mounted on a slide with 5% Noble agar dissolved in ddH₂O. Epifluorescence and

DIC images were taken using a Zeiss AxioImager A2 microscope with an attached Zeiss AxioCam camera. Images were processed using the Zeiss AxioVision software. Image montages were generated using Fiji [75].

QUANTIFICATION AND STATISTICAL ANALYSIS

Statistical analyses and power analyses to determine appropriate sample sizes were conducted using GraphPad Prism 6. When one-way and two-way ANOVAs are utilized, we report multiplicity-adjusted p values. K-means clustering was performed using PAST 3.19 [77].

Chapter 6

Molecular mechanisms for olfactory-driven host seeking and in-host development in skin-penetrating nematodes

Introduction

Skin-penetrating parasitic nematodes including threadworms of the *Strongyloides* genus and hookworms of the *Necator* and *Ancylostoma* genera are gastrointestinal human parasites that infect hundreds of millions of people in tropical and sub-tropical regions around the world [1,2]. These infections can lead to chronic gastrointestinal distress, anemia, stunted growth and cognitive impairment in children, and in the case of *Strongyloides stercoralis*, occasionally death in immunocompromised individuals [3,4]. While effective anthelmintic treatments for parasitic nematodes have been in use since the 1960's, they have not eliminated disease burden, in part due to high re-infection rates and inadequate drug distribution in low-resource settings [2,5,6]. Furthermore, mass administration of anthelmintics comes with the risk of resistance mechanisms emerging in some human-infective nematode populations, as has been observed in livestock-parasitic nematodes [1,7].

One attractive complementary strategy for reducing the disease burden caused by skin-penetrating nematodes is to interfere with their ability to target and infect human hosts. Skin-penetrating nematodes live in the environment as developmentally arrested third-stage larvae (iL3s). iL3s must navigate through the soil to find a host, cross the host's skin barrier, and traverse through multiple host tissues to eventually establish an infection in the intestinal tract (Fig. 1) [8]. Thus, blocking the ability of iL3s to execute any of these steps could serve as an effective way to decrease infection rates. iL3s are only able to infect a narrow range of host species [9-13]. Given the limited host range for each skin-penetrating nematode species, it has been speculated that iL3s might use sensory mechanisms to discriminate a permissive host from other non-host mammals [14]. Supporting this hypothesis, we and others have demonstrated that iL3s of many parasitic nematode species engage in host-seeking behaviors in the presence of host-emitted thermosensory, olfactory, and gustatory cues, suggesting a critical role for chemosensation in directing iL3s toward hosts in the environment [8,15-17]. Similarly, sensory function has also been implicated in allowing iL3s to resume of development upon entering the host for both skin-penetrating *Ancylostoma* and *Strongyloides* species [18-21]. However, the molecular mechanisms underlying these critical sensory-driven behaviors

have been largely unexplored. As a result, our ability to develop new measures to prevent harmful nematode infections had remained limited.

Here, we provide the first molecular-level evidence that skin-penetrating iL3s require functional chemosensory pathways to both engage in host-seeking behaviors and initiate development after entering the host. We used human-infective *S. stercoralis* as a genetically tractable model for investigating the mechanisms underlying these important sensory-driven parasitic behaviors [22-24]. First, to identify host-emitted odorant cues that might be important for *S. stercoralis* iL3s to find human hosts, we undertook a broad comparative chemotaxis study to investigate how *S. stercoralis*' olfactory preferences change between environmentally-dwelling free-living adult and iL3 life stages. We found that many host-emitted skin, sweat, and fecal odorants were attractive for free-living adults. However, only a limited number of odorants abundant in skin and sweat were also attractive for iL3s, suggesting that the responses to these select odorants may be retained at the iL3 life stage for host seeking purposes. To investigate the molecular mechanisms underlying olfactory-driven host seeking, we focused on exploring how *S. stercoralis* iL3s respond to 3-methyl-1-butanol (hereafter 3m1b). 3m1b was identified as an attractive odorant for *S. stercoralis* iL3s in our chemotaxis panel and is commonly found in mammalian skin, sweat, and is produced by skin microbiota [17,25-28]. We found that individual wild-type *S. stercoralis* iL3s navigate toward 3m1b. However, iL3s with CRISPR-Cas9-mediated disruption of the cyclic nucleotide-gated channel subunit *tax-4* were unable to chemotaxis toward 3m1b, suggesting that interfering with chemosensory mechanisms may be a useful strategy for inhibiting host-seeking behavior [24]. Finally, we examined if sensory cues that are important for iL3s to navigate in the environment are also important for initiating development following skin penetration. We found that mammalian body temperatures of 37°C, and elevated CO₂ concentrations, are essential sensory cues for iL3s to initiate feeding behavior inside the host [21]. Similar to our observations for olfactory-driven host seeking, *S. stercoralis tax-4* knockout iL3s were unable to initiate development in host-like culture conditions. Together, these results suggest that

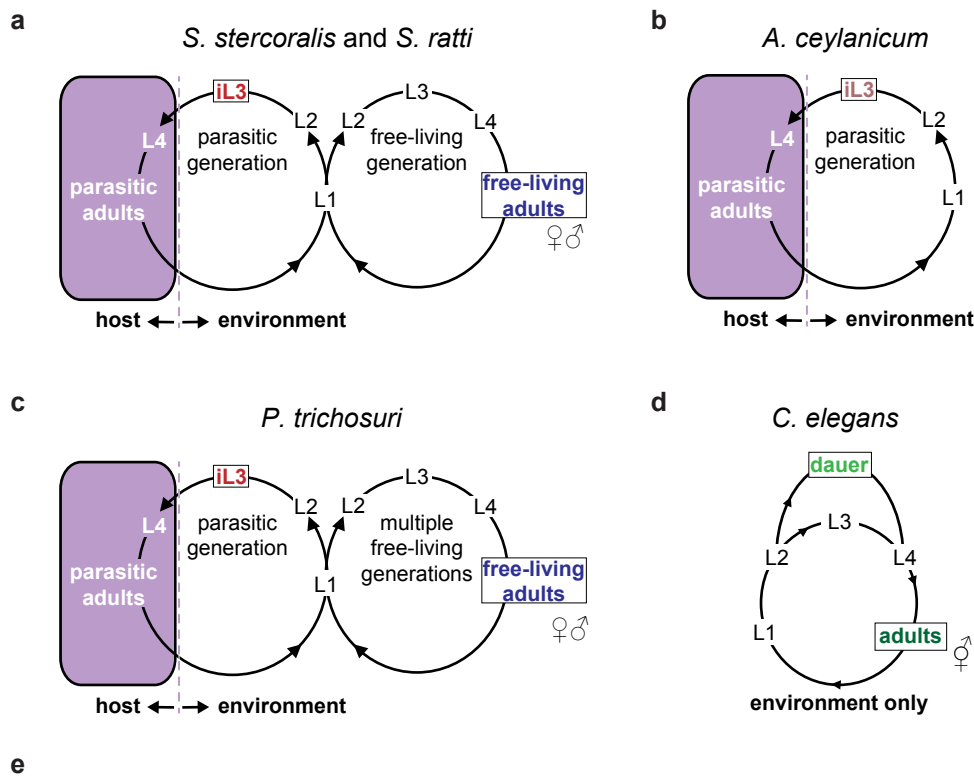
disrupting chemosensory mechanisms in iL3s may be novel strategy for controlling human-parasitic nematode infections.

Results

Olfactory preferences reflect species-and-life-stage specific ecological requirements

All skin-penetrating nematode species develop into iL3s that must eventually find and infect a mammalian host to survive. However, different skin-penetrating species have unique developmental trajectories in the environment. For example, *S. stercoralis* nematodes are excreted in host feces as young larvae. These larvae can either develop directly into iL3s or can undergo one free-living generation outside the host (Fig. 1a) [22]. By contrast, hookworm species such as *A. ceylanicum* lack a free-living generation in the environment; larvae can only develop into iL3s that must infect a host to continue the life cycle (Fig. 1b). Which chemosensory cues are important for iL3s of different skin-penetrating species to target mammalian hosts? Given presence of both non-infective and infective life stages in the environment, we hypothesized that an investigation of life-stage specific olfactory preferences might reveal host-emitted odor cues that are specifically important for iL3s to engage in host-seeking behaviors. Supporting this hypothesis, in a preliminary investigation we observed distinct odorant response profiles for *Strongyloides* iL3, non-infective larval, and free-living adult life stages [17]. However, these life-stage-specific variations were only investigated within the *Strongyloides* genus against a small number of host-emitted odorants. Thus, how the life-stage-specific changes in olfactory preferences we observed in *Strongyloides* compared to other nematode species, with different environmental ecology, was not thoroughly explored.

To investigate the life-stage-specific olfactory preferences of skin-penetrating nematodes in more detail, we examined the responses of *S. stercoralis* free-living adults and iL3s to a large panel of odorants emitted from mammalian skin, sweat, skin microbiota, feces, breath, as well as fecal odor (Fig. 1a, Supplementary Table 1). The responses of each life stage were quantified using a chemotaxis assay (Supplementary Figure 1) [17]. The life-stage-



Nematode Species	Common Name	Host Range	Life Stages Tested
<i>S. stercoralis</i>	threadworm	humans, primates, dogs	free-living adults iL3s
<i>S. ratti</i>	threadworm	rats, mice	free-living adults iL3s
<i>A. ceylanicum</i>	hookworm	humans, south Asian carnivores	iL3s
<i>P. trichosuri</i>	threadworm	Australian brushtail possum	free-living adults iL3s
<i>C. elegans</i>	none	none	adults dauers

Fig 1. Life cycles and ecology of nematode species. **a** *S. stercoralis* and *S. ratti* larvae from host feces either develop directly into iL3s or can develop through one free-living generation in the environment. All progeny from free-living adult males and females become iL3s that must infect a host to continue the life cycle. **b** *A. ceylanicum* larvae can only develop into iL3s and must infect a new host each generation. **c** *P. trichosuri* larvae can develop directly into iL3s or can undergo many free-living generations in the environment without infecting a host. **d** Non-parasitic *C. elegans* completes its life cycle in the environment. Under environmental stress, some individuals become developmentally arrested dauer larvae, which is the analogous life stage to the skin-penetrating iL3 [29]. **e** Summary of the nematode species, host ranges, and life stages tested in this study. In **a-e** the life stages tested are color coded: blue = free-living adults of parasitic threadworms, red = iL3s of parasitic threadworms, pink = iL3s of parasitic hookworms, dark green = non-parasitic *C. elegans* adults, green = non-parasitic *C. elegans* dauers. L1-L4 = larval stages; iL3 = third-stage infective larvae.

specific olfactory preferences of *S. stercoralis* were then compared to three other species that also have environmentally dwelling adults and developmentally arrested third-stage larvae: *S. ratti*, a rat parasite which has a similar life cycle to *S. stercoralis* (Fig. 1a) [10]; *P. trichosuri*, a uniquely complex parasite of Australian brushtail possums which can undergo many free-living generations without infecting a host, and thus represents an evolutionary

intermediate between facultative and obligate parasitism (Fig. 1c) [30,31]; and non-parasitic *C. elegans*, which reproduces as hermaphroditic adults whose larval progeny can enter a developmentally arrested dauer stage under stressful environmental conditions (Fig. 1d) [32]. *C. elegans* dauers are morphologically analogous to parasitic iL3s [29].

Each species, and life-stage, tested against the mammalian odorant panel exhibited a unique response profile (Fig. 2a). A quantitative comparison of odor response profiles across the four different nematode species tested which have both environmental adults and developmentally arrested third-stage larvae revealed that olfactory preferences closely reflect ecology and life stage (Fig. 2b). The odorant preferences of non-parasitic *C. elegans* adults and dauers were more similar to each other than to any of parasitic species tested, regardless of life stage (Fig. 2b). These results suggest that non-parasitic and parasitic nematode species have distinct olfactory preferences that reflect their respective environmental niches. However, within the parasitic nematode species tested, life stage was more reflective of olfactory preference than species (Fig 2b). Interestingly, *S. stercoralis*, *S. ratti*, and *P. trichosuri* iL3s had more similar odorant response profiles than any species did to their respective free-living adult life stage (Fig. 2b). Our results indicate that, irrespective of host range and obligate vs. facultative parasitic lifestyle, the transition to the iL3 life stage represents a dramatic shift in odorant preferences relative to free-living adults in the environment.

What accounts for the life-stage-specific olfactory preferences observed in skin-penetrating nematodes? Our preliminary analysis suggested a model in which free-living adults, which feed on bacteria in the host's feces, are highly attracted to fecal odor while iL3s are neutral to fecal odor [10,17]. Our expanded analysis across a large panel of odorants and species supported this model. For example, *S. stercoralis* adults were attracted to animal feces and wide range of individual odorants emanating from skin and feces (Fig. 2d). However, *S. stercoralis* iL3s were neutral to many of these odorants; attraction for *S. stercoralis* iL3s was restricted to a small subset of host-emitted odorants that are found in skin, sweat, and feces (Fig. 2e). Similar shifts from odorant attraction at the adult stage, to neutrality at the iL3 stage, were also observed in *S. ratti* and *P. trichosuri* (Fig. 2a). In summary, our results

indicate that free-living life stages are retained on host feces by strong attraction to feces and fecal odorants. However, at the iL3 life stage, attraction to fecal odorants is downregulated allowing iL3s to disperse into the environment in search of hosts [17]. Odorants that remain attractive at the iL3s stage may represent host-emitted odorants that are specifically detected during host-seeking behavior.

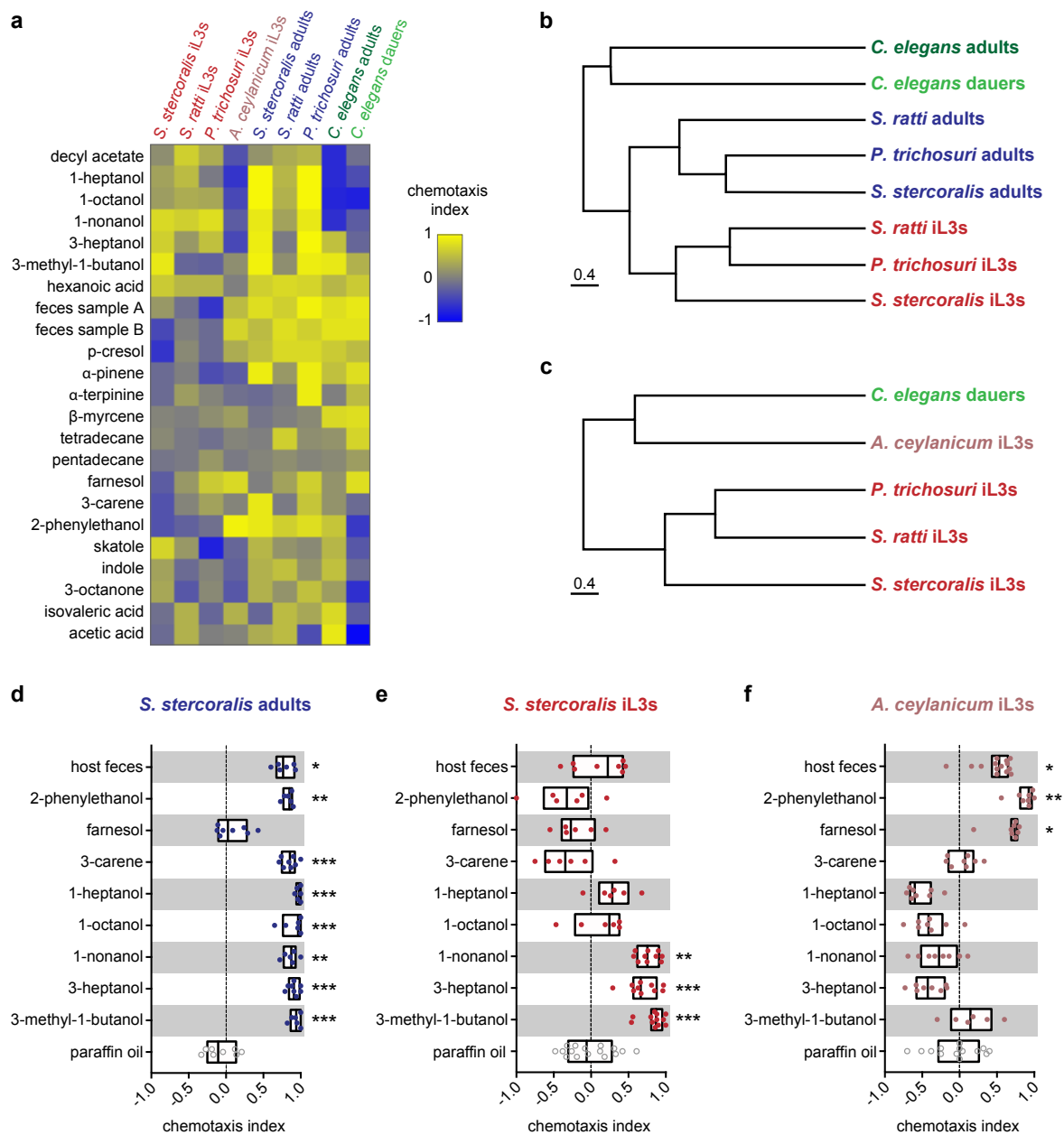


Fig 2. Olfactory responses are species and life-stage specific. **a** Responses of skin-penetrating and free-living nematode species to mammalian skin, sweat, fecal odorants, and feces across different life stages. Response magnitudes are color-coded according to the scale shown to the right of the heat map. Odorants are ordered based on hierarchical cluster analysis [33]. $n = 6-20$ trials for each odorant, species, and life stage combination. The nematode species and life stages are color-coded as shown in Fig. 1. Each species and life

stage had a unique response profile to the odorant panel. **** $P < 0.0001$, two-way ANOVA with Tukey's post-test. Some data for *S. ratti* and *S. stercoralis* are from Castelletto *et al.*, 2014 [17]. **b,c** Olfactory preferences of skin-penetrating threadworms reflect life stage rather than species (**b**); iL3s of the hookworm *A. ceylanicum* have distinct olfactory preferences from iL3s of the skin-penetrating threadworm species (**c**). The behavioral dendrograms were constructed from the odorant response profiles in **a**. Hierarchical clustering was performed using Unweighted Pair Group Method with Arithmetic Mean (UPGMA). Euclidean distance was used as a similarity measurement (Coph. Corr. = 0.85 for **b** and 0.90 for **c**) [33]. **d** Responses of *S. stercoralis* adults to select skin, sweat, fecal odorants, and host fecal odor. * $P < 0.05$, ** $P < 0.01$, *** $P < 0.001$. $n = 6-8$ trials for each odorant. **e** Responses of *S. stercoralis* iL3s to select odorants. ** $P < 0.01$, *** $P < 0.001$. $n = 6-16$ trials for each odorant. **f** Responses of *A. ceylanicum* iL3s to select odorants. * $P < 0.05$, ** $P < 0.01$. $n = 6-14$ trials for each odorant. For **d-f** significant responses were calculated relative to the paraffin oil control, Kruskal-Wallis test with Dunn's post-test. Each dot represents an individual chemotaxis assay. Lines indicate medians and interquartile ranges.

Human-infective *S. stercoralis* and *A. ceylanicum* have distinct olfactory preferences

Approximately 100 million people worldwide are infected with *S. stercoralis*; 500 million people harbor hookworm infections from *Ancylostoma duodenale*, *Necator americanus* or zoonic transmission of *A. ceylanicum*, with billions at risk around the world [13,34,35]. Despite the prevalence of these neglected tropical parasites, very little is known about the similarities, or differences, by which threadworm and hookworm iL3s target humans. To address this question, we investigated the olfactory preferences of the hookworm *A. ceylanicum* in response to our mammalian odorant panel (Fig. 2a, Supplementary Table 1). The responses of *A. ceylanicum* iL3s were then compared to those of iL3s from threadworm species *S. stercoralis*, *S. ratti*, and *P. trichosuri*, as well as *C. elegans* dauers. Surprisingly, quantitative analysis of odor responses across iL3s and dauers revealed that *A. ceylanicum* iL3s had distinct odorant preferences from those of skin-penetrating threadworm species. In fact, the odorant preferences of *A. ceylanicum* iL3s more closely reflected those of non-parasitic *C. elegans* dauers than the parasitic species examined (Fig. 2c). A key determinate of this divergence in odorant preferences between *A. ceylanicum* and the skin-penetrating threadworm species was their respective responses to feces and fecal odorants. For example, *S. stercoralis* iL3s were shown to be neutral to host feces and fecal odorants (Fig. 2e) [17]. By contrast, *A. ceylanicum* iL3s were attracted to both host feces and odorants prevalent in mammalian feces (Fig. 2f). Together, these results argue that, despite the fact that *S. stercoralis* and *A. ceylanicum* iL3s both target humans, these two species may employ very

different strategies for host seeking. Intriguingly, *A. ceylanicum* iL3s can infect by both oral and skin-penetration routes while *S. stercoralis* is thought to infect mainly by skin penetration [10,13]. Thus, infection mode may play an important role in the olfactory-driven behaviors for each species. The odorant responses of *S. stercoralis* iL3s may reflect a stronger requirement for locating host skin while *A. ceylanicum* iL3s may be less dependent on skin-penetration as a primary strategy for infection.

***S. stercoralis* and *A. ceylanicum* iL3s have different environmental dispersal behaviors**

The contrasting chemotactic responses of *S. stercoralis* and *A. ceylanicum* iL3s to host fecal odor, and individual odorants prevalent in host feces, raised the question of whether these human-infective species have different environmental dispersal strategies. To test this question, we performed fecal dispersal assays on *S. stercoralis* and *A. ceylanicum* iL3s (Fig. 3a) [15]. We placed iL3s on uninfected feces from permissive laboratory hosts for each species (gerbils for *S. stercoralis*; hamsters for *A. ceylanicum*) and monitored the frequency with which iL3s migrated away from the fecal pellet [36,37]. We found that, on average, 70% of *A. ceylanicum* iL3s remained on the fecal pellet while only 40% of the *S. stercoralis* iL3s remained on feces at the end of a 1-hour assay (Fig. 3b). In addition, for *A. ceylanicum*, of the 30% of iL3s that left the fecal pellet, the majority those of iL3s stayed near the feces; only approximately 10% of all iL3s tested migrated to the outer zone of the assay plate. By contrast, greater than 50% of all *S. stercoralis* iL3s migrate to the outer zone in the same timeframe (Fig. 3b).

To further compare the host seeking behaviors of *S. stercoralis* and *A. ceylanicum* iL3s, we also examined nictation behavior for each species. Nictation is a strategy employed by some parasitic nematode species whereby the infective larva elevates its body and waves its head to facilitate attachment to a passing host [8]. We previously found that *S. stercoralis* iL3s exhibit very low nictation frequencies with only approximately 20% of iL3s displaying nictation behavior, instead preferring a cruising strategy to disperse into the environment [17].

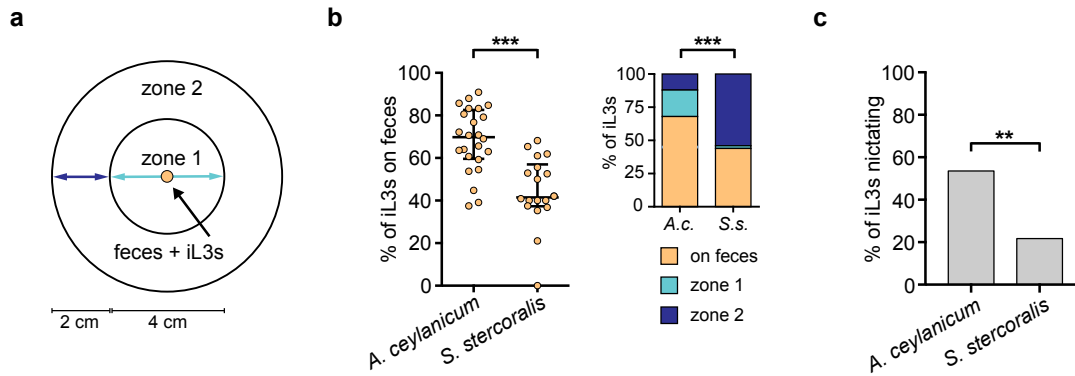


Fig 3. *A. ceylanicum* and *S. stercoralis* have distinct fecal dispersal behaviors. **a** Fecal dispersal assay for skin-penetrating iL3s. iL3s were placed on host feces in the center of the plate and were allowed to crawl for 1 hour. The total number of iL3s remaining on the feces (orange circle), in zone 1 (light blue line), or in zone 2 (dark blue line) was then quantified. **b** Left: The percentage of iL3s remaining on feces after 1 hour for *A. ceylanicum* and *S. stercoralis*. *** $P < 0.001$, Mann-Whitney test. $n = 18-24$ trials per species. Right: The proportion of iL3s on feces, in zone 1, and in zone 2 after 1 hour for *A. ceylanicum* and *S. stercoralis*. The percentage of iL3s in all three regions differed significantly between *A. ceylanicum* and *S. stercoralis*. *** $P < 0.001$, chi-square test. $n = 367-605$ iL3s across 18-24 trials. **c** Nictation frequencies differed between *A. ceylanicum* and *S. stercoralis*. ** $P < 0.01$, Fisher's exact test. $n = 23-71$ iL3s per species. For **b** and **c**, *S. stercoralis* data are from Castelletto *et al.*, 2014 [17].

By contrast, nearly 50% of *A. ceylanicum* iL3s tested under the same conditions displayed nictation behaviors, indicating that this species may prefer more of an ambusher-like (“sit-and-wait”) strategy for infecting hosts (Fig. 3c) [17].

The behaviors of *S. stercoralis* and *A. ceylanicum* iL3s suggest very different host seeking approaches for each species. While *S. stercoralis* iL3s were neutral to fecal odor, *A. ceylanicum* iL3s were highly attracted to fecal odor. This difference was reflected in fecal dispersal assays, where *A. ceylanicum* iL3s preferred to stay on-or-near the fecal pellet while *S. stercoralis* iL3s dispersed further into the environment. Finally, nictation assays indicated that *A. ceylanicum* iL3s may spend more time nictating on host feces while *S. stercoralis* prefer to crawl away from feces. Taken together, our results indicate that *A. ceylanicum* may rely on waiting for potential host to pass by fecal deposits before engaging in host seeking behaviors while *S. stercoralis* iL3s may migrate further into the environment and actively search for potential hosts to infect.

***S. stercoralis tax-4* is required for olfactory-driven host seeking**

Our investigation of life-stage-specific olfactory preferences revealed that iL3s were attracted to a smaller number of odorants than free-living adults. We hypothesized that the select odorants that remained attractive at the iL3 stage might be important for olfactory-driven host-seeking behaviors. To test this hypothesis, we examined how *S. stercoralis* iL3s respond to 3m1b, one of the attractive host-emitted odorants for this species at the iL3 life stage (Fig. 2e) [17]. We imaged real-time migration of individual *S. stercoralis* iL3s in a modified chemotaxis assay where the iL3 was given a choice between two odorants: 3m1b, or a paraffin oil control, which is non-volatile and elicits a neutral response from iL3s in standard chemotaxis assays (Fig. 2e) [17]. Wild-type iL3s preferred to navigate toward 3m1b over paraffin oil when given a choice between the two odorants; approximately 65% of all iL3s tested crawled into the 3m1b scoring region while only approximately 10% of iL3s tested entered the paraffin oil scoring region (Supplementary Figure 2a,c, Supplementary Video 1). To verify that the response to 3m1b was a true chemotactic preference, and not an artifact of the assay design, we also performed single iL3 tracking where both scoring regions contained paraffin oil control; we observed no difference in the frequency with which wild-type iL3s entered the left or right scoring regions containing paraffin oil (Supplementary Figure 2b,d, Supplementary Video 2). Interestingly, the presence of 3m1b in the assay affected iL3 crawling speed. Wild-type iL3s tested in 3m1b vs. paraffin oil control assays showed increased average crawling speeds relative to iL3s tested in paraffin oil vs. paraffin oil assays (Supplementary Figure 2e). The combination of consistent migration toward 3m1b and increased crawling speeds in the presence of 3m1b suggests that host-emitted 3m1b may be an important cue for active host-seeking behavior in *S. stercoralis* iL3s.

At present, the molecular basis for chemosensation has not been explored in any parasitic nematode species, in part due to the historic genetic intractability of these organisms [38]. However, the molecular mechanisms underlying olfactory chemosensation in *C. elegans* are well characterized [39,40]. In *C. elegans*, the cyclic nucleotide gated channel TAX-4/TAX-2 is required for sensory transduction in many sensory neurons, including

olfactory neurons [40]. We previously identified the *S. stercoralis* homolog of *C. elegans tax-4*, disrupted its function with CRISPR-Cas9, and demonstrated that *Ss-tax-4* is required for temperature-driven host seeking in *S. stercoralis* iL3s [16,24]. We reasoned that *Ss-tax-4* might similarly be required for olfactory-driven host seeking. To test this hypothesis, we used CRISPR-Cas9-mediated mutagenesis to generate *S. stercoralis* iL3s with homology-directed homozygous insertions at the *Ss-tax-4* locus (Methods, Supplementary Figure 3a-d) [16]. As a control, we performed our CRISPR-Cas9 method, but omitted the Cas9 construct and generated “no-Cas9-control” iL3s that lacked disruption of the *Ss-tax-4* gene.

As observed in wild-type iL3s, individual no-Cas9-control iL3s tested in a 3m1b versus paraffin oil chemotaxis assay consistently migrated toward 3m1b; approximately 70% of all iL3s tested entered the 3m1b scoring region while only 15% of iL3s entered the paraffin oil control (Fig. 4a,c, Supplementary Video 3). In contrast, *Ss-tax-4* iL3s showed no preference for 3m1b or paraffin oil control (Fig. 4b,d, Supplementary Video 4). In addition, *Ss-tax-4* iL3s displayed slower crawling speeds than no-Cas9-control iL3s the presence of 3m1b, indicating that these worms were less active in the presence of host-emitted odor (Fig. 4e). Thus, our results suggest that *Ss-tax-4* is required for normal olfactory-driven chemotaxis in iL3s, and that detection of host-emitted odorants may be a critical navigational strategy allowing iL3s to find human hosts in the environment.

***S. stercoralis tax-4* is required for development inside the host**

Host seeking is only the first step for skin-penetrating nematodes to successfully establish an infection inside a mammalian host. Following skin penetration, iL3s are thought to migrate through the host’s circulatory system to the lungs where they are coughed up, swallowed, pass through the stomach, and eventually develop into parasitic adults in the intestine (Fig. 1) [3]. One of the initial developmental steps for iL3s as they migrate through the host is activation. Activation is a process whereby the developmentally arrested, non-feeding iL3 resumes pharyngeal pumping and feeding behavior [18,21]. Given the fact that the transition from the soil to inside the host represents a major environmental shift for iL3s, one reasonable hypothesis is that iL3s might use chemosensory to detect host factors

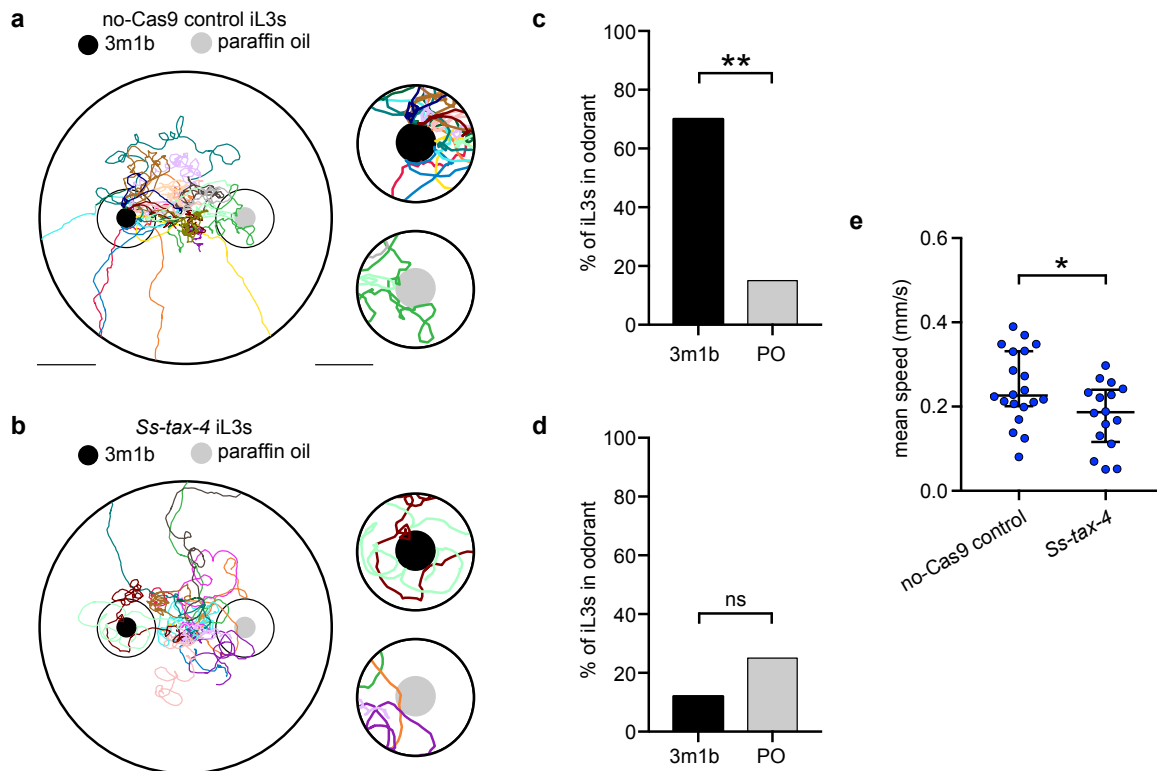


Fig 4. The *S. stercoralis tax-4* gene is required for olfactory-driven host seeking. **a,b** CRISPR-Cas9 disruption of the *Ss-tax-4* gene results in iL3s with reduced preference for host-emitted 3-methyl-1-butanol (3m1b). Tracks of no-Cas9-control iL3s (**a**) and CRISPR-Cas9-edited *Ss-tax-4* iL3s (**b**) migrating for approximately 5 minutes in an odor gradient. Each colored line indicates the track of a single iL3. The full assay arena is shown on the left; scale bars = 1 cm. An enlarged view of the scoring region around the odorants is shown on the right; scale bars = 5 mm. Black dot = placement area of a 5 μ L drop of 3m1b; grey dot = placement area of a 5 μ L drop of paraffin oil control (PO). **c** The percentage of no-Cas9 control iL3s entering the 3m1b and PO scoring regions; no-Cas9 control iL3s migrate preferentially towards 3m1b. $**P < 0.01$, Fisher's exact test. $n = 20$ iL3s. **d** The percentage of *Ss-tax-4* iL3s entering the 3m1b and PO scoring regions; *Ss-tax-4* iL3s display no preference for 3m1b or PO control. $P = 0.653$, Fisher's exact test. $n = 16$ iL3s. **e** No-Cas9 control iL3s display increased crawling speed in the presence of 3m1b. $*P < 0.05$, Welch's t test.

and initiate activation upon host entry. Supporting this hypothesis, studies examining activation of *Ancylostoma* species identified several host stimuli that were required for, or enhanced, iL3 activation including elevated temperatures, CO₂, host serum, and reduced glutathione [18-20]. Similarly, laser ablation studies targeting amphidal sensory neurons of *S. stercoralis* iL3s resulted in reduced activation rates [21]. However, the molecular mechanisms required for in-host activation were not characterized in these studies.

To investigate the host cues that are important for iL3s to resume development in more detail, we modified a previously described *in vitro* activation assay (Fig. 5a) [21]. We exposed

S. stercoralis iL3s to host-like conditions including DMEM tissue culture media, 37°C temperatures, and a 5% CO₂ atmosphere for 21 hours. The iL3s were then incubated with fluorescein isothiocyanate under the culture conditions for 3 hours; resumption of feeding, indicating transition out of the iL3 life stage, was then assessed by visualizing FITC staining in the nematode pharynx (Fig. 5b). We found that, on average, approximately 50% of the

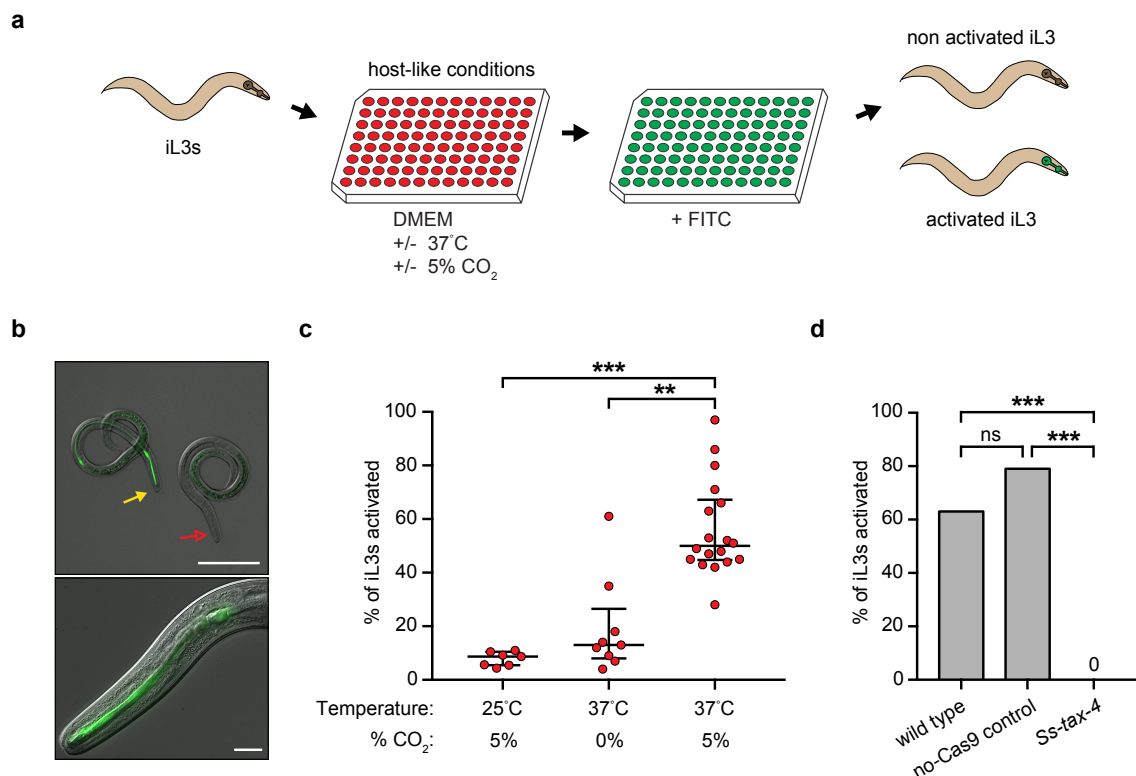


Fig 5. The *S. stercoralis tax-4* gene is required to detect sensory cues inside the host. **a** Schematic of an *in vitro* assay for iL3 activation. Developmentally arrested iL3s are incubated in host-like conditions in DMEM culture medium at 37°C and 5% CO₂ atmosphere. After 21 hours of incubation, fluorescein isothiocyanate (FITC) is added to the medium and iL3s are returned to the culture conditions. Following 3 hours of incubation with FITC the iL3s are washed, anesthetized, plated, and screened for FITC ingested in the nematode pharynx indicating resumption of feeding behavior and exit from the iL3 stage. **b** Top: Representative DIC + epifluorescence overlay of an activated iL3 with FITC staining the pharynx (closed yellow arrow) and an iL3 that failed to activate following 24 hours of incubation (open red arrow). Scale bar = 100 μm. Bottom: magnified DIC + epifluorescence overlay of an activated iL3 with FITC staining the pharynx. Scale bar = 10 μm. **c** Heat and CO₂ are required for iL3 activation in *S. stercoralis*. ***P* < 0.01, ****P* < 0.001, Kruskal-Wallis test with Dunn's post-test. *n* = 7-18 trials per condition. % activation = # FITC-positive activated iL3s / total # iL3s scored. Red dots = % activation for each trial, ~100 iL3s scored per trial. Lines show medians and interquartile ranges. **d** CRISPR-Cas9-edited *Ss-tax-4* iL3s fail to activate in host-like conditions. ****P* < 0.001, chi-square test with Bonferroni correction. *n* = 21-40 iL3s per genotype.

S. stercoralis iL3s activated after 24 hours in host-like conditions. However, removal of either heat, or the 5% CO₂ atmosphere, from the culture conditions dramatically reduced activation rates (Fig. 5c). These results were similar to those observed for *in vitro* activation of the canine hookworm *Ancylostoma caninum*, but the requirement for CO₂ observed here was more pronounced [18]. 37°C and 5% CO₂ culture conditions were also required for *in vitro* activation of *S. ratti* and *P. trichosuri* iL3s (Supplementary Figure 4).

The fact that elevated temperatures, and CO₂ concentrations, are critical activation cues across multiple skin-penetrating species supports the hypothesis that sensory mechanisms play an important role for iL3 development inside the host. Therefore, we asked if *Ss-tax-4* iL3s were able to activate when exposed to host-like conditions. While individual wild-type iL3s and no-Cas9-control iL3s consistently activated under host-like conditions, we never observed activation in any of the *Ss-tax-4* iL3s tested (Fig. 5d). Thus, thermosensory and chemosensory pathways that contribute to iL3 host seeking are also important for iL3s to trigger development upon entering the host.

Discussion

Here, we conducted a large scale quantitative behavioral analysis to determine how life stage and parasitic vs. non-parasitic ecology affect the olfactory preferences of different nematode species. We found that both parasitic and non-parasitic nematode species show life-stage-specific olfactory preferences that fit their distinct environmental needs. Free-living adults of skin-penetrating threadworm species were broadly attracted to mammalian-emitted odorants found in skin, sweat, breath, and feces. However, the odorant preferences for iL3s were more restricted (Fig. 2). Free-living adults likely feed on fecal bacteria to as a nutrition source. However, iL3s have little incentive to remain on, or near, feces since they are non-feeding [10]. Thus, threadworm iL3s appear to downregulate responses to odorants that are important for environmental feeding behaviors and instead favor odorants that may facilitate finding a mammalian host, which is essential for their continued development.

Intriguingly, iL3s of the hookworm *A. ceylanicum* had distinct olfactory preferences when compared to iL3s of skin-penetrating threadworm species (Fig. 2c). *A. ceylanicum* iL3s

had a strong attraction to host feces and fecal odorants, tended to disperse shorter distances into the environment, and had a higher propensity to nictate than *S. stercoralis* iL3s (Fig. 2f, Fig. 3). Taken together, the respective responses of hookworm and threadworm iL3s to feces and fecal odorants appears to represent a critical difference in host-seeking strategy between these species. This disparity is especially notable when comparing *A. ceylanicum* and *S. stercoralis* iL3s since both species can infect humans, indicating that each species may have evolved different approaches to infect the same host. In a previous study from our lab, we characterized the host-seeking behaviors of the passively ingested murine parasite *Heligmosomoides polygyrus*. Like *A. ceylanicum*, *H. polygyrus* iL3s were attracted to host feces [15]. Fecal attraction is thought to allow *H. polygyrus* iL3s to optimally position themselves for being swallowed during coprophagy [15]. Oral infection has been documented in many hookworm species including *A. ceylanicum*, *A. duodenale*, *A. caninum*, and *N. americanus* [13,41,42]. Therefore, attraction to feces may facilitate oral infection for hookworms in a similar manner as *H. polygyrus*, even if their animal hosts are not necessarily coprophagic. In contrast to olfactory-driven behaviors, *A. ceylanicum* iL3s also show robust positive thermotaxis and engage in thermosensory-driven host seeking [16]. Thus, as an alternative to oral infection, *A. ceylanicum* iL3s may elect to stay near fecal deposits, wait for mammalian host to pass by, and initiate thermosensory-driven host seeking to infect by skin penetration. We note that *A. ceylanicum* infections in humans are considered to be zoonotically acquired, typically from domesticated animals [13]. In the future, studies examining the host-seeking behaviors of iL3s from other human-infective hookworm species, such as *A. duodenale* or *N. americanus*, would be valuable to determine how reflective our observations of *A. ceylanicum* iL3s are of hookworms in general.

Based on our observations of life-stage-specific olfactory preferences, we identified 3-methyl-1-butanol (3m1b), a volatile odorant emitted from mammalian skin, sweat, skin microbiota, and feces, as an attractant for *S. stercoralis* iL3s (Fig. 2e) [17,25-28]. We tracked the responses of individual wild-type iL3s to 3m1b in a chemotaxis assay and found that they navigated toward a point source of the 3m1b; iL3s also increase their speed when 3m1b

present, suggesting this odorant may be an important cue for olfactory-driven host seeking (Supplementary Figure 2). While individual iL3s reliably navigated to 3m1b, we note that their overall trajectory toward the odorant was not direct, but highly curved, and resembled previously described local search behaviors (Supplementary Figure 2, Supplementary Video 1) [16,17]. This is in contrast to thermosensory-driven host seeking where *S. stercoralis* iL3s move rapidly up a thermal gradient in relatively straight trajectories and only engage in local search at temperatures approximating that of a mammalian host [16]. These results indicate that different host-emitted sensory cues elicit distinct host seeking behaviors in iL3s. Future studies interrogating the underlying sensory neural circuits that drive chemosensory and thermosensory host-seeking behaviors will allow us to better understand how iL3s interpret different cues to successfully target hosts in the environment.

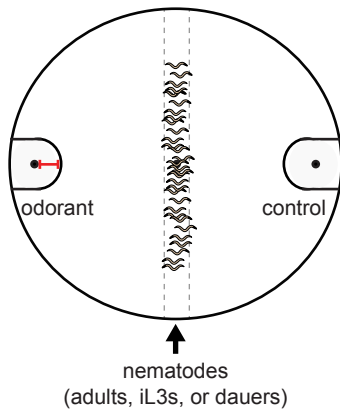
To identify molecular mechanisms that might be required for olfactory-driven host seeking, we used a previously described CRISPR-Cas9 method to generate *S. stercoralis* iL3s with putative homozygous disruptions of the *Ss-tax-4* gene [24]. We found that *Ss-tax-4* iL3s were unable to navigate toward a 3m1b point source and showed slower speeds than control iL3s in the presence of 3m1b (Fig. 4). Our results represent the first molecular evidence that chemosensory mechanisms are required for iL3s to detect and navigate toward host-emitted odorants. These results strongly suggest that odorant detection is a critical component of parasitic behaviors for skin-penetrating iL3s. Interestingly, 3m1b is also a known attractant for *C. elegans*, and the underlying neural circuitry that results in chemotaxis towards 3m1b is well characterized [39]. Volatile 3m1b is detected by *tax-4*-expressing AWC olfactory neurons in the nematode amphid [40]. Decreasing concentrations or removal of 3m1b elicits depolarization of AWC sensory neurons, which activates downstream AIB interneurons; AIB activation signals downstream to increase the frequency with which the worm turns while crawling [43]. This behavior is thought to allow the worm to reorient towards higher concentrations of 3m1b using a biased random walk [43]. Electron microscopic reconstructions of *S. stercoralis* sensory neuroanatomy indicate the presence of AWC-like sensory neurons in the amphid [44]. Are the *Ss-tax-4*-dependent responses to 3m1b we

observed in *S. stercoralis* iL3s similarly mediated by AWC neurons? In addition, has this chemosensory circuit been adapted for iL3s engaging in host-seeking behavior? Future examination of the sensory neurons mediating iL3 attraction to 3m1b will provide more clarity on how important this odorant is for targeting human hosts.

In addition to examining the role of chemosensation in iL3 host seeking, we asked if sensory mechanisms might also be required for in-host development. We found that host-like 37°C temperatures and elevated CO₂ concentrations are vital cues for iL3 activation (Fig. 5c). Thus, thermosensory and chemosensory pathways that are required for host seeking also appear to be necessary for triggering the developmental program of iL3s following host entry. We found that *Ss-tax-4* iL3s were unable to activate (Fig. 5d). Previous laser ablation studies targeting ASJ sensory neurons in *S. stercoralis* iL3s reduced activation rates. However, approximately half of ASJ-ablated animals still activated normally, indicating that ablation of one neuron pair is insufficient to completely eliminate iL3 activation [21]. Here, *Ss-tax-4* knockout iL3s showed no evidence for activation (Fig. 5d). Our results suggest that proper activation likely requires multiple sensory inputs across many sensory neurons, as was previously predicted [21]. We hypothesize that multisensory integration is likely critical for iL3 activation, as it would decrease the chance of iL3s improperly developing outside the host. For example, multisensory activation would be a beneficial adaptation in many tropical regions of the world where environmental temperatures frequently exceed 37°C. In such environments, entirely thermosensory-driven activation would come with the risk of premature iL3 activation. A multisensory approach for in-host development may not only allow iL3s to properly time development but may also assist in migration through the host tissues. Further investigation of the host cues that are important for iL3 activation will allow us to better understand how successful infection is achieved after skin penetration.

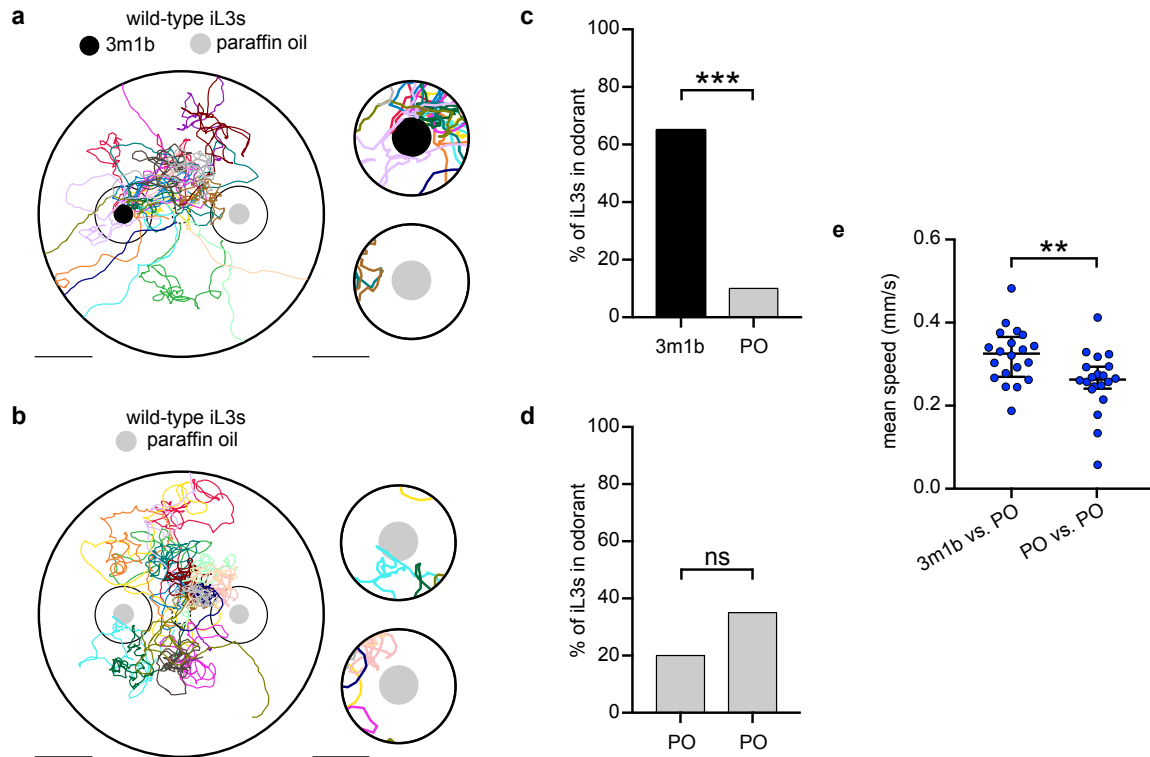
Here, we have used the human-infective skin-penetrating *S. stercoralis* as a model to elucidate chemosensory mechanisms that promote host seeking and activation. Our results provide a foundation for understanding the sensory mechanisms that allow skin-penetrating

iL3s to target mammalian hosts in the environment and successfully establish an infection inside the host. In the future, a deeper investigation of these mechanisms may allow for the development of novel approaches to prevent harmful infections caused by skin-penetrating hookworm and threadworm species.

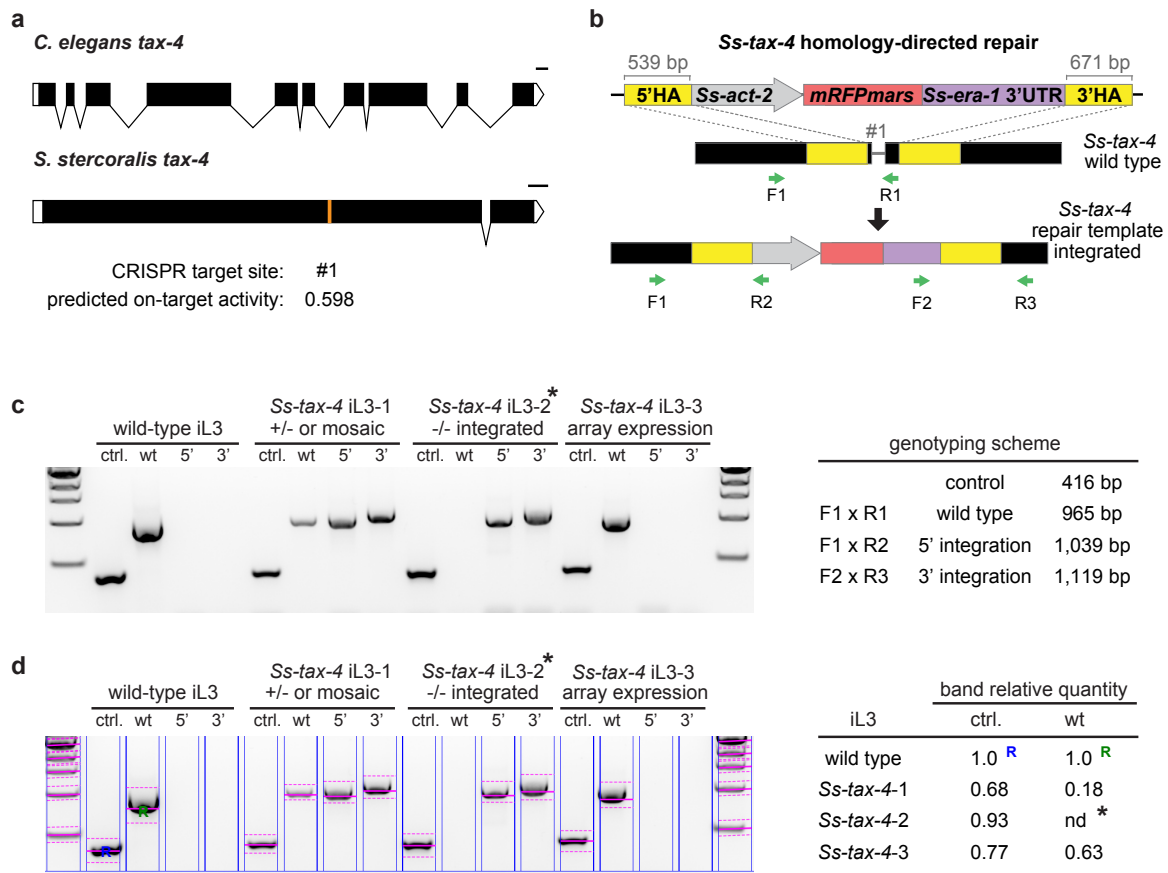


$$\text{chemotaxis index} = \frac{(\# \text{ of worms at odorant}) - (\# \text{ worms at control})}{(\# \text{ of worms at odorant}) + (\# \text{ worms at control})}$$

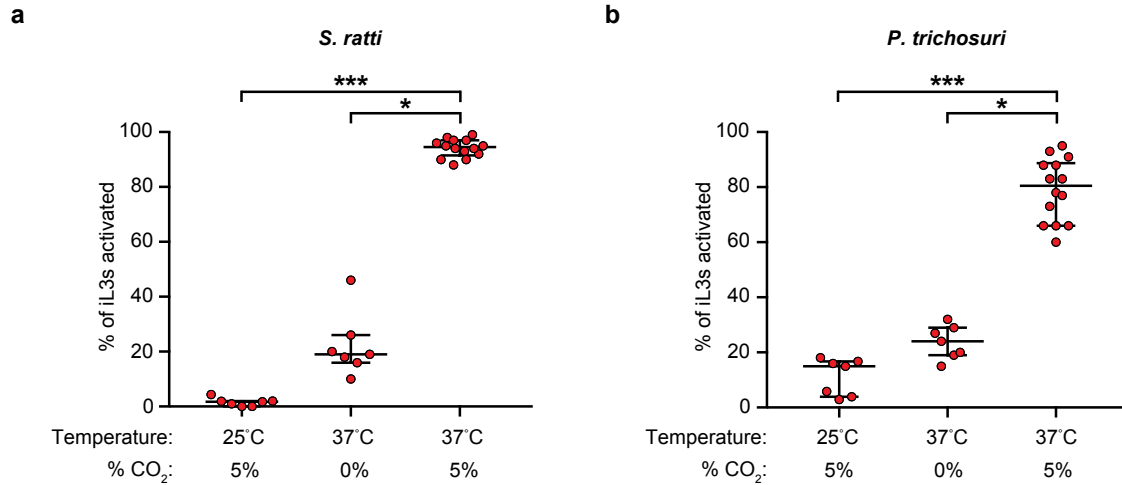
Supplementary Figure 1. Nematode chemotaxis assay. Each nematode species, and life stage (free-living adults, iL3s, or non-parasitic dauers), were assayed using the same format. Nematodes were spread vertically along the center of the plate; approximately 100-200 animals per plate. Odorant and control were placed on each side of the plate (black dots). The nematodes were allowed to migrate in the odor gradient for 3 hours. The number of animals in the scoring regions (extended circles around the black dots) was counted. The chemotaxis index was then calculated as shown. The chemotaxis index ranges from +1 to -1 with positive values indicating attraction to the host odorant and negative values indicating repulsion to the host odorant. Red scale bar = 1 cm. The figure was modified from Gang *et al.* 2016 [8].



Supplementary Figure 2. *S. stercoralis* wild-type iL3s navigate to host-emitted 3-methyl-1-butanol. **a,b** Tracks of wild-type iL3s migrating for approximately 5 minutes in a 3-methyl-1-butanol (3m1b) odor gradient (**a**) or in a control assay where paraffin oil (PO) was added to each scoring region (**b**). Each colored line indicates the track of a single iL3. The full assay arena is shown on the left; scale bars = 1 cm. An enlarged view of the scoring region around the odorants is shown on the right; scale bars = 5 mm. Black dot = placement area of a 5 μ L drop of 3m1b; grey dot = placement area of a 5 μ L drop of PO control. **c** The percentage of wild-type iL3s entering the 3m1b and PO scoring regions; wild-type iL3s migrate preferentially towards 3m1b. $***P < 0.001$, Fisher's exact test. $n = 20$ iL3s. **d** The percentage of wild-type iL3s entering the scoring regions when only PO control is added to the plate; wild-type iL3s show no preference for the left or right scoring regions. $P = 0.48$, Fisher's exact test. $n = 20$ iL3s. **e** Wild-type iL3s display increased crawling speed in the presence of 3m1b. $**P < 0.01$, Mann-Whitney test. $n = 20$ iL3s per condition.



Supplementary Figure 3. Strategy for CRISPR-Cas9-mediated targeted mutagenesis of *Ss-tax-4* and genotyping for homology-directed repair (HDR). **a** The *C. elegans* and *S. stercoralis tax-4* genes. The *Ss-tax-4* CRISPR target site and predicted on-target activity score is indicated (orange line) [45]. Scale bar = 100 bp. **b** HDR strategy for *Ss-tax-4*. iL3s expressing *mRFPmars* along the full nematode body wall (Methods) were selected as integration candidates and genotyped using the PCR primer sets indicated. **c** Left; representative gel and inferred genotypes of a wild-type iL3 and three *mRFPmars*-expressing F₁ iL3 progeny collected from *Ss-tax-4* CRISPR-injected adults. gDNA from each iL3 was evenly divided into four reactions: ctrl. = reaction amplifying 416 bp of the first exon of the *Ss-act-2* gene to confirm successful gDNA isolation; wt = reaction amplifying the *Ss-tax-4* wild-type CRISPR locus where primer R1 overlaps the predicted cut site; 5' = reaction for HDR at the 5' border of the integrated cassette; 3' = reaction for HDR at the 3' border of the integrated cassette. 5' and 3' integration primer pairs amplify only following successful integration of *Ss-act-2::mRFPmars* into the *Ss-tax-4* target locus. For iL3 genotypes: array expression = *mRFPmars* expressing iL3 that showed no evidence for integration; +/- or mosaic = *mRFPmars* expressing iL3 that showed integration but also showed wild-type DNA remaining at the target locus; -/- integrated = putative *Ss-tax-4* homozygous disruption (asterisk) showing 5' and 3' integration and no amplicon for the wild-type locus. Right; summary of the PCR-genotyping scheme and predicted amplicon sizes. Size markers = 3kb, 2 kb, 1.5 kb, 1 kb, and 500 bp from top to bottom. **d** Automated detection of PCR amplicons and relative quantification of bands. The relative amount of DNA for each *mRFPmars*-expressing F₁ iL3 was quantified based on the wild-type control as a reference. "R" indicates the wild-type reference band: Blue R = reference band for quantification of the *act-2* control reactions; Green R = reference band for quantification of the *Ss-tax-4* wild-type locus reactions; nd^{*} = no PCR-amplicon was detected, thus this iL3 was considered a putative *Ss-tax-4* homozygous disruption.



Supplementary Figure 4. *In vitro* activation assay for *S. ratti* and *P. trichosuri* iL3s. **a** Heat and CO₂ are required for iL3 activation in *S. ratti*. * $P < 0.05$, *** $P < 0.001$, Kruskal-Wallis test with Dunn's post-test. $n = 7-14$ trials per condition. **b** Heat and CO₂ are required for iL3 activation in *P. trichosuri*. * $P < 0.05$, *** $P < 0.001$, Kruskal-Wallis test with Dunn's post-test. $n = 7-14$ trials per condition. For **a,b** % activation = # FITC-positive activated iL3s / total # iL3s scored. Red dots = % activation for each trial, ~100 iL3s scored per trial. Lines show medians and interquartile ranges.

Supplementary Table 1. Mammalian derived odorants tested. Superscripts denote the control used in chemotaxis assays and the diluent used to make 10^{-1} odorant solutions as described in the methods: p = paraffin oil, w = dH₂O, e = 200 proof ethanol. Odorant sources are not exhaustive.

odorant ^(control)	class	source	CAS #	references
3-methyl-1-butanol ^p	alcohol	[human]: sweat, feces, skin microbiota	123-51-3	[25-28]
1-heptanol ^p	alcohol	[human]: sweat, feces, hair, scalp [dog]: feces [rabbit]: feces	111-70-6	[25,26,46-48]
1-octanol ^p	alcohol	[human]: sweat, feces, hair, scalp, microbiota [rabbit]: feces	111-87-5	[25,26,28,46,48]
1-nonanol ^p	alcohol	[human]: sweat, feces, hand, hair, scalp, microbiota	143-08-8	[25,26,28,46]
farnesol ^p	alcohol	[human]: sebum [dog]: feces [rat]: preputial gland	4602-84-0	[47,49,50]
3-heptanol ^p	alcohol	[human]: attractant for anthropophilic mosquitoes	589-82-2	[51]
2-phenylethanol ^p	alcohol	[rabbit]: feces	60-12-8	[48]
isovaleric acid ^p	acid	[human]: sweat, feces, foot, back/arm, skin microbiota [dog]: feces	503-74-2	[25-27,47,52-54]
acetic acid ^w	acid	[human]: sweat, foot, hand, skin, back/arm, hair, scalp, breath, skin microbiota	64-19-7	[25,28,46,52,53,55-57]
hexanoic acid ^p	acid	[human]: sweat, feces, skin, microbiota	142-62-1	[25,26,54-56]
decyl acetate ^p	acetate	fecal microbiota	112-17-4	[28]
3-octanone ^p	ketone	[human]: feces [rabbit]: feces	106-68-3	[26,48]
β-myrcene ^p	hydrocarbon	[human]: feces	123-35-3	[26]
tetradecane ^p	hydrocarbon	[human]: feces, hair, scalp, skin [rat]: preputial gland [rabbit]: feces	629-59-4	[26,46,48,49,55]
pentadecane ^p	hydrocarbon	[human]: hair, scalp, skin [rabbit]: feces	629-62-9	[46,48,55]
p-cresol ^e	aromatic	[human]: skin, back/arm, feces [rabbit]: feces	106-44-5	[26,48,56]
α-terpinene ^p	aromatic	[human]: urine	99-86-5	[58]
skatole ^e	aromatic heterocyclic	[human]: feces	83-34-1	[59]
indole ^e	aromatic heterocyclic	[human]: sweat, feces, forearm skin microbiota [dog]: feces [rat]: preputial gland	120-72-9	[25,26,28,55,59-61]
α-pinene ^p	bicyclic monoterpene	[human]: feces, breath	7785-70-8	[26,62]
(+)-3-carene ^p	bicyclic monoterpene	[human]: feces, breath	498-15-7	[26,62]
feces ^w	---	dog, rat, Australian brushtail possum, hamster, gerbil	---	---

Supplementary Table 2. Plasmid vectors used in this study. pPV540 was modified from pPV402, which is described in Shao *et al.* 2012 [63]. pEY11 was modified from pAJ50, which is described in Junio *et al.* 2008 [64].

construct	description	backbone
pPV540 (<i>Sr-eef-1A_p::Cas9::Ss-era-1</i> 3'UTR)	<i>Strongyloides</i> codon-optimized Cas9	pPV402
pMLC47 (<i>Sr-U6_p::Ss-tax-4-sgRNA::Sr-U6</i> 3'UTR)	sgRNA for <i>Ss-tax-4</i>	pUC57-Kan
pEY11 (<i>5'HA::Ss-act-2_p::mRFP_{mars}::Ss-era-1</i> 3'UTR::3'HA)	HDR construct for <i>Ss-tax-4</i>	pAJ50

Supplementary Table 3. Oligonucleotides used in this study.

oligonucleotide set (5' to 3')	description	Size (bp)	notes
F: GTTTAAACTGGTTATCCTCTGACTTGATAGCTG R: TCAATATTTTGTACTGGACCAGGAAC	<i>Ss-tax-4</i> 5' homology arm in pEY11	539 bp	
F: TCGATGATTTCCAATATGTCTGCTG R: TCCACTGTATTTTGTCTTCTGGTG	<i>Ss-tax-4</i> 3' homology arm in pEY11	671 bp	
F: TGTTTAGTTGACAGTAATTGGACGG R: TTATAACCTTCTTCTCCTTCCGGTG	<i>Ss-gcy-9</i> 5' homology arm for pSSG04	556 bp	
F: TCAGATGATGAAAATGATGGAGGACT R: AGTACTTTCCATACGAGAAGCCATA	<i>Ss-gcy-9</i> 3' homology arm for pSSG04	583 bp	
F: GTATCCCTTCTATTGTTGGAAGACC R: CCTTCATAGATTGGTACAGTGTGAG	<i>Ss-act-2</i> exon 1 gDNA control	416 bp	Control in Supplementary Figure 3
F: TTCTAATTCTTCAAAAATGCCAAAGTCC R: TTGTAGCAAAAATTAACCCACC	<i>Ss-tax-4</i> wild-type locus	965 bp	F1 x R1 Supplementary Figure 3
F: TTCTAATTCTTCAAAAATGCCAAAGTCC R: CGAGGTACCTCTTTCCACACTT	<i>Ss-tax-4</i> 5' integration	1,039 bp	F1 x R2 Supplementary Figure 3
F: AAACAGAAACAGATTGGGTCTCT R: AGGTTTGTAAGTCAATGCATCTTGG	<i>Ss-tax-4</i> 3' integration	1,119 bp	F2 x R3 Supplementary Figure 3

Supplementary Table 4. Summary of *Ss-tax-4* microinjections, F₁ iL3 screening, and genotyping of *Ss-tax-4* knockout iL3s. Percentages in the last two columns were calculated based on the # red iL3s genotyped by PCR. na = not available; iL3s counts were not recorded for this experiment.

# free-living adults injected	# iL3s screened	# red iL3s collected	# red iL3s genotyped	# repair-template integrated (%)	# <i>Ss-tax-4</i> knockouts (%)
20	na	40	22	17 (77%)	8 (36%)
15	333	12	12	6 (50%)	3 (25%)
17	680	6	6	4 (66%)	3 (50%)
30	487	18	18	14 (77%)	6 (33%)
23	160	12	12	9 (75%)	4 (33%)
25	256	10	10	8 (80%)	5 (50%)
130	1,916	98	80	58 (73%)	29 (36%)

Methods

Ethics Statement

Gerbils were used as hosts to passage *S. stercoralis*. Rats were used as hosts to passage *S. ratti*. Hamsters were used as hosts to passage *A. ceylanicum*. Procedures and protocols for animal subjects were approved by the UCLA Office of Animal Research and Oversight (2011-060-22) which follows AAALAC standards and the *Guide for the Care and Use of Laboratory Animals*.

Maintenance of *Strongyloides stercoralis*

S. stercoralis UPD strain (provided by Dr. James Lok, University of Pennsylvania) was serially passaged in male and female Mongolian gerbils obtained from Charles River Laboratories. Gerbil infections were carried out by collecting *S. stercoralis* iL3s from fecal-charcoal cultures by Baermann apparatus as described [22]. iL3s were cleansed of fecal debris by suspension in ~0.5% low-gelling-temperature agarose; iL3s that crawled out of the agarose were collected and washed in sterile 1x PBS 5 times. Gerbils were anesthetized with isoflurane and inoculated with ~2,250 iL3s suspended in 200 μ L sterile 1x PBS by inguinal subcutaneous injection. After a 14-day pre-patency period, feces infested with *S. stercoralis* were collected by placing infected gerbils on wire cage racks with wet cardboard lining the cage bottom to prevent the feces from desiccating. Fecal pellets were collected the next morning, softened with dH₂O, mixed in a 1:1 ratio with autoclaved charcoal granules (bone char from Ebonex Corp., Cat # EBO.58BC.04), and stored in 10-cm diameter x 20-mm height Petri dishes lined with filter paper moistened with dH₂O. *S. stercoralis* infested feces were collected between days 14-45 after initial infection. *S. stercoralis* free-living adults were collected by storing fecal-charcoal cultures at 20°C for 48 h, or at 25°C for 24 h; adults were isolated using the Baermann technique. iL3s were collected by storing fecal-charcoal cultures at 23°C for 6-14 days; iL3s were isolated using the Baermann technique.

Maintenance of *Strongyloides ratti*

S. ratti ED321 strain (provided by Dr. James Lok, University of Pennsylvania) was serially passaged in Sprague Dawley rats obtained from Envigo. Rat infections were carried

out by collecting *S. ratti* iL3s from fecal-charcoal cultures by Baermann apparatus. iL3s were washed in 1x PBS 5 times and rats were inoculated with ~800 iL3s in 300 μ L sterile 1x PBS by subcutaneous injection. After a 7-day pre-patency period, feces infested with *S. ratti* were collected as described above. *S. ratti* infested feces were collected between days 7-23 after initial infection. *S. ratti* free-living adults and iL3s were isolated using the Baermann technique as described above.

Maintenance of *Ancylostoma ceylanicum*

A. ceylanicum Indian strain, US National Parasite Collection Number 102954 (provided by Dr. John Hawdon, George Washington University) was serially passaged in male Syrian golden hamsters from Envigo. Hamster infections were carried out by collecting *A. ceylanicum* iL3s from fecal-charcoal cultures by Baermann apparatus. iL3s were washed in sterile dH₂O and hamsters were inoculated with ~70-100 iL3s in 100 μ L sterile water by oral gavage. After a 14-day pre-patency period, feces infested with *A. ceylanicum* were collected as described above. *A. ceylanicum* infested feces were collected between days 14-44 after initial infection. *A. ceylanicum* iL3s were collected by storing fecal-charcoal cultures at 23°C for 14-21 days.

Maintenance of *Parastrongyloides trichosuri*

P. trichosuri (provided by Dr. Warwick Grant, La Trobe University) was a mixed population of wild isolates collected from *Trichosurus vulpecula* brushtail possum feces in Upper Hutt, New Zealand and Kioloa State Forest, New South Wales, Australia. *In vitro* cultures of free-living *P. trichosuri* were maintained as described, with modifications [30,65]. Briefly, 6-cm Nematode Growth Media (NGM) plates with *Escherichia coli* OP50 were prepared using standard methods [66]. For optimal *P. trichosuri* growth, 3% agar plates were used to limit nematode penetration into the agar and 1/10 the standard peptone was added to the NGM media. Autoclaved fecal pellets collected from New Zealand white rabbits was deposited in the center of the NGM plate on the OP50 lawn. The fecal pellet was punctured, saturated with OP50 solution, and was allowed to dry overnight. The next day, *P. trichosuri* free-living cultures containing all life stages were pipetted on the OP50-saturated feces (~100-

200 nematodes per plate). The free-living cultures were maintained at room temperature and passaged every 3-4 days by pouring BU salt solution into the plate and floating nematodes off the bacterial lawn and fecal pellet. The nematodes were washed 5 times in BU and pipetted onto fresh NGM + rabbit feces plates. *P. trichosuri* free-living adults were collected by transferring BU washed nematodes to a watch glass; adults were gravity settled to the bottom of the dish and other life stages were removed in the BU suspension. *P. trichosuri* iL3s were collected by taking nematode-infested rabbit feces and preparing 6-cm fecal charcoal cultures as described above. Fecal-charcoal cultures were stored at 23°C and iL3s were collected 7-21 days later by Baermann technique.

Maintenance of *Caenorhabditis elegans*

C. elegans wild isolate “Hawaii” (CB4856) was cultured at room temperature on 6-cm 2% NGM plates with *E. coli* OP50 bacteria lawns using standard methods [66]. Adult hermaphrodites were collected by washing them off plates with M9 solution. The nematodes were washed 3x in M9 and transferred to a watch glass; adults were gravity settled to the bottom of the dish and other life stages were removed in the M9 suspension. To collect dauer larvae, 4-5 young adults were picked to fresh NGM plates with OP50. The plates were grown without passage for 10-14 days. Dauers were collected from water droplets on the lids of starved cultures [67].

Host odorant and fecal odor assays

Odorant assays were performed on 9-cm chemotaxis plates as described (Supplementary Figure 1) [17]. Populations of ~100-200 adults, iL3s, or dauers were spread vertically along the center of the plate. 5 μ L of host odorant, or control odorant (paraffin oil, dH₂O, or ethanol), was then pipetted on each side of the plate in the center of 2 cm diameter scoring region. The scoring regions were aligned horizontally along the center of the plate with the odorants placed 1 cm from the edge of the plate. The worms were allowed to crawl undisturbed in the odorant gradient for 3 hours at room temperature on a vibration-insulating platform. The chemotaxis index (CI) was calculated as: $CI = (\# \text{ worm in odorant scoring region} - \# \text{ worms in control scoring region}) / (\# \text{ worms in both scoring regions})$. CI values range from

+1 to -1 with a positive CI indicating attraction to the tested odorant, and a negative CI indicating repulsion to the odorant. All adult assays were performed with odorants diluted 10^{-1} in either paraffin oil, dH₂O, or ethanol. iL3 and dauer assays were performed with undiluted odorant to account for thickened body wall cuticle, closed oral orifices, and clogged amphid openings potentially dampening responses [68]. To account for directional bias, two identical assays were performed simultaneously with the test odorant placed in scoring regions on opposite sides. All assays where the absolute difference in CI for the two plates was ≥ 0.9 were discarded. Assays were also discarded if < 7 total worms moved into the scoring regions on one, or both, of the plates. Details on preparation of odorants, and diluents for each odorant, are described in Supplementary Table 1. Chemotaxis assays with odor from animal feces were performed essentially as described [15,17]. Gerbil, dog, rat, hamster, and rabbit feces were collected fresh the morning of assays from cage bottoms; possum feces were collected from uninfected *T. vulpecula* housed at La Trobe University in Melbourne, Australia and stored at -20°C until assays were performed.

Fecal dispersal assays

Fecal dispersal assays were performed as described [15]. Fresh fecal pellets were collected from cage bottoms on the morning of assays; gerbil feces were used for *S. stercoralis* and hamster feces were used for *A. ceylanicum*. A single ~0.03 g fecal pellet was placed in the center of a chemotaxis plate and 15-35 iL3s were pipetted onto the feces in $< 5 \mu\text{L}$ of dH₂O. The plates were left undisturbed for 1 hour on a vibration-insulating platform. The number of iL3s remaining on feces, off feces but in a 4-cm diameter area around the feces (zone 1), or off feces in a 4-cm diameter outermost area of the plate (zone 2) were counted (Fig. 3a). iL3s stuck to, and trapped, on plate walls were counted as part of zone 2. Since iL3s on the feces were not visible, the number of iL3s on feces was counted by subtracting the number of iL3s in zones 1 + 2 from the total number of iL3s placed at the beginning of the assay.

Nictation assay

Nictation assays were performed as described [15]. Briefly, PDMS molds with near-microscopic pillars were used to cast chips made from 4% agar dissolved in ddH₂O. Agar poured over the PDMS mold was allowed to solidify and the agar chip was then separated from the mold and placed at 37°C for 2 hours to dry. The agar chip was then cooled at room temperature for at least 1 hour before assays were performed. A 5 µL drop of dH₂O containing 10-20 iL3s was pipetted onto the center of the agar chip. Once the dH₂O dried, the iL3s were left for 10 minutes to acclimate to the agar chip. Individual iL3s were then observed for a 2-minute period on the agar chip. The near-microscopic pillars on the chip reduce the surface tension between the iL3 and the chip, thus allowing the iL3 to stand if desired. If at any point during the 2 minutes the iL3 raised at least half its body from the plate for at least 5 seconds, it was counted as nictating. The process was then repeated for other iL3s on the same agar chip.

CRISPR-Cas9-mediated targeted mutagenesis of *Ss-tax-4*

Targeted mutagenesis of the *S. stercoralis tax-4* gene (SSTP_0000981000) was performed as previously described using the same CRISPR target site [16,24]. *Ss-tax-4* was identified based on sequence homology with *C. elegans tax-4*; the *Ss-tax-4* gene was also predicted as an ortholog of *Ce-tax-4* on WormBase parasite [31]. The CRISPR target site and gRNA were selected using Geneious 9 software [69]. gRNA design parameters used for optimized CRISPR-Cas9 mutagenesis in *C. elegans* were similarly used for *S. stercoralis* [45,70]. The single guide RNA (sgRNA) expression construct targeting *Ss-tax-4* (pMLC47) was synthesized by GENEWIZ to include the 500-bp of the *S. ratti* U6 promoter and 277-bp of the *S. ratti* U6 3'UTR flanking the *Ss-tax-4* sgRNA. For homology-directed repair at *Ss-tax-4*, a construct (pEY11) was made by sub-cloning 539-bp 5' and 671-bp 3' homology arms flanking the *Ss-tax-4* CRISPR site into the *Ss-act-2::mRFPmars* vector pAJ50, which drives mRFPmars expression in the nematode body wall (Supplementary Figure 4) [24,64]. Cas9 endonuclease was expressed from the vector pPV540, in which *Strongyloides* codon-optimized Cas9 expression is driven by the *S. ratti eef-1A* promoter [24]. The pMLC47,

pEY11, and pPV540 vectors were mixed and microinjected into the syncytial gonad free-living adult females; F₁ iL3 progeny were screened for potential *Ss-tax-4* disruptions as described below. Microinjections were either done at 100 ng/μL or 200 ng/μL total DNA using the following recipes: 60 ng/μL pMLC47, 20 ng/μL pEY11, and 20 ng/μL pPV540; or 80 ng/μL pMLC47, 80 ng/μL pEY11, and 40 ng/μL pPV540. No-Cas9 control injections were performed using the same recipe, but with pPV540 omitted from the mix. Primers used to amplify the *Ss-tax-4* homology arms from *S. stercoralis* gDNA can be found in Supplementary Table 3. Gene structure diagrams for *C. elegans* and *S. stercoralis tax-4* (Supplementary Figure 4), were generated with Exon-Intron Graphic Maker (Version 4, www.wormweb.org).

Microinjection of *S. stercoralis*

Microinjection of syncytial gonads of *S. stercoralis* free-living adult females was performed using standard methods from *C. elegans* and *Strongyloides* species, with modifications [24,64,71]. Briefly, microinjected females were recovered from injection slides and transferred to 6-cm 2% NGM plates seeded with OP50; free-living males were added to the plate for mating. After a minimum recovery time of 30 minutes on NGM, the plate was flooded with dH₂O and all worms were pipetted to 6-cm fecal-charcoal plates made with fresh gerbil feces from uninfected animals, collected as described above. Fecal-charcoal cultures were maintained at 23°C for 6-14 days to collect F₁ iL3s.

Selection of *Ss-tax-4* iL3s

iL3 progeny from microinjected females were recovered by Baermann apparatus and stored in ~ 2 mL of BU in a watch glass. To screen for *mRFPmars* expression, ~15-20 μL of iL3s in BU (~100 worms) were pipetted onto a 6-cm 2% NGM plate seeded with OP50. Freely crawling iL3s were screened for *mRFPmars* expression under a Leica M165 FC microscope. *mRFPmars* expressing iL3s were picked into a small watch glass for storage prior to assays. The fluorescent iL3s collected for behavioral experiments and subsequent genotyping were selected based on “integrated-like” expression of *mRFPmars* along the full body wall of the iL3. iL3s with patchy or faint *mRFPmars* expression were not collected, as these iL3s were

unlikely to have CRISPR-Cas9-mediated HDR at the target, as described in Gang *et al.* 2017 [24]. A summary of free-living adult microinjections, and iL3 screening, for *Ss-tax-4* can be found in Supplementary Table 4.

Single iL3 odorant chemotaxis assays

Wild-type, no-Cas9 control, or *Ss-tax-4* iL3s were stored in BU in a small watch glass prior to chemotaxis assays. A single iL3 was pipetted in 2 μ L of BU from the watch glass and transferred to the center of a 9-cm chemotaxis plate without odor. The iL3 was acclimated to chemotaxis plate for 10 minutes prior to the odor assay. During the acclimation period, the iL3 was allowed to crawl freely on the agar surface. To account for any damage done to the animal during Baermann collection, *mRFPmars* screening, or pipetting, the iL3 had to crawl out of a 2-cm diameter circle in the center of the acclimation plate; any iL3 that failed to leave the 2-cm circle during the 10-minute acclimation period was discarded. iL3s that successfully navigated out of the 2-cm circle were collected at the end of the acclimation period and transferred in \sim 2 μ L ddH₂O to the center of a 5-cm odor-chemotaxis arena drawn on a fresh 9-cm chemotaxis plate. 5 μ L of a 10⁻¹ dilution of 3-methyl-1-butanol, or 5 μ L if paraffin oil, was placed 1-cm away from the iL3 on each side (as shown in Fig. 4 and Supplementary Figure 2). The plate was then placed on top of two light diffusers arranged orthogonally on a raised plexiglass surface. The imaging surface was bottom-illuminated with a white LED box covered with a red-light filter. The entire imaging setup was placed in an opaque enclosure with the LED box as the only light source. Imaging was started immediately as the dH₂O drop containing the iL3 dried. iL3 movements were monitored with a 5 mega-pixel CMOS camera (BTE-B050-U, Mightex Systems) suspended above the chemotaxis plate. Images were collected by triggering TTL pulses with a USB DAQ device (U3-LV, LabJack Corp) using custom MATLAB script (Mathworks) [16]. Images were collected for 6 minutes at 0.5 frames/second, or until the iL3 left the 5-cm arena. Any recordings where the iL3 did not move for at least 60 seconds were discarded. iL3s were then recovered from the assay plate for single iL3 genotyping, as described below. The trajectories of iL3s in the odorant arena were measured in Fiji using the

Manual Tracking plugin. Custom MATLAB scripts were used to translate x/y coordinates into the tracks shown in Fig. 4 and Supplementary Figure 2. The MATLAB scripts also calculated mean speed for each iL3 tested [16]. To calculate odorant responses, 1-cm diameter circle was drawn around the center of the odorant placement point in FIJI. Any iL3 that entered the 1-cm scoring area was counted as responsive to that odorant. To account for directional bias, the location of the odorant stimulus was alternated between the left and right scoring regions for each assay. For presentation purposes, half of tracks shown in Fig. 4 and Supplementary Figure 2. were flipped 180° to show the odorant in the same orientation.

***In vitro* activation assays**

In vitro activation assays for skin-penetrating iL3s were performed as described, with modifications [21]. For *S. stercoralis*, *S. ratti*, and *P. trichosuri* iL3 population assays shown in Fig. 5c and Supplementary Figure 3. iL3s were collected by Baermann apparatus, washed 3 times in BU, and pelleted by centrifugation. Pelleted iL3s were then resuspended in 10 mL of BU supplemented with 100 µL of 100x Penicillin-Streptomycin (10,000 U/mL, Gibco 15140-122) 100 µL of 100x Amphotericin B (250 µg/mL, Gibco 15290-018), and 10 µL of 1000x Tetracycline hydrochloride dissolved in ddH₂O (5 mg/mL, Sigma-Aldrich T7660-5G). iL3s were axenized for 3 hours in the antibiotic solution, in the dark, at room temperature. The iL3s were then pelleted by centrifugation and the supernatant was removed. 5 µL of the pellet containing ~100-200 iL3s was then transferred to one well of a 96-well plate containing 100 µL DMEM. Typically, iL3s were aliquoted to 6-12 wells containing DMEM, per condition, per assay. The 96-well plate was then transferred to a tissue culture incubator set to the desired experimental conditions (37°C and 5% CO₂, 25°C and 5% CO₂, or 37°C and 0% CO₂). iL3s were incubated for 21 hours, after which 2.5 µL of fluorescein isothiocyanate (FITC, 20mg/mL in N,N-dimethylformamide, Acros organics 119252500) was added to each well. The iL3s were then returned to the culture conditions for 3 hours. Wells containing iL3s were then pipetted into a 15 mL conical tube and filled with BU solution. The iL3s were washed 5 times with BU to remove excess FITC on the outer cuticle of the worms. The iL3s were then transferred to a

chemotaxis plate and paralyzed by applying 1% nicotine solution diluted in ddH₂O. The iL3s were screened for FITC ingested in the nematode pharynx, indicating resumption of feeding behavior and exit from the iL3 stage, under a Leica M165 FC microscope. The percentage of activated iL3s was calculated as: (# FITC-positive activated iL3s) / (total # iL3s scored). For *in vitro* activation assays on single iL3s, as shown in Fig. 5d, the procedure was modified such that each iL3 was axenized in 100 μ L of BU + antibiotics in its own well in a 96-well plate. Each iL3 was then pipetted into its own well containing 100 μ L of DMEM and was incubated as described above. Each iL3 recovered from incubation and FITC staining was washed by pipetting up-and-down in a watch glass filled with \sim 2 mL dH₂O. The iL3s were then transferred to a chemotaxis plate, scored for activation, and collected for gDNA isolation as described below.

Media preparation for *in vitro* activation assays

To assess the requirements of 37°C temperature and 5% CO₂ atmosphere for iL3 activation, shown in Fig. 5c and Supplementary Figure 3, we prepared DMEM without sodium bicarbonate to ensure that the only source of CO₂ or HCO₃⁻ was supplied by the tissue culture incubator. To prepare sodium bicarbonate-free DMEM, we added 0.4044 g DMEM powder (4.5 g/L glucose, L-glutamine & sodium pyruvate without sodium bicarbonate, Corning 50-003-PB) to 30 mL of ddH₂O. 300 μ L of Pen-Strep, 300 μ L of Amphotericin B, and 30 μ L of Tetracycline-HCl was added, as described above, to inhibit growth of bacteria transferred with iL3s from fecal charcoal plates. As an alternative buffering agent to sodium bicarbonate, 0.1788g HEPES (25 mM final concentration, Fisher BP310-100) was added to the solution. For 37°C and 5% CO₂, and 37°C and 5% CO₂ assay conditions, the room temperature pH was titrated to \sim 8.0 with 5M NaOH. For the 37°C and 0% CO₂ condition, the room temperature pH was titrated to \sim 7.0 and 2M sodium gluconate was added to balance the molar ratio of Na⁺ with the 5% CO₂ conditions. The DMEM solutions were filter sterilized through a 0.22 μ m membrane (Millipore Millex-GV SLGV033RS) connected to a Luer-lok syringe into a sterile 50 mL conical tube. 100 μ L aliquots were then pipetted into individual wells of 96-well plate as

described above. The 96-well plate was incubated in the desired heat and % CO₂ for at least 1 hour. Following 1 hour of incubation, the pH of the media was checked to ensure pH ~7.0 prior to adding iL3s for overnight incubation. For single iL3 assays tested in the 37°C and 5% CO₂, standard DMEM media with sodium bicarbonate was used (4.5 g/L glucose, L-glutamine & sodium pyruvate, Corning 10-013-CV).

Single iL3 genotyping

To extract genomic DNA from individual *S. stercoralis* iL3s we followed the previously described procedure[24]. A single iL3 was transferred to a PCR tube containing 5-6 µL of nematode lysis buffer (50 mM KCl, 10 mM Tris pH 8, 2.5 mM MgCl₂, 0.45% Nonidet-P40, 0.45% Tween-20, 0.01% gelatin in dH₂O) supplemented with ~0.12 µg/µL Proteinase-K and ~1.7% 2-mercaptoethanol. Tubes were placed at -80°C for at least 20 min, then transferred to a thermocycler for digestion: 65°C (2 h), 95°C (15 min), 10°C (hold). For long term storage, iL3s were left iL3s undigested at -80°C and thermocycler digestion was performed the day of PCR genotyping. To genotype wild-type iL3s, *Ss-tax-4* no-Cas9 control, or CRISPR-Cas9-mediated disruptions of *Ss-tax-4*, PCR reactions were performed with GoTaq G2 Flexi DNA Polymerase (Promega, Cat. # M7801) or Herculase II Fusion DNA Polymerase (Agilent Cat. # 600675) using the following thermocycler conditions: denature 95°C (2 min); PCR 95°C (30 s), 55°C (30 s), 72°C (1 min) x 35 cycles; final extension 72°C (5 min); 10°C (hold). The 5-6 µL single iL3 gDNA preparation was split evenly across control, wild-type locus, 5' integration, and 3' integration reactions, as shown in Supplementary Figure 4. Primer sets used for *Ss-tax-4* genotyping can be found in Supplementary Table 3.

Fluorescent microscopy

Fluorescent microscopy was performed essentially as described [16,24]. Activated iL3s shown in Fig. 5 were collected from chemotaxis plates, described above, and were pipetted onto a 5% Noble agar pad dissolved in ddH₂O. The slide was mounted under a Zeiss Axiomager A2 microscope and epifluorescence images were taken with a Zeiss AxioCam camera. Images were processed using Zeiss AxioVision software.

References

1. Boatman BA, Basanez MG, Prichard RK, Awadzi K, Barakat RM, Garcia HH, et al. A research agenda for helminth diseases of humans: towards control and elimination. *PLoS Negl Trop Dis*. 2012;6(4):e1547.
2. Pullan RL, Smith JL, Jasrasaria R, Brooker SJ. Global numbers of infection and disease burden of soil transmitted helminth infections in 2010. *Parasit Vectors*. 2014;7:37.
3. Schafer TW, Skopic A. Parasites of the small intestine. *Curr Gastroenterol Rep*. 2006;8(4):312-20.
4. Nutman TB. Human infection with *Strongyloides stercoralis* and other related *Strongyloides* species. *Parasitology*. 2017;144(3):263-73.
5. Grover JK, Vats V, Uppal G, Yadav S. Anthelmintics: a review. *Trop Gastroenterol*. 2001;22(4):180-9.
6. Holden-Dye L, Walker RJ. Anthelmintic drugs. *WormBook*. 2007:1-13.
7. Kaplan RM. Drug resistance in nematodes of veterinary importance: a status report. *Trends Parasitol*. 2004;20(10):477-81.
8. Gang SS, Hallem EA. Mechanisms of host seeking by parasitic nematodes. *Mol Biochem Parasitol*. 2016;208(1):23-32.
9. Haley AJ. Biology of the rat nematode *Nippostrongylus brasiliensis* (Travassos, 1914). I. Systematics, hosts and geographic distribution. *J Parasitol*. 1961;47:727-32.
10. Viney ME, Lok JB. The biology of *Strongyloides* spp. In *WormBook*, www.wormbook.org 2015:1-17.
11. Viney M, Kikuchi T. *Strongyloides ratti* and *S. venezuelensis* - rodent models of *Strongyloides* infection. *Parasitology*. 2017;144(3):285-94.
12. Nolan TJ, Zhu X, Ketschek A, Cole J, Grant W, Lok JB, et al. The sugar glider (*Petaurus breviceps*): a laboratory host for the nematode *Parastrongyloides trichosuri*. *J Parasitol*. 2007;93(5):1084-9.
13. Traub RJ. *Ancylostoma ceylanicum*, a re-emerging but neglected parasitic zoonosis. *Int J Parasitol*. 2013;43(12-13):1009-15.
14. Ashton FT, Li J, Schad GA. Chemo- and thermosensory neurons: structure and function in animal parasitic nematodes. *Vet Parasitol*. 1999;84(3-4):297-316.
15. Ruiz F, Castelletto ML, Gang SS, Hallem EA. Experience-dependent olfactory behaviors of the parasitic nematode *Heligmosomoides polygyrus*. *PLoS Pathog*. 2017;13(11):e1006709.
16. Bryant AS, Ruiz F, Gang SS, Castelletto ML, Lopez JB, Hallem EA. A critical role for thermosensation in host seeking by skin-penetrating nematodes. *Curr Biol*. 2018;28(14):2338-47 e6.
17. Castelletto ML, Gang SS, Okubo RP, Tselikova AA, Nolan TJ, Platzer EG, et al. Diverse host-seeking behaviors of skin-penetrating nematodes. *PLoS Pathog*. 2014;10(8):e1004305.

18. Hawdon JM, Schad GA. Serum-stimulated feeding in vitro by third-stage infective larvae of the canine hookworm *Ancylostoma caninum*. J Parasitol. 1990;76(3):394-8.
19. Hawdon JM, Volk SW, Pritchard DI, Schad GA. Resumption of feeding in vitro by hookworm third-stage larvae: a comparative study. J Parasitol. 1992;78(6):1036-40.
20. Hawdon JM, Schad GA. *Ancylostoma caninum*: reduced glutathione stimulates feeding by third-stage infective larvae. Exp Parasitol. 1992;75(1):40-6.
21. Ashton FT, Zhu X, Boston R, Lok JB, Schad GA. *Strongyloides stercoralis*: Amphidial neuron pair ASJ triggers significant resumption of development by infective larvae under host-mimicking in vitro conditions. Exp Parasitol. 2007;115(1):92-7.
22. Lok JB. *Strongyloides stercoralis*: a model for translational research on parasitic nematode biology. 2007;In WormBook, www.wormbook.org.
23. Lok JB, Shao H, Massey HC, Li X. Transgenesis in *Strongyloides* and related parasitic nematodes: historical perspectives, current functional genomic applications and progress towards gene disruption and editing. Parasitology. 2017;144(3):327-42.
24. Gang SS, Castelletto ML, Bryant AS, Yang E, Mancuso N, Lopez JB, et al. Targeted mutagenesis in a human-parasitic nematode. PLoS Pathog. 2017;13(10):e1006675.
25. Meijerink J, Braks MAH, Brack AA, Adam W, Dekker T, Posthumus MA, et al. Identification of olfactory stimulants for *Anopheles gambiae* from human sweat samples. J Chem Ecol. 2000;26(6):1367-82.
26. Garner CE, Smith S, de Lacy Costello B, White P, Spencer R, Probert CS, et al. Volatile organic compounds from feces and their potential for diagnosis of gastrointestinal disease. FASEB J. 2007;21(8):1675-88.
27. Verhulst NO, Beijlveld H, Knols BG, Takken W, Schraa G, Bouwmeester HJ, et al. Cultured skin microbiota attracts malaria mosquitoes. Malar J. 2009;8:302.
28. Tait E, Perry JD, Stanforth SP, Dean JR. Use of volatile compounds as a diagnostic tool for the detection of pathogenic bacteria. TrAC Trends in Analytical Chemistry. 2014;53:117-25.
29. Hotez P, Hawdon J, Schad GA. Hookworm larval infectivity, arrest and amphiparatensis: the *Caenorhabditis elegans* Daf-c paradigm. Parasitol Today. 1993;9(1):23-6.
30. Grant WN, Stasiuk S, Newton-Howes J, Ralston M, Bisset SA, Heath DD, et al. *Parastrongyloides trichosuri*, a nematode parasite of mammals that is uniquely suited to genetic analysis. Int J Parasitol. 2006;36(4):453-66.
31. Hunt VL, Tsai IJ, Coghlan A, Reid AJ, Holroyd N, Foth BJ, et al. The genomic basis of parasitism in the *Strongyloides* clade of nematodes. Nat Genet. 2016;48(3):299-307.
32. Hu PJ. Dauer. WormBook. 2007:1-19.
33. Hammer Ø HD, Ryan PD. PAST: Paleontological statistics software package for education and data analysis. Palaeontol Electronica. 2001;4: 9pp.

34. Bartsch SM, Hotez PJ, Asti L, Zapf KM, Bottazzi ME, Diemert DJ, et al. The Global Economic and Health Burden of Human Hookworm Infection. *PLoS Negl Trop Dis*. 2016;10(9):e0004922.
35. Schar F, Trostorf U, Giardina F, Khieu V, Muth S, Marti H, et al. *Strongyloides stercoralis*: Global Distribution and Risk Factors. *PLoS Negl Trop Dis*. 2013;7(7):e2288.
36. Nolan TJ, Megyeri Z, Bhopale VM, Schad GA. *Strongyloides stercoralis*: the first rodent model for uncomplicated and hyperinfective strongyloidiasis, the Mongolian gerbil (*Meriones unguiculatus*). *J Infect Dis*. 1993;168(6):1479-84.
37. Garside P, Behnke JM. *Ancylostoma ceylanicum* in the hamster: observations on the host-parasite relationship during primary infection. *Parasitology*. 1989;98 Pt 2:283-9.
38. Ward JD. Rendering the intractable more tractable: tools from *Caenorhabditis elegans* ripe for import into parasitic nematodes. *Genetics*. 2015;201(4):1279-94.
39. Bargmann CI, Hartweg E, Horvitz HR. Odorant-selective genes and neurons mediate olfaction in *C. elegans*. *Cell*. 1993;74(3):515-27.
40. Bargmann CI. Chemosensation in *C. elegans*. *WormBook*. 2006:1-29.
41. Haas W, Haberl B, Syafruddin, Idris I, Kallert D, Kersten S, et al. Behavioural strategies used by the hookworms *Necator americanus* and *Ancylostoma duodenale* to find, recognize and invade the human host. *Parasitol Res*. 2005;95(1):30-9.
42. Landmann JK, Prociv P. Experimental human infection with the dog hookworm, *Ancylostoma caninum*. *Med J Aust*. 2003;178(2):69-71.
43. Chalasani SH, Chronis N, Tsunozaki M, Gray JM, Ramot D, Goodman MB, et al. Dissecting a circuit for olfactory behaviour in *Caenorhabditis elegans*. *Nature*. 2007;450(7166):63-70.
44. Ashton FT, Bhopale VM, Fine AE, Schad GA. Sensory neuroanatomy of a skin-penetrating nematode parasite: *Strongyloides stercoralis*. I. Amphidial neurons. *J Comp Neurol*. 1995;357(2):281-95.
45. Doench JG, Hartenian E, Graham DB, Tothova Z, Hegde M, Smith I, et al. Rational design of highly active sgRNAs for CRISPR-Cas9-mediated gene inactivation. *Nat Biotechnol*. 2014;32(12):1262-7.
46. Goetz N, Kaba G, Good D, Hussler G, Bore P. Detection and identification of volatile compounds evolved from human hair and scalp using headspace gas chromatography. *J Soc Cosmet Chem*. 1988;39:1-13.
47. Arnould C, Malosse C, Signoret J, Descoins C. Which chemical constituents from dog feces are involved in its food repellent effect in sheep? *J Chem Ecol*. 1998;24(3):559-76.
48. Goodrich BS, Hesterman ER, Shaw KS, Mykytowycz R. Identification of some volatile compounds in the odor of fecal pellets of the rabbit. *J Chem Ecol*. 1981;7(5):817-27.
49. Ponmanickam P, Palanivelu K, Govindaraj S, Baburajendran R, Habara Y, Archunan G. Identification of testosterone-dependent volatile compounds and proteins in the preputial gland of rat *Rattus norvegicus*. *Gen Comp Endocrinol*. 2010;167(1):35-43.

50. Nicolaides N. Skin Lipids. IV. Biochemistry and Function. J Am Oil Chem Soc. 1965;42:708-12.
51. Smallegange RC, BukovinszkinÉ-Kiss G, Otieno B, Mbadi PA, Takken W, Mukabana WR, et al. Identification of candidate volatiles that affect the behavioural response of the malaria mosquito *Anopheles gambiae* sensu stricto to an active kairomone blend: laboratory and semi-field assays. Physiological Entomology. 2012;37(1):60-71.
52. Ara K, Hama M, Akiba S, Koike K, Okisaka K, Hagura T, et al. Foot odor due to microbial metabolism and its control. Can J Microbiol. 2006;52(4):357-64.
53. Caroprese A, Gabbanini S, Beltramini C, Lucchi E, Valgimigli L. HS-SPME-GC-MS analysis of body odor to test the efficacy of foot deodorant formulations. Skin Res Technol. 2009;15(4):503-10.
54. Cork A, Park KC. Identification of electrophysiologically-active compounds for the malaria mosquito, *Anopheles gambiae*, in human sweat extracts. Med Vet Entomol. 1996;10(3):269-76.
55. Bernier UR, Kline DL, Barnard DR, Schreck CE, Yost RA. Analysis of human skin emanations by gas chromatography/mass spectrometry. 2. Identification of volatile compounds that are candidate attractants for the yellow fever mosquito (*Aedes aegypti*). Anal Chem. 2000;72(4):747-56.
56. Gallagher M, Wysocki CJ, Leyden JJ, Spielman AI, Sun X, Preti G. Analyses of volatile organic compounds from human skin. Br J Dermatol. 2008;159(4):780-91.
57. Phillips M, Herrera J, Krishnan S, Zain M, Greenberg J, Cataneo RN. Variation in volatile organic compounds in the breath of normal humans. J Chromatogr B Biomed Sci Appl. 1999;729(1-2):75-88.
58. Wahl HG, Hoffmann A, Luft D, Liebich HM. Analysis of volatile organic compounds in human urine by headspace gas chromatography-mass spectrometry with a multipurpose sampler. J Chromatogr A. 1999;847(1-2):117-25.
59. Moore JG, Jessop LD, Osborne DN. Gas-chromatographic and mass-spectrometric analysis of the odor of human feces. Gastroenterology. 1987;93(6):1321-9.
60. Zhang JX, Sun L, Zhang JH, Feng ZY. Sex- and gonad-affecting scent compounds and 3 male pheromones in the rat. Chem Senses. 2008;33(7):611-21.
61. Syed Z, Leal WS. Acute olfactory response of *Culex* mosquitoes to a human- and bird-derived attractant. Proc Natl Acad Sci U S A. 2009;106(44):18803-8.
62. Mochalski P, King J, Klieber M, Unterkofler K, Hinterhuber H, Baumann M, et al. Blood and breath levels of selected volatile organic compounds in healthy volunteers. Analyst. 2013;138(7):2134-45.
63. Shao H, Li X, Nolan TJ, Massey HC, Jr., Pearce EJ, Lok JB. Transposon-mediated chromosomal integration of transgenes in the parasitic nematode *Strongyloides ratti* and establishment of stable transgenic lines. PLoS Pathog. 2012;8(8):e1002871.
64. Junio AB, Li X, Massey HC, Jr., Nolan TJ, Todd Lamitina S, Sundaram MV, et al. *Strongyloides stercoralis*: cell- and tissue-specific transgene expression and co-

transformation with vector constructs incorporating a common multifunctional 3' UTR. *Exp Parasitol.* 2008;118(2):253-65.

65. Stasiuk SJ, Scott MJ, Grant WN. Developmental plasticity and the evolution of parasitism in an unusual nematode, *Parastrongyloides trichosuri*. *Evodevo.* 2012;3(1):1.

66. Brenner S. The genetics of *Caenorhabditis elegans*. *Genetics.* 1974;77(1):71-94.

67. Karp X. Working with dauer larvae. *WormBook.* 2018:1-19.

68. Wolkow CA, Hall DH. Dauer Neuroanatomy. *WormAtlas.* 2012.

69. Kearse M, Moir R, Wilson A, Stones-Havas S, Cheung M, Sturrock S, et al. Geneious Basic: an integrated and extendable desktop software platform for the organization and analysis of sequence data. *Bioinformatics.* 2012;28(12):1647-9.

70. Farboud B, Meyer BJ. Dramatic enhancement of genome editing by CRISPR/Cas9 through improved guide RNA design. *Genetics.* 2015;199(4):959-71.

71. Mello C, Fire A. DNA transformation. *Methods Cell Biol.* 1995;48:451-82.

Chapter 7

Conclusions and future work

Conclusions:

Locating a host in the environment, and successfully establishing an infection inside the host, are essential for the survival of skin-penetrating iL3s. However, the cellular and molecular processes promoting host-seeking and host-infection behaviors are not well characterized. Over the course of these studies, we have rigorously examined the unstimulated motility, thermosensory, and chemosensory-driven behaviors of skin-penetrating nematode species to better understand how these medically important parasites target mammalian hosts. We have demonstrated that parasitic nematodes with different infection modes have unique strategies for targeting their natural hosts. Importantly, our studies comparing the chemosensory behaviors of the skin-penetrating, human-infective, threadworm *S. stercoralis* and hookworm *A. ceylanicum* have revealed distinct mechanism that each species may employ to target humans. Such information could help inform public health strategies for preventing and controlling both hookworm and threadworm infections. To gain insight into the molecular mechanisms underlying the behaviors of skin-penetrating iL3s, we developed CRISPR-Cas9 mutagenesis in human-parasitic *S. stercoralis*. Our implementation of CRISPR-Cas9 is the first described method for using reverse genetics to generate phenotypes in parasitic nematodes, and thus represents a critical advance in understanding parasitic nematode biology. We used CRISPR-Cas9 to generate *S. stercoralis* iL3s with sensory deficiencies by targeting the *Ss-tax-4* gene. We found that *Ss-tax-4* iL3s are unable to engage in thermosensory and chemosensory-driven host-seeking behaviors. Similarly, *Ss-tax-4* iL3s were unable to properly resume development upon entering host-like culture conditions. Together, these results demonstrate that sensory perception is vital for the parasitic lifestyles of skin-penetrating iL3s. In the future, our results may open the door for the development of novel approaches for preventative intervention of parasitic nematode infections. By inhibiting sensory-driven host seeking, or development inside the host, it may be possible to block iL3 infectivity without the need for drug-based anthelmintic therapies.

Follow-up experiments and future work:

Dissecting sensory neural circuits required for host seeking and host infection

Over the course of this study, we have implicated *Ss-tax-4*-dependent pathways as important sensory mechanisms for iL3 behaviors. Reporter-based experiments have shown that *Ss-tax-4* is expressed in a large set of *S. stercoralis* sensory neurons that respond to thermal and chemical cues [1]. However, the neural circuits that detect individual sensory cues have yet to be clearly defined in any skin-penetrating nematode species. One remaining question is how functionally conserved sensory microcircuits are across nematode species. To answer this question, we are in the process of leveraging known sensory circuit information from the model nematode *C. elegans* to examine if similar circuits exist in *S. stercoralis*. Because sensory neuroanatomy is largely conserved across *C. elegans* and *S. stercoralis*, we are testing the hypothesis that sensory neurons in similar anatomical positions might respond to similar sensory cues, and that these responses may have evolved to mediate parasite-specific behaviors in skin-penetrating iL3s [2].

In a preliminary investigation, we have asked how well-conserved CO₂ perception is across *C. elegans* and *S. stercoralis*. In *C. elegans*, adult nematodes are repelled by CO₂ while dauers are attracted to CO₂. *C. elegans* is known to detect CO₂ through a receptor guanylate cyclase GCY-9 specifically expressed in BAG sensory neurons; ablation of BAG neurons, or disruption of the *gcy-9* gene, eliminates CO₂ response in *C. elegans* [3,4]. Our results show that *S. stercoralis* iL3s are repelled by CO₂ in a dose-dependent manner, suggesting that CO₂-detecting chemosensory mechanisms are also present in parasitic nematodes [5]. We identified a *gcy-9* homolog in *S. stercoralis*, and a *Ss-gcy-9::GFP* reporter construct revealed that *Ss-gcy-9* is expressed in one pair of sensory neurons in roughly the same anatomical position as the *C. elegans* BAG neurons (Fig. 1a). We generated a *Ss-gcy-9::GCaMP3* reporter construct and observed CO₂-evoked BAG activity in *S. stercoralis* iL3s that was similar to the BAG response in *C. elegans* (Fig. 1b,c). Excitingly, to our knowledge, these results represent the first *in vivo* neural imaging from a parasitic nematode

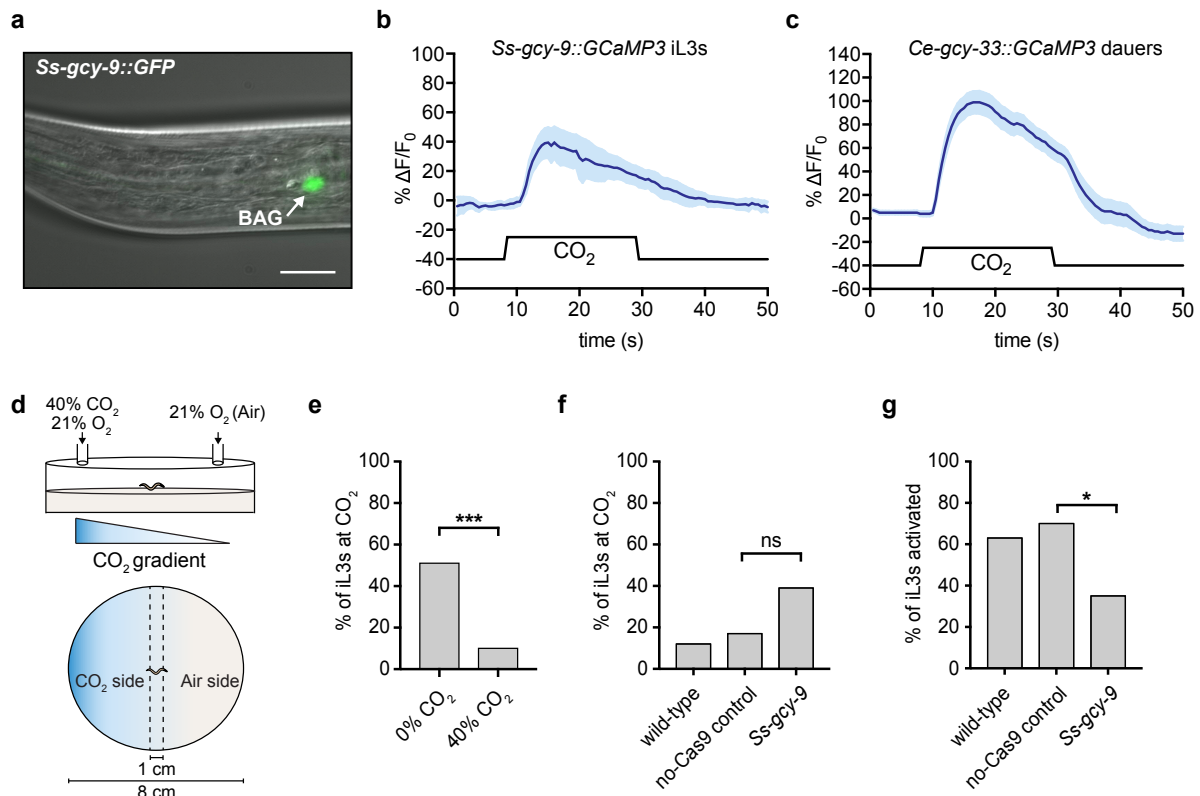


Fig 1. The *S. stercoralis gcy-9* gene may be required for detection of CO₂. **a** *Ss-gcy-9_p::GFP* is expressed in the putative BAG sensory neurons of an *S. stercoralis* larva. Scale bar = 10 μ m. **b,c** *S. stercoralis* iL3s expressing *Ss-gcy-9_p::GCaMP3* in putative BAG neurons (**b**) and *C. elegans* dauers expressing *Ce-gcy-33_p::GCaMP3* in BAG neurons (**c**) respond to CO₂. Graphs show calcium responses to a 10% CO₂ stimulus. Solid blue lines indicate the average calcium responses; light blue shading represents SEMs. Black lines indicate the CO₂ pulse. *n* = 5 for *S. stercoralis*; 19 for *C. elegans*. **d** Schematic of a CO₂ assay for iL3s. Populations or individual iL3s were placed at the center of an 8 cm agar plate. A CO₂ gradient was established by delivering 40% CO₂ or 21% O₂ (air) through holes in the lid on each side of the plate. The iL3s were allowed to crawl in the gradient for 10 minutes. At the end of the assay iL3s were scored as crawling on the CO₂ or air side of the plate. iL3s that failed to leave a 1 cm width area in the center of the plate were not counted. The CO₂ side was flipped for each assay to establish a gradient in the opposite direction. **e** Populations of wild-type *S. stercoralis* iL3s are repelled by CO₂. 0% CO₂ = both sides of the plate received air input only; wild-type iL3s show no preference for the air side or “CO₂ side” of the plate. 40% CO₂ = a 40% CO₂ gradient was established as shown in **d**; wild-type iL3s are repelled by CO₂ relative to the air-only condition. ****P* < 0.001, *n* = 69-84 iL3s for each condition; Fisher’s exact test. **f** *Ss-gcy-9* iL3s may not be repelled by CO₂. However, a large enough data set has not yet been collected to determine this conclusively. **g** *Ss-gcy-9* iL3s may show decreased ability to activate in host-like conditions. However, a large enough data set has not yet been collected to determine this conclusively.

and suggest that interrogation of other sensory neural circuits involved in parasitic behaviors may be feasible. Our results also indicate that, at the sensory neuron level, BAG responses are conserved across *C. elegans* and *S. stercoralis*. In *C. elegans* the downstream interneurons that regulate CO₂ response are well characterized [6]. However, neural imaging

from the interneurons of parasitic nematodes has not been performed. Given that *S. stercoralis* iL3s are repelled by CO₂ while *C. elegans* dauers are attracted to CO₂, it will be interesting to determine if the CO₂ microcircuit has been altered downstream of BAG to mediate parasitic-specific behaviors in iL3s, or if CO₂ detection represents a conserved circuit across species.

To ask if *Ss-gcy-9* is required for the CO₂-dependent behaviors of iL3s, we used CRISPR-Cas9 to disrupt *Ss-gcy-9* [7]. While our results are very preliminary, it appears *Ss-gcy-9* may be important for CO₂-induced repulsion for iL3s in the environment (Fig. 1d-f). In addition, perception of CO₂ via *Ss-gcy-9* may also be required for iL3 activation, as *Ss-gcy-9* iL3s show reduced activation rates relative to control iL3s (Fig. 1g). CO₂ detection as a necessary component of activation is consistent with results describe in Chapter 6 of this thesis. Thus, CO₂ likely represent a critical cue for iL3 development inside the host. If this response is *Ss-gcy-9* dependent, inhibition of *Ss-gcy-9* activity could serve as one method for preventing *S. stercoralis* infections. The microcircuits for thermosensory and olfactory behaviors in *C. elegans* are also well described [8,9]. In the future, a similar strategy described for dissecting the *S. stercoralis* BAG-dependent CO₂ response will be applied for dissecting sensory neural circuits required for thermosensory and olfactory-driven host seeking behaviors described in Chapters 5 and 6.

Interrogation of additional sensory cues detected by iL3s

The thermosensory and olfactory behaviors of iL3s describe here only represent a portion of the environmental cues that may be important for host-seeking behavior. *C. elegans* is known to respond to cations and anions, pheromones, light, humidity, and vibrational stimuli [10]. *C. elegans* has dedicated sensory pathways for gustatory chemotaxis, mechanosensory-driven taxis, phototaxis, and hygrotaxis; some of these behaviors have been observed in parasitic nematodes as well [11]. However, how each of these distinct sensory modalities is involved in the host-seeking behaviors of skin-penetrating iL3s has not been thoroughly explored. Furthermore, which combinations of sensory cues are sufficient to initiate skin penetration, and how these signals are perceived by iL3s, remains unclear. By interrogating

the sensory microcircuits required for these other behaviors we may be able to identify key host factors that allow each skin-penetrating nematode species to differentiate a permissive host from another non-host animal. These studies may also reveal additional insight into how iL3s navigate in the environment, for example, how the activity of iL3s changes on diurnal timescales, or how sensory perception is modulated as environmental conditions change.

Implications for other helminths

Skin-penetrating nematodes represent only a portion of human helminth infections. Together, soil-transmitted helminths, filarial nematodes, schistosomes, and other helminths infect billions worldwide [12]. Traditionally, genetic intervention in these important parasites has been difficult [13]. However, the CRISPR-Cas9 system has been revolutionary for targeted mutagenesis in many model and non-model organisms [14]. Here, we have described a significant advancement in better understanding helminths by developing CRISPR-Cas9 approaches in *S. stercoralis*. Our approach demonstrates that CRISPR-Cas9 machinery is functional in parasitic worms and expands on preliminary evidence, also conducted in *Strongyloides*, that targeted mutagenesis is possible in helminth parasites [15]. In the future, with additional technical development, the expansive CRISPR toolkit may be similarly implementable in other helminths. Such advancements would revolutionize our ability to combat the widespread neglected tropical diseases caused by helminth infections.

References

1. Bryant AS, Ruiz F, Gang SS, Castelletto ML, Lopez JB, Hallem EA. A critical role for thermosensation in host seeking by skin-penetrating nematodes. *Curr Biol*. 2018;28(14):2338-47 e6.
2. Ashton FT, Bhopale VM, Fine AE, Schad GA. Sensory neuroanatomy of a skin-penetrating nematode parasite: *Strongyloides stercoralis*. I. Amphidial neurons. *J Comp Neurol*. 1995;357(2):281-95.
3. Hallem EA, Sternberg PW. Acute carbon dioxide avoidance in *Caenorhabditis elegans*. *Proc Natl Acad Sci U S A*. 2008;105(23):8038-43.
4. Hallem EA, Spencer WC, McWhirter RD, Zeller G, Henz SR, Ratsch G, et al. Receptor-type guanylate cyclase is required for carbon dioxide sensation by *Caenorhabditis elegans*. *Proc Natl Acad Sci U S A*. 2011;108(1):254-9.
5. Castelletto ML, Gang SS, Okubo RP, Tselikova AA, Nolan TJ, Platzer EG, et al. Diverse host-seeking behaviors of skin-penetrating nematodes. *PLoS Pathog*. 2014;10(8):e1004305.
6. Guillermin ML, Carrillo MA, Hallem EA. A Single Set of Interneurons Drives Opposite Behaviors in *C. elegans*. *Curr Biol*. 2017;27(17):2630-9 e6.
7. Gang SS, Castelletto ML, Bryant AS, Yang E, Mancuso N, Lopez JB, et al. Targeted mutagenesis in a human-parasitic nematode. *PLoS Pathog*. 2017;13(10):e1006675.
8. Aoki I, Mori I. Molecular biology of thermosensory transduction in *C. elegans*. *Curr Opin Neurobiol*. 2015;34:117-24.
9. Hart AC, Chao MY. From Odors to Behaviors in *Caenorhabditis elegans*. In: Menini A, editor. *The Neurobiology of Olfaction*. Frontiers in Neuroscience. Boca Raton (FL)2010.
10. Bargmann CI. Chemosensation in *C. elegans*. *WormBook*. 2006:1-29.
11. Gang SS, Hallem EA. Mechanisms of host seeking by parasitic nematodes. *Mol Biochem Parasitol*. 2016;208(1):23-32.
12. Lustigman S, Prichard RK, Gazzinelli A, Grant WN, Boatman BA, McCarthy JS, et al. A research agenda for helminth diseases of humans: the problem of helminthiases. *PLoS Negl Trop Dis*. 2012;6(4):e1582.
13. Ward JD. Rendering the intractable more tractable: tools from *Caenorhabditis elegans* ripe for import into parasitic nematodes. *Genetics*. 2015;201(4):1279-94.
14. Chen L, Tang L, Xiang H, Jin L, Li Q, Dong Y, et al. Advances in genome editing technology and its promising application in evolutionary and ecological studies. *Gigascience*. 2014;3:24.
15. Lok JB, Shao H, Massey HC, Li X. Transgenesis in *Strongyloides* and related parasitic nematodes: historical perspectives, current functional genomic applications and progress towards gene disruption and editing. *Parasitology*. 2017;144(3):327-42.